FINAL REPORT

Tracking the Uptake, Translocation, Cycling, and Metabolism of Munitions Compounds in Coastal Marine Ecosystems Using Stable Isotopic Tracer

SERDP Project ER-2122

MAY 2019

Dr. Craig Tobias
University of Connecticut

SERDP
DOD ▪ EPA ▪ DOE

Page Intentionally Left Blank

Page Intentionally Left Blank

REPORT DOCUMENTATION PAGE

Form Approved
OMB No. 0704-0188

1. REPORT DATE *(DD-MM-YYYY)*	**2. REPORT TYPE**	**3. DATES COVERED** *(From - To)*
05-29-19	SERDP Final Report	May 2011 – Dec 2018

4. TITLE AND SUBTITLE
Tracking the Uptake, Translocation, Cycling and Metabolism of Of Munitions Compounds in Coastal Marine Ecosystems Using Stable Isotopic Tracers

5a. CONTRACT NUMBER
W912HQ11C0051/W912HQ18P000

5b. GRANT NUMBER

5c. PROGRAM ELEMENT NUMBER

6. AUTHOR(S)
Craig Tobias

5d. PROJECT NUMBER
ER-2122

5e. TASK NUMBER

5f. WORK UNIT NUMBER

7. PERFORMING ORGANIZATION NAME(S) AND ADDRESS(ES)

University of Connecticut
438 Whitney Rd
Storrs, CT 06269

8. PERFORMING ORGANIZATION REPORT NUMBER

ER-2122

9. SPONSORING / MONITORING AGENCY NAME(S) AND ADDRESS(ES)
SERDP
4800 Mark Center Dr
Suite 16F16
Alexandria, VA 22350

10. SPONSOR/MONITOR'S ACRONYM(S)
SERDP

11. SPONSOR/MONITOR'S REPORT NUMBER(S)
ER-2122

12. DISTRIBUTION / AVAILABILITY STATEMENT

DISTRIBUTION A. Approved for public release: distribution unlimited.

13. SUPPLEMENTARY NOTES

14. ABSTRACT

Stable isotope-labeled TNT and RDX were used in benchtop, aquaria, and large mesocosm experiments to quantify the fate these compounds in coastal marine ecosystems. Both compounds underwent conversion to organic derivatives, sediment sorption, uptake and turnover by biota, and mineralization to inert inorganic constituents. The isotope label was used to quantify the magnitude of each of these fates. Biota was a small sink for both TNT and RDX. Bioconcentration factors (BCFs) were several orders of magnitude below those of hydrophobic compounds known to bioaccumulate. Differences between tissue RDX and TNT concentrations and isotope tracer indicated high amounts of internal processing of both compounds after uptake. Abiotic sorption to sediments, while only a minor fate, was higher than that reported for freshwater sediment. Mineralization to inorganic constituents was the dominant fate (50-60%) for RDX particularly in high organic sediments. Production of an unmeasured aqueous organic derivative was the primary fate for TNT. The BCFs, and uptake and elimination constants for biota can benefit stakeholders because they can be directly used to parameterize transport and/or risk models. Isotopic evidence of mineralization provides proof of concept that similar tracer approaches can be used at contaminated sites to evaluate natural attenuation in-situ.

15. SUBJECT TERMS
Uptake, Translocation, Cycling, Metabolism, Munitions Compounds, Coastal Marine Ecosystems, Stable Isotopic Tracer

16. SECURITY CLASSIFICATION OF:			**17. LIMITATION OF ABSTRACT**	**18. NUMBER OF PAGES**	**19a. NAME OF RESPONSIBLE PERSON**
a. REPORT	**b. ABSTRACT**	**c. THIS PAGE**			Craig Tobias
UNCLASS	UNCLASS	UNCLASS	UNCLASS	256	**19b. TELEPHONE NUMBER** *(include area code)* 860-405-9140

Standard Form 298 (Rev. 8-98)
Prescribed by ANSI Std. Z39.18

Page Intentionally Left Blank

TABLE OF CONTENTS

LIST OF TABLES

LIST OF FIGURES

LIST OF ACRONYMS

2A-DNT	2-aminodinitrotoluene
4A-DNT	4-aminodinitrotoluene
^{15}N	The rare heavy stable isotope of nitrogen
ACS	American Chemical Society
ASTM	American Society for Testing and Materials
BCF	Bioconcentration Factor
CT	Connecticut
CV	Coefficient of Variance
DON	Dissolved Organic Nitrogen
DIN	Dissolved Inorganic Nitrogen
DOC	Dissolved Organic Carbon
DNB	Dinitrobenzene
DNX	Hexahydro-1,3-dinitroso-5-nitro-1,3,5-triazine
DOD	Department of Defense
EA-IRMS	Elemental Analyzer Isotope Ratio Mass Spectrometry
EPA	Environmental Protection Agency
ER	Environmental Restoration
GB-IRMS	Gas Bench Isotope Ratio Mass Spectrometry
GC-IRMS	Gas Chromatography Isotope Ratio Mass Spectrometry
GC-ECD	Gas Chromatography Electron Capture Detector
GT	Gas Transfer coefficient
HPLC	High Performance Liquid Chromatography
IRMS	Isotope Ratio Mass Spectrometry
KCL	Potassium Chloride
KOH	Potassium Hydroxide
Kow	Octanol-Water Partition Coefficient
LIS	Long Island Sound
MADNT	Monoaminodinitrotoluene
MC	Munitions Constituent
MEDINA	Methylenedinitramine
MNX	Hexahydro-1-nitroso-3,5-dinitro-1,3,5-triazine
N	Nitrogen
N_2	Dinitrogen gas
NA	Natural Attenuation
NDAB	4-nitro-2,4-diazabutanal
NH_3	Ammonia
NH_4+	Ammonium
N_2O	Nitrous oxide
NO_2^-	Nitrite
NO_3^-	Nitrate
NPL	National Priorities List
NT	Nitrotoluene
OC	Organic Carbon
PC	Principal Component

PCA	Principal Components Analysis
PES	Polyethersulfone
PSU	Partial Salinity Units
PTFE	Polytetrafluoroethylene
RDX	Hexahydro-1,3,5-trinitro-1,3,5-triazine
∑RDX	RDX + all measured organic RDX derivatives
RMSE	Root Mean Square Error
SERDP	Strategic Environmental Research and Development Program
SETAC	Society for Toxicology and Chemistry
SF6	Sulfur Hexafluoride
SON	Statement of Need
SPOM	Suspended Particulate Organic Matter
SRB	Sulfate Reducing Bacteria
TAT	Triaminotoluene
TNT	2,4,6 Trinitrotoluene
∑TNT	TNT + all measured organic TNT derivatives
TNX	Hexahydro-1,3,5- trinitroso1,3,5-triazine
UCONN	University of Connecticut
USGS	United States Geological Survey
UXO	Unexploded Ordnance
VA	Virginia
VNTR	Vieques Naval Training Range
XRD	X-ray Diffractometer

KEYWORDS

RDX, TNT, munitions, marine, stable isotope tracer, ^{15}N, mineralization, sediments, sorption, biota, bioconcentration factor

ACKNOWLEDGMENTS

We would like to thank the SERDP ER Program for supporting this project and for providing valuable guidance, suggestions, and course corrections along the way. Additional thanks to Paul Hatzinger for insights on the isotope tracer synthesis, and to Gui Lotufo for his comments on all things biotic. The thoughtful and constructive reviews from anonymous journal reviewers and associate editors were instrumental in helping to disseminate our findings. Finally, this work would not have been possible without the hard work from Charlie Woods who runs the Rankin Seawater Lab, and David Cady who runs the Stable Isotope Lab at the University of Connecticut.

ABSTRACT

Objective

This work quantified ecosystem processing of the legacy munitions compounds RDX (hexahydro-1,3,5-trinitro-1,3,5-triazine) and TNT (2,4,6-trinitrotoluene) in coastal marine environments. Sorption to sediments, mineralization, and uptake / elimination by macrobiota were examined. The project responded to the SERDP Core Statements of Need (11 ER01-008): 1) *Assess the predominant fate and transport mechanisms and the kinetics of such reactions at environmentally relevant concentrations in the sediment and water column.* 2) *Assess the impacts of munitions constituents to relevant ecological receptors in the marine environment.*

Technical Approach

Stable isotope (^{15}N) -labeled and unlabeled RDX and TNT were used in benchtop and mesocosm tracer experiments. These experiments were designed to quantify *removal and mineralization* in water and sediment, as well as *uptake and elimination* by macrobiota.

Results

Removal and Mineralization - The presence of sediments had a major influence on the removal kinetics of all compounds detected. RDX degraded only in the presence of sediment, and TNT degraded significantly faster in the presence of sediment. RDX and TNT removal from the overlying water increased with decreasing grain-size. Photodegradation at light levels typical of temperate coastal waters was not a factor in RDX or TNT removal from the water column.

Sediment effects on aqueous RDX and TNT concentrations resulted partly from high sorption to marine sediment. Abiotic sorption tests in anaerobic sediment slurries showed that marine sediments had significantly higher uptake rates for both compounds relative to freshwater sediment of similar grain size. Equilibrium partition constants were on the same order of magnitude for marine and freshwater silt (1.1 – 2.0 $Lkg^{-1}sed$), but lower for marine sand.

Anaerobic slurry conditions promoted mineralization of both TNT and RDX as evidenced by conversion of ^{15}N labeled parent compound to various dissolved inorganic nitrogen (DIN) constituents. Two percent of the TNT added was mineralized through denitration, and deamination which resulted in primarily NH_4^+. Multivariate analyses suggested that iron and sulfate reduction facilitated mineralization. Anaerobic RDX mineralization resulted in primarily NH_4^+. Six times more RDX was mineralized relative to TNT.

More realistic aquaria experiments using ^{15}N- RDX with intact sediment with aerobic / anaerobic gradients showed a linkage between RDX mineralization and denitrification. Modeling the evolution of $^{15}N_2O$ and $^{15}N_2$ showed mineralization of 11% of the added RDX after 22 days , and 29% of the total removed RDX-N was identified as $^{15}N_2$. Denitrifiers were not responsible for the RDX degradation but rather that they used RDX mineralization products as a substrate. The result documented that RDX mineralization supplied N generally to the marine N cycle.

Aerobic/anaerobic aquaria-scale ^{15}N- TNT experiments indicated that the dominant TNT mineralization product remained as NH_4^+ even under mixed redox conditions. The ^{15}N tracer mass balance revealed that the majority of TNT was not mineralized, but instead transformed into an unidentified derivative. We used principal components analysis to constrain the steps leading to the derivative production and to infer that the major transformation pathway was the deamination of TNT, promoted by sorption to SPM and oxic surface sediments.

Larger mesocosms containing water, sediment, biota, and ^{15}N-RDX were used to evaluate RDX mineralization among three different marine ecotypes: 1) subtidal low carbon sand, 2) subtidal higher organic carbon vegetated silt, 3) intertidal salt marsh. RDX processing was largest (50%) in the high carbon and redox variable intertidal marsh, and smallest in the low carbon sand mesocosm (25% of added RDX). The nitroso derivatives MNX, DNX, and TNX, comprised only 2-3% of the RDX loss. Mineralization of RDX, resulted in primarily N_2O and N_2, and was the fate of 47-70% of the RDX lost from the water column. Similar mesocosm experiments with ^{15}N TNT showed ~78% loss of TNT from the overlying water that was independent of ecotype. TNT -^{15}N partitioning to sediment was greater than RDX, but with little mineralization. Poor isotope mass balances in the TNT mesocosms, similar to that found in the TNT aquaria experiments, suggested that TNT processing largely resulted in the formation of an unidentified organic derivative. Analysis of the dissolved organic nitrogen pool did not further constrain the nature of the derivative.

Uptake and Elimination by Macro-organism - Exposure of common coastal marine flora and fauna to RDX and TNT yielded bioconcentration factors (BCFs) that were similar to freshwater organisms of similar trophic level and lifestyle. Uptake into tissues was rapid. Primary nitroso derivatives for RDX were a small fraction of the tissue RDX concentrations, but amino-dinitrotoluenes (dominated by 4-ADNT) were 20% of the TNT concentration. Highest BCF was measured in lipid rich crab eggs, but generally RDX, TNT and their primary derivatives yielded low BCFs (<50 ml g^{-1}) that were reasonably well-predicted by the octanol-water partition coefficient (Kow) of the compounds.

First order modeling of RDX and ^{15}N tracer concentrations in tissues revealed high rates of uptake offset by rapid elimination and redistribution of tracer into bulk biomass. Tissue ^{15}N tracer exceeded intact ^{15}N-RDX by 10-fold. Modeled uptake rates were similar to published values, but elimination rates were several orders of magnitude smaller (0.05 to 0.7 day^{-1}). Low elimination rates were offset high rates of retention of ^{15}N in some unknown form. Four different biotransformation pathways were proposed to explain the ^{15}N retention. Some of these pathways indicate photosynthetic utilization of RDX derived N, while others suggest the formation of undetected metabolites and/or adduct formation between metabolites and cellular constituents.

The uptake, retention, and transformation of ^{15}N-RDX measured in 13 marine species were independent of coastal ecotype. Despite different levels of RDX loss and mineralization between sand, vegetated silt, and intertidal marsh mesocosms, the variance in the tissue RDX and ^{15}N concentrations were similar. Limited correlation between aqueous and tissue RDX concentrations suggested that post uptake transformations were as important as aqueous RDX concentrations in setting tissue RDX levels. Extrapolating mesocosm results to ecosystem scales revealed that macrobiotic RDX retention and processing scaled linearly with expected species biomass, with “hot spots” of high retention and/or transformation in marsh macrophyte roots.

Benefits

Results provide end-user benefits in two categories. **I)** ER-2122 yielded constants for direct parameterization of models that support risk assessments (Abstract Graphic #1). The water column half-lives and sorption isotherms measured across range of sediment types can be incorporated into transport models that predict MC mobility and migration off-site. The BCFs and associated uptake and elimination constants measured for over a dozen marine biota species, including those consumed by humans, provide calibration factors for human exposure models. **II)** ER-2122 vetted a technology that can be used to quantify in-situ natural attenuation of MC

(munitions constituents) at aquatic sites under field conditions (Abstract Graphic #2). The detection of mineralization species unique to the isotope labeled MC, coupled with high recovery of total labeled RDX products in large mesocosms identified a sensitive tool for quantifying natural attenuation (NA) rates in-situ. The in-situ mineralization rates can be evaluated relative to transport times of MC off-site and/ or to sensitive human health / ecological targets to determine suitability of NA as a remediation option. Implementation of this technology in MC contaminated ground or surface waters would require tagging existing contamination with small amounts of isotope labeled MC, accounting for dilution during transport, and analyses of labeled mineralization products over time.

Transfer of the RDX results to end users with respect to both Categories I and II can be done with high confidence. Data gaps remain for transfer of the TNT results whose primary fate was an unmeasured aqueous organic derivative. Identification of this aqueous derivative is a critical missing piece of information needed to provide end-users with guidance on TNT mineralization or human health / ecological risk.

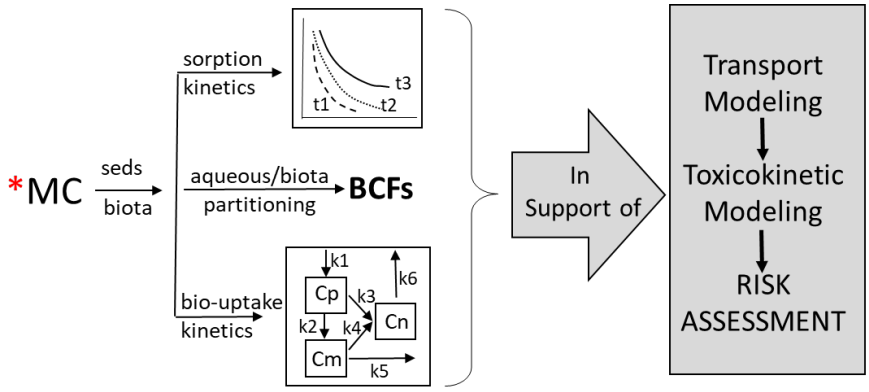

Abstract Graphic #1. Sediment and biological kinetic parameters established as part of ER-2122 can be directly used to calibrate site assessment models. ER-2122 results include multiple sediment types and aquatic species. Data can be used by site specific end-users for assessing MC mobility, potential for bioaccumulation, and ultimately ecological and human health risk.

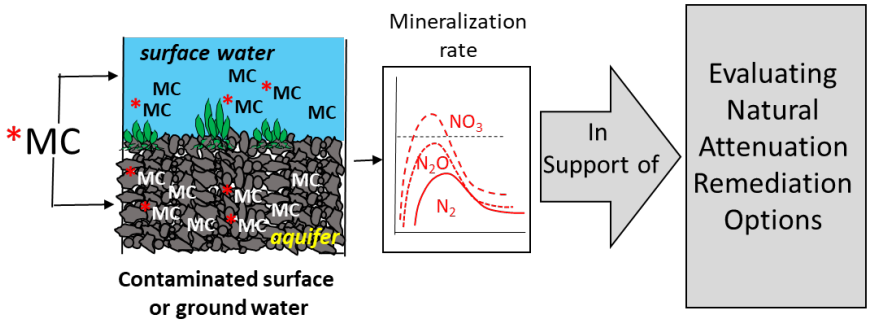

Abstract Graphic #2. Isotope tracer approaches used in ER-2122 to quantify mineralization of MC can be applied to MC contaminated sites. Existing MC contamination in surface or ground waters can be tagged with isotope labeled MC (*MC) and used to estimate in-situ mineralization rates. These rates will frame the efficacy of natural attenuation (NA) relative to rates of MC transport off-site. This site specific NA measurement permits better evaluation of NA in the context of other remediation alternatives by RPMs and regulatory agencies.

1.0 PROJECT OBJECTIVES AND BACKGROUND

1.1. Objectives

The overall goal of this work was to quantify ecosystem processing of the legacy munitions compounds RDX (hexahydro-1,3,5-trinitro-1,3,5-triazine) and TNT (2,4,6-trinitrotoluene) in coastal marine environments. Sorption to sediments, mineralization, and uptake / elimination by macrobiota were examined. The project responded to the SERDP Core Statements of Need 11 ER01-008. The following six specific objectives were targeted: 1) quantify the effect of marine sediments on aqueous munitions concentrations, 2) determine the contributions of sediment sorption and biodegradation under strictly anaerobic conditions to munitions uptake from the water column, 3) quantify how much of the munitions loss could be attributed to complete mineralization for RDX and TNT independently, 4) establish baseline bioconcentration factors for both compounds in a suite of common coastal marine flora and fauna, 5) model the organismal rates of uptake, retention, and elimination of RDX, 6) examine how the rates and pathways of compound mineralization and processing by macrobiota are affected by different environmental variables characteristic of three common coastal marine ecotypes. We hypothesized a dominant role of sediments in mineralization of both compounds particularly in higher organic carbon environs. Further, RDX would be more likely to completely mineralize relative to TNT which would produce more stable organic derivatives. For marine flora and fauna, low RDX bioconcentration factors and high rates of biotransformation were expected.

1.2. Background

Within the contiguous 48 United States, there are approximately 41 active DOD installations located within the coastal zone. Munitions operations on active facilities consist of storage, loading, packing, and live fire exercises. Several active installations maintain live fire ranges in intertidal and subtidal marine habitats. The number of active bases, combined with decommissioned facilities with historical TNT /RDX contamination, and offshore munitions dump sites indicate the probable likelihood that multiple marine habitats at multiple locations receive exposure to TNT and RDX. Exposure of marine/estuarine ecosystems at some sites like Eagle River Flats and the Yorktown Weapons Station is well documented (Walsh et al., 2010), while other sites have documented contamination inland with no available data beyond the shoreline. Still other sites have the potential for contact but little to no characterization with respect to munitions compounds migration into marine ecosystems.

Near-shore marine habitats play an important role in retaining and transforming nutrients/contaminants derived from anthropogenic sources. These ecosystems exhibit strong feedbacks between loading, organic matter decomposition, redox variability, and primary production in both water column and sediments. They serve as focal points for enhanced benthic primary production, sediment-water nutrient exchange (McGlathery et al., 2001; Anderson et al., 2003) and provide critical ecosystem services including fish and shellfish production. Reactive nitrogen is the primary limiting nutrient for biological production in marine environments (Howarth et al., 2000), and both TNT and RDX are N-rich. Ecosystem responses to munitions input may be evident in localized areas. Similarly, toxicity effects and alterations of species composition of marine organisms may also be limited to hotspots (Darrach et al., 1998; Lotufo et

al., 2001). Further background on previous research is expanded in the following Sections (2.0 – 10.0). Generally this past work was limited to freshwater environments, toxicological studies, and/or identification of pathways of derivative production. Here we focused on mineralization and sub lethal uptake / biotransformation of RDX and TNT in marine systems.

The following Sections 2.0 – 10.0 include Materials and Methods, Results, and Discussion/Conclusions of individual experiments. They are presented in similar formats and reflect the format of the peer-review journals in which they were published. The final Section 11.0 presents future research directions and recommendations for implementation based upon conclusions drawn collectively from Sections 2.0 – 10.0.

2.0. Removal Rates of Dissolved Munitions Compounds in Coastal Marine Systems

This chapter was published, as follows:

Smith, R.W., Vlahos, P., Tobias, C., Ballentine, M., Ariyarathna, T., and Cooper, C. 2013. Removal rates of dissolved munitions compounds in seawater. Chemosphere, 92: 898-904.

Abstract

The historical exposure of coastal marine systems to munitions compounds is of significant concern due to the global distribution of impacted sites and known toxicological effects of nitroaromatics. In order to identify specific coastal regions where persistence of these chemicals should be of concern, it is necessary to experimentally observe their behavior under a diversity of relevant oceanographic conditions. Here, we conduct a mesocosm scale pulse addition experiment to document the behavior of two commonly used explosives, 2,4,6-trinitrotoluene (TNT) and hexahydro-1,3,5-trinitro-1,3,5-triazine (RDX) in simulated marine systems containing water and sediments collected from Long Island Sound, CT. The addition of sediments and sediment grain-size had a major influence on the removal kinetics of all compounds detected. RDX degraded only in the presence of sediment, and TNT degraded significantly faster in the presence of sediment. Both compounds were removed from the system faster with decreasing grain-size. Based on these findings and a thorough review of the literature, we hypothesize that TNT removal rates in coastal marine waters are controlled by sorption and rapid surface-mediated bacterial transformation, while RDX removal rates are controlled by diffusion into sedimentary anoxic regions and subsequent anaerobic bacterial mineralization. A comparison of published removal rates of RDX and TNT highlights the extreme variability in measured degradation rates and identifies physicochemical variables that covary with the breakdown of these munitions compounds.

2.1. Introduction

Coastal military activity has resulted in exposure of marine habitats to munitions compounds in both dissolved and particulate phases (Darrach et al., 1998; Rodacy et al., 2000). Unexploded ordnance (UXOs) enter the marine environment through their use in the field and ongoing training exercises, through incomplete detonation, as well as disposal at sea (Rosenblatt et al., 1991; Morley et al., 2006), and contamination can persist for several decades (Darrach et al., 1998).

2,4,6-trinitrotoluene (TNT) and hexahydro-1,3,5-trinitro-1,3,5-triazine (RDX) are two of the most commonly used munitions compounds, and are proven toxins in marine systems (Won et al., 1976; Nipper et al., 2001). Sublethal bioaccumulation of RDX and TNT in the tissues of marine organisms may also pose a threat to human health from seafood consumption (Lotufo et

al., 2010; Belden et al., 2005). The duration of environmental exposure after munitions compounds become solubilized is a function of their residence time in seawater, determined by a number of factors including sediment adsorption, biotic and abiotic transformation, and remineralization (Brannon et al, 2005; Hawari et al., 2000). Therefore, reliable estimates of removal rates of TNT and RDX under a number of geographic locations and oceanographic conditions, has the potential to greatly simplify fate and transport models and/or contaminant management schemes.

A wealth of information exists on the fate of RDX and TNT in terrestrial environments such as soils, groundwater, and surface freshwater (Juhasz and Naidu 2007; Bradley et al., 1992; Pennington and Patrick 1990; Zheng et al., 2009); yet how the rates and mechanisms of removal translate to the marine environment is not fully understood (Brannon et al., 2005), especially considering the geochemical differences between soils, freshwater sediments and marine sediments (Hedges and Oades, 1997). Also, observed breakdown and transformation rates in marine systems vary greatly (Brannon et al., 2005; Harrison and Vane, 2010; Yost et al., 2007; Chappell et al., 2011), outlining the need for additional experiments and a thorough comparison of existing data.

In this study, we describe the behavior of RDX and TNT at environmentally relevant concentrations in the marine setting, with a focus on the role of sediments. Removal rates, first order rate constants and half-lives, are calculated for RDX, TNT, and TNT transformation products (2a-DNT and 4a-DNT). Incubations are performed in series of mesocosm scale treatments replicating coastal conditions in Long Island Sound. The observed rates are compared with existing rates to highlight potential sedimentary indicators of munitions persistence.

2.2. Methods

2.2.1 Experimental Design

Four experimental treatments were used in the study: seawater only- light (SW_L); seawater only - dark (SW_D); seawater + fine grained sediment (SED_{FG}); and seawater + coarse grained sediment (SED_{CG}). Two paired mescosms (70 L glass tanks containing seawater or seawater and sediment) were used for each treatment, connected to a common recirculating reservoir (Figure 2.1). Seawater was supplied to the mesocosms directly from Long Island Sound. Sediments used in the SED_{FG} and SED_{CG} mesocosms were collected from a Long Island Sound shallow subtidal habitat near Groton, CT, and added to the mesocosms to a sediment thickness of ~10 cm depth. The SW_D treatment, to control for photochemical degradation, was kept in the dark using a black cloth. All other treatments were exposed to ambient light conditions. Sediments and seawater were added to the tanks with active recirculation two weeks before the start of the experiment, in order for redox and chemical conditions to stabilize. The seawater was kept recirculating through the mesocosms and reservoirs as a closed system throughout the course of the experiment.

To examine the behavior of dissolved TNT and RDX under each of the experimental conditions, each of the mesocosms received single pulse additions of concentrated TNT and RDX in methanol (10 ml) simultaneously, targeting environmentally relevant concentrations of

0.3 mg L^{-1} for RDX and 1.3 mg L^{-1} for TNT. Following the addition of TNT and RDX, time series sampling of the overlying water was conducting starting at day 0, and sampling continued for a period of 28 (SW_L & SW_D) to 45 (SED_{FG} & SED_{CG}) days.

2.2.2 Water Chemistry

Dissolved oxygen (DO), salinity, and temperature in the water column were monitored with a YSI probe. Munitions sampling and analysis methods were adapted from EPA method 8330 (US EPA, 1994) as modified by Agilent. Briefly, 5 ml of methanol were immediately added to a 5 ml seawater sample, shaken and filtered through a 0.45µm PTFE syringe tip filter. 20 µl of the solution was injected onto an Agilent 1200 series ultra-violet high-performance liquid chromatograph (UV-HPLC) equipped with a Zorbax Eclipse column (4.2 x 150 mm, 3 µm; Agilent) maintained at 30 ºC. Munition compounds were eluted isocratically with 25% MeOH and 75% ammonium formate buffer (pH 6) at a flow rate of 1.7 mL min^{-1}. UV peak areas at 254 nm were identified based on retention time and converted to mg L^{-1} concentrations with an external calibration curve containing 14 munitions compounds (EPA Mix A:EPA Mix B, 1:1, Accustandard). All values are reported as n = 4 (two water samples from each mesocosm, two mesocosms per treatment), and precision was on the order of approximately 1% (Supplementary Table S-2.1).

Rate constants (k) and half-lives of munitions compounds, when degradation was observed, were calculated by fitting a first-order best-fit exponential curve to the time series profiles with Sigmaplot v.11.

2.2.3 Sediment Chemistry

Sediments were sampled at the beginning and end of the experiment for percent organic carbon, grain-size, and munitions concentrations. Freeze-dried sediment was analyzed for %OC using the acid fumigation and EA method of Hedges and Stern (1984). For grain size characterization, ~2 g of sediment was passed through a series of sieves ranging in size from 2 mm to 63 µm. The fraction of sediment retained on each sieve was weighed. The mass of each size fraction was converted to particle "counts" assuming a perfectly spherical shape and a density of 2.65 g cm^{-3}, typical of aluminosilicates. Sediment that passed through the 63 µm sieve was deemed to be the silt/clay fraction. Therefore % sand and % silt/clay represents a percentage of the number of particles in each size range present under 2 mm (particles above 2 mm were excluded, and include cobbles and discrete woody fragments). Munitions were extracted following a method adapted from US EPA (1994). Briefly, 2 g of freeze-dried sediment was extracted by sonicating for 1 hr with acetonitrile at a 2:1 liquid to solid ratio. The extract was filtered through a 0.45µm PTFE syringe tip filter, and a 3 µl aliquot was injected into the HPLC.

2.3. Results and Discussion

2.3.1 Mesocosm Geochemistry

The temperature of the LIS water used in all the tanks remained stable at ~19 ºC. (Supplementary Table S-2.1). Salinity was initially ~31, and increased linearly to ~35 to 38 in

all the mesocosms as water evaporated over the long duration of the experiment. Salinity was used as a conservative tracer to correct for evaporative volume changes. The water column of all treatments remained aerobic: DO values ranged from 3.0 – 8.1 mg L^{-1}, with the lowest values observed in SED_{FG}. Initial concentrations of RDX and TNT vary slightly around the target values based on small differences in seawater volume among tanks.

Coarse-grained sediments in SED_{CG} and SED_{FG} contained 0.03 % and 0.38 % OC (w/w) and 0.5 % and 26.5 % silt/clay (particle counts), respectively. In both treatments with sediments, no munitions compounds were detected in sediment extracts, and therefore the rest of the discussion is based around dissolved values in the water column.

The nearly identical behavior of RDX, TNT, and TNT derivatives in SW_L and SW_D suggests that ambient light levels in our experiment were not strong enough to cause photochemical breakdown (Figure 2.2; Supplementary Table S-2.2). Similar behavior of all observed compounds in these treatments highlights the reproducibility of this experimental setup, and therefore the average of these two treatments is reported in the discussion for comparison with treatments containing sediment.

2.3.2 Contaminant Behavior

2.3.2.1 TNT

In all three treatments, dissolved TNT exhibited first-order degradation to levels below detection, ranging from 3 days in the presence of fine-grained sediment, 11 days in coarse-grained sediment, to 28 days in the absence of sediment (Figure 2.3). TNT half-lives were 3.83 days in the absence of sediment, 1.87 days in the presence of coarse-grained sediment, and 0.439 days in the presence of fine-grained sediment (Table 2.1). 2a-DNT and 4a-DNT were the only detected TNT transformation products. In the absence of sediment, these derivatives were stable and approached values of 0.113 and 0.157 mg L^{-1} (SW_L and SW_D, respectively) around day 16. However, in the presence of sediment, these compounds exhibit first-order degradation (Figure 4). Calculated half-lives are 28 and 2.74 days for 2a-DNT and 41.1 and 8.48 days for 4a-DNT in SED_{CG} and SED_{FG}, respectively (Table 2.1).

The observed first-order degradation of TNT and production of DNT derivatives in simulated marine environments is consistent with most studies in the literature, although time scales vary (Table 1). Maximum DNT yields in SED_{FG} (0.180 mg L^{-1}) and SED_{CG} (0.194 mg L^{-1}) accounted for only 12% and 13% of spiked TNT, respectively, while in the SW treatments the maximum yield (0.270 mg L^{-1}) accounted for 21%. Therefore, the fate of the bulk of TNT is unknown. TNT is readily reduced or transformed to breakdown products by heterotrophic bacteria involving the reduction of nitro (-NO_2) functional groups to nitroso (-NO), hydroxylamino (-NHOH) and amino (-NH_2) moieties, or complete removal of these groups from the ring (Esteve-Nunez et al., 2001). As US EPA method 8330 does not include reduced products beyond 2a-DNT, and 4a-DNT, undetected transformation products of TNT were likely to exist in our system. Additionally, TNT can be mineralized to CO_2 and N gases, reported to occur by lignolytic fungi (Hawari et al., 2000) and natural microbial communities in marine sediments (Montgomery et al., 2011). Rates of 3 – 270 μgC kg^{-1} d^{-1} suggest this removal process was likely quantitatively significant in our treatments, although confirmation requires the use of isotopically labeled TNT ([^{15}N]-TNT).

An alternative fate of the spiked TNT as opposed to breakdown is removal via biological assimilation, or irreversible sorption to sediments. It is unclear if phytoplankton, introduced to the tanks in LIS seawater, assimilate TNT similar to macroalgae, and this mechanism of removal cannot be ruled out (Cruz-Uribe et al. 2007). Finally, through the dimerization of reduced TNT derivatives to azoxy compounds, TNT can be irreversibly covalently bonded to active sites on minerals (Vasilyeva et al., 2002; Yong et al. 2008). These previous studies suggest this removal process can be very significant, and would help to explain the disappearance of TNT from the water column despite the absence of extractable TNT in sediments.

2.3.2.2 RDX

Dissolved RDX was removed from the mesocosms at a slower rate than TNT in all treatments. Concentrations remained stable throughout the course of the experiment in SW_L and SW_D, but significantly decreased in the presence of sediments (Figure 2.4). In SED_{CG}, RDX removal was not complete, however we estimate RDX would drop below detection limits after 332 days, based on its half-life. In SED_{FG}, removal was complete (under detection limits) after 28 days. Half-lives in SED_{CG} and SED_{FG} were 41.1 and 8.48 days, respectively, and are in the range of both freshwater and seawater removal rates published by Brannon et al. (2005).

Unlike TNT, no RDX transformation products are included in US EPA method 8330, and therefore its fate is unknown. However, it is known that a consortia of microbes in marine sediments can degrade RDX including sulfate-reducing and denitrifying bacteria (Bhatt et al., 2005; Hawari et al., 2000; Zhao et al., 2004a,b; Singh et al., 2009) and fungi (Bhatt et al., 2006; Sheremata and Hawari, 2000). Several abiotic mechanisms also exist with varying rates of removal and optimum conditions, such as reduction by hydrogen sulfide (Kemper et al. 2008; Xu et al. 2010) black carbon (Xu et al., 2010; Gustafsson and Gschwend, 1998), or reduced iron minerals (Gregory et al., 2004), as well as by alkaline hydrolysis (Hoffsommer et al., 1977; Monteil-Rivera et al., 2008). A more thorough analysis of RDX dynamics using isotopic tracers (^{15}N) is necessary to fully understand the role of these competing mechanisms.

2.3.3 The Role of Sediments in Munitions Breakdown

A handful of studies exist comparing breakdown rates of TNT and RDX to variable conditions in simulated marine systems. These efforts and the data presented here suggest that TNT will be removed faster with increasing water temperature and sediment surface area and % OC content, based on controlled experiments examining the effect of single variables (Table 1 and references therein). RDX rates have only been published in a limited number of studies, and therefore have only been linked to %OC content and grain-size (Table 2.1).

In general, TNT half-lives observed based on these variable conditions ranged by a factor of 2, and at most just over an order of magnitude. However, the range of TNT half-lives between studies is over 4 orders of magnitude. Therefore, there are conditions other than those determined previously that exert large controls on the persistence of munitions in marine systems. Linear regression statistics between measured sedimentary characteristics and TNT k values are calculated in an attempt to identify these controlling parameters. Sedimentary pH and %OC are the only properties that correlate significantly with TNT k values (Supplementary Table S-2.3). The correlation between sedimentary pH and TNT k values was particularly strong ($R^2 = 0.9$), with more acidic pore-waters coinciding with faster degradation rates. This

relationship between porewater pH and TNT degradation has been previously observed (Ullah et al., 2010), although pH may just be tracing *in situ* heterotrophic microbial respiration promoted by the addition and breakdown of TNT (and subsequent nitrate release) (Morse and Mackenzie, 1990; Esteve-Nunez et al., 2001).

The observed covariance of sedimentary characteristics and munitions residence time may hint towards a mechanistic explanation of removal that could explain variables not yet considered in controlled experiments. We suggest that observed increases in TNT removal rates is the result of sediment surface-mediated abiotic and biotic transformation of TNT. TNT sorbs strongly to clay in soils (Pennington and Patrick, 1990; Eriksson et al., 2004) and it is well documented that sorbed TNT is readily bioavailable (Robertson and Jjemba, 2005; Ullah et al., 2010; Chappell et al. 2011). Additionally, it has been suggested that the lack of extractable munitions in marine incubation experiments is due to rapid bacterial utilization of sorbed TNT. Sorption is therefore a rate-limiting step, and the observed covariance of temperature and %OC with TNT degradation rates may be indirect through the effect these parameters have on sorption efficiency to sediments.

RDX however exhibits minimal sorption to particles (Singh et al., 1998; Dontsova et al., 2006, 2008), yet breakdown is impacted similarly in the presence of sediments as with TNT. We hypothesize that RDX degrades in the presence of sediment via aqueous transport to anaerobic zones in deeper sediment layers and subsequent bacterial utilization. Bacterial mineralization of RDX is well known to occur primarily under anaerobic conditions (Hawari et al., 2000; Zhao et al., 2004a; Bhatt et al., 2005), and oxygen penetration into marine sediments is generally restricted to 1 cm in undisturbed conditions (Aller, 1982; Archer, 1990). Increases in sediment surface area and %OC therefore facilitate the removal of RDX by restricting oxygen penetration into the sediments and facilitating oxygen removal through OC remineralization.

While further experiments using isotopically labeled munitions are necessary to confirm these hypotheses, it is clear sediments exert a major influence over the persistence of these compounds in coastal zones. Breakdown will be favored in shallow marine depositional environments where dissolved munitions can interact with fine-grained sediments and associated bacteria.

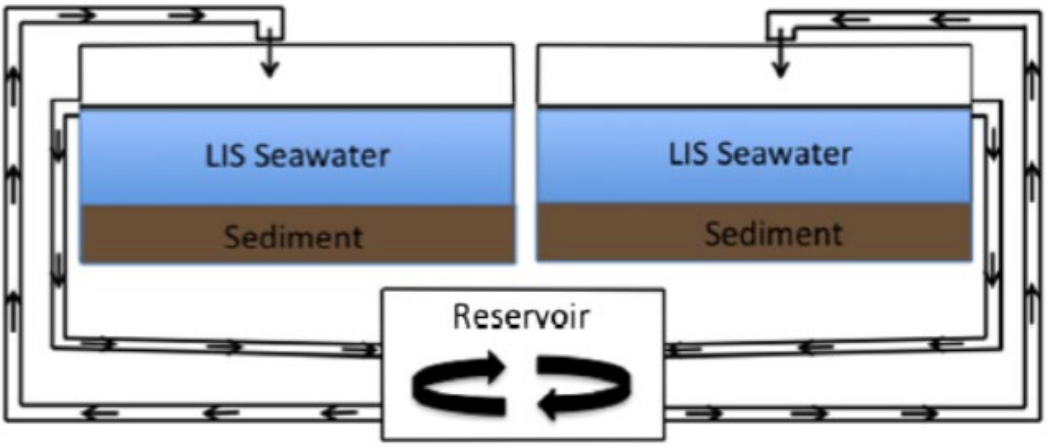

	Sediment	Label
Treatments	No Sed. (light)	SW_L
	No Sed. (dark)	SW_D
	Fine-grained (light)	SED_{FG}
	Coarse-grained (light)	SED_{CG}

Figure 2.1. Diagram of a single recirculating mesocosm. Arrows indicate the direction of water flow.

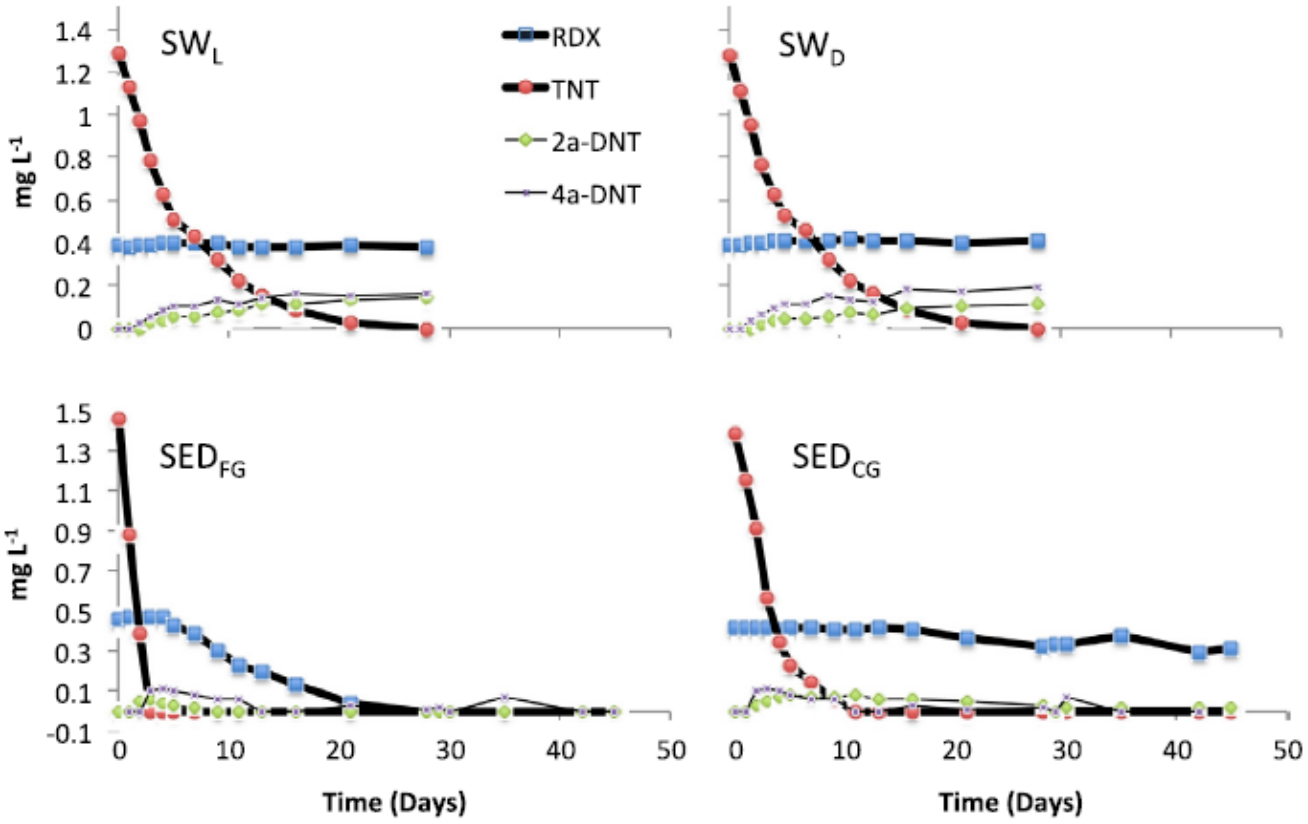

Figure 2.2. Time-series concentrations of TNT, RDX, and detected derivatization products in the four mesocosms constructed. Mesocosms SW_L and SW_D were both carried out under the same conditions with no sediment and are shown as evidence of repeatability of the experiment. Mesocosms SED_{FG} and SED_{CG} were carried out with the same water type (Long Island Sound coastal water) but with fine- and coarse-grained sediment from LIS, respectively. Concentrations along the y axis are in mg L^{-1}.

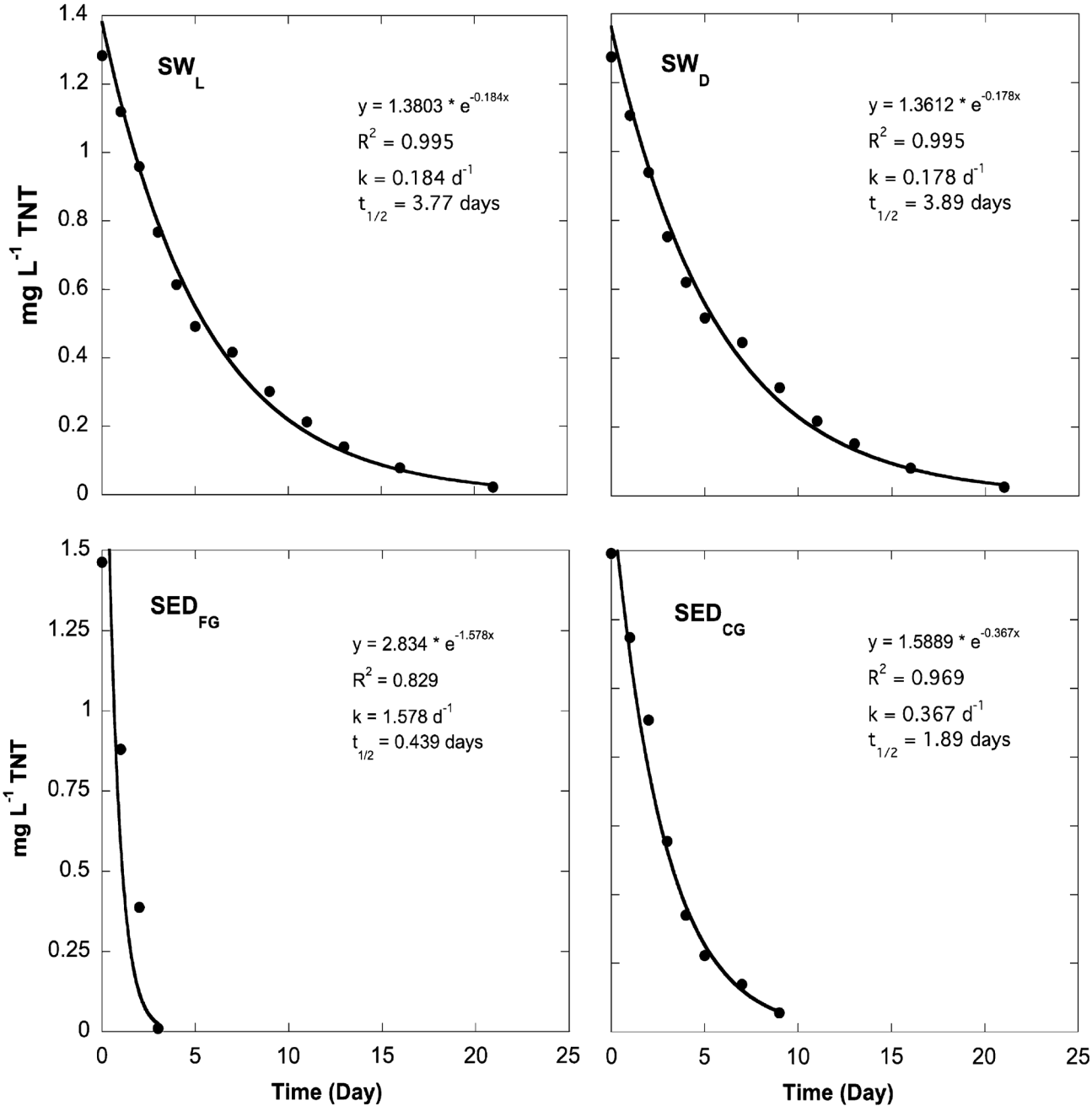

Figure 2.3. Time-series concentrations of 2,4,6-trinitrotoluene (TNT) in the four mesocosms described in the text. Mesocosms SW_L and SW_D are replicates.

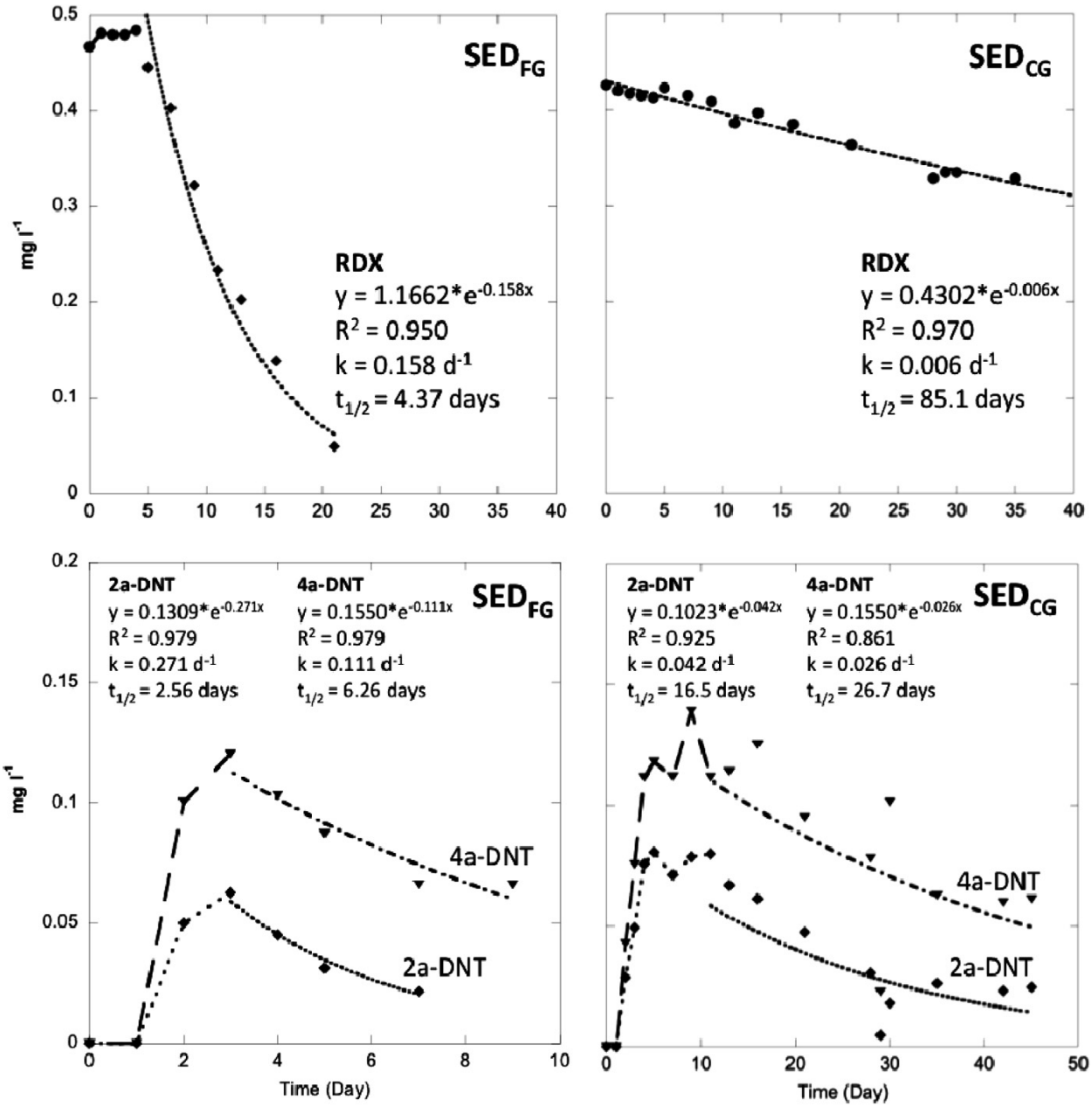

Figure 2.4. Time-series concentrations of RDX, and 2-aminodinitrotoluene (2a-DNT) and 4-aminodinitrotoluene (4a-DNT), produced from the reduction of TNT in the mesocosm experiments. These compounds did not degrade after production in the replicate mesocosms with no sediment present, and therefore only the experiments including sediment in which degradation occurred are shown. For TNT derivatives, exponential breakdown curves were started at the point in which TNT was completely removed from the system, in order to avoid bias from production.

Table 2.1. Comparison of published removal rates (k and t1/2) of TNT, RDX, 2a-DNT and 4a-DNT, with sedimentary characteristics when given. Sediment types are classified based on arbitrary %OC and %clay cutoff points in order to highlight comparable sediments among studies. - : data not measured or cannot be calculated. Groundwater and freshwater references are included for comparison with marine data.

Study	Water type/location	°C	Salinity	Sediment location	Sed type	Sediment characteristics				TNT		2a-DNT		4a-DNT		RDX	
						%OC	%Clay	pH	CEC	k	$t_{1/2}$	k	$t_{1/2}$	k	$t_{1/2}$	k	$t_{1/2}$
This study	Long Island Sound	18	31-39	Long Island Sound, CT	No sed	-	-	7.7	-	0.181	3.83	0	-	0	-	0	-
					Coarse, low OC	0.03	0.5	7.6	-	0.367	1.89	0.042	16.5	0.026	26.7	0.006	85.1
					Fine, low OC	0.38	28.5	7.8	-	1.578	0.439	0.271	2.56	0.111	6.26	0.158	4.37
Chappell et al. (2011)	Artificial (marine)	8	20	Aransas Bay, TX	Coarse, low OC	0.12	2.4	8	22	0.0096	72	-	-	-	-	-	-
		25								0.1176	5.9	-	-	-	-	-	-
		8		San Diego Bay, CA	Medium, low OC	0.84	10	8.2	53	0.1968	3.5	-	-	-	-	-	-
		25								0.6336	1.1	-	-	-	-	-	-
		8		Sequim Bay, WA	Fine, high OC	2.27	40	7.9	188	0.456	1.5	-	-	-	-	-	-
		25								0.8952	0.77	-	-	-	-	-	-
Harrison and Vane (2010)	North Sea	7	31-35	North Sea, UK	No sed	-	-	-	-	0.0004	1925	-	-	-	-	-	-
					Coarse, low OC	0.1	2	-	-	0.0023	305	-	-	-	-	-	-
					Fine, high OC	2.23	19.5	-	-	0.0054	129	-	-	-	-	-	-
Yost et al. (2007)	Artificial (marine)	24	20	Aransas Bay, TX	Coarse, low OC	0.1	11	7.8	1	0.0116	60	-	-	-	-	-	-
				San Diego Bay, CA	Coarse, low OC	0.6	12	8.6	5.3	0.02	35	0.004	1.79	0.003	263	-	-
				Sequim Bay, WA	Fine, high OC	3.6	22.5	7.6	49	0.0139	50	0.003	2.21	0.006	111	-	-
Brannon et al. (2005)	Artificial (marine)	20	20	University Lake	Medium, high OC	7.41	14	5.4	47	4.752	0.15	-	-	-	-	0.026	26.8
				Browns Lake	Medium, low OC	0.83	11	6.8	13	2.52	0.28	-	-	-	-	0.012	59.8
				Texas Lake	Fine, high OC	1.92	39	6.6	40	2.364	0.3	-	-	-	-	0.161	4.29
Brannon et al. (2005)	DI (fresh)	20	0	University Lake	Medium, high OC	7.41	14	5.4	47	2.448	0.28	-	-	-	-	0.089	7.8
				Browns Lake	Medium, low OC	0.83	11	6.8	13	5.856	0.12	-	-	-	-	0.022	32.1
				Texas Lake	Fine, high OC	1.92	39	6.6	40	3.792	0.18	-	-	-	-	0	-
Best et al. (1998)	Groundwater			No sed		-	-	-	-	0.23	3	-	-	-	-	0	-
				Wetland		-	-	-	-	0.55	1.3	-	-	-	-	0.05	13.8
				Gravel		-	-	-	-	0.57	1.2	-	-	-	-	0.01	69.3

Supplementary Material

Supplementary Table S-2.1. Water chemistry parameters for tanks spiked with TNT and RDX. The no sediment treatment represents the average of 4 tanks (2 separate recirculating reservoirs), and the fine- and coarse-grained sediment treatments each represent the average of 2 tanks (one common recirculating reservoir).

Treatment	Day	Temp. (°C)	Salinity	DO (%)	DO (mg L^{-1})	pH
$SW_L + SW_D$	0	19.0	31.2	103	7.9	7.6
(Mean)	1	18.7	31.1	99.2	7.7	7.2
	2	18.8	31.3	100	7.8	N.M.
	3	18.9	31.4	97.6	7.5	7.8
	4	18.7	31.6	109	8.4	7.9
	5	18.7	31.7	98.9	7.7	7.7
	7	18.5	31.8	105	8.1	7.8
	9	19.0	32.1	96.5	7.4	8.1
	11	19.1	N.M.	85.9	6.6	N.M.
	13	18.6	N.M.	88.9	6.9	N.M.
	16	18.8	N.M.	89.4	6.9	N.M.
	21	19.0	34.0	94.3	7.1	N.M.
	28	18.4	34.6	91.4	6.9	N.M.
SED_{FG}	0	19.0	31.0	96.5	7.4	7.5
	1	18.7	31.0	96.7	7.5	7.9
	2	18.9	31.3	91.5	7.1	N.M.
	3	19.1	31.4	48.2	3.7	6.9
	4	18.6	31.6	98.0	7.6	7.8
	5	18.7	31.8	93.8	7.2	7.6
	7	18.8	32.0	102	7.8	7.7
	9	18.9	32.4	92.1	7.1	8.1
	11	18.9	N.M.	81.0	6.3	N.M.
	13	18.3	N.M.	71.8	5.6	N.M.
	16	19.0	N.M.	83.0	6.4	N.M.
	21	19.0	34.8	94.2	7.1	N.M.
	28	17.6	36.3	40.8	3.1	N.M.
	29	17.4	36.4	32.1	2.5	N.M.
	30	17.3	36.5	28.7	2.2	N.M.
	35	17.1	N.M.	33.1	2.6	N.M.
	42	17.2	38.0	39.7	3.0	N.M.
	45	17.4	38.5	38.9	3.0	N.M.
SED_{CG}	0	18.5	30.4	98.5	7.7	7.5
	1	18.3	30.3	97.4	7.6	7.4
	2	18.4	30.6	93.1	7.3	N.M.
	3	18.7	30.7	84.5	6.6	7.3
	4	18.1	30.8	93.3	7.3	7.7
	5	18.2	31.5	91.5	7.2	7.6
	7	18.4	31.1	99.1	7.7	7.7
	9	18.4	31.5	94.3	7.3	7.9
	11	18.7	N.M.	82.9	6.4	N.M.
	13	17.9	N.M.	78.8	6.3	N.M.
	16	18.6	N.M.	84.9	6.5	N.M.
	21	18.8	33.3	93.1	7.1	N.M.
	28	18.0	34.8	76.9	5.9	N.M.
	29	17.1	34.8	74.3	5.8	N.M.
	30	16.9	34.9	63.7	5.0	N.M.
	35	16.7	N.M.	74.3	5.8	N.M.
	42	16.2	36.1	70.4	5.6	N.M.
	45	16.3	36.4	67.7	5.3	N.M.

Supplementary Table S-2.2. Concentrations of detected explosive compounds using EPA method 8330. Compound acronyms are defined in the text. N.D. = Not detected (under detection limits). n=8 (4 tanks, 2 samples from each) in the 'no sediment' treatment, and n=4 (two tanks, 2 samples from each) in the fine- and coarse-grained sediment treatments.

Treatment	Day	RDX (mg/L)	TNT (mg/L)	2a-DNT (mg/L)	4a-DNT (mg/L)
SW_L + SW_D	0	0.394 ± 0.004	1.279 ± 0.005	N.D.	N.D.
(Mean)	1	0.384 ± 0.003	1.112 ± 0.007	N.D.	N.D.
	2	0.392 ± 0.005	0.949 ± 0.007	N.D.	0.029 ± 0.002
	3	0.393 ± 0.005	0.760 ± 0.014	0.020 ± 0.001	0.062 ± 0.003
	4	0.398 ± 0.003	0.617 ± 0.002	0.033 ± 0.003	0.085 ± 0.005
	5	0.401 ± 0.001	0.504 ± 0.002	0.048 ± 0.003	0.108 ± 0.005
	7	0.399 ± 0.002	0.431 ± 0.005	0.046 ± 0.001	0.107 ± 0.005
	9	0.399 ± 0.012	0.308 ± 0.007	0.062 ± 0.001	0.135 ± 0.005
	11	0.383 ± 0.003	0.215 ± 0.001	0.076 ± 0.002	0.120 ± 0.005
	13	0.390 ± 0.004	0.146 ± 0.002	0.083 ± 0.007	0.125 ± 0.004
	16	0.388 ± 0.004	0.080 ± 0.002	0.098 ± 0.002	0.158 ± 0.004
	21	0.388 ± 0.002	0.024 ± 0.001	0.110 ± 0.003	0.150 ± 0.005
	28	0.383 ± 0.007	N.D.	0.113 ± 0.008	0.157 ± 0.005
SED_{FG}	0	0.467 ± 0.004	1.463 ± 0.008	N.D.	N.D.
	1	0.479 ± 0.002	0.880 ± 0.008	N.D.	N.D.
	2	0.477 ± 0.002	0.388 ± 0.004	0.049 ± 0.001	0.099 ± 0.002
	3	0.475± 0.004	N.D.	0.062 ± 0.002	0.118 ± 0.010
	4	0.474 ± 0.005	N.D.	0.044 ± 0.005	0.101 ± 0.002
	5	0.433 ± 0.003	N.D.	0.030 ± 0.003	0.085 ± 0.002
	7	0.388 ± 0.003	N.D.	0.021 ± 0.003	0.063 ± 0.004
	9	0.307 ± 0.011	N.D.	N.D.	0.063 ± 0.002
	11	0.220 ± 0.003	N.D.	N.D.	N.D.
	13	0.189 ± 0.002	N.D.	N.D.	N.D.
	16	0.127 ± 0.002	N.D.	N.D.	0.028 ± 0.005
	21	0.044 ± 0.004	N.D.	N.D.	0.006 ± 0.008
	28	N.D.	N.D.	N.D.	0.018 ± 0.003
	29	N.D.	N.D.	N.D.	N.D.
	30	N.D.	N.D.	N.D.	0.059 ± 0.010
	35	N.D.	N.D.	N.D.	N.D.
	42	N.D.	N.D.	N.D.	N.D.
	45	N.D.	N.D.	N.D.	N.D.
SED_{CG}	0	0.426 ± 0.002	1.393 ± 0.009	N.D.	N.D.
	1	0.420 ± 0.004	1.148 ± 0.010	N.D.	N.D.
	2	0.417 ± 0.003	0.908 ± 0.020	0.028 ± 0.003	0.042 ± 0.003
	3	0.415 ± 0.007	0.555 ± 0.008	0.049 ± 0.004	0.074 ± 0.005
	4	0.413 ± 0.005	0.340 ± 0.003	0.074 ± 0.001	0.109 ± 0.004
	5	0.423 ± 0.003	0.222 ± 0.003	0.079 ± 0.004	0.115 ± 0.002
	7	0.415 ± 0.002	0.138 ± 0.001	0.069 ± 0.003	0.108 ± 0.004
	9	0.409 ± 0.008	0.056 ± 0.005	0.076 ± 0.005	0.134 ± 0.002
	11	0.386 ± 0.007	N.D.	0.076 ± 0.001	0.106 ± 0.004
	13	0.397 ± 0.002	N.D.	0.063 ± 0.003	0.107 ± 0.007
	16	0.385 ± 0.001	N.D.	0.057 ± 0.003	0.116 ± 0.001
	21	0.364 ± 0.003	N.D.	0.043 ± 0.004	0.087 ± 0.006
	28	0.329 ± 0.007	N.D.	0.027 ± 0.003	0.069 ± 0.006
	29	0.335 ± 0.006	N.D.	0.004 ± 0.001	0.020 ± 0.004
	30	0.335 ± 0.003	N.D.	0.016 ± 0.006	0.089 ± 0.004
	35	0.329 ± 0.005	N.D.	0.023 ± 0.004	0.054 ± 0.005
	42	0.297 ± 0.006	N.D.	0.019 ± 0.001	0.050 ± 0.002
	45	0.308 ± 0.005	N.D.	0.020 ± 0.001	0.051 ± 0.002

Supplementary Table S-2.3. Linear correlation coeffecients of measured sediment properties and TNT k values in marine simulations only from Table 1. Parameters in bold have statistically significant correlations, as identified by ANOVA statistical analysis ($p < 0.005$).

Sediment Property	n	R^2
pH	12	0.903
%OC	13	0.502
Temperature	18	0.061
%Clay	13	0.028
CEC	9	0.002

3.0. Sorption Kinetics of TNT and RDX in Anaerobic Freshwater and Marine Sediments: Batch Studies

This chapter was published, as follows:

Ariyarathna, T., Vlahos, P., Tobias, C., and Smith R. 2016. Sorption kinetics of TNT and RDX in anaerobic freshwater and marine sediments: batch studies. Environmental Toxicology and Chemistry, 35: 47–55.

Abstract

Examining the partitioning of explosives onto sediment in marine environments is critical to predict the toxicological impacts of worldwide explosive-contaminated sites adjacent to estuaries, wetlands, and the coastal ocean. Marine sediments have been identified as sites of enhanced munitions removal, yet most studies addressing these interactions focus on soils and freshwater sediments. This study measures the kinetics of 2,4,6-trinitrotoluene (TNT) and hexahydo-1,3,5-trinitro-1,3,5-triazine (RDX) sorption onto two marine sediments of varying grain-sizes (silt vs. sand) and organic carbon (OC) content. Abiotic sediment sorption tests were performed at 23°C, 15°C and 4°C by spiking TNT and RDX solutions directly into anaerobic sediment slurries. Marine sediments showed significantly higher compound uptake rates (0.30 - 0.80 hr^{-1}) than freshwater silt (0.0046 – 0.0065 hr^{-1}) for both compounds likely because of lower compound solubilities and a higher pH in marine systems. Equilibrium partition constants are on the same order of magnitude for marine silt (1.1 – 2.0 Lkg^{-1}sed) and freshwater silt (1.4 – 3.1 Lkg^{-1}sed) but lower for marine sand (0.72 - 0.92 Lkg^{-1}sed). Total organic carbon content in marine sediments varied linearly with equilibrium partition constants for TNT and moderately linear for RDX. Uptake rates and equilibrium constants of explosives are inversely correlated to temperature regardless of sediment type because of kinetic barriers associated with low temperatures.

3.1. Introduction

The explosive compounds TNT and RDX are common components of military munitions worldwide (Jenkins et al., 2007; Pennington et al., 2006). Contamination of soil, surface water, groundwater, wetlands and coastal ecosystems with TNT and RDX has become a global environmental issue (Pichtel, 2012; Mittal, 2003). TNT has been identified in at least 20 of the 1,397 hazardous waste sites on the United States Environmental Protection Agency National Priorities List (USEPA-NPL; ASTDR, 1995) and RDX has been identified at 31 out of the 1,699 hazardous waste sites that have been proposed for inclusion on USEPA-NPL (ASTDR, 1995; 2012). TNT and RDX enter into the environment mainly through low order detonations, manufacturing, improper handling and disposal of unexploded ordnances (Kalderis et al., 2011). These sources lead to levels of contamination that can be toxic to ecological receptors at impacted sites and nearby areas subjected to offsite migration of TNT and RDX (Kalderis et al.,

2011). RDX concentrations of sediment samples from army depots and composts prepared from contaminated sediments have been identified ranging from <0.1 to 3,574 mg/kg and >2.9–896 mg/kg, respectively. Groundwater contamination levels of RDX in munition plants in the United States (<1– 14,100 μg/L) and Germany (21–3,800 μg/L) have been documented (ASTDR, 2012). These concentrations are above accepted drinking water values for both TNT and RDX (2 μg/L) established by United States environmental protection agency (US EPA, 2014a; 2014b). TNT has been linked to liver damage and anemia in humans and both TNT and RDX are classified as possible human carcinogens (Group C) by USEPA (US EPA, 2014a; 2014b) and under Group 3 in IARC carcinogenic categorization (IARC, 1996).

The fate of contaminants in the environment is determined by physico-chemical properties of the compounds and environmental conditions (Kalderis et al., 2011). Sorption to sediments and particles in aquatic systems can significantly attenuate freely dissolved concentrations and alter bioavailability in both sediments and overlying water. Existing studies of TNT and RDX sorption are primarily focused on terrestrial soils and freshwater sediments where equilibrium partition coefficients for TNT are an order of magnitude higher than RDX (Yamamoto et al., 2004; Sheremata et al., 2001; Chappell et al., 2011; Ainsworth et al., 1993; Brannon et al., 1992). Similar studies in marine systems are comparatively less available (Chappell et al., 2011; Harrison and Vane, 2010) and no marine studies are available on RDX although it is believed to be more persistent in the environment compared to TNT (Spalding and Fulton, 1988). TNT and RDX can be sorbed onto minerals, amorphous grain coatings of metal oxide, humic materials, and organic/inorganic colloids present in sediment (Juhasz and Naidu, 2007). The rate and extent of sorption can be influenced by the hydrophobicity of compounds, temperature, ionic strength of the water, surface area and nature of the sorbent and energy input. For example, the salting-out effect in saline systems, decreases the solubility of explosives and increases the fugacity in water (Brannon, 2002; Lynch et al., 2002; Zhao et al., 2003).

Geochemical differences in sediments are critical variables in adsorption of explosive compounds onto sediment. Grain size, clay content and type, and quantity of organic carbon (Yamamoto et al., 2004; Harrison and Vane, 2010) affect equilibrium partition constants of TNT and RDX. Seasonal temperature changes in the environment may cause differences in sorption and release of TNT and RDX into the aqueous phase and transport processes. For example, organic contaminants such as atrazine, simazine, naphthalene have shown a 50% decrease in equilibrium partition coefficients by increasing temperatures from 0 to 50 °C (Site, 2001). Characterizing the temperature dependence on sorption kinetics of these explosives is valuable for environmental process descriptors that have not been studied extensively and for which available data is inconsistent (Chappell et al., 2011; Ainsworth et al., 1993). Marine systems are significantly different from freshwater environments in terms of pH, ionic strength and sulfate concentration which can result in different sorption kinetics for these compounds. Although anion exchange is not likely a dominant mechanism in sorption, principal component analysis done by Chappell et al., 2011 supports that higher elemental sulfur content in the sediment correlates with higher sorption rates for some sediments (Chappell et al., 2011). A comparative study of sorption kinetics of munitions in fresh and marine environments has yet to be done in order to reveal the importance of sorption as a sink for explosives from the aqueous environment. Herein, sorption kinetics of TNT and RDX and the formation of degradation products are evaluated for two sediment types (fine and coarse grained) in freshwater and marine systems in order to compare differences in kinetics and the potential for long term preservation of these

compounds. The objective of this study is to fill the data gap in the literature on sorption characteristics of TNT and RDX including the determination of uptake and equilibrium partition coefficients, examination of abiotic compound breakdown using a mass balance approach, and an evaluation of sorption kinetics.

3.2. Materials and Methods

3.2.1 Experimental Approach

In order to examine sorption kinetics of TNT and RDX, we conducted a series of abiotic slurry experiments using a single freshwater and two marine sediment types. Fine-grained freshwater sediment samples were collected from a pond in eastern Connecticut (41°19′13.93″N / 72°04′01.80″W). Fine grained (silt), and coarse grained (sand) marine sediments were collected from 41°18′03.42″N / 72°07′14.09″W and 41°19′04.50″N / 72°04′00.52″W in the intertidal zones of Waterford and Groton, Connecticut, USA respectively. Freshwater and sea water were also collected from the same sampling locations of sediments respectively. All experiments were performed at three temperatures for the purpose of yielding sorption kinetics. The data were used to calculate sorption rates and sediment-water equilibrium partition coefficients for TNT and RDX.

3.2.2 Sediment Characterization

All sediments were characterized for total organic carbon (TOC), total nitrogen (TN) and sulfur (S) using a Perkin Elmer elemental analyzer (NA 1500). Sediment texture was determined using a mechanical sieve analyzer with a set of sieves from 0.063 mm to 2.0 mm. Clay compositions in the sediment were determined by X-ray diffractometer (XRD) (Rigaku Ultima IV / Cu Kα (λ = 0.15406 nm) radiation; beam voltage 40 kV; beam current 44 mA). Redox potential of sediment systems were measured using platinum electrode (Paleo Terra, Amsterdam) relative to Ag/AgCl reference electrode (Fisher Scientific) over the course of the experiment.

3.2.3 Incubation Experiments

Two types of marine sediments were each mixed with filtered (polyethersulfone- 0.2µm) sea water (30 ‰) at a mass ratio of 1:4 (Pennington et al., 1995) with 100g of sediment, in 500mL glass bottles. Freshwater sediment slurries were prepared the same way using filtered (polyethersulfone- 0.2µm) freshwater. Biological activity in sediment slurries was inhibited by adding mercuric chloride and bottles were covered with aluminum foil to inhibit photo-degradation. Sediment slurries were mixed with continuous stirring on magnetic stirrer plates in temperature controlled chambers of 4^0C, 15^0C and 23^0C over the course of the experiment and selected as representative seasonal environmental temperature ranges.

Target compounds in this study, TNT and RDX (>99 purity) were purchased from Naval Munitions Command, China Lake, CA, USA. Sediment slurries were allowed to equilibrate for 24 hr prior to spiking. After 24 hr, slurries were spiked with target compounds dissolved in (1 ml) acetonitrile to achieve concentrations of 4 mgL^{-1} and 2.5 mgL^{-1} for TNT and RDX respectively. The acetonitrile slug was less than 0.25 % of the total volume such that the final concentration was 0.04 M acetonitrile and substantially diluted to avoid any co-solvent

interferences. These target concentrations of TNT and RDX adequately represent the underwater point source concentrations from military related activities and disposal of unexploded ordnance before substantial dilution in the environment (Craig and Taylor, 2011). All treatments were done in duplicate and included two controls; sediment slurries with no compound introduction and a compound-spiked control with no sediment in order to correct for matrix effects and any compound loss in the absence of sediment.

Samples to quantify aqueous munitions concentrations were collected at preset intervals (7 total) over the 2 week duration of the experiment. The 1 mL samples were filtered through 0.2µm polyethersulfone filters and mixed with 1 mL of acetonitrile. A modified salting out method (Miyares, 1990) was adapted for smaller sample sizes wherein 0.65 g of sodium chloride was added to each sample, sonicated 15 minutes and vortexed for 5 minutes to extract the munition compounds from sediment slurries. The extraction was repeated twice and extracts were combined. An average recovery of 99.1 ± 0.5% was obtained for known amounts of 1, 2-dinitrobenzene (1,2-DNB) in water extractions. Sediment bound munitions were measured at the end of the experiment. Sediment samples were extracted (adapted from US EPA 8330) (US EPA, 1994) using 10 mL of acetonitrile and 2 g of freeze dried sediments. After one hour of sonication and 5 minutes of vortexing, samples were centrifuged for 10 minutes to separate the supernatant from the sediment. Filtrate was blown to dryness with N_2 followed by an addition of 2 mL of acetonitrile. Average recoveries of munitions from sediment samples were 82 ± 7 % based 1,2-DNB added to the replicate sediment samples. Both water and sediment extractions were analyzed using gas chromatography (GC)/electron-capture detection (ECD) following the methods described by (Pan et al., 2005; US EPA, 2007; Zhang et al., 2007; Zhang et al., 2005)**.** 3, 4-dinitrotoluene was added to each extract prior to injection to monitor detection efficiency. Explosive analysis was performed with an Agilent GC/ECD (Pan et al., 2005) equipped with an HP-DB5 column (30 m x 320 µm, 0.25-µm; Agilent). 1 µl of sample was injected onto a splitless liner in pulsed injection mode. Helium was used as a carrier gas at a flow rate of 11.9 mL min^{-1}. The oven temperature was maintained at 90 ^{0}C with two ramps: ramp 1 was 10.9 min to 200^{0}C and held for 1.5 min, and ramp 2 was 14.2 min to 250 ^{0}C held for 1.9 min. Quantification was based on an external calibration curve of available standard munitions TNT, 2-amino-4,6-dinitrotoluene (2-ADNT), 4-amino-2,6-dinitrotoluene (4-ADNT), RDX, Hexahyro-1-nitroso-3,5-dinitro-1,3,5-triazine (MNX), Hexahyro-1,3-dinitroso-5-nitro-1,3,5-triazine (DNX), and Hexahyro-1,3,5-trinitroso-1,3,5-nitro-1,3,5-triazine (TNX) (AccuStandard, New Haven, CT). The average reporting limit for all compounds was 7.8 ng mL^{-1} (See Table S3 for compound specific reporting limits). Sample chromatograms of GC/ECD for parent compounds and derivatives are shown in Figure S-3.1.

3.3. Data analysis

3.3.1. Sorption Uptake Model

The measured time series concentrations of TNT and RDX in water [C_i], for each sediment type were used to calculate sorption rate constants according to equation 1,

$$\ln [C_i] = -kt + \ln [C_i]_{t=0} \quad (1)$$

where t is time (hr) and k is the first order sorption rate constant in hr^{-1}.

3.3.2. Equilibrium Partitioning Model and Sorption Energetics

Equilibrium partition constants, (Kd) of target compounds were calculated using measured concentrations of compounds in sediment (C_{is}) and in water (C_{iw}) when equilibrium was reached at the end of the experiment as follows:

$$K_d = (C_{is}) / (C_{iw}) \quad (2)$$

Aqueous concentrations were further analyzed for partitioning of TNT and RDX onto dissolved colloidal organic matter using the following equation.

$$C_{iw} = C_{iaq} + C_{iaq} [K_{oc}.DOC] \quad (3)$$

where C_{iw} is the total compound concentration in water, C_{iaq} is the truly dissolved aqueous compound concentration, K_{oc} is the experimental partition coefficient to organic carbon calculated using K_d and the organic carbon fraction of sediment (f_{OC}) and DOC is the dissolved organic carbon concentration in water. The second term on the right hand side of equation 3 is the functionally soluble portion of the total dissolve concentration that is associated with DOC. f_{OC} is determined using acid fumigation and EA analysis after of Hedges and Stern (1984) while DOC in the aqueous phase was analyzed using 40 mL samples acidified to a pH value of 2 followed by TOC analysis on a Shimadzu TNM-1. Experimental values of K_{oc} for TNT and RDX were calculated using modeled K_{oc} and organic carbon fraction of sediment ($K_d = K_{oc}/f_{OC}$) and compared to those derived from Di Toro's equation (Di Toro, 1985),

$$\log K_{oc} = 0.00028 + (0.983 + \log K_{ow}) \quad (4)$$

where K_{ow} is Octanol–Water partition coefficient for the compounds. The Di Toro's relationship was used because it has been shown to be consistent with observations of a large set of absorption-desorption data of non-ionizing hydrophobic organic compounds.

3.3.3. Mass Balancing Model

At the end of the experiment, the total amount of target compounds and their identifiable degradation products in both water and sediment phases were quantified to obtain a mass balance for each system and identify losses that were not accounted for wherein,

$$M_{TNT\ spiked} = M_{TNT,dissolved} + M_{TNT,particles} + M_{2A\text{-}DNT,dissolved} + M_{4A\text{-}DNT,particles} + M_{2A\text{-}DNT,dissolved} + M_{4A\text{-}DNT,particles} + \text{unknown} \quad (5)$$

$$M_{RDXspiked} = M_{RDX,dissolved} + M_{RDX,particles} + M_{MNX,dissolved} + M_{MNX,,particles} + M_{DNX,dissolved} + M_{DNX,particles} + M_{TNX,dissolved} + M_{TNX,particles} + \text{unknown} \quad (6)$$

In above equations, $M_{X,\ spiked}$, $M_{X,\ dissolved}$ and $M_{X,\ particles}$ represent the mass of compound X

spiked to the system, mass of compound X in the aqueous phase at equilibrium (truly dissolved and sorbed to DOC) and the mass of compound X partitioned onto sediment at equilibrium, respectively.

3.4. Results

3.4.1 Sediment Characterization

Sediments used in incubation experiments were chemically and texturally different to each other as shown in Table 3.1. Sediments were classified as freshwater silt, marine silt and marine sand based on grain size. Grain size increased in the order of marine silt, freshwater silt and marine sand considering their graphic mean ($0.16 < 0.37 < 0.41$ mm) and median ($0.11 < 0.31 < 0.36$ mm). Fine-grained freshwater sediment was rich in organic carbon (9.32 mg g^{-1}sed) and considerably poor in elemental sulfur (0.40 mg g^{-1}sed) compared to both marine sediments. Fine-grained marine silt had a higher organic carbon (4.10 mg g^{-1}sed) and elemental sulfur level (3.70 mg g^{-1}sed) than medium to coarse-grained marine sand (organic carbon and sulfur contents of 0.038 mg g^{-1}sed and 1.00 mg g^{-1}sed respectively). Marine sand had negligible clay content (0.8 %) whereas marine silty sediment and freshwater sediment contain 56% and 34% of silt and clay contents respectively. XRD spectrums showed that both marine silt and freshwater silt have smectite group clays and feldspar (Menking et al., 1993; Figure S-3.2).

3.4.2 Behavior of Explosives in Freshwater Systems

Both TNT and RDX were rapidly removed from the aqueous phase in freshwater slurries at all three temperatures, followed by a slow removal that approached equilibrium (Figure 1, Figure S-3). Table 3.2 summarizes the kinetic parameters of uptake of the target explosives (TNT and RDX) onto freshwater sediment at the three temperatures. Uptake rate constants of both TNT and RDX increase with decreasing temperature for freshwater sediments. In this study, uptake rate constants ranged between 0.0046 - 0.0065 hr^{-1} and 0.0048 - 0.0060 hr^{-1} for TNT and RDX respectively in anaerobic freshwater sediment slurries at three different temperatures. Corresponding half-lives of TNT and RDX (110 – 150 hr) consistently increase with increasing temperature.

Equilibrium partition constants (K_d) measure the distribution of explosives in water and sediment phases at equilibrium. Values of K_d of both TNT and RDX for freshwater silt range in 1.4 - 3.1 Lkg^{-1}sed (Table 3.2) and decrease with increasing temperatures (Figure 3.2). The amount of TNT and RDX partitioned onto dissolved organic matter in the freshwater sediment slurry represented 0.5 and 0.4 % of the total aqueous phase concentrations for both compounds. Mass balances of TNT in the freshwater systems showed that 55% of the TNT was in the dissolved phase while 38% was in the particle phase at these mixing ratios and that the balance was reasonably closed with only 2-7% unknowns. 34 – 35% of the spiked RDX was unidentifiable after the 14 day period and 29% and 11% remained in water and sediment phases respectively without degradation (Table 3.3). 25% of spiked RDX was accounted for as the derivatives MNX, DNX, and TNX in freshwater systems at all three temperatures (Table S-3.2).

3.4.3 Behavior of Explosives in Marine Systems

Similar to the freshwater silt incubations, both compounds were rapidly removed from the slurry water in marine sand and silt as shown in Figure 3.1 and Figure S-3.3. Uptake rate constants in marine sediments (Table 3.2) were ~100 times higher than those in freshwater silt. Observed sorption rates were in the ranges of 0.48 - 0.80 hr^{-1} and 0.30 - 0.36hr^{-1} for TNT and RDX respectively. Marine silt had slightly higher uptake rate constants for TNT (0.53 - 0.80 hr^{-1}) and RDX (0.31 - 0.36 hr^{-1}) than marine sand (0.48 - 0.62 hr^{-1} and 0.30 - 0.34 hr^{-1}) respectively at all temperatures at 95% confidence ($p \leq 0.05$) based on a paired T test. Uptake rate constants of TNT for both marine silt (0.53 hr^{-1}) and sand (0.48 hr^{-1}) at 23^0C are lower than those at 4^0C (0.64 hr^{-1} and 0.58 hr^{-1} respectively). RDX in marine silt showed a consistent decrease in uptake rates from 0.36 hr^{-1} to 0.31 hr^{-1} with increasing temperature from 4 ^{0}C to 23 ^{0}C.

K_d values for marine sediments in this study (Table 2) decrease with increasing temperature (Figure 3.2). Equilibrium partitioning of TNT (0.82 – 2.0 Lkg^{-1}sed) onto marine sediments is higher than that of RDX (0.72 - 1.3 Lkg^{-1}sed) in anaerobic sediment slurries. K_d values of explosives were on the same order of magnitude for both freshwater silt (1.4 - 3.1 Lkg^{-1}sed) and marine silt (1.1 – 2.0 Lkg^{-1}sed), although marine silt exhibits rapid sorption with uptake rates which are 100 times greater than freshwater silt. Marine sand has lower K_d values (0.72 - 0.92 Lkg^{-1}sed) than marine silt (1.1 – 2.0 Lkg^{-1}sed) and freshwater silt (1.4 - 3.1 Lkg^{-1}sed) for both compounds at all treatments except one K_d value observed for TNT at 4^0C (1.3 Lkg^{-1}sed). Partitioning of TNT and RDX onto dissolved organic matter in marine silt slurry water is 0.25 and 0.19 % of the aqueous phase concentrations for both compounds. Similarly, for marine sand, TNT and RDX partitioned onto dissolved organic matter represented 0.17 and 0.13 % of the total aqueous phase concentrations for both compounds.

After 14 days, 22 - 43% of TNT remained in the systems (Table 3.3). Approximately 3% of the spiked TNT abiotically degraded into identifiable compounds forming mostly 4-aminodinitrotoluene, leaving a considerable portion (64%) of unknowns at all three temperatures in both marine systems. Nearly 58% of the spiked RDX remained unchanged in the marine systems while 24% was abiotically transformed to identifiable compounds in 14 days (Table 3.3, Table S-3.2). The unaccounted portion of RDX (18%) is comparatively less than for TNT in all the marine treatments. These results differ from the freshwater systems.

3.5. Discussion

Removal of dissolved TNT and RDX at a rapid rate in our incubations regardless of the sediment type indicates the importance of uptake of energetic compounds onto sediments. Redox potentials of the sediment systems were in the range of 100 - 150 mV maintaining anaerobic conditions (Delaune, 2005) throughout the experiment. Both compound removals were consistent with first order kinetics and attained equilibrium with sediment in all treatments of marine systems within two hours after spiking, which was consistent with previous studies (Chappell et al., 2011; Zhao et al., 2003), as opposed to 96 - 240 hr in freshwater incubations. The uptake rate constants onto marine sediments were nearly 100 times higher than for freshwater sediment in this study. The lower solubility of compounds in seawater (salinity of 30‰ in these experiments) may drive rapid uptake onto marine sediments through hydrophobic

bonding, chemisorption and electrostatic interactions as they are polarizable organic compounds (Site, 2001). Hydrophobic sorption should have an important role for these compounds since they exhibit some hydrophobicity. This is also true for several of the degradation products such as triaminotoluene, (an anaerobic degradation product of TNT) that is also known to partition to sediments (Hammett, 1937). Electrostatic interactions may also occur between variable charged surfaces, such as soil organic matter, mineral oxides and on the edge sites of layered silicate minerals (feldspar and smectite group clays) and these explosive compounds. The charges on these surfaces arise most commonly through protonation and deprotonation reactions, and are highly pH dependent (Weber et al., 1983). Freshwater systems have lower pH values (7.0) than marine systems (7.9) and more protonation may lead to competition between studied munition compounds (TNT, RDX) and H^+ which can be reversibly sorbed on to the sites of exchangeable cations and OH^- of clay surfaces in sediment (Site, 2001). Marine sediments with higher pH values may experience less site-specific competition and higher uptake of TNT and RDX (0.30 - 0.80 hr^{-1}) than that in freshwater sediments (0.0046 - 0.0065 hr^{-1}).

As for many other organic compounds, sorption is also influenced by the organic matter and clay content in the sediment, as has been observed for both marine and freshwater sediments (Pichtel, 2012; Yamamoto et al., 2004; Chappell et al., 2011; Site, 2001; Weissmahr and Sedlak, 2000). Considering the mineralogy of the sediments used in this study, marine sand contained a negligible amount of clay compared to both marine and freshwater silts. Finer-grains, higher clay content, high TOC and TN levels in marine silt compared to marine sand may facilitate sorption resulting in higher uptake rates and K_d values. Although higher clay contents may increase sorption of compounds, presence of similar clay types in both silts suggests that clay mineralogy has a secondary role on sorption of munitions onto silts. However, it appears that the difference in K_d values for all slurries is sufficiently described linearly by the TOC content of the sediment for TNT (Figure 3.3A).The linearity of TOC content in sediment and K_d of TNT (R^2=0.99) was further confirmed from the Pearson correlation coefficient (PCC) values which are in the range of 0.95-0.98. For RDX, K_d and TOC content in sediment show a moderate-linear relationship (R^2 = 0.94-0.98, PCC = 0.51-0.85) that suggests RDX sorption may undergo secondary sorption that may be significant at low TOC concentrations (Figure 3.3B). Although the uptake rates are much higher in marine sediments (0.30 - 0.80 hr^{-1}) relative to freshwater silt (0.0046 - 0.0065 hr^{-1}), equilibrium partition constants are on the same order of magnitude for both freshwater silt (1.4 – 3.1 L kg^{-1} sed) and marine silt (1.1 – 2.0 L kg^{-1} sed). Equilibrium partition constants for both freshwater and marine systems are consistent with reported literature values (US EPA, 2014a; Yamamoto et al., 2004; Sheremata et al., 2001; US EPA, 1994; US EPA, 2007). Marine sand has the lowest equilibrium partition constants in the range of 0.72 - 0.92 L kg^{-1} sed. These results suggest fast sorption of TNT and RDX through electrostatic forces to marine sand (that may be reversible) followed by small fraction of less reversible organic carbon sorption. Both marine silt and freshwater silt partitioning may be dominated by relatively high hydrophobic sorption of compounds, as both sediments contain considerable amounts of organic carbon (Table 3.1) and negative free energies of sorption (Table 3.2). Strong linear correlations between organic carbon and equilibrium partition constants of TNT (Figure 3.3A) further confirmed the importance of hydrophobic sorption of TNT onto the sediments. Partitioning of TNT and RDX onto DOC was not significant in the slurries studied. Percentages of total aqueous munitions sorbed onto DOC are on the order of 0.13 to 0.49% among all sediment types. This is due to the dilution of the sediments into seawater and it is expected that porewaters of intact sediments would have DOC

concentrations that are at least 10 times higher (Moore, 2003) and therefore the fraction of munitions on DOC in intact sediment porewaters would be on the order of 1 to 5 %. The experimental partition coefficients derived in these experiments (K_{oc}) for TNT (320±57 L/kg) and RDX (260±25 L/kg) are on the same order of magnitude as values reported in the literature (US EPA, 2014a; 2014b; Rosenblatt et al., 1991; Spanggord et al., 1980). Predicted K_{oc} values using equation 4 from Di Toro (1985) for TNT were higher (920 L/kg) than those obtained experimentally for TNT and significantly lower for RDX (71 L/kg). Differences between predicted values based on hydrophobic parameters and those obtained experimentally may help identify secondary sorption processes that are important. Quantitative structure-activity relationships (QSAR's) based on Hammett substituent constants were consistent with derived K_{oc} values and reaction constants of 0.22 and 0.80 for TNT and RDX respectively (Hammett, 1937). It is possible that the experimental K_d values for RDX contain both hydrophobic partitioning as would be predicted in the 71 L/kg and secondary sorption mechanism that accounts for the additional sorption. Further research is required to address these differences.

Higher sorption rates of TNT (0.48 - 0.80 hr^{-1}) were observed than for RDX (0.30 - 0.35 hr^{-1}) on both marine sediments. These results are consistent with published data that includes sorption rates for TNT and RDX of 0.1-0.2 and 0.0005-0.0067 hr^{-1} respectively (Brannon et al., 2005). A higher octanol-water partition constant (K_{ow}) of TNT supports hydrophobic sorption of TNT onto the organic matter in the sediment (Haderlein et al., 1996). K_d of TNT and RDX clearly decrease as temperature increases for both freshwater and marine sediments (Figure 3.2) and the same trend is observed for uptake rate constant except the 15^0C treatment of marine sediments which has the least precision in data. Low temperatures are kinetically unfavorable for dissolution (Brannon, 2002; Lynch et al., 2002) resulting in more sorption onto sediments (Figure 3.2). Negative Gibb's free energies of sorption indicate that sorption of TNT and RDX onto freshwater and marine silt is spontaneous whereas it is non-spontaneous for all the marine sand treatments except at 4°C for TNT. It further reveals that marine sand cannot act as a sink for these compounds as it does for both marine and freshwater silts. Spontaneity of the sorption reaction increases with decreasing temperature for both marine silt and freshwater silt (Table 3.2). Marine systems show faster abiotic degradation than freshwater systems for TNT as alkaline hydrolysis of TNT is facilitated by higher alkalinity in marine systems (Pichtel, 2012). For TNT, the transformation product triaminotoluene, which is not identified in this study, may be covalently bound onto the sediment (Hawari et al., 2000) and comprise a significant portion of unknowns of the TNT pool. Gregory et al., (2004) has identified ring-cleaved intermediate transformation products of RDX including NH_4^+, N_2O and formaldehyde end products as a result of sequential reduction of RDX. In our study, we did not analyzed ring-cleaved intermediate transformation products of RDX that could be key components to close the mass balance.

Comprehensive analysis of available data in the literature to date (Yamamoto et al., 2004; Sheremata et al., 2001; Chappell et al., 2011; Ainsworth et al., 1993; Brannon et al., 1992; Brannon et al., 2005; Dontsova et al., 2006; Xue et al., 1995; Sharma et al., 2013; Pennington and Patrick, 1990) shows agreement with our K_d values for TNT in all published data. Organic carbon is a reliable predictor for K_d of both compounds and equilibrium partition constant values are in reasonable agreement between freshwater and marine systems (Figure 3.4). There is not enough uptake data at high salinities (this is the only study for RDX) to complete a comprehensive comparison. However, among the three abiotic studies in Table S-3.1, there was an exponential increase in uptake rates with salinity. A modest to negligible increase occurs

between sorption rates from salinities between 0 and 20‰, however, between 20 and 30 ‰, the increase appears to be very significant (>50x). There does not appear to be a relationship between uptake rate and percent organic carbon in this study though the only three sediment types were tested. This study provides the lower rate limit of transport and fate of these environmentally significant compounds. These constraints permit more robust modeling of total compound fate (biotic and abiotic) in marine settings.

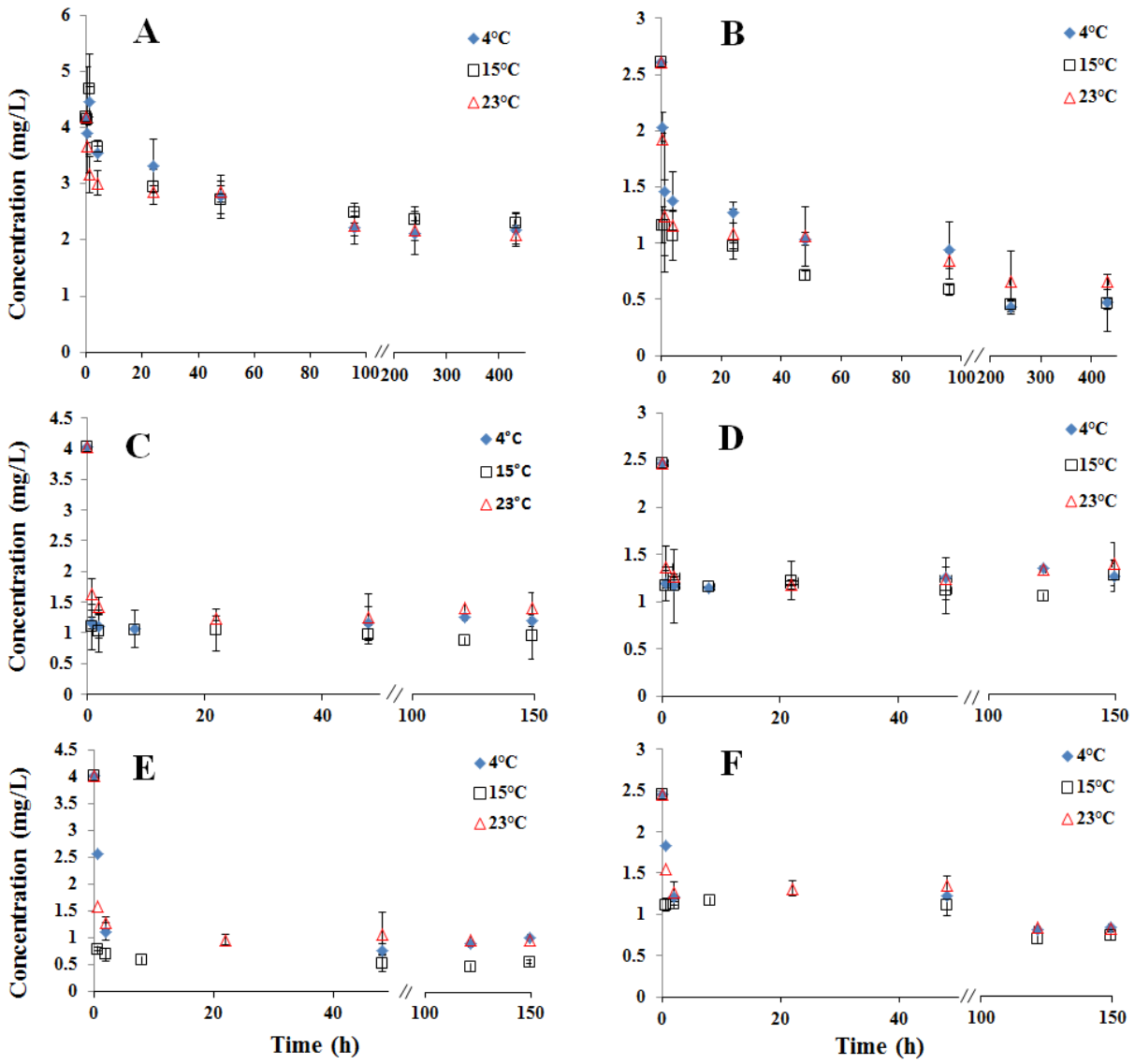

Figure 3.1. Time series aqueous concentrations of (A) 2,4,6-trinitrotoluene (TNT) in the freshwater silt system, (B) hexahydro-1,3,5-trinitro-1,3,5-triazine (RDX) in the freshwater silt system, (C) TNT in the marine sand system, (D) RDX in the marine sand system, (E) TNT in the marine silt system, and (F) RDX in the marine silt system at 3 different temperatures: 4 °C, 15 °C, and 23 °C. Error bars represent standard deviations of measurements.

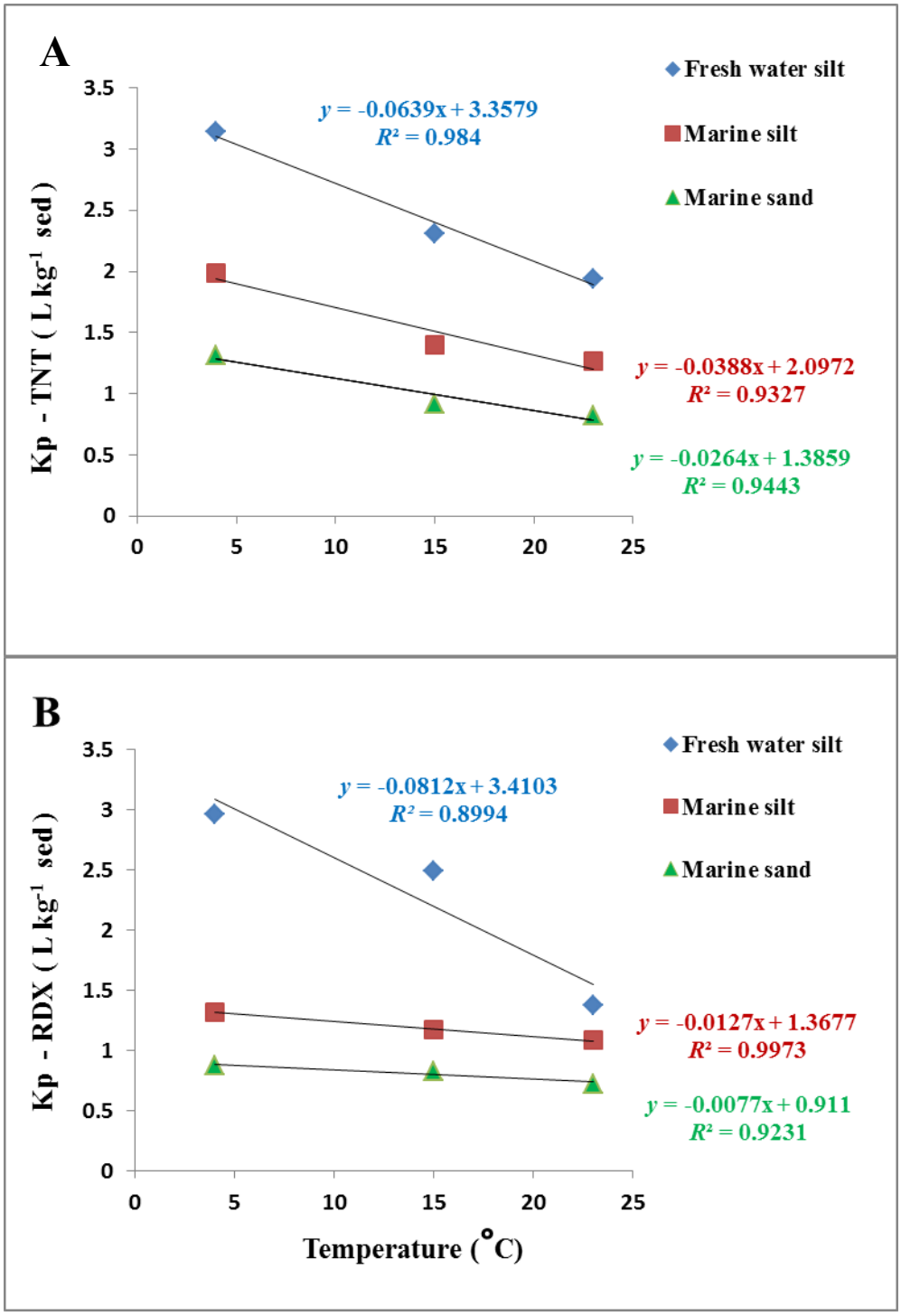

Figure 3.2. Correlation between temperature and equilibrium partition coefficient (Kp) of (A) 2,4,6-trinitrotoluene (TNT) and (B) hexahydro-1,3,5-trinitro-1,3,5-triazine (RDX) for freshwater silt, marine silt, and marine sand.

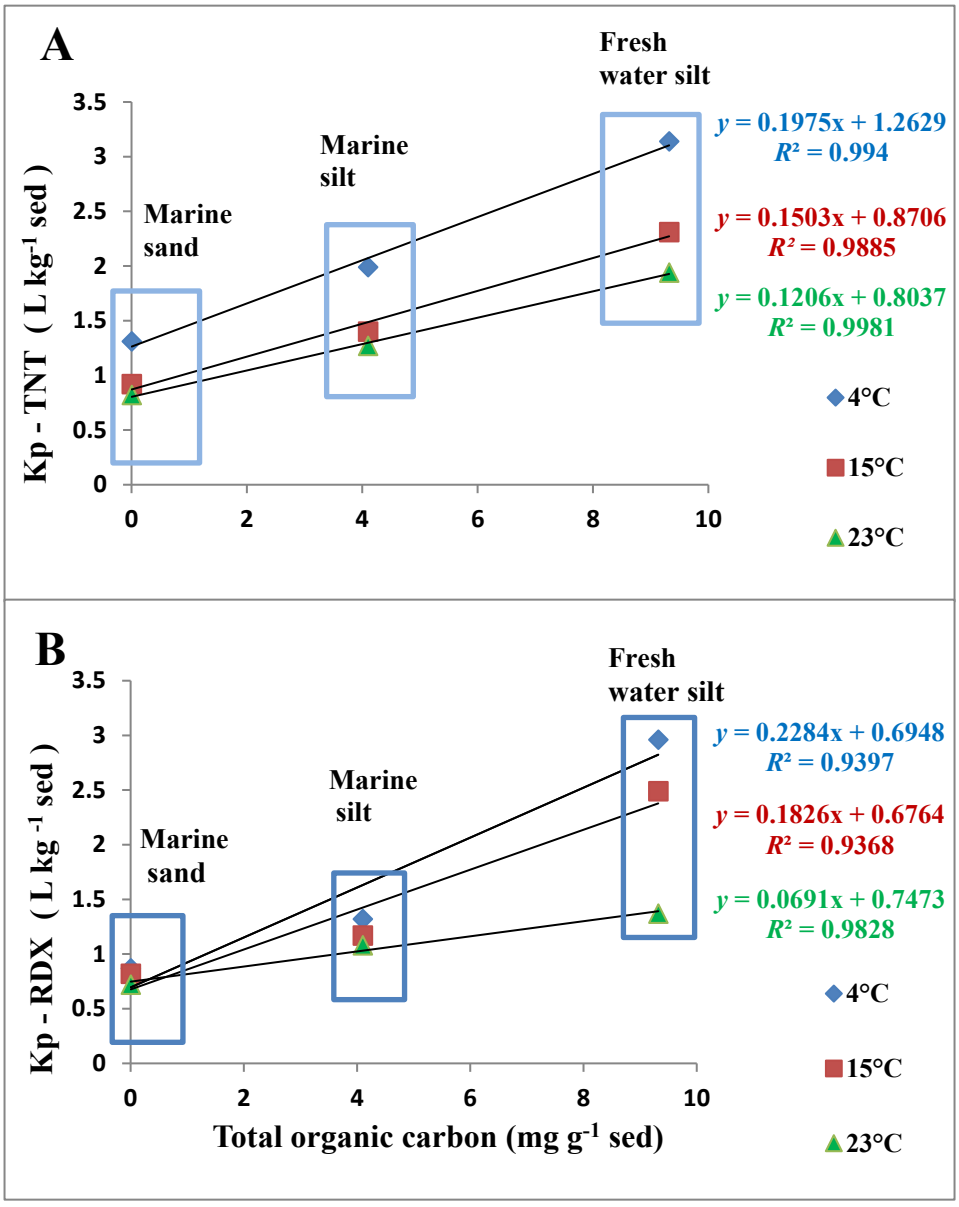

Figure 3.3. Correlation between total organic carbon of sediment and equilibrium partition coefficient (Kp) of (A) 2,4,6-trinitrotoluene (TNT) and (B) hexahydro-1,3,5-trinitro-1,3,5-triazine (RDX) at three temperatures.

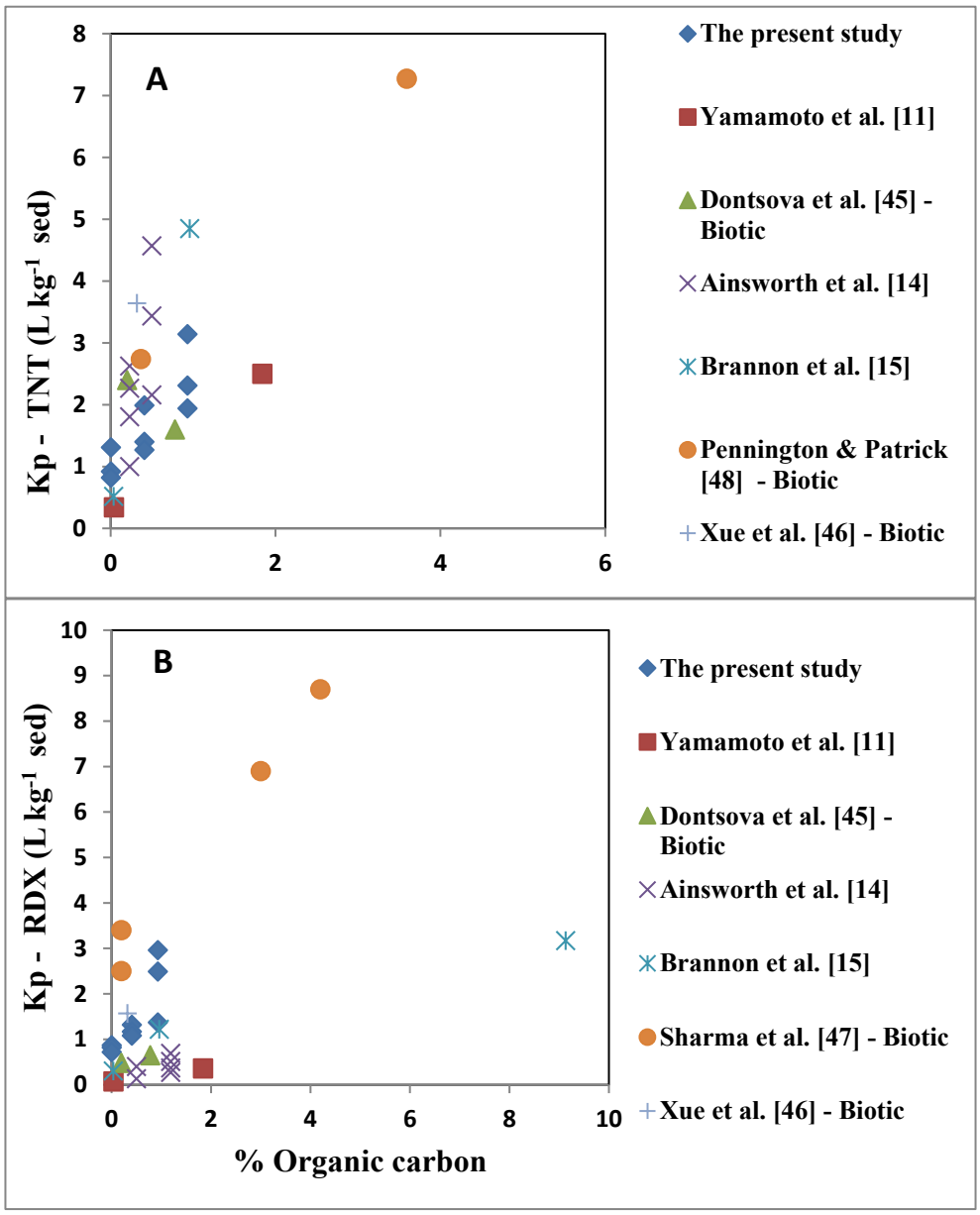

Figure 3.4. Relationship between percent organic carbon and equilibrium partition coefficient (Kp) of (A) 2,4,6-trinitrotoluene (TNT) and (B) hexahydro-1,3,5-trinitro-1,3,5-triazine (RDX) for sediments in freshwater and marine systems under different conditions published in the literature, including the present study.

Table 3.1. Chemical and textural properties of sediments and slurry-water used in this study (n=2).

	Property	Freshwater silt	Marine silt	Marine sand
Particle size	Sand (%)	66	44	99.2
distribution	Silt & clay (%)	34	56	0.8
data	Statistical parameters			
	1.Graphic mean (mm)	0.37	0.16	0.41
	2.Median (mm)	0.31	0.11	0.36
	3.IGSD (mm)	0.63	0.16	0.25
Physical	Bulk density(gcm^{-3})	1.3	1.4	1.7
properties	Porosity (%)	48.3	45.6	31.0
	pH	7.0	7.9	7.9
	Salinity (‰)	0.1	30.0	30.0
Chemical	DOC (µM)	1350±11	550 ± 27	250±14
properties	TOC ($mgg^{-1}sed$)	9.320 ± 0.070	4.101 ± 0.694	0.038 ± 0.007
	TN ($mgg^{-1}sed$)	0.559 ± 0.001	0.615 ± 0.252	0.060 ± 0.002
	S ($mgg^{-1}sed$)	0.4 ± 0.1	3.7 ± 0.3	1.0 ± 0.5

IGSD = Inclusive Graphic Standard Deviation; DOC = Dissolved Organic carbon; TOC = Total Organic Carbon; TN = Total Nitrogen; S = Elemental Sulfur

Table 3.2. Sorption kinetic parameters of explosives onto marine and freshwater sediments at three different temperatures.

Temp.	Sediment	TNT				RDX			
(^{0}C)	Type	k (hr^{-1})	$T_{1/2}$ (hr)	K_p (Lkg^{-1} sed)	ΔG ($kJmol^{-1}$)	k (hr^{-1})	$T_{1/2}$ (hr)	K_p (Lkg^{-1} sed)	ΔG ($kJmol^{-1}$)
4	Freshwater	0.0065 (R^2= 0.92)	110	3.1	-2.6	0.0060 (R^2= 0.83)	120	3.0	-2.5
	Marine Silt	0.64 (R^2= 0.99)	1.1	2.0	-1.6	0.36 (R^2=0.99)	2.0	1.3	-0.65
	Marine Sand	0.58 (R^2= 0.64)	1.2	1.3	-0.63	0.33 (R^2=0.64)	2.2	0.87	0.33
15	Freshwater	0.0053 (R^2= 0.81)	130	2.3	-2.0	0.0052 (R^2= 0.69)	130	2.5	-2.0
	Marine Silt	0.80 (R^2= 0.68)	0.9	1.4	-0.80	0.35 (R^2=0.60)	2.0	1.2	-0.37
	Marine Sand	0.62 (R^2= 0.66)	1.1	0.92	0.20	0.34 (R^2=0.62)	2.1	0.82	0.48
23	Freshwater	0.0046 (R^2= 0.71)	150	1.9	-1.6	0.0048 (R^2= 0.79)	140	1.4	-0.78
	Marine Silt	0.53 (R^2= 0.78)	1.3	1.3	-0.58	0.31 (R^2=0.87)	2.2	1.1	-0.18
	Marine Sand	0.48 (R^2= 0.72)	1.5	0.82	0.50	0.30 (R^2=0.71)	2.3	0.72	0.82

Experimental data was fit to the first-order kinetic equation, $\ln [C_i] = -kt + \ln [C_i]_{t=0}$.

Table: 3.3. Mass balance of target compounds in fresh water and marine systems at three different temperatures.

Sediment type	Treatment	Physical phase	Compound Name	Compound %		
				4 ^{0}C	15 ^{0}C	23 ^{0}C
Fresh Water silt	TNT	Aqueous	TNT	48.8	57.9	56.9
			To. Tr. Pro.[a]	1.4	1.4	1.1
		Particle	TNT	41.6	36.7	35.7
			To. Tr. Pro.[a]	1.2	1.7	1.9
		Unknown		7.1	2.3	4.4
	RDX	Aqueous	RDX	26.9	29.0	30.4
			To. Tr. Pro.[c]	16.1	15.2	15.6
		Particle	RDX	12.8	10.9	8.7
			To. Tr. Pro.[d,e]	8.5	10.4	10.9
		Unknown		35.6	34.5	34.4
Marine Silt	TNT	Aqueous	TNT	23.6	15.6	21.8
			To. Tr. Pro.[a]	2.22	2.0	2.0
		Particle	TNT	7.6	7.2	9.0
			To. Tr. Pro.[a]	0.1	0.2	-
		Unknown		66.6	75.0	67.1
	RDX	Aqueous	RDX	52.0	48.4	52.2
			To. Tr. Pro.[c,e]	29.1	16.0	0.4
		Particle	RDX	8.7	13.4	14.3
			To. Tr. Pro.[c,d]	3.6	4.6	4.61
		Unknown		6.7	17.6	28.6
Marine Sand	TNT	Aqueous	TNT	34.1	25.9	32.4
			To. Tr. Pro.[a,b]	5.2	2.8	2.4
		Particle	TNT	8.8	3.2	8.4
			To. Tr. Pro.[a]	0.1	-	0.1
		Unknown		51.8	68.1	56.7
	RDX	Aqueous	RDX	53.3	45.0	48.6
			To. Tr. Pro.[c,e]	20.0	17.2	42.9
		Particle	RDX	0.1	7.4	5.3
			To. Tr. Pro.[c]	-	2.2	1.1
		Unknown		26.5	28.2	2.0

To. Tr. pro. = Total transformation products

[a] 4-amino-2,6-dinitrotoluene (4A-DNT)

[b] 2-amino-4,6-dinitrotoluene (2A-DNT)

[c] Hexahyro-1-nitroso-3,5-dinitro-1,3,5-triazine (MNX)

[d] Hexahyro-1,3-dinitroso-5-nitro-1,3,5-triazine (DNX)

[e] Hexahyro-1,3,5-trinitroso-1,3,5-nitro-1,3,5-triazine(TNX)

Supplementary Material

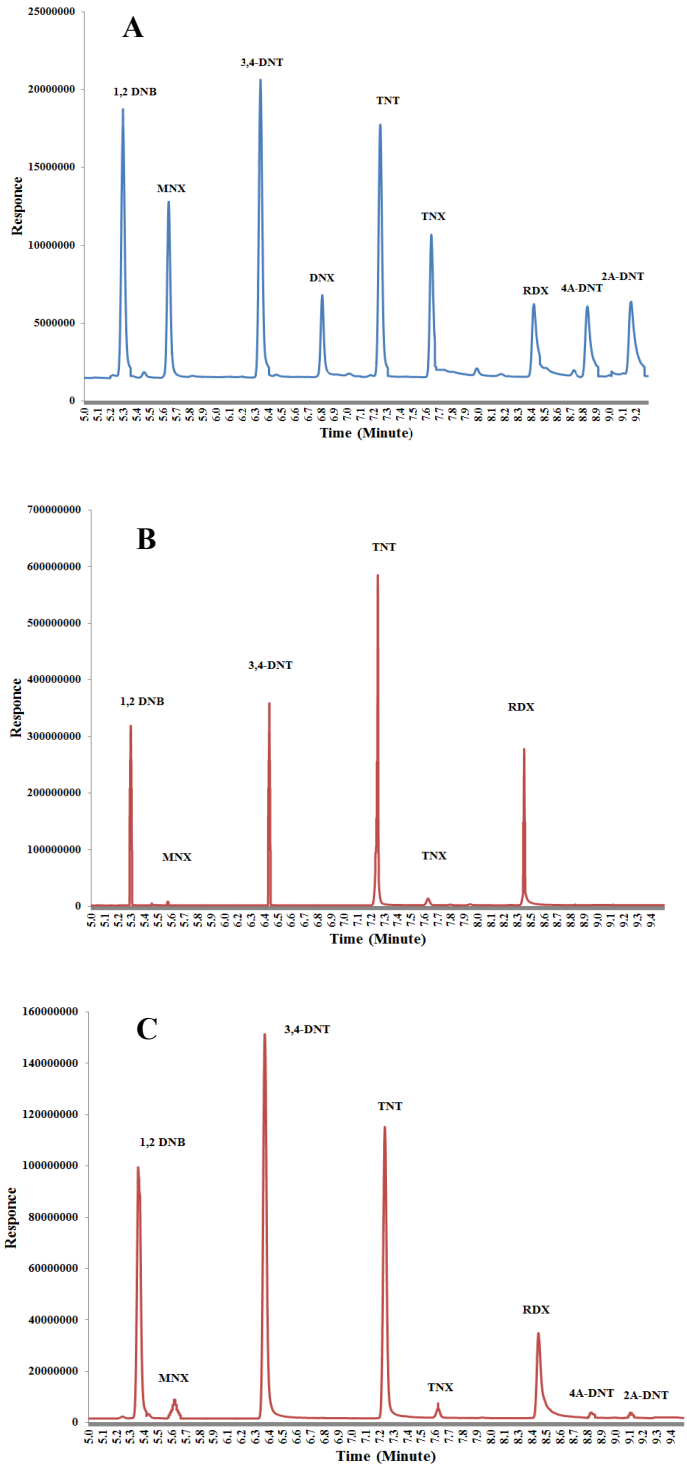

Supplementary Figure S-3.1. GC-ECD chromatograms of munition compounds of A) standards B) water extraction from marine sand system C) sediment extraction from marine sand system

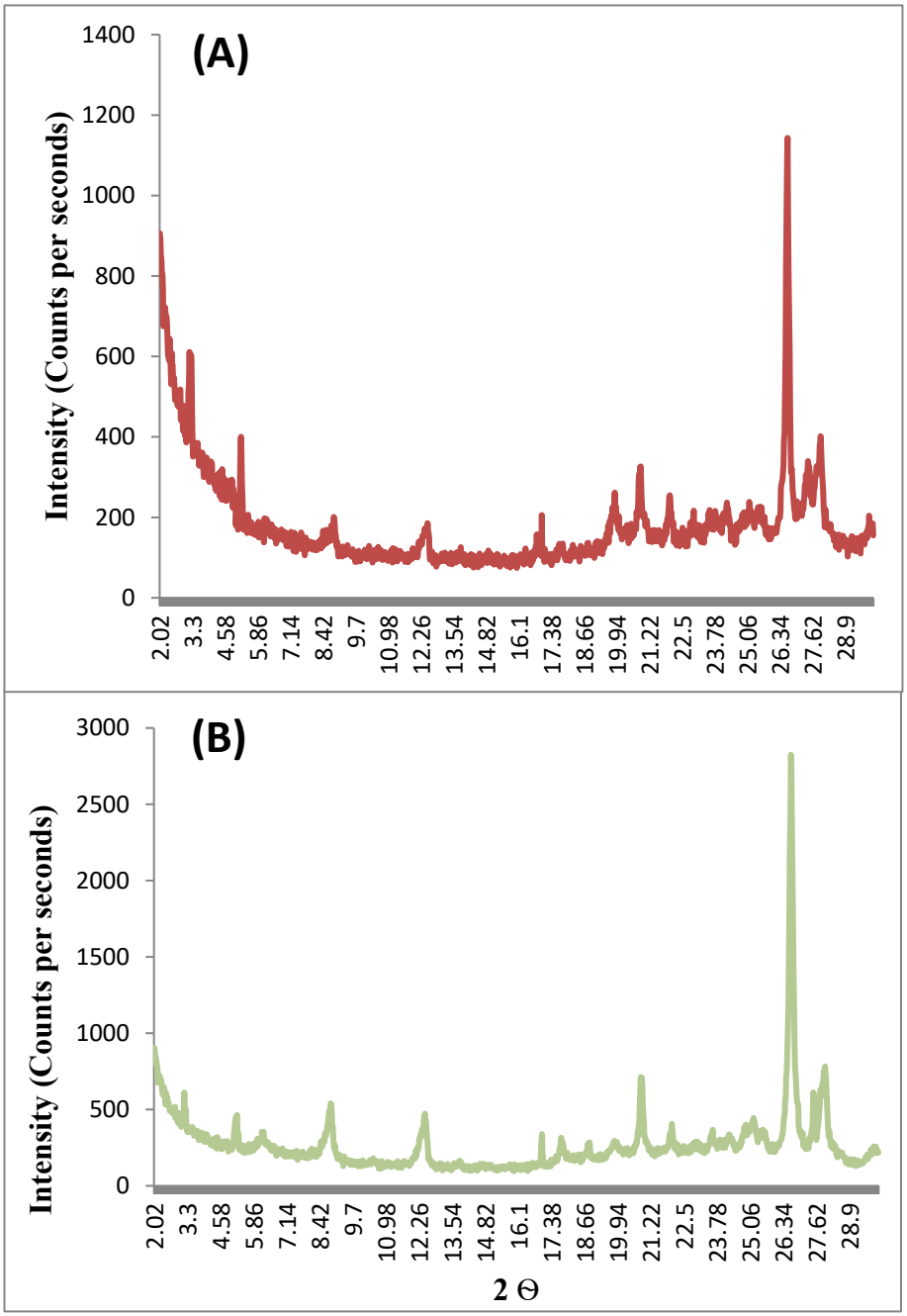

Supplementary Figure S-3.2. X-ray diffractometer (XRD) spectrums of clay compositions of A) freshwater silt B) Marine silt ; Peaks corresponds to plagioclase (Na-feldspar), k-feldspar and smectite group clays are shown at series of 2Θ angles of (3.18, 27.9) , (3.24, 27.5) and (5.2, 17) respectively. (Reference: Open-File Report, US geological Survey)

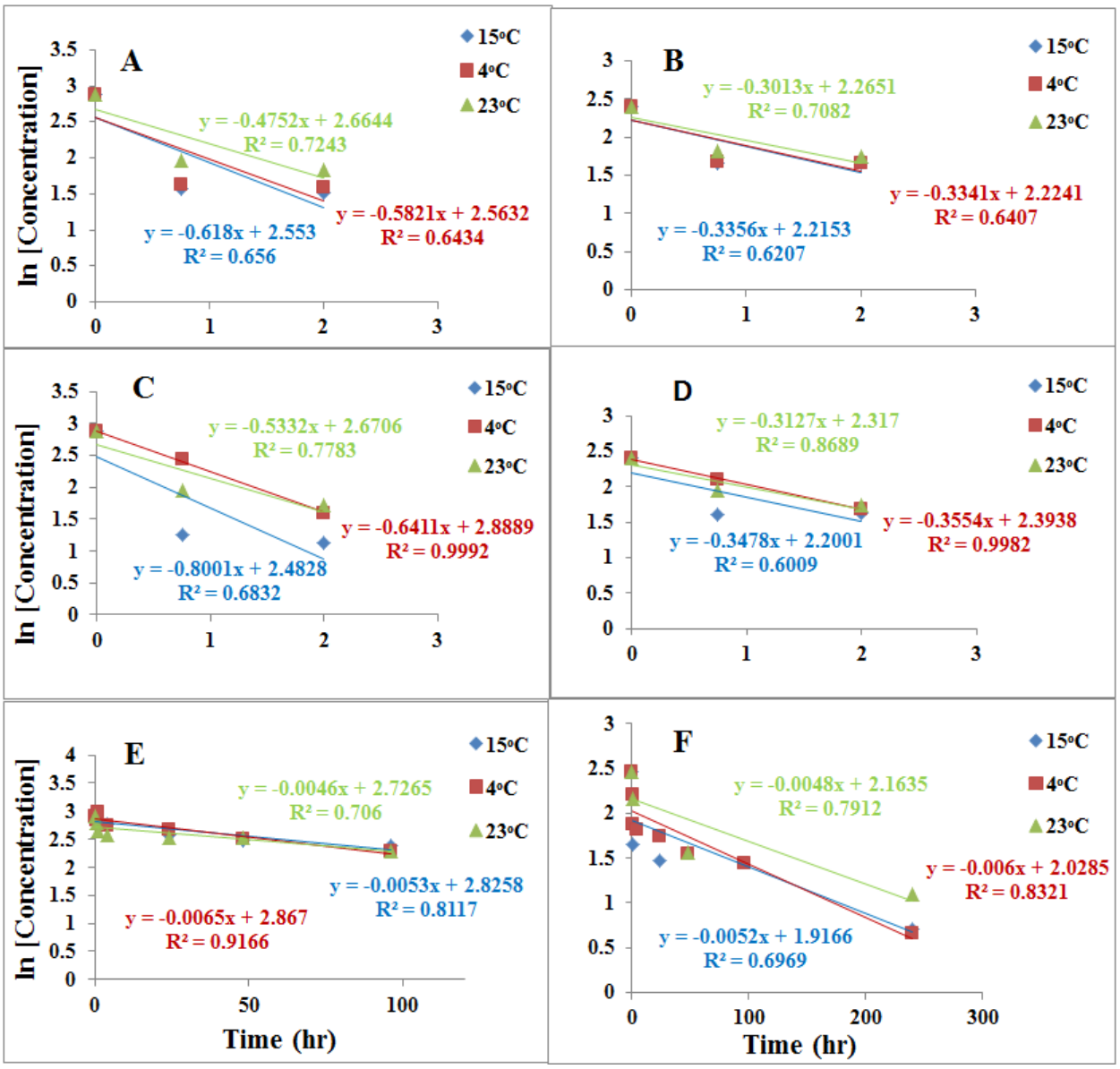

Supplementary Figure S-3.3. Time series ln values of aqueous concentrations of A) TNT in the marine sand system B) RDX in the marine sand system C) TNT in the marine silt system D) RDX in the marine silt system E) TNT in the freshwater silt system F) RDX in the freshwater silt system at three different temperatures, 4^0C, 15^0C, 23^0C.

Supplementary Table S-3.1. Published sorption parameters of TNT and RDX under abiotic and biotic conditions

Study	Water type/Location	Sediment Type	Sediment Characteristics			System Characteristics		Kinetic parameters			
								TNT		RDX	
			% OC	Clay%	CEC (cmolkg^{-1})	Temp (^{0}C)	pH	k (hr^{-1})	K_p (Lkg^{-1}sed)	k (hr^{-1})	K_p (Lkg^{-1}sed)
This Study	Marine/Long Island Sound (30 ppt)	Upper tidal sand	0.0038	0.80	-	4	7.9	0.5821	1.31	0.3163	0.87
						15		0.6180	0.92	0.3356	0.82
						23		0.4752	0.82	0.3013	0.72
		Intertidal silt	0.4101	56	-	4	7.9	0.6411	1.99	0.3554	1.32
						15		0.8001	1.40	0.3348	1.17
						23		0.5332	1.27	0.3120	1.08
	Fresh/Avery Point, CT (0.1ppt)	Fresh water silt	0.9320	34	-	4	7.0	0.0065	3.14	0.0060	2.96
						15		0.0053	2.31	0.0052	2.49
						23		0.0046	1.94	0.0048	1.37
Chappel et al., (2011)	Marine (Artificial, 20ppt)	Coarse, Low OC	0.12	2.4	22	8	8.0	0.0115	-	-	-
						15		0.0040	-	-	-
						25		0.0016	-	-	-
		Medium, Low OC	0.84	10.0	53	8	8.2	0.0040	-	-	-
						15		0.0045	-	-	-
						25		0.0084	-	-	-
		Fine, High OC	2.27	40.0	188	8	7.9	0.0113	-	-	-
						15		0.0110	-	-	-
						25		0.0141	-	-	-
Yamamoto et al., (2010)	Ground water/MMR, MA	Surface soil	1.84	7.9	9.20	22	4.73	0.00295*	2.5	0.00126*	0.36
		Deep soil	0.04	2.7	1.17		6.12	0.00144*	0.34	0.0031*	0.072
Sheremata et al., (2001)	Deionized water (Fresh)	Agricultural top soil /	8.4	4	14.6	25	5.6	-	-	0.0043*	0.83
Brannon et	Marine/Artificial	Medium, high OC	7.41	14	47	20	5.4	0.105	-	0.00048	-

al., (2005) - **Biotic**	(20ppt)	Medium, low OC	0.83	11	13		6.8	0.198	-	0.00108	-
		fine, high OC	1.92	39	40		6.6	0.0985	-	0.00671	-
	Deionized water (Fresh, 0 ppt)	University Lake	7.41	14	47	20	5.4	0.102	-	0.00037	-
		Browns Lake	0.83	11	13		6.8	0.244	-	0.0009	-
		Texas Lake	1.92	39	40		6.6	0.158	-	0	-
Dontsova et al., (2006) - **Biotic**	Fresh water	Plymouth loamy sand/	0.78	5.0	7.05	-	5.1	-	1.6	-	0.65
		Alder silt loam	0.20	4.5	7.83	-	8.2	-	2.4	-	0.48
Ainsworth et al., (1993)	Fresh water	Soil,Horizon C	0.23	13	55.00	10	7.1	-	2.625*	-	-
						20	-	-	1.804*	-	-
						23	-	0.012*	2.267*	-	-
						50	-	-	0.999*	-	-
		Soil,Horizon BC	0.50	44	162.00	10	6.7	-	4.569*	-	0.400*
						20	-	-	3.435*	-	0.132*
						50	-	-	2.159*	-	-
		Soil,Horizon AP	1.19	11	2.49	10	5.3	-	-	-	0.514*
						20	-	-	-	-	0.370*
						23	-	-	-	0.0036*	0.690*
						50	-	-	-	-	0.274*
Brannon et al., (1992)	Fresh water	Massonry sand	0.036	2.5	1.73	-	-	-	0.517	-	0.305
		Tunica silt	0.960	6.3	73.00	-	-	-	4.850	-	1.220
		Muck soil	9.130	-	168.00	-	-	-	-	-	3.170
Pennington & Patrick, (1990) - **Biotic**	Fresh water	High OC	3.592	23.8	102.0	-	6.77	0.7156*	7.2725	-	-
		Low OC	0.367	10.6	16.3	-	4.40	0.5637*	2.7377	-	-
Xue et al., (1995) - **Biotic**	Fresh water	Norwood soil	0.32	18.0	4.10	-	7.4	-	3.64	-	1.57
		Kolin soil	-	10.6	16.3	-	4.4	-	2.66	-	1.59
Sharma et al., (2013) - **Biotic**	Fresh water	Low OC	0.2	6.9	1.8	25	4.6	-	-	-	3.4
		Low OC, Soil horizon B	0.2	9.7	1.8	25	4.3	-	-	-	2.5
		High OC, Soil horizon E	3.0	1.5	3.9	25	3.8	-	-	-	6.9
		High OC	4.2	<1	7.1	25	5.2	-	-	-	8.7

Supplementary Table S-3.2. Mass balance of target compounds in fresh water and marine systems at three different temperatures.

Sediment type	Treatment	Physical phase	Compound Name	Compound %		
				4 °C	15 °C	23 °C
Fresh Water silt	TNT	Aqueous	TNT	48.8	57.9	56.9
			4A-DNT	1.4	1.4	1.1
		Particle	TNT	41.6	36.7	35.7
			4A-DNT	1.2	1.7	1.9
		Unknown		7.1	2.3	4.4
	RDX	Aqueous	RDX	26.9	29.0	30.4
			MNX	16.1	15.2	15.6
		Particle	RDX	12.8	10.9	8.7
			DNX	2.6	2.8	2.7
			TNX	5.9	7.6	8.2
		Unknown		35.6	34.5	34.4
Marine Silt	TNT	Aqueous	TNT	23.6	15.6	21.8
			4A-DNT	2.2	2.0	2.1
		Particle	TNT	7.6	7.2	9.0
			4A-DNT	0.1	0.2	-
		Unknown		66.6	75.0	67.1
	RDX	Aqueous	RDX	52.0	48.4	52.2
			MNX	1.5	-	-
			TNX	27.6	15.9	0.4
		Particle	RDX	8.7	13.4	14.3
			MNX	1.2	2.2	2.2
			DNX	2.4	2.4	2.4
		Unknown		6.7	17.6	28.6
Marine Sand	TNT	Aqueous	TNT	34.1	25.9	32.4
			4A-DNT	4.7	2.8	2.4
			2A-DNT	0.6	-	-
		Particle	TNT	8.8	3.2	8.4
			4A-DNT	0.1	-	0.1
		Unknown		51.8	68.1	56.7
	RDX	Aqueous	RDX	53.3	45.0	48.6
			MNX	6.5	7.8	18.7
			TNX	13.5	9.4	24.2
		Particle	RDX	0.1	7.4	5.3
			MNX	-	2.2	1.1
		Unknown		26.5	28.2	2.0

Supplementary Table S-3.3. Compound specific recoveries and detection limits for parent and transformation products.

Compound	Detection limit (ng/mL)
TNT	7.8
2A-DNT	7.5
4A-DNT	7.5
RDX	7.2
MNX	7.4
DNX	7.3
TNX	7.4

4.0. Biodegradation and mineralization of isotopically labeled TNT and RDX in anaerobic marine sediments

This chapter was published, as follows:

Ariyarathna, T., Vlahos, P., Smith, R., Böhlke, JK, Fallis, S., Groshens, T., and Tobias C**.** 2017**.** Biodegradation and mineralization of isotopically labeled TNT and RDX in anaerobic marine sediments. Environmental Toxicology and Chemistry, 36: 1170-1180.

Abstract

The lack of knowledge on fate of explosive compounds, 2,4,6-trinitrotoluene (TNT) and hexahydro-1,3,5-trinitro-1,3,5-triazine (RDX) particularly in marine ecosystems constrains the application of bioremediation techniques in explosive-contaminated coastal sites. Here, we present a comparative study on anaerobic biodegradation and mineralization of ^{15}N-nitro group isotopically labeled TNT and RDX in organic-carbon-rich, fine-grained marine sediment with native microbial assemblages. Separate sediment slurry experiments were carried out for TNT and RDX at 23°C for 16 days. Dissolved and sediment-sorbed fractions of parent and transformation products, isotopic compositions of sediment and mineralization products of the dissolved inorganic nitrogen (DIN) pool ($^{15}NH_4^+$,$^{15}NO_3^-$,$^{15}NO_2^-$ and $^{15}N_2$) were measured. TNT was removed from the aqueous phase at a faster rate (0.75 hr^{-1}) than RDX (0.37 hr^{-1}) and ^{15}N accumulation in sediment was higher in the TNT microcosms (13%) than RDX (2%). Mono-amino-dinitrotoluenes were identified as intermediate biodegradation products of TNT. TNT-N (2% of the total spiked) was mineralized to DIN through two different pathways: denitration, and deamination and formation of NH_4^+, facilitated by iron and sulfate reducing bacteria in the sediments. Majority of the spiked TNT-N (85%) was in unidentified pools by day 16. For RDX, 10% biodegraded to nitroso-derivatives, while 13% of RDX-N in nitro groups was mineralized to DIN anaerobically by the end of the experiment. NH_4^+ was the primary identified mineralization end-product of RDX (40%). A moderate level of N_2 production (13% of RDX loss) was seen in the RDX system but not in the TNT system. RDX-N (68% of the total spiked) was in an unidentified pool by day16 and may have included unquantified mineralization products dissolved in water.

4.1. Introduction

Though the disposal of explosives into the ocean has been prohibited in the United States since the “ocean dumping act” in 1972 (Bearden, 2007), intact, breached or buried munitions from past disposal activities slowly release explosive chemicals into the adjacent marine settings through corrosion and leaking resulting in potential risks to human health and the marine resources (Craig and Taylor, 2011). Ongoing Military training and weapon testing activities of the Department of Defense (DoD), which owns more than 10% of the 1,240 sites currently on the National Priorities List (Schmidt, 2004), may also be a continuous source of explosives to coastal

environments where marine aquatic life is exposed, as are humans through direct exposure and/or the food chain (Pichtel, 2012). Energetic compounds are not expected to persist over timescales of several years in coastal environments, but, explosive dumping sites and areas proximal to military training sites have shown elevated concentrations of energetic compounds (Bearden, 2007; Craig and Taylor, 2011).

TNT has been linked to altered liver function and anemia in humans (Schmidt, 2004) and both TNT and derivatives including 1,3,5-trinitrobenzene, 2,4,6-trinitrobenzaldehyde , 4,6-dinitroanthranil, 2,4,6-trinitrobenzonitril and N-hydroxylamines have shown toxicity and mutagenic potential in *Salmonella Typhimurium* strains, mammals, and aquatic species (fathead minnow, rainbow trout, channel catfish, worms, oyster larvae; Pichtel, 2012). RDX is considered a known neurotoxin for humans (Pichtel, 2012) and both TNT and RDX are classified as possible human carcinogens under group 3 in the International Agency for Research on Cancer carcinogenic categorization, and Group C by the United States Environmental Protection Agency (USEPA).

Munitions contamination from explosives is widespread globally, including areas off the US coasts and Hawaii, Gulf of Mexico, North Sea, Baltic Sea, Mediterranean Sea and off the coasts of Europe and Russia (Bearden, 2007). Since the estimated cost of complete cleanup at active military installations, closed bases, and other former military properties is in the tens of billions of US dollars (Bearden, 2007), it is extremely important to have a better understanding of natural biodegradation, mineralization pathways and rates to plan cost effective bioremediation techniques. Currently available literature on biodegradation of TNT and RDX address freshwater and groundwater systems extensively (Pichtel, 2012; Smith et al., 2013) and a limited number of studies have been focused on marine environment in terms of characterizing metabolites and mass balancing in the systems (Montgomery et al., 2011; Montgomery et al., 2013; Smith et al., 2015b). As nitrogen containing compounds, TNT and especially RDX with high N/C ratios may be quite susceptible to microbial breakdown in nitrogen-limited marine ecosystems (Montgomery et al., 2013).

The breakdown of TNT and RDX is determined by both the environment and the physical-chemical properties of the compounds which include solubility, octanol-water partition constants, vapor pressure, Henry's Law constants and bond energies (Ariyarathna et al., 2016). It is well established that TNT and especially RDX anaerobically biodegrade forming various reduced by-products although significant uncertainties are observed in breakdown pathways (Smith et al., 2015a; 2015b; Halasz and Hawari, 2011). Anoxic sediment is a favorable biodegradation zone of TNT and RDX in natural coastal habitats (Smith et al., 2015a; 2015b) and the extent of biodegradation relies on sediment properties including organic carbon content, surface charge and oxidation state, sediment texture and mineralogy, diversity and quantity of microbial populations and redox conditions (Ariyarathna et al., 2016; Smith et al., 2013). It has been documented that nitro groups of TNT are reduced to amino groups forming mono, di and tri-aminotoluenes under anaerobic conditions (Pichtel, 2012; Esteve-Núñez et al., 2001; Drzyzga et al, 1998). Mineralization of TNT also has been reported in nitrate reducing (Boopathy, 2014) and sulfate reducing conditions (Drzyzga et al., 1998; Boopathy, 2014), but the extent and pathways of complete mineralization remain controversial (Montgomery et al., 2011; Montgomery et al., 2013; Smith et al., 2015a). RDX is known to anaerobically biodegrade through sequential reduction to form more toxic nitroso-derivatives (McCormick et al., 1981).

Though it has been identified that denitration, denitrification, deamination and ring breakdown are involved in further mineralization of RDX (Smith et al., 2015a; Halasz and Hawari, 2011; Hawari et al., 2000), the relative importance of these mechanisms in natural systems, particularly marine settings, is unknown.

Most of the existing studies evaluating the breakdown of TNT and RDX in sediments incubate pure microbial strains in nutrient rich media under laboratory controlled conditions (McCormick et al., 1981; Spain, 1995). A few studies have used natural coastal microbial assemblages to study TNT and RDX breakdown using isotopically ^{14}C labeled (Montgomery et al., 2011; Montgomery et al., 2013) and ^{15}N labeled compounds (Smith et al., 2015a; 2015b) suggesting the necessity of more experiments to characterize the metabolites and kinetic pathways of these compounds in marine sediments.

In this study, bench-top sediment slurry experiments using fine grained, organic rich marine sediment were conducted using ^{15}N isotopically labelled TNT and RDX. Separate experiments were conducted for the two compounds over 16 days and time series data was obtained for a subset of degradation and mineralization products of target compounds over the course of the experiment. The data were combined to calculate transformation rates, trace the degradation pathways and develop mass balance models for TNT and RDX. Further, this study allows for comparison of the removal of TNT and RDX from aqueous phases via both sorption and degradation under biotic conditions with that of a previous study performed under abiotic conditions (Ariyarathna et al., 2016) which had been conducted using a similar experimental set-up and sediment from the same field location, offering a novel and incremental comparison and this type of study has not been done related to the explosives in the past. The use of ^{15}N labeled compounds in tracing the breakdown pathways of TNT and RDX entering inorganic nitrogen pools such as ammonium (NH_4^+), nitrates (NO_3^-), nitrites (NO_2^-) and nitrogen gas (N_2) provides the nitrogen-based mass balance of the systems that will help to reveal pathways (Smith et al., 205b). Identification and quantification of prominent pathways/ultimate pools of TNT and RDX facilitate determining the most suitable bioremediation techniques applied to marine sediments in coastal environments. Moreover, this approach may provide insight to favorable conditions for bioremediation including sediment properties and environmental parameters such as pH, redox, reduced sulfur and iron species.

4.2. Materials and Methods

TNT and RDX (>99 purity) with and without isotopically labeled nitro groups were synthesized at the Naval Munitions Command, China Lake, CA, USA. All standards were purchased from Accustandard, New Haven, CT and solvents were high purity from Fisher Scientific. Sediment and sea water were collected from 41°18′03.42″N / 72°07′14.09″W and 41°19′04.50″N / 72°04′00.52″W in the intertidal zones of Waterford and Groton, Connecticut, USA respectively.

4.2.1 Incubation Experiments

Fine grained, organic rich marine sediment (100g) was mixed with filtered (polyethersulfone- 0.2µm) sea water (30 ‰) at a mass ratio of 1:4 (Pennington et al., 1995) in

500mL glass bottles covered with aluminum foil to inhibit photo-degradation. Sediment slurries were continuously mixed on magnetic stirrer plates at 23^0C over the course of the experiment. After a 24 hr equilibration time, slurries were separately spiked with 36 µL of nitro group labeled ^{15}N-TNT (15 atom % ^{15}N total) or 41 µL ^{15}N-RDX (7.5 atom% ^{15}N total) dissolved in acetone to achieve concentrations of 4 mg L^{-1} and 2.5 mg L^{-1} for TNT and RDX respectively. The final concentration of acetone was less than 0.01% by volume. Two separate experiments for TNT and RDX were conducted including three controls for each. Samples were collected in triplicates at preset intervals (5 total) over the 2 week duration of the experiment and each slurry was sacrificed at the time of sampling. Aqueous samples were collected for quantifying target and breakdown products including a subset of transformation and mineralization products while sediment samples were analyzed for target and breakdown products and sediment bulk ^{15}N.

4.2.2 System Characterization

Physical parameters of the systems including pH, temperature and salinity were measured using a YSI probe (YSI 556 MPS). Redox potentials of sediment systems were measured using a platinum electrode (Paleo Terra, Amsterdam) relative to an Ag/AgCl reference electrode (Fisher Scientific) over the course of the experiment. Water samples were filtered through polyethersulfone - 0.2µm (0.2 µM PES) syringe tip filters and analyzed for nutrients including NH_4^+ and total NO_3^- and NO_2^- using a Smartchem nutrient analyzer (Westco-W12623) following cadmium azo-dye and phenol hypochlorite methods, respectively. A 40 ml water sample was filtered (0.2 µM PES) and acidified with hydrochloric acid to a pH of 2 for dissolved organic carbon (DOC) analysis using a total organic carbon (TOC) analyzer (Shimadzu TNM-1). 3 ml of water were filtered (0.2 µM PES) and analyzed using a ferrozine method (Stookey, 1970) and methylene blue method (Cline, 1969) for dissolved ferrous and hydrogen sulfide respectively in aqueous phase by UV/Vis spectrophotometer (Hitachi-U-30110).

Sediment was characterized for TOC, total nitrogen (TN) and total elemental sulfur (S) using a Perkin Elmer elemental analyzer (NA 1500). Sediment texture was determined using a mechanical sieve analyzer with a set of sieves from 0.063 mm to 2.0 mm. Clay compositions in the sediment were determined by X-ray diffractometer (XRD; Rigaku Ultima IV / Cu Kα). with λ radiation was = 0.15406 nm, beam voltage set at 40 kV, and the beam current was 44 mA.

4.2.3 Explosives Analysis

Reduced degradation products, including TNT-derived 2-amino-4,6-dinitrotoluene (2-ADNT) and 4-amino-2,6-dinitrotoluene (4-ADNT), and RDX-derived Hexahyro-1-nitroso-3,5-dinitro-1,3,5-triazine (MNX), Hexahyro-1,3-dinitroso-5-nitro-1,3,5-triazine (DNX), and Hexahyro-1,3,5-trinitroso-1,3,5-nitro-1,3,5-triazine (TNX), were analyzed in aqueous and sediment samples. A modified salting-out method (Miyares and Jenkins, 1990) adapted for smaller sample sizes was used for extraction of munition compounds from aqueous samples following methods described in Ariyarathna et al. (2015). An average recovery of 99.1 ± 0.5% was obtained for known amounts of 1, 2-dinitrobenzene (1,2-DNB) in water extractions. Sediment bound munitions were extracted using 2g of freeze dried sediments and average recoveries of munitions from sediment samples were 82 ± 7 % based on 1,2-DNB added to the triplicate sediment samples. Both water and sediment extractions were analyzed using gas chromatography (GC)/electron-capture detection (ECD) following the methods described by

Ariyarathna et al. (2015). 3, 4-dinitrotoluene (3,4-DNT) was added to each extract prior to injection to monitor detection efficiency. Explosive analysis was performed with an Agilent GC/ECD equipped with an HP-DB5 column (30 m x 320 µm, 0.25-µm; Agilent). Quantification was based on an external calibration curve of available standard munitions TNT, 2-ADNT, 4-ADNT, RDX, MNX, DNX and TNX. (AccuStandard, New Haven, CT). The average reporting limit for all compounds was 7.8 ng mL^{-1}.

4.2.4 Bulk ^{15}N Analysis in Sediment

Freeze dried sediment samples were analyzed using a continuous flow elemental analyzer – isotope ratio mass spectrometry (EA-IRMS: Delta V, Thermofisher) at the University of Connecticut for ^{15}N enrichments. Nitrogen isotope ratios are reported in δ notation as follows:

$$\delta^{15}N = [(R_{sample} - R_{STD})/R_{STD}] \quad (1)$$

where R_{STD} is the $^{15}N/^{14}N$ ratio of atmospheric nitrogen and R_{sample} is the $^{15}N/^{14}N$ ratio of the sample. $\delta^{15}N$ values are reported in parts per mil (‰) and external isotope and mass calibration was done using glutamic acid standards purchased from US Geological Survey. Triplicate sediment samples replicated with coefficient of variance of 0.35. Excess ^{15}N tracer was calculated as

$$^{15}N \text{ mols Excess} = N \text{ mols} * (X^{15}N_t - X^{15}N_{t0}) \quad (2)$$

where the total N mass, and mole fractions of ^{15}N at time t ($X^{15}N_t$) and time 0 ($X^{15}N_{t0}$) were obtained from an elemental analyzer – isotope ratio mass spectrometry EA-IRMS (Delta V, Thermofisher).

4.2.5 Mineralization Product Analysis

The mineralization products, $^{15}NH_4^+$, $^{15}N_2$ and total $^{15}NO_2^- + {}^{15}NO_3^-$ ($^{15}NO_X$) in the aqueous phase, were quantified using IRMS techniques. Filtered (0.2 µM PES), frozen water samples were extracted for NH_4^+ following the methods from Holmes et al., (1998). NH_4^+ in aqueous samples was converted to ammonia using magnesium oxide and absorbed onto glass fiber filters trapped in a sealed acidified filter packet. Dried glass fiber filters were analyzed for ^{15}N using a continuous flow EA-IRMS similar to the analysis of bulk ^{15}N in sediments. Microcosm samples where done in triplicates at each time point and replicated with coefficient of variance of 0.8% while extraction efficiencies were between 95-105% based on the recovery of NH_4NO_3 standards. Moles of $^{15}NH_4^+$ were calculated using NH_4^+ concentrations and mole fractions of ^{15}N ($X^{15}N_t$ and $X^{15}N_{t0}$) obtained from Smartchem nutrient analyzer and EA-IRMS respectively (equation 3).

$$^{15}NH_4^+ \text{ mols Excess} = NH_4^+ \text{ mols} * (X^{15}N_t - X^{15}N_{t0}) \quad (3)$$

$^{15}N_2$ in water samples was determined using continuous flow isotope ratio mass spectrometry on a Thermo Delta V Plus with a Gas Bench interface (GB-IRMS). Triplicate gas samples were collected at each time point by pumping unfiltered seawater into 30 ml serum bottles that had previously been sealed, pre-loaded with 750µl of 2M KOH (for preservation), and flushed with He for 12 minutes (Smith et al., 2015a). After at least 6 hours of headspace

equilibration, the isotopic composition of N_2 ($\delta^{15}N_2$) was measured with coefficient of variance of 0.2. By applying Henry's law (Schwarzenbach et al., 2003), dissolved N_2 mols in aqueous phase, N_2 mols,aq was calculated by using N_2 determined based on air standards, N_2 mols,air and dimensionless Henry's law constant, K_H (equation 4).

$$N_{2\ mols,aq} = N_{2\ mols,air} / K_H \quad (4)$$

$^{15}N_2$ aq was calculated from the measured mole fraction of dissolved N_2 ($X^{15}N_2$) and aqueous N_2 concentration.

$\delta^{15}NO_X$ (total $^{15}NO_2^-$ and $^{15}NO_3^-$) values were obtained via the denitrifier method using *Pseudomonas aureofaciens* (Smith et al., 2015b) at the US Geological Survey (USGS) in Reston, VA on water samples filtered through a 0.2µM PES filters and frozen. Moles of $^{15}NO_X$ were calculated using NO_X concentration and mole fractions of ^{15}N ($X^{15}N_t$ and $X^{15}N_{t0}$) obtained from Smartchem nutrient analyzer and GB-IRMS respectively (equation 5).

$$^{15}NO_X \text{ mols Excess} = NO_X \text{ mols} * (X^{15}N_t - X^{15}N_{t0}) \quad (5)$$

4.2.6 Data Analysis

The measured time series concentrations of TNT and RDX in water [C_i] were used to calculate removal rate constants of compounds according to equation 6,

$$\ln [C_i] = -k_{r,i}t + \ln [C_i]_{t=0} \quad (6)$$

where t is time (hr) and $k_{r,i}$ is the first order removal rate constant of compound i in hr^{-1}.
The rate of formation of mineralization product j was used to derive the first order formation rate constant ($k_{f,j}$) wherein for n first order degradation products,

$$k_{r,i} = k_{f,1} + k_{f,2} + \ldots + k_{f,n} \quad (7)$$

The measured time series concentrations of degradation products, $C_{product\ j}$ were used to estimate the removal rate constants wherein

$$k_{f,j}[C_{parent\ i}] - k_{r,j}[C_{product\ j}] = k_{r,j}[C_{product\ j}]_{net} \quad (8)$$

where t is time (hr) and k is the first order rate constant in hr^{-1}.

Removal rate constants (Equation 6) represent the total of sorption, biotic and abiotic transformation while degradation and mineralization rate constants (Equation 7, 8) consist of biotic and abiotic transformation. Furthermore, the total biotic component was obtained by subtracting aquatic concentrations in abiotic treatments from the aquatic concentrations in biotic treatments (Total of biotic and abiotic) based on biotic removal rate constants of TNT and RDX were calculated using equation 7 and 8.

A mass balancing approach was based on ^{15}N equivalents in masses of each analyzed N-containing parent and derivative pools and illustrated in following equations (Equations 9 and 10).

$$^{15}N\text{-}TNT_{system} = {}^{15}N\text{-}TNT_{water} + {}^{15}N\text{-}TNT_{sediment} + {}^{15}N\text{-}2A\text{-}DNT_{water} + {}^{15}N\text{-}2A\text{-}DNT_{sediment} + {}^{15}N\text{-}4A\text{-}DNT_{water} + {}^{15}N\text{-}4A\text{-}DNT_{sediment} + {}^{15}N\text{-}NH_4^+{}_{water} + {}^{15}N\text{-}N_{2\ water} + {}^{15}N\text{-}NO_{X\ water} + \text{unidentified } {}^{15}N\text{-compounds}_{\text{ water and/or sediment}} \quad (9)$$

where, ^{15}N-TNTsystem represents total mols of ^{15}N-TNT spiked into the system and all the other terms represent ^{15}N moles measured in different TNT-derived metabolites in water and sediment.

$$^{15}N\text{-}RDX_{system} = {}^{15}N\text{-}RDX_{\ water} + {}^{15}N\text{-}RDX_{\ sediment} + {}^{15}N\text{-}MNX_{water} + {}^{15}N\text{-}MNX_{sediment} + {}^{15}N\text{-}DNX_{water} + {}^{15}N\text{-}DNX_{sediment} + {}^{15}N\text{-}TNX_{water} + {}^{15}N\text{-}TNX_{sediment} + {}^{15}N\text{-}NH_4^+{}_{water} + {}^{15}N\text{-}N_{2\ water} + {}^{15}N\text{-}NO_{X\ water} + \text{unidentified } {}^{15}N\text{-compounds}_{\text{ water and/or sediment}} \quad (10)$$

where, ^{15}N-RDX system represents total mols of ^{15}N-RDX spiked into the system and all the other terms represent ^{15}N measured in different RDX-derived metabolites in water and sediment. Bacterial incorporation of nitrogen from the energetics were calculated using incorporation rates published in Montgomery et al., (2013) and were 27.3 µg C L^{-1} d^{-1} and 4 µg C L^{-1} d^{-1} for TNT and RDX, respectively at salinity of 30 PSU.

Principal component analysis (PCA) was carried out to obtain a better understanding of transformation pathways and to evaluate the effect of geochemical variables on the breakdown of TNT and RDX in anaerobic marine sediment systems. PCA was performed using all measured pools of ^{15}N and geochemical variables as metrics at 16 days for both TNT and RDX microcosms separately using 'Excelstat'. Metrics used in PCA were mean normalized, and missing gaps in the data were filled using the values of the detection limit of the instruments of particular analysis.

4.3. Results

4.3.1 Removal of TNT and RDX from the Aqueous Phase

Incubation experiments for TNT and RDX were conducted anaerobically (Delaune and Reddy, 2005) with redox potential varying from 53mV to -133mV and from 83mV to -231mV

respectively (Table 4.1) throughout the experiment. Table 4.1 summarizes the physical system over the time series.

TNT was rapidly removed from 17.6 µM to 0.028 µM in the aqueous phase following first order kinetics with a rate constant of 0.75 ± 0.08 hr^{-1}. This was greater than that in a similar experimental set-up under abiotic conditions which contained a different batch of sediment samples from the same field location determined in Ariyarathna et al. (2015) of 0.53 ± 0.08 hr^{-1} (Table 4.2). The total TNT removal rate constant solely from the biotic component (biodegradation and biotic mineralization) is estimated as 0.22 ± 0.11 hr^{-1} (Supplemental Data, Table S-4.1). 2-aminodinitrotoluene (2A-DNT) and 4-aminodinitrotoluene (4A-DNT) were identified as measurable derivatives of TNT in the aqueous phase (Figure 4.1A), rapidly forming until t = 2.5 hr at rates of 0.028 hr^{-1} (R^2 = 0.99) and 0.030 hr^{-1} (R^2 = 0.99) respectively (Table 4.2). Monoaminodinitrotoluenes (MADNTs) further degraded to just above detection limits in the aqueous phase by day 10. The first order removal rate constants of 2A-DNT and 4A-DNT from the aqueous phase are 0.52 hr^{-1} and 0.56 hr^{-1} respectively (Table 4.2). The TNT removal rate is 1.4 times higher compared to the removal rates of monoamino-derivatives from the aqueous phase. The ratio of aqueous MADNTs to TNT increased from 0.05 - 0.58 until 2.5 hr (Table 4.3). RDX was removed in water from 11.3 µM to 0.89 µM and the removal (0.37 ± 0.01 hr^{-1}) was greater than that of the abiotic system (0.31 ± 0.06 hr^{-1}) [15] (Table 4.2, Figure 4.1B). This yields a smaller RDX removal rate constant that can be attributed solely to biotic components (biodegradation and biotic mineralization) of 0.06 ± 0.06 hr^{-1} (Supplemental Data, Table S-4.1). TNX was the only identified nitroso-derivative of RDX and it appeared in the aqueous phase at 0.75 hr after spiking and remained constant throughout the experiment (14 days). The ratio of TNX to RDX increased from 0.17 to 1.29 in the aqueous phase over the experiment (Table 3). Removal rate constants of TNT and RDX in the aqueous phase increased by up to 42% and 19% respectively in the presence of marine microbial assemblages compared to abiotic conditions under the same experimental set-ups as shown in Table 4.2 (Ariyarathna et al., 2016). Aqueous munition profiles of parent and daughter products comparing biotic and abiotic treatments are shown in Table S-4.2 in supplemental section.

4.3.2 Partitioning of TNT, RDX and their Derivatives onto Sediment

Marine silty sediments with a medium grain size of 0.5 mm comprised of 56 % silt and clay with smectite group clays and feldspar as the dominant clay types were used for slurries in the experiment (chemical and textural properties of sediment are shown in Supplemental Data, Table S-4.3). The sediments had an organic carbon content of 4.10 mg g^{-1}sed (0.41 % OC) (Table S-4.3) which raised the dissolved organic carbon content by 239-369µM in the aqueous phase of the slurries above that of normal seawater (185µM) at time 0 (Table 4.1). The spike added 1471-1675µM DOC due to acetone and 15-55µM DOC due to the compounds.

Bulk ^{15}N in sediment during TNT treatments increased rapidly (0.017 hr^{-1}; Table 4.2) from an initial $\delta^{15}N$ value of 6‰, to 165‰ (Table S-4.2) within 2 days (Figure 4.2A). Only 0.1 – 5.6 % of total^{15}N in sediments during TNT treatments was identified as TNT, 4A-DNT and 2A-DNT (∑TNT) and the majority (94.4 – 99.9 %) resided in other pools (Figure 4.2B). The average ratio of mono-amino-derivatives to TNT found in sediment throughout the experiment was 1.2 ± 0.8 (Table 4.3). However, TNT, 4A-DNT and 2A-DNT concentrations started decreasing in sediment after 0.45 hr, 0.45 hr and 2.5 hr respectively. Over this time, bulk ^{15}N in sediment continued rising for 2 days where it then plateaued.

In RDX treatments, bulk ^{15}N in sediment varied from a $\delta^{15}N$ value of 9‰ to 47‰ (Table S-4.4) and rapidly increased to a peak value of 7.7 x 10^{-4}µmol g^{-1} sed within 0.75 hr after spiking, followed by a slow decrease at a rate of 0.0021 hr^{-1} (Table 4.2, Figure 4.2A). Between 88-22% of total ^{15}N in sediment was identified as RDX, DNX and TNX (∑ RDX), and 12 – 78% resided in other pools for over the duration of the experiment (Figure 4.2C). RDX disappeared from the sediment at a rate of 0.0091 hr^{-1} (Table 4.2), and nitroso-derivatives DNX and TNX were first observed in sediment at 0.75 hr. Sediment concentrations of DNX and TNX slowly decreased following rate constants of 0.0006 hr^{-1} and 0.0012 hr^{-1} after day 3 of spiking respectively (Table 4.2). The ratio of RDX to identified nitroso-derivatives in sediments decreased from 6.1 to 0.2 over the course of the experiment (Table 4.3). Sediment-sorbed munition profiles of parent and daughter products comparing biotic and abiotic treatments are shown in Table S-4.2 in supplemental section.

4.3.3 Mineralization of Munitions to Dissolved Inorganic Nitrogen (DIN)

Measured aqueous mineralization products including NH_4^+, NO_X and N_2 show elevated enrichments for $\delta^{15}N$ relative to the natural levels in sediment slurries (Table 4.4). Excess $^{15}NO_X$ concentrations in slurry water during TNT treatments rapidly increased within 0.45 hr from spiking, followed by a first order decay after 0.45hr (0.0067 hr^{-1}; $R^2 = 0.85$) and almost disappeared after the two-week time period (Tables 4.2, 4.4). In RDX treatments, excess $^{15}NO_X$ concentrations in slurry water increased until day 3 with a formation rate of 0.014 hr^{-1}(R^2 = 0.99) and were removed by day 10 (Tables 4.2, 4.4). TNT derived NH_4^+ production approached steady state conditions after 10 days from spiking (Figure 4.3) and the formation rate constant was 0.048 hr^{-1} ($R^2 = 0.42$; Table 4.2). δ $^{15}NH_4^+$ in RDX treatments continuously increased (Table 4.4) also approaching steady state after 10 days after a reduction in the formation rate from 0.017 hr^{-1} ($R^2 = 0.83$) to 0.0061 hr^{-1} ($R^2 = 0.87$; Figure 4.3). Elevated $\delta^{15}N$ enrichments for N_2 were observed in RDX treatments, although, no N_2 production was detected in TNT treatments (Table 4.4). RDX-N derived N_2 was produced linearly over time at a rate of 0.041 hr^{-1} ($R^2 = 0.91$) (Figure 4.3) until day 3, where it reached steady state (with the exception of the last two time points, where sampling may have increased gas transfer losses).

Mineralization of RDX into all DIN pools including NH_4^+, NO_X and N_2 was 1 – 13 %, 10 times higher than the fraction observed for TNT (1% - 2%) throughout the experiment. Mineralization products in TNT sediment slurries increased until day 10 and stayed constant (1.9% relative to total TNT-N added) for the rest of the experimental time period while for RDX the percent mineralized increase from 0.8% to 13% throughout the experiment (16 days; Table 4.4). NH_4^+ made up 42-86% and NO_X accounted for 58-14% of measured mineralization products for TNT sediment slurries. For RDX treatments, NH_4^+, NO_X and dissolved N_2 gas were responsible for 10-39%, 86-48% and 5-13% of total mineralization, respectively.

4.3.4 Mass Balancing Approach of TNT and RDX Systems

Time series mass balances of TNT and RDX systems in terms of ^{15}N equivalents include the mineralization products (NH_4^+, NO_X and N_2), aqueous parent compound, selected derivatives, partitioning of compounds onto bulk sediment and unidentified ^{15}N incorporation onto sediments through other processes (Figure 4.4). Aqueous TNT dropped from 49 % to 0.2 % over the two weeks. Between 3 % -13% of spiked TNT partitioned onto sediment during the experiment. Insignificant mineralization of TNT in terms of NH_4^+ and NO_X (1% - 2%) was

observed while unidentifiable ^{15}N pools increased from 45% to 85% for TNT treatments throughout the experiment. Based on uptake rates from Montgomery et al. (Montgomery et al., 2013), up to 0.002 – 2.0 µmol of TNT may be incorporated into the bacterial biomass over the duration of the experiment. Bacterial incorporation could account for 0.4% of the unidentified pool at 0.45 hr but up to 100% at 10 days (Supplemental Data, Table S-4.5).

The percent of RDX remaining in the dissolved phase was higher than for TNT although it decreased from 53 % to 8 % over time. TNX remained in the water at an average constant percentage of 9.4% of total spiked RDX (Table 4.3). The percentage of spiked RDX that partitioned onto sediment was comparatively less than TNT and it decreased from 3.8 % to 1.8 % over the experiment. Nitrogen containing mineralization products (NH_4^+, NO_X and N_2) accounted for 1% -13% of spiked RDX throughout the experiment and unidentifiable ^{15}N pools increased for RDX treatments from 33% at the 0.75hr after spiking to 68% at the end of the experiment. For RDX, bacterial incorporation ranges from 0.0003 to 0.2 µmols and 0.1- 34% of unidentifiable pools have been identified as incorporated biomass in bacteria (Table S-4.5).

4.4. Discussion

4.4.1 Fate of TNT in Anaerobic Sediments

TNT is rapidly removed from the aqueous phase following first order kinetics through initial sorption and abiotic degradation (Ariyarathna et al., 2016) and via biodegradation by microbes in anaerobic sediments (Esteve-Núñez et al., 2001; Drzyzga et al., 1998; Spain, 1995). TNT removal rate constants decrease from highest to lowest in the order of: biotic marine organic carbon (OC) rich silt > abiotic marine OC rich silt > abiotic marine OC poor sand > abiotic freshwater OC rich silt. Increases in removal rates constants of TNT from the aqueous phase up to 42% in the presence of microbes illustrates the importance of native microbial assemblages in marine sediment towards TNT remediation. Removal rate constants of compounds in the abiotic system are composed of two parameters; sorption onto sediment and abiotic transformation. Based on the production rates of measured transformation products, abiotic transformation could account for 2% of total spiked TNT and up to 9% through sorption (Ariyarathna et al., 2016). Therefore, sorption plays a major role in removing TNT from the aqueous in all systems and is the major removal in abiotic systems. In biotic systems, biotic transformation of TNT is up to 9% of total spiked TNT (in terms of measured transformation products confirming biotransformation) is a significant removal process. Integrated sorption and biodegradation becomes the most effective removal mechanism of TNT particularly since sediments act as a biofilm carriers by providing a surface for microbes to attach (Smith et al., 2015b; Chusova et al., 2015) and enhancing the dual sorption, biodegradation effects. TNT biodegrades to MADNTs (2A-DNT and 4A-DNT) along the pathway of forming further reduced transformation products (Esteve-Núñez et al., 2001; Khan et al., 2013) however, diaminomononitrotoluenes (DANTs) and triaminotoluene (TAT) were not quantified in this study. Formation of TAT requires a redox potential below -200mV (Smith et al., 2015b; Esteve-Núñez et al., 2001) which was not reached in our anaerobic sediment microcosms where redox potentials ranged from 53mV to -133mV. However, the appearance and subsequent disappearance of MADNTs soon after the TNT sorption maximum suggests that 2A-DNT and

4A-DNT are intermediates of TNT break down pathways (Esteve-Núñez et al., 2001; Khan et al., 2013). TNT is removed from the aqueous phase faster (1.4 times) than for MADNTs revealing other possible pathways of TNT breakdown under anaerobic conditions (Esteve-Núñez et al., 2001; Khan et al., 2013) than the reduction through amino derivatives. Even though rapid biodegradation of TNT is reported in this study, observed production of derivatives, 2A-DNT and 4A-DNT, is small (0.1-8.6% of spiked TNT). The persistence of MADNTs implies that the production rates and removal rates are balanced while the removal of the 2A-DNT and 4A-DNT overtakes their respective production rates as they do not persist.

Partitioning of 13% of spiked TNT onto sediment highlights the role of sediment in reducing the bioavailability of TNT and derivatives in aquatic systems (Ariyarathna et al., 2016; Pennington et al., 2011) and further proposes new insights for sediment sorption related bioremediation techniques. Bulk ^{15}N values in sediment rapidly increased, followed by a plateau, strongly suggesting that TNT and then its derivatives must have been sorbed onto the sediment (Smith et al., 2015b) and maintained steady state or persisted relatively high percentages of silt and clays (56%; Haderlein et al., 1996) and organic carbon (4.1 mg g^{-1} sed; Yamamoto et al., 2004) found in the marine sediment used in this experiment facilitate the sorption of TNT and amino derivatives through electrostatic forces and hydrophobic partitioning (Ariyarathna et al., 2016). TNT and mono amino derivatives are responsible for a small percentage of bulk ^{15}N in sediment (2%) and also disappear soon after they reached maximum production, leaving the majority of bulk ^{15}N in sediment unaccounted for. The most likely pools for this ^{15}N include unquantified degradation products including DANTs and TAT (Smith et al., 2015b) or incorporation of ^{15}N into microbial biomass (Montgomery et al., 2011; Montgomery et al., 2013).

Mineralization of dissolved TNT and derivatives by anaerobic marine microbial assemblages (Montgomery et al., 2011; Montgomery et al., 2013; Smith et al., 2015b) to DIN, including NH_4^+ and NO_X is reported in this study, although the relatively small yields (2% of spiked TNT) agrees with previously published experiments (Montgomery et al., 2011; Montgomery et al., 2013). Principal component analysis (PCA) of time series ^{15}N pools reveals two possible pathways of mineralization of TNT under our experimental conditions (Figure 4.5A). Measurements (PCA scores) found as clusters in the PCA plot are influenced by the same underlying factors. PC1 reflects the duration of the experiment, with fresh TNT in both dissolved and sorbed phases plotting in the far right quadrant, and mineralization products in the far left quadrant. PC2 represents aqueous and sediment geochemical variables, specifically, the pH and %OC content. $^{15}NH_4^+$ and $^{15}NO_X$ are negatively correlated in the PCA plot suggesting these products are involved in two different pathways of mineralization. Denitration of TNT takes place (Esteve-Núñez et al., 2001; Qiao et al., 2011) in the early phase of the experiment when less reduced transformation products are available and redox potentials are 41 to 54 mV. The NO_X's formed are likely being removed by bacteria in the aqueous phase of the microcosms over the latter part of the experiment when redox ranges between 40mV and -26mV. The second pathway involves deamination of reduced transformation products (2A-DNT, 4A-DNT etc.) forming NH_4^+ (Smith et al., 2015b; Boopathy, 2014) towards the end of the experiment, as illustrated in the PCA plot.

The PCA plot also suggests ammonia formation may be associated with iron and sulfate reducing bacteria (Boopathy, 2014) in sediment, as $^{15}NH_4^+$, bulk ^{15}N in sediment and reduced

forms of iron and sulfur (Fe^{+2}, H_2S) are correlated in the PCA plot (Figure 4.5A - circled region). Microbially mediated degradation of TNT by iron reducers has been previously documented (Pichtel, 2012). Continuous production of Fe^{2+} from the interaction of *Shewanella putrefaciens* and iron bearing soil minerals was identified as the key factor to enhanced degradation of TNT via electron transfer (Cho et al., 2012). This is further confirmed in our study as demonstrated by the linear relationship between dissolved $^{15}NH_4^+$ and Fe^{2+} concentrations (R^2=0.4) and continuous production of Fe^{2+} throughout the TNT experiment. Moreover, *Shewanella putrefaciens* has shown enhanced growth by elemental sulfur reduction to hydrogen sulfide (H_2S; Moser and Nealson, 1996) which was observed towards the end of the experiment in this study. It can also indirectly affect TNT biodegradation via Fe^{2+} production. Sulfate reducing bacteria (SRB; *Clostridium*, *Desulfovibrio*) plays an important role in anaerobic marine environments in converting sulfates to H_2S by sulfate reductase. These organisms use the nitro groups present in the TNT molecule as either an electron acceptor or a nitrogen source (Boopathy, 2014). H_2S production observed towards the end of the experiment suggests that degradation of TNT is facilitated by SRB in this study.

NH_4^+ concentrations were steady towards the end of the experiment and no further N_2 production from either NO_X or NH_4^+ was observed over 16 days. It strongly reveals that NH_4^+ serves as a terminal mineralization product of TNT in DIN pools under anaerobic conditions. However, modest production of N_2 has been reported in an aerated water column of mesocosm studies (Smith et al., 2015b). Mineralization tracking as described in this study is limited to the ring attached functional groups as the TNT ring contains no N; but it is supported with the idea of ring stability with an aromatic π system described in Hawari et al. (2000). Further, the limited number of previous studies that describe ring breakdown of TNT to CO_2 confirms that ring carbon mineralization accounts for a lower percentage of TNT metabolic fate (Montgomery et al., 2011; Montgomery et al., 2013). Based on recent studies, environmental factors such as matrix effects, solution chemistry, sediment texture and chemistry etc. also control, and likely enhance the decomposition of TNT (Marín-Spiotta et al., 2014; Han et al., 2016). Lower remineralization in the system supports the incorporation of nitrogen from energetics as an organic nitrogen source rather than catabolization in bacteria. Total carbon demand of the system may have affected the remineralization of microbially incorporated carbon or nitrogen from the energetics. Bacterial incorporation of carbon and nitrogen from TNT is higher than that of RDX based on the incorporation rates published in Montgomery et al. (2013) and consistent with previously published data (Montgomery et al., 2011; Montgomery et al., 2013). The unidentified TNT-N pool at the last day of the experiment (85% of spiked TNT) could be fully explained by microbial incorporation based on the calculations above.

Here, we provide evidence that TNT is likely removed from the dissolved phase primarily through partitioning onto sediment and biotransformation at relatively equal amounts rather than undergoing abiotic mineralization in anaerobic sediment systems. This is supported by the modest yield of mineralization products in terms of DIN. However, from a mass balancing point of view, there is still a significant portion of TNT which has not been traced that remains in the dissolved phase as a transformation product of TNT. Further research needs to be done to obtain full mass balances of the system by widening the analytical window to quantify additional transformation products and bulk ^{15}N in water, as well as to include measurements of additional pools such as non-particle associated microbes. Increases in the unaccounted for portion of

spiked TNT (Figure 4) over the duration of the experiment suggests that unidentified (as yet unknown) or unmeasured (eg: DANTs, TAT) transformation products are accumulating with time, as has been suggested (Delaune and Reddy, 2005). Further research is necessary to confirm the identity of these potentially toxic products.

4.4.2 Fate of RDX in Anaerobic Sediments

RDX is removed from the dissolved phase following first order kinetics though removal is not as rapid as for TNT. Removal rate constants of RDX from the aqueous phase increases by up to 19% in the presence of anaerobic microbes in biotic system compared to the abiotic systems with different environmental conditions including freshwater, marine organic carbon rich and poor sediments described in Ariyarathna et al. (2015). Abiotic transformation and sorption of RDX could account for 5% and 14% of total spiked RDX respectively (Ariyarathna et al., 2016) while biotic transformation of RDX up to 9-10% in terms of measured transformation products confirming the significance of biotransformation. RDX (9.4%) biodegrades to TNX by sequential reduction through the nitroso-derivatives MNX and DNX, while keeping the nitroamine ring intact (Halasz and Hawari, 2011). TNX is found to be relatively stable (Paquet et al., 2011) in both dissolved and sorbed phases over 16 days. RDX sorbs onto the sediment reversibly through electrostatic forces (Ariyarathna et al., 2016) and is subsequently removed from sediment following first order kinetics via three possible mechanisms: abiotic transformation by mineral-bound ferrous (Gregory et al., 2004), enhanced biotransformation by microbes attached to the sediment particles and organic matter (Finneran et al., 2007) and desorption (Selim and Iskandar, 1994). TNX accounts for the majority of identified degradation products in sediment due to its relative stability (Paquet et al., 2011). However, 26-70% of bulk ^{15}N in sediment was still unidentified showing an ascending trend with time similarly to TNT. This may be due to microbial assimilation and unquantified derivatives. Interestingly, unlike TNT, elevated bulk ^{15}N values of sediment in RDX treatments did not stay constant, rather, slowly decreased with a first order decay constant via either desorption of RDX, other unquantified derivatives initially sorbed onto the sediment (eg: hydrazine; McCormick et al., 1981), or mineralization to water soluble products (Halasz and Hawari, 2011). However, unlike TNT, the sediment was not an ultimate sink for RDX and its derivatives since the sediment contained less RDX derived ^{15}N over the experiment and decreased with time.

Both dissolved RDX (Halasz and Hawari, 2011) and nitroso-derivatives (MNX and DNX; Smith et al., 2015a) were mineralized (13%) by anaerobic microbes forming N_2 in addition to other DIN species and ultimately in the nitrogen cycle as the best case scenario of removal of RDX and derivatives from marine ecosystems. Similarly to TNT systems, PCA gives robust interpretations for identifying pathways of anaerobic mineralization of RDX (Figure 4.5B). PC1 reflects the duration of the experiment, with fresh RDX in both dissolved and sorbed phases plotting in the far right quadrant, and continual production of NH_4^+ approaching steady state as a mineralization product in the far left quadrant. Two distinct shaded regions, 1 and 2 in the PCA plot of RDX systems suggest two possible pathways of anaerobic mineralization of RDX including production of NH_4^+ (region 1) and N_2 (region 2) in marine sediments and the proposed mechanisms are illustrated in Figure 4.6. NH_4^+ production approached steady state by end of the experiment confirming NH_4^+ as one of the final mineralization products of RDX that

resulted from mono-denitration of RDX leading to the predominant formation of methylenedinitramine (MEDINA) which is unstable in water and decomposes to NH_4^+ and formaldehyde in anaerobic conditions (Halasz and Hawari, 2011). Moreover, NH_4^+ production, reduced sulfur and iron species were clustered together in the PCA plot inferring the involvement of iron and sulfate reducers in the sediment on NH_4^+ production from RDX in agreement with previously published work (Pichtel, 2012; Boopathy et al., 1998). The second mineralization pathway includes steady state production of N_2 via denitration of RDX and/or nitroso derivatives followed by denitrification of resulted NO_X (Smith et al., 2015a), which act as intermediates in the process. The maximum measured NO_X production is 2% in our anaerobic slurries whereas (Fuller et al., 2016) has reported the nitrite production and isotopic fractionation in both anaerobic and aerobic systems, giving a nitrite yield up to around 16% in the apparent absence of coexisting nitrite reduction. NH_4^+ production out-competes N_2 formation since almost 40% of detected mineralization products were accounted by NH_4^+ at the end of the experiment in this study. Missing ^{15}N in the system also showed a strong linear correlation (R^2= 0.83) with NH_4^+ production suggesting the majority of missing ^{15}N is related to unquantified mineralization products resulting from the pathway of NH_4^+ formation, as was seen for TNT. It has been documented that nitrous oxide (N_2O), though not quantified in this study, can also be formed via both pathways of mineralization discussed in this study which include breakdown of MEDINA (Halasz and Hawari, 2011) and denitrification of NO_X (Smith et al., 2015a). Therefore, further research is recommended for improved mass balancing of the system that includes tracing N_2O production.

Finally, unlike TNT, mineralization was more prominent in the RDX system because of its structural properties and the prevailing anaerobic conditions in these sediment systems. Lack of aromatic stability, weaker (<2 kcal/mol), inner C-N bonds (Hawari et al., 2000), lower sorption of RDX onto sediment (which results in lower shielding of RDX from decomposition; Han et al., 2016) facilitate higher mineralization rates of RDX in marine sediments compared to TNT. Unidentified pools of N-RDX in nitro groups at the end of the experiment (69% of spiked RDX) may include unquantified mineralization products and bacterial incorporated nitrogen which accounts for 0.1% to 34% of the unknown pool (from 0.75hr to end of the experiment) based on the published bacterial incorporation rates in marine sediments (Montgomery et al., 2013).

It is clear that marine sediment plays an important role in mineralization providing favorable anaerobic conditions, iron bearing minerals and natural microbial assemblages that enhance transformation of RDX. Overall mineralization in terms of measured nitrogen containing mineralization products (NH_4^+ and N_2) dominates sorption and biodegradation of RDX as the most significant removal mechanism from marine ecosystems.

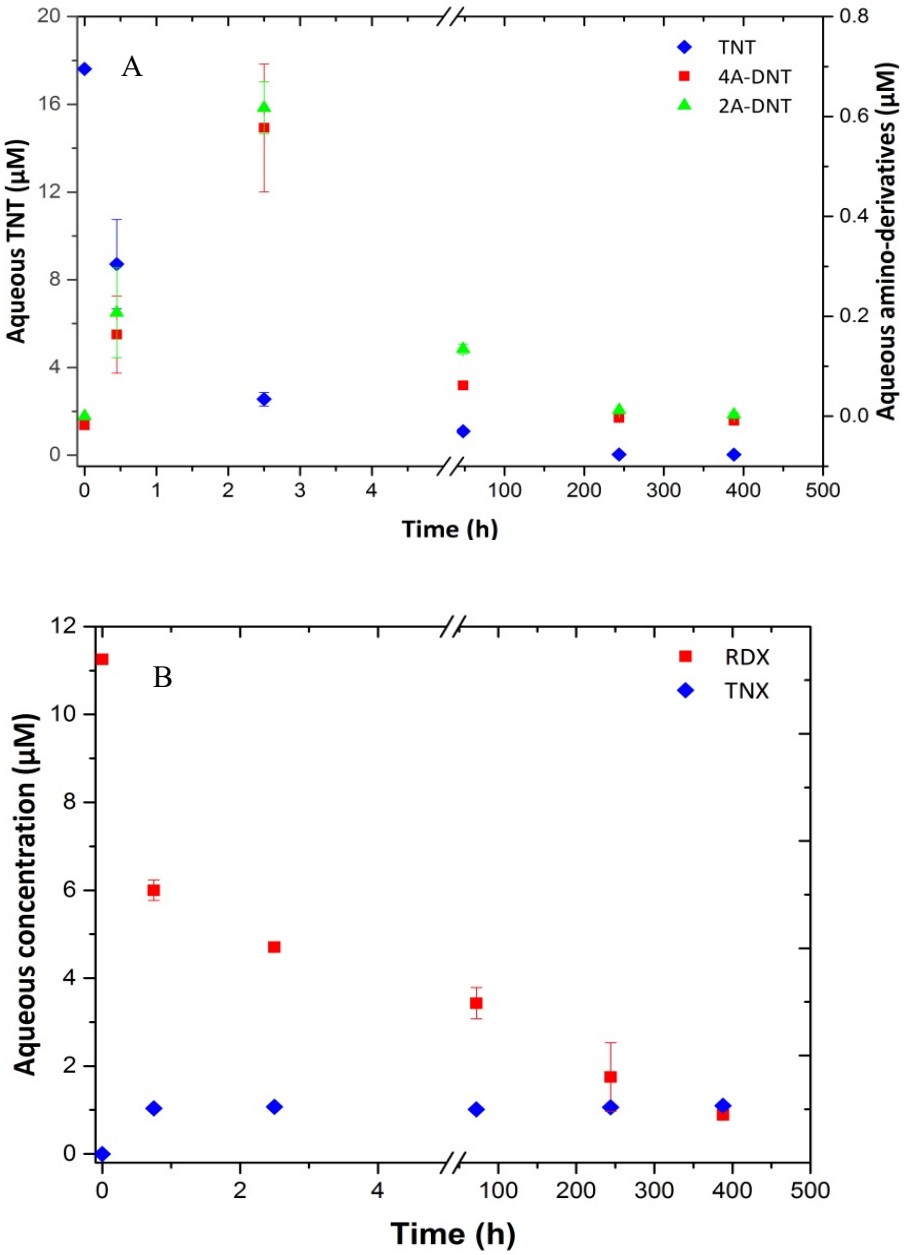

Figure 4.1. Time series aqueous concentrations of (A) 2,4,6-trinitrotoluene and amino derivatives and (B) hexahydro-1,3,5-trinitro-1,3,5-triazine and nitroso derivatives. 2A-DNT-2-amino-4,6-dinitrotoluene; 4A-DNT- 4-amino-2,6-dinitrotoluene; RDX-hexahydro-1,3,5-trinitro-1,3,5-triazine; TNT-2,4,6-trinitrotoluene; TNX-hexahyro-1,3,5-trinitroso-1,3,5-nitro- 1,3,5-triazine.

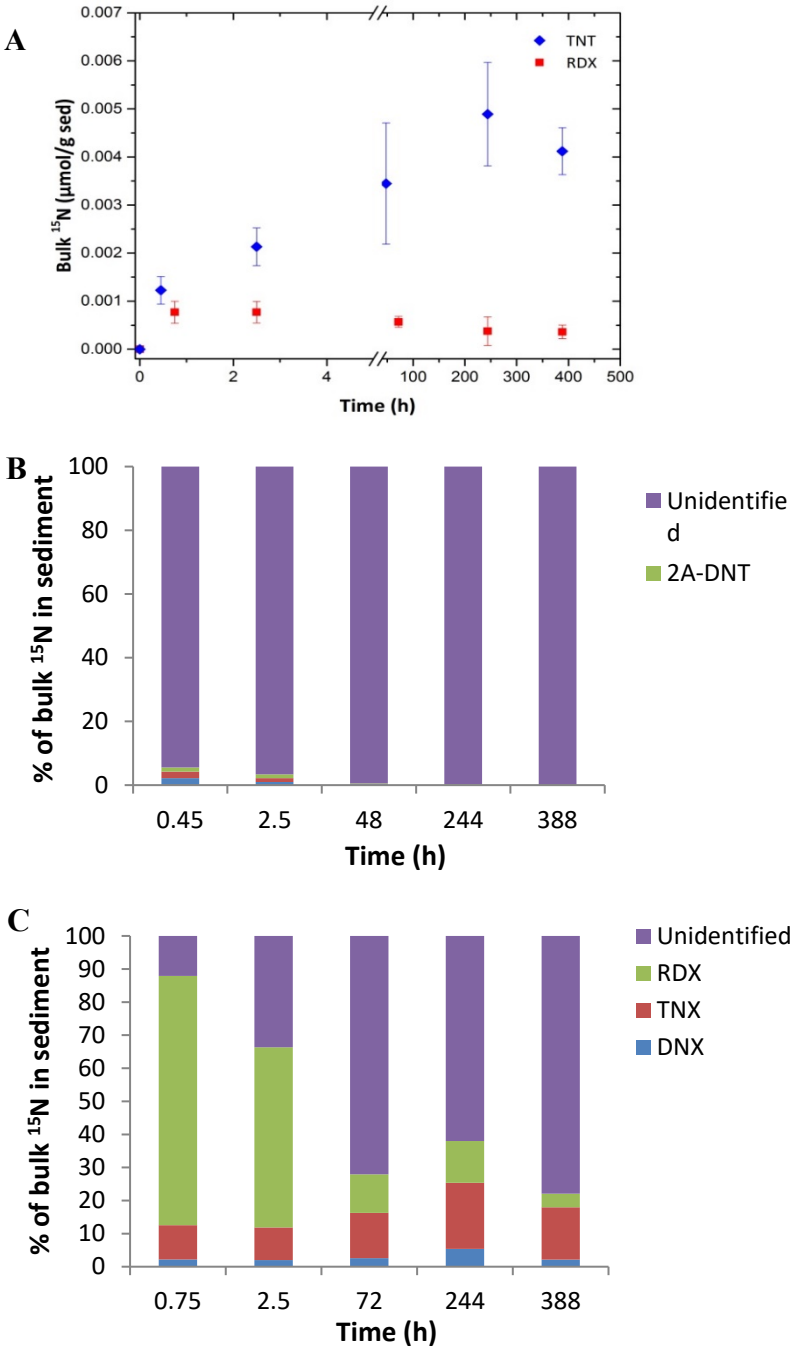

Figure 4.2. Time series (A) bulk ^{15}N concentrations in sediments for 2,4,6- trinitrotoluene (TNT) and hexahydro-1,3,5-trinitro-1,3,5-triazine (RDX) treatments. (B) Contribution of total ^{15}N in sediment by munitions for TNT treatments. (C) Contribution of total ^{15}N in sediment by munitions for RDX treatments. 2A-DNT=2-amino-4,6-dinitrotoluene; 4A-DNT=4-amino- 2,6-dinitrotoluene; DNX¼hexahyro-1,3-dinitroso-5-nitro-1,3,5-triazine; RDX=hexahydro-1,3,5-trinitro-1,3,5-triazine; TNT=2,4,6-trinitrotoluene; TNX=hexahyro-1,3,5-trinitroso-1,3,5-nitro-1,3,5-triazine.

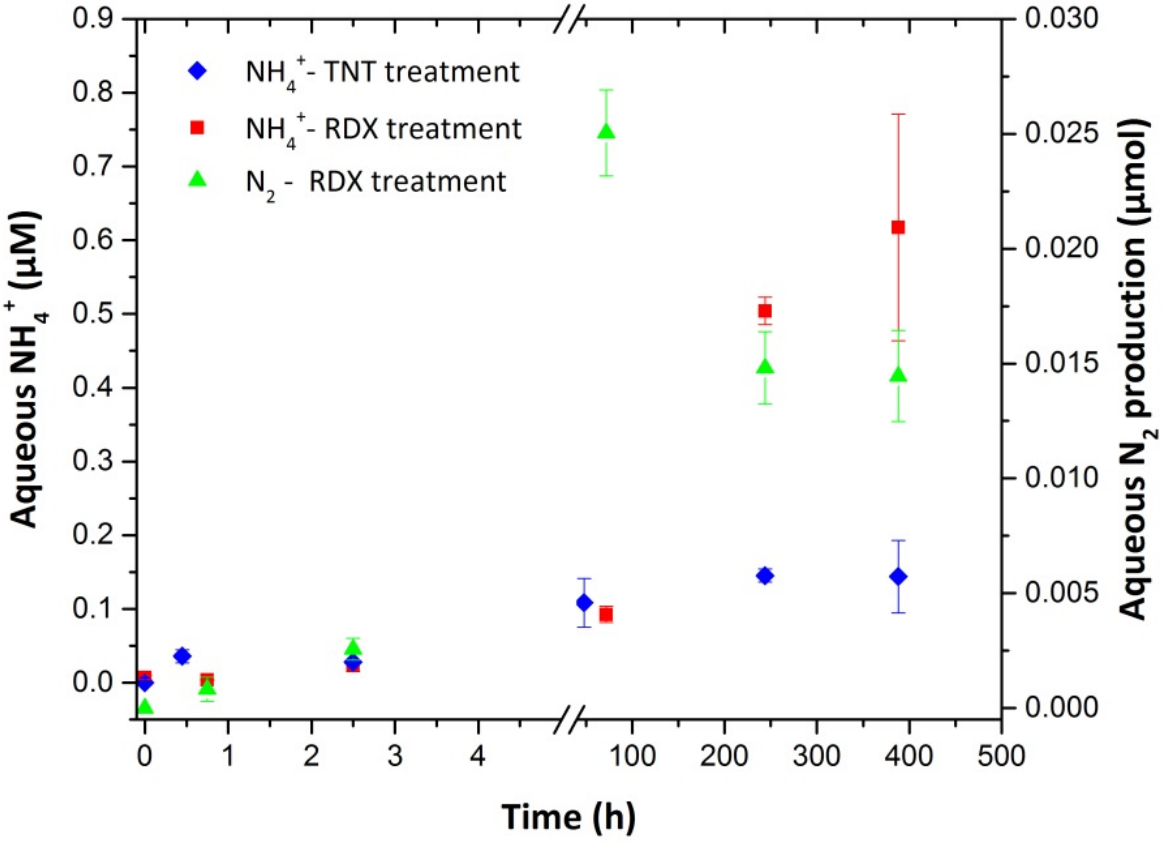

Figure 4.3. Time series variation of munition-derived NH_4^+ and N_2 in both 2,4,6-trinitrotoluene (TNT) and hexahydro-1,3,5-trinitro-1,3,5-triazine (RDX) sediment slurries.

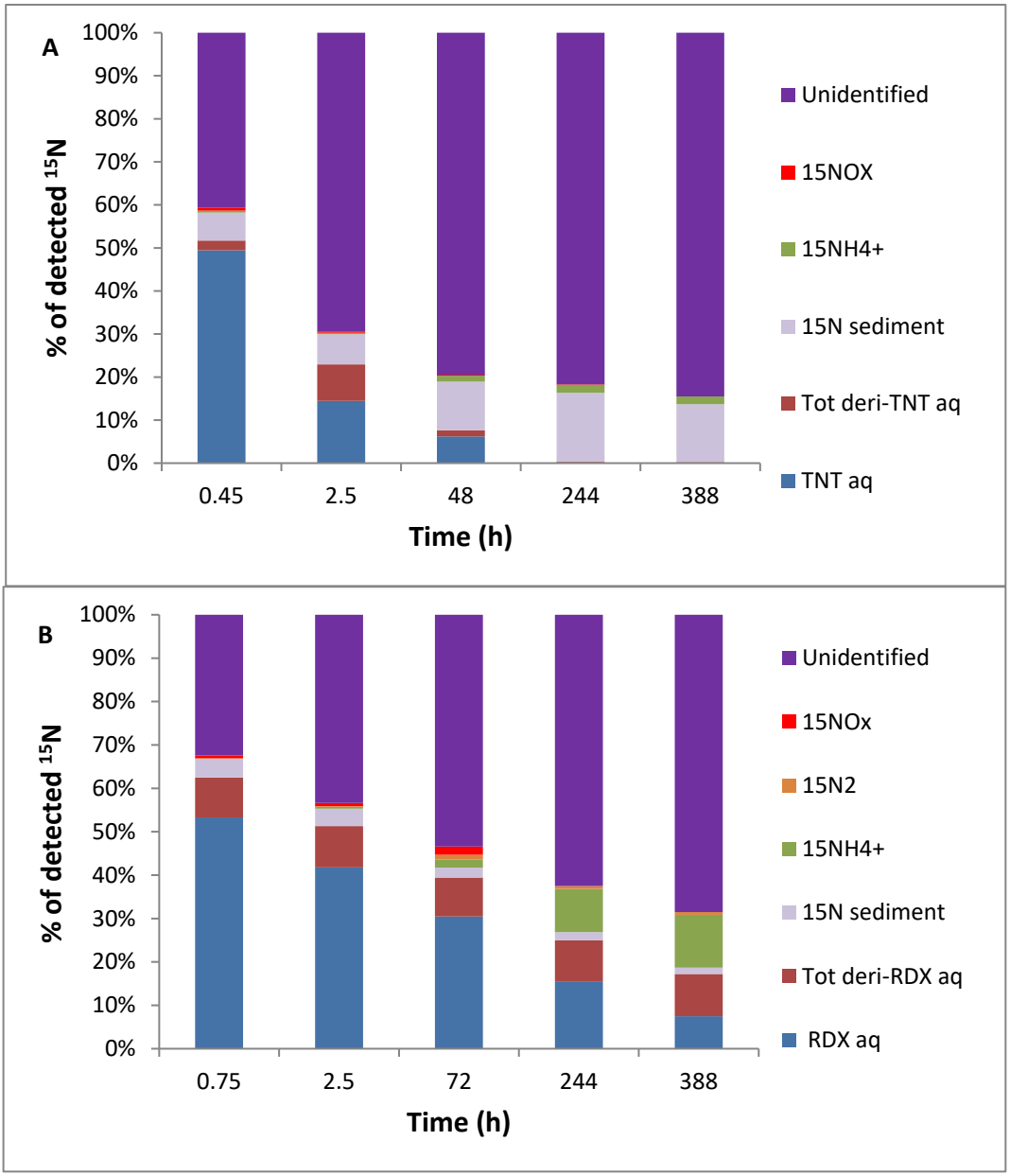

Figure 4.4. Time series full ^{15}N mass balance based on ^{15}N added to the system for (A) 2,4,6-trinitrotoluene treatments and (B) hexahydro-1,3,5- trinitro-1,3,5-triazine treatments. RDX=hexahydro-1,3,5-trinitro-1,3,5- triazine; TNT=2,4,6-trinitrotoluene; Tot deri-RDX Aq=aqueous hexahydro-1,3,5-trinitroso-1,3,5-nitro-1,3,5-triazine; Tot deri-TNT Aq=aqueous 2-amino-4,6-dinitrotoluene and 4-amino-4,6-dinitrotoluene.

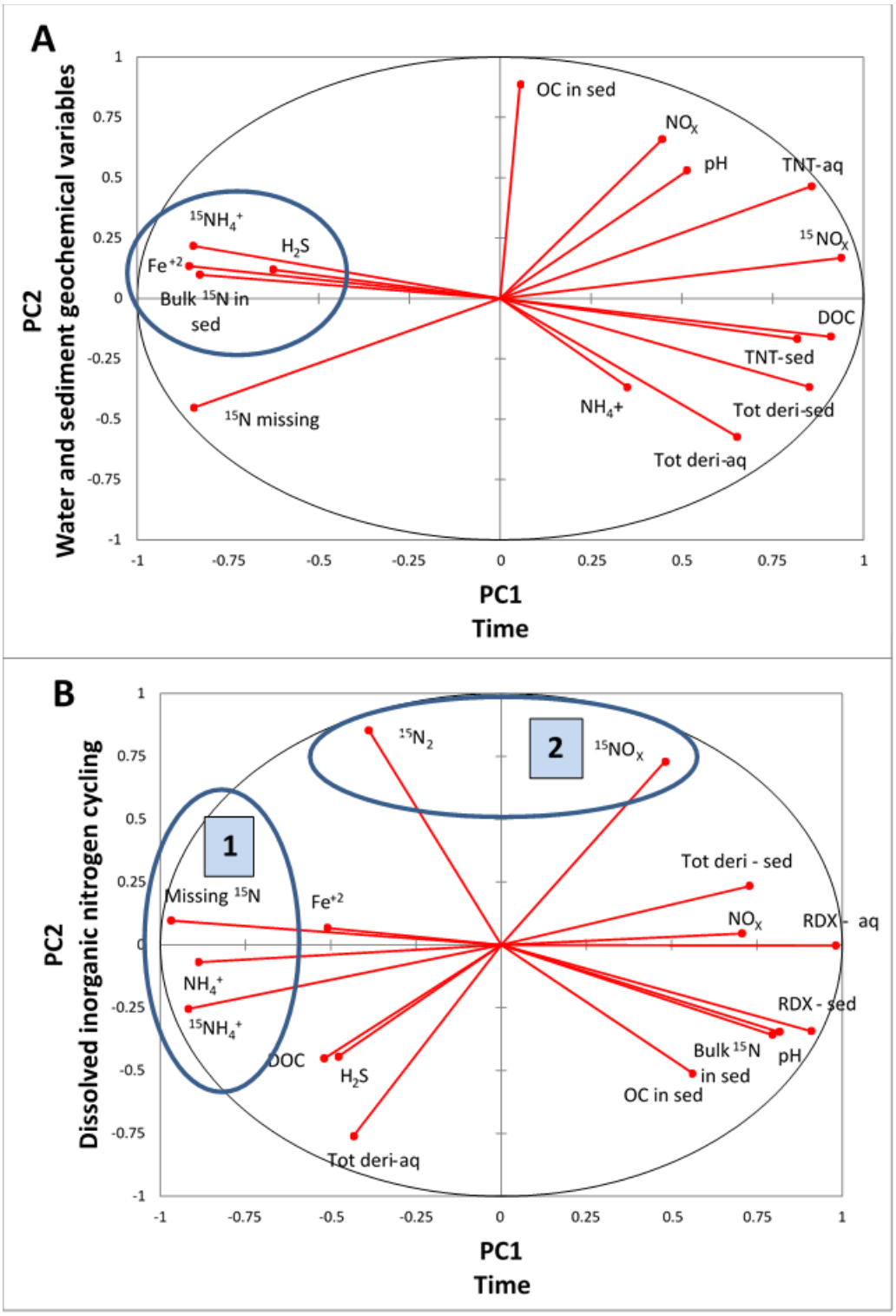

Figure 4.5. Principal component (PC) analysis of (A) 2,4,6-trinitrotoluene microcosm. Circled box shows correlation of $^{15}NH_4^+$ production and reduced iron and sulfur species in sediment; PC1 and PC2 represent 54% and 17% variability, respectively. (B) Hexahydro-1,3,5-trinitro-1,3,5- triazine microcosm; PC1 and PC2 have 52% and 20% variability, respectively.

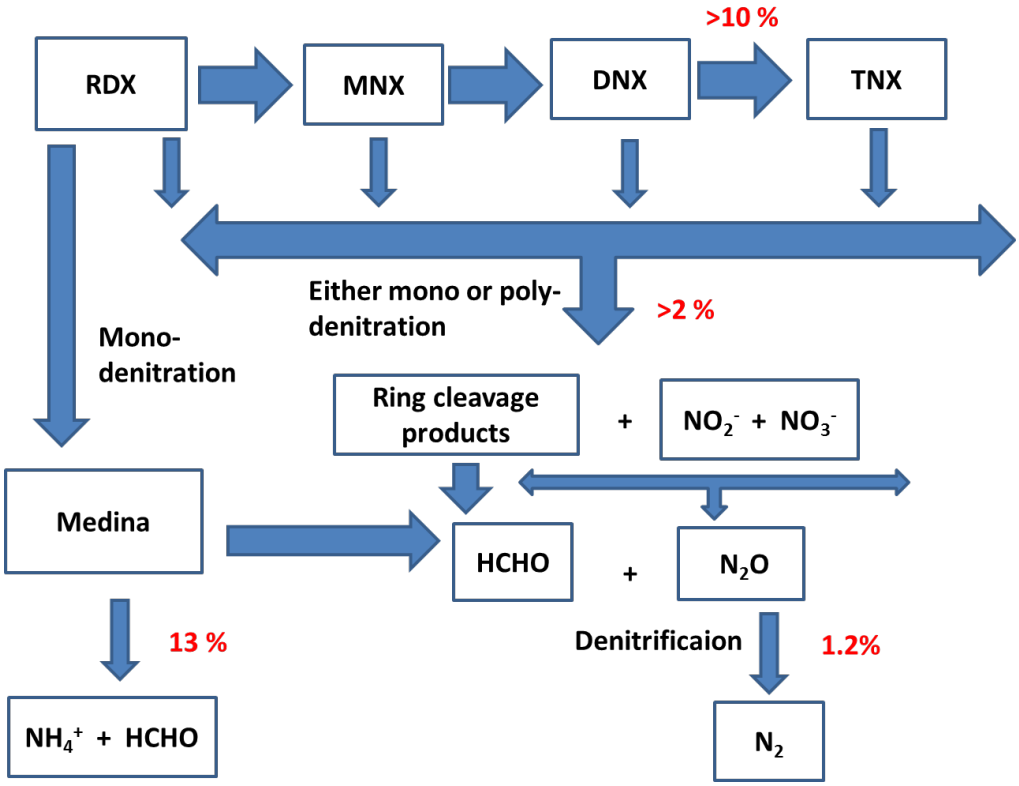

Figure 4.6. Proposed hexahydro-1,3,5-trinitro-1,3,5-triazine anaerobic mineralization pathway. Modified from Smith et al. (2015) and Halasz and Hawari (2001).

Table 4.1. Time series variation of chemical and physical properties of slurry water for 2,4,6-trinitrotoluene and hexahydro-1,3,5-trinitro-1,3,5-triazine experiments.

Treatment	Time point	Physical properties		Chemical properties				
		pH	Redox(mV)	DOC (μM)	NH_4^+ (μM)	Tot. NO_2^- & NO_3^- (μM)	H_2S (μM)	Fe^{+2} (μM)
TNT	T0	7.41±0.01	41.13±2.66	1685±56	36±4	3.4±1.2	ND	2.20±0.08
	T1	7.33±0.05	54.30±2.59	2437±405	70±16	7.6±3.0	ND	2.54±0.19
	T2	7.03±0.02	39.93±5.20	2419±68	78±8	0.22±0.22	ND	4.30±1.33
	T3	7.19±0.09	29.40±3.93	2066±569	86±25	2.1±0.4	ND	3.48±1.26
	T4	6.97±0.05	-26.1±19.95	909±20	24±15	3.5±1.8	ND	18.15±6.62
	T5	7.10±0.18	-133.5±4.95	918±184	21±16	ND	70.41±0.39	33.27±0.39
RDX	T0	7.50±0.08	83.37±2.00	1912±27	196±1	1.3±0.8	ND	6.94±2.34
	T1	7.53±0.16	73.97±0.91	2423±8	27±3	4.2±2.7	ND	3.95±0.63
	T2	7.38±0.05	69.57±0.90	2669±312	48±4	4.6±2.5	ND	4.10±0.36
	T3	7.17±0.01	59.33±1.53	2432±323	136±91	3.8±0.9	ND	12.62±1.53
	T4	7.03±0.12	47.03±22.3	1759±435	398±236	0.19±0.08	ND	33.92±18.32
	T5	7.14±0.09	-231±64.37	1262±263	373±61	0.17±0.09	530.94±20.32	91.54±10.26

T0, T1, T2, T3, T4 and T5 represent 0, 0.45, 2.5, 48, 244, 388 hr for TNT treatments and 0, 0.75, 2.5, 72, 244, 388 hr for RDX treatments throughout the experimental time periods.

DOC = Dissolved organic carbon includes the spike of munitions

NH_4^+ = ammonium

Tot. NO_2^- & NO_3^- = Total nitrite and nitrate

H_2S = Hydrogen Sulfide

Fe^{+2} = Ferrous

ND = not detected

Table 4.2. First-order rate constants of production and loss of analytes in anaerobic marine sediment slurries at 23°C.

Treatment	Medium	Analyte	Rate constant (hr^{-1})	
			Production Rate	Loss Rate
TNT/Abiotic	Aqueous	TNT	-	0.53 (R^2 = 0.78)
TNT/Biotic	Aqueous	TNT	-	0.75 (R^2=0.94)
		4A-DNT	0.030 (R^2=0.99)	0.56 (R^2=0.85)
		2A-DNT	0.028 (R^2=0.99)	0.52 (R^2=0.98)
		NH_4^+	0.047 (R^2=0.42)	Steady state at day10
		NO_X	0.47 (R^2=1)	0.0067 (R^2=0.85)
	Sediment	Bulk ^{15}N	0.017 (R^2=0.99)	Steady state at day 2
		TNT	Peaks at 0.45hr	0.0049 (R^2=0.89)
		4A-DNT	0.095 (R^2=1)*	0.046 (R^2=0.54)
		2A-DNT	0.19 (R^2=1)*	0.16 (R^2=0.59)
RDX/Abiotic	Aqueous	RDX	-	0.31 (R^2 = 0.87)
RDX/Biotic	Aqueous	RDX	-	0.37 (R^2=0.79)
		TNX	Peaks at 0.75hr	Steady state at 0.75hr
		NH_4^+ -initial	0.017 (R^2=0.83)	Approaching steady state
		NH_4^+ -final	0.0061 (R^2=0.87)	after16 days
		NO_X	0.0138 (R^2=0.99)	Not calculated
		N_2	0.041 (R^2=0.91)	Steady state at day 3
	Sediment	Bulk ^{15}N	Peaks at 0.75hr	0.0021 (R^2=0.86)
		RDX	Peaks at 0.75hr	0.0091 (R^2=0.87)
		DNX	Peaks at 0.75hr	0.0006 (R^2=0.88)
		TNX	0.0005 (R^2 =0.69)*	0.0012 (R^2=0.80)

Abiotic removal rates were obtained from Ariyarathna et al., 2015 under similar experimental conditions. Loss rate of NOx was not calculated due to the limited data availability not enough measurable data points to calcultion.

*Rates of DNT's and TNX in sediments are appearance rates and represent both sorption equilibrium with the dissolved phase and transformation of TNT on the sediment

Table 4.3. Time series aqueous, sediment, and total percentages of parent and transformation products in TNT and RDX microcosms.

-

Treatment	Time (hr)	Parent compound %			Trans. products %		
		Aq	Sed	Tot	Aq	Sed	Tot
TNT	0	100.00	0	100.00	0	0	0
	0.45	49.47	0.09	49.56	2.25	0.13	2.38
	2.5	14.49	0.08	14.57	8.45	0.17	8.62
	48	6.19	0.04	6.23	1.46	0.04	1.50
	244	0.20	0.02	0.22	0.19	0.03	0.22
	388	0.16	0.01	0.17	0.09	0	0.09
RDX	0	100.00	0	100.00	0	0	0
	0.75	53.28	2.67	55.95	9.20	0.44	9.64
	2.5	41.79	1.98	43.77	9.50	0.43	9.93
	72	30.46	0.36	30.82	8.97	0.44	9.41
	244	15.54	0.11	15.65	9.46	0.33	9.79
	388	7.52	0.07	7.59	9.73	0.29	10.02

Trans. = Transformation products

Aq = Aqueous

Sed = Sediment

Tot = Total in aqueous and sediment

ND = No data

Table 4.4. Dissolved inorganic nitrogen (NH_4^+, N_2, and NO_X) production from TNT and RDX.

Treatment	Time (hr)	δ $^{15}NH_4^+$	δ $^{15}NO_X$	δ $^{15}N_2$	nmol Excess $^{15}NH4^+$	nmol Excess $^{15}NO_X$	nmol Excess $^{15}N_2$	Munition derived DIN %
TNT	0	12.69	11.84	-1.77	0.83	0.300	0	0
	0.45	144.5	3203	-0.08	15.99	21.76	0	1.07
	2.5	89.01	6295	-0.70	12.48	10.89	0	0.66
	48	376.5	4654	-0.34	48.15	7.84	0	1.59
	244	2987	3424	-0.93	64.55	2.85	0	1.92
	388	1714	0	-0.67	63.85	0	0	1.81
RDX	0	10.06	0	-1.23	3.08	0	0	0
	0.75	100.9	1123	0.5	1.73	15.57	0.83	0.81
	2.5	159.9	1089	2.39	10.20	16.84	2.57	1.32
	72	311.7	9227	23.97	41.17	42.65	25.04	4.84
	244	420.5	0	14.92	223.9	0	14.81	10.61
	388	463.9	0	14.08	274.2	0	14.46	12.66

Values correspond to 0 hr indicate before spiking background levels and all the other data points are corrected for background values. Spiked ^{15}N equivalents of TNT and RDX treatments are 3520 nmol and 2250nmol respectively.

ND = No data

Supplementary Material

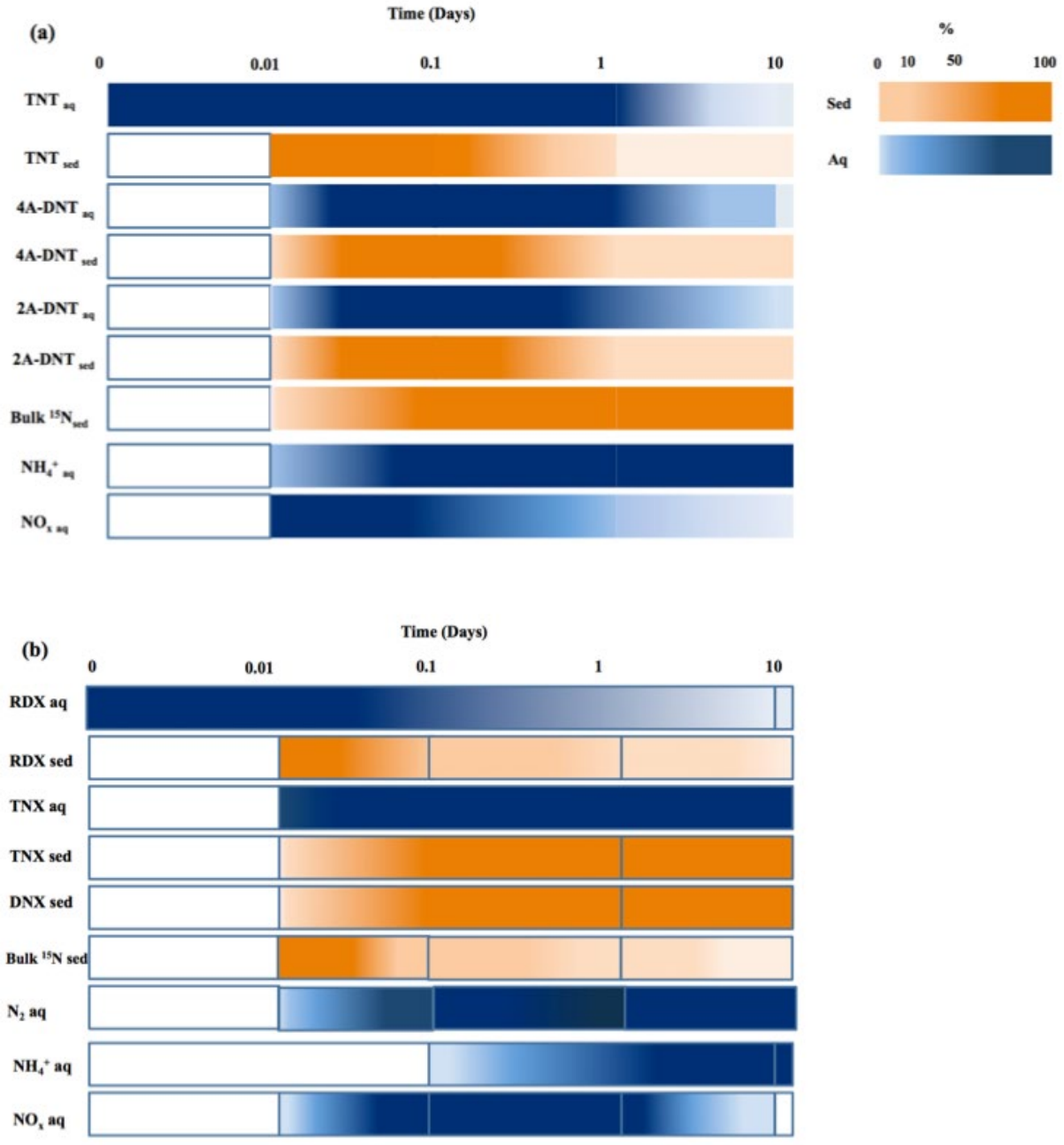

Supplementary Figure S-4.1. Gantt Chart for timeline of events a) TNT microcosms b) RDX microcosms. Blue (aqueous) and orange (sediment) color intensities denote relative contributions to total compound loss.

Supplementary Table S-4.1. Concentrations of TNT and RDX removed by biotic component in microcosms.

Time (hr)	Biotically removed TNT (μM)	Biotically removed RDX (μM)
0.45	2.7	-
0.75	-	1.0
2.5	1.3	1.6
48	3.7	-
72	-	2.7
244	4.2	4.0
388	4.2	4.8

It was calculated by subtracting abiotic aquatic concentrations (Ariyarathna et al., 2015) from aquatic concentrations in biotic treatment in current study.

Supplementary Table S-4.2. Munition profile comparison of a) TNT b) RDX microcosms.

a)

Treatment	Time (hr)	Dissolved (µM)			Sediment (ng/g sed)		
		TNT	4A-DNT	2A-DNT	TNT	4A-DNT	2A-DNT
Biotic	0.45	8.7	0.25	0.23	14	10	7.9
	2.5	2.6	0.81	0.68	12	12	12
	48	2.0	0.11	0.15	5.6	1.3	3.7
	244	0.035	0.02	0.013	2.4	0.9	2.8
	388	0.028	0.01	0.0035	1.9	BD	BD
Abiotic	0.75	7.0	0.46	0.012	-	-	-
	2	5.6	0.42	0.052	-	-	-
	48	4.8	0.4	0.041	-	-	-
	122	4.3	0.39		-	-	-
	150	4.2	0.36		1067	BD	BD

b)

Treatment	Time (hr)	Dissolved (µM)				Sediment (ng/g sed)			
		RDX	MNX	DNX	TNX	RDX	MNX	DNX	TNX
Biotic	0.75	6.0	BD	BD	1.0	267	BD	6.6	29
	2.5	4.7	BD	BD	1.1	198	BD	6.2	28
	72	3.4	BD	BD	1.0	36	BD	6.1	30
	244	1.8	BD	BD	1.1	11	BD	5.3	21
	388	0.89	BD	BD	2.0	7	BD	5.3	21
Abiotic	0.75	7.0	3.4	BD	4.0	-	-	-	-
	2	5.7	3.1	3.2	3.6	-	-	-	-
	48	6.1	3.0	BD	3.6	-	-	-	-
	122	5.7	BD	BD	3.6	-	-	-	-
	150	5.6	BD	BD	3.8	794	104	101	BD

Data related to the abiotic treatment was taken from Ariyarathna et al., 2015.

BD = below detection

Supplementary Table S-4.3. Chemical and textural properties of marine sediment used for both TNT and RDX systems in this study (n=3).

	Property	Value
Particle size distribution data	Sand (%)	44
	Silt & clay (%)	56
	Statistical parameters	
	1.Graphic mean (mm)	0.16
	2.Median (mm)	0.11
	3.IGSD (mm)	0.16
Physical properties	Bulk density(gcm^{-3})	1.4
	Porosity (%)	45.6
Chemical properties	TOC (mgg^{-1}sed)	4.10 ± 0.69
	TN (mgg^{-1}sed)	0.62 ± 0.25
	S (mgg^{-1}sed)	3.7 ± 0.3

IGSD = Inclusive Graphic Standard Deviation

TOC = Total Organic Carbon

TN = Total Nitrogen

S = Elemental Sulfur

Supplementary Table S-4.4. Time series bulk $\delta^{15}N$ values in sediment in TNT and RDX microcosms.

Time (hr)	Bulk $\delta^{15}N$ (‰)	
	TNT microcosm	RDX microcosm
0	6	9
0.45	122	-
0.75	-	31
2.5	148	34
48	165	-
72	-	47
244	170	29
388	171	30

Supplementary Table S-4.5. Bacterial incorporation of ^{15}N from TNT and RDX in microcosms.

Time (hr)	Incorporated µmols		Incorporated %	
	TNT	RDX	TNT	RDX
0.45	0.002	-	0.5	-
0.75	-	0.0003	-	0.1
2.5	0.01	0.001	2	0.3
48	0.2	-	26	-
72	-	0.03	-	8
244	1	0.1	100	23
388	2	0.2	100	34

Bacterial incorporated quantity is in µmols TNT and µmols RDX; Incorporated % represents percentage of bacterial incorporation of unidentified pool in TNT and RDX microcosms; Bacterial incorporation rates in marine sediments from Montgomery et al., 2013 was used for the calculations.

5.0. Mineralization of RDX-derived Nitrogen to N_2 via Denitrification in Coastal Marine Sediments

This chapter was published, as follows:

Smith, R. W.; Tobias, C.; Vlahos, P.; Cooper, C.; Ballentine, M.; Ariyarathna, T.; Fallis, S.; Groshens, T. J. Mineralization of RDX-derived nitrogen to N_2 via denitrification in coastal marine sediments. Environmental Science and Technology, DOI: 10.1021/es505074v.

Abstract

Hexahydro-1,3,5-trinitro-1,3,5-triazine (RDX) is a common constituent of military explosives. Despite widespread RDX contamination at U.S. military facilities and its mobility to aquatic systems, the fate of RDX in marine systems remains largely unknown. Here, we provide RDX mineralization pathways and rates in seawater and sediments, highlighting for the first time the importance of the denitrification pathway in determining the fate of RDX-derived N. ^{15}N nitro group labeled RDX (^{15}N-[RDX], 50 atom %) was spiked into a mesocosm simulating natural shallow marine conditions of coastal Long Island Sound, and the ^{15}N enrichment of N_2 ($\delta^{15}N_2$) was monitored via gas bench isotope ratio mass spectrometry (GB-IRMS) for 21 days. The ^{15}N tracer data were used to model RDX mineralization within the context of the broader coastal marine N cycle using a multi-compartment time-stepping model. Estimates of RDX mineralization rates based on the production and gas transfer of $^{15}N_2O$ and $^{15}N_2$ ranged from 0.8 to 10.3 μmol d^{-1}. After 22 days, 11% of the added RDX had undergone mineralization, and 29% of the total removed RDX-N was identified as N_2. These results demonstrate the important consideration of sediment microbial communities in management strategies addressing prevention and cleanup of contaminated coastal sites by military explosives.

5.1. Introduction

The 15 million acres of former and current military sites in the U.S. known or suspected to be contaminated with munitions is expected to cost $8 billion to $35 billion in cleanup over 75 years, incentivizing research into the transport and fate of explosive chemicals in the environment (GAO, 2003). Hexahydro-1,3,5-trinitro-1,3,5-triazine (RDX) is one of the most common chemical constituents in munitions, produced in enormous quantities during and after WWII (USAEHA, 1985). RDX is extremely mobile in the environment, and groundwater contamination at military sites has been well documented (USEPA, 1999). The ease of transport to aquatic environments has created concerns of RDX contamination in marine systems such as wetlands, estuaries, and coastal waters adjacent to contaminated military sites (Walsh et al., 2010); for example the Waikoloa Maneuver Area on Hawaii Island (GAO, 2003, Alavi et al., 2011) and the Vieques Naval Training Range (VNTR) on Bahia Salinas del Sur Vieques, Puerto Rico (McDonald, 2009).

Mineralization of RDX to soluble and/or gaseous inorganic N and C compounds (i.e. CO_2, CH_4, N_2O, N_2, NO_3^-, NO_2^-) represents a "best case" scenario of removal from the environment (Hawari et al., 2000a). Accurate estimation of RDX mineralization rates in the environment is a key factor in evaluating the feasibility of monitored natural attenuation remediation strategies of RDX contaminated sites, and informs assessments of long-term human and environmental health impacts (Pennington et al., 1999). In soils, the extent of RDX mineralization is only on the order of a few percent over annual timescales (Sheremata et al., 2001), and can be further inhibited through the presence of TNT, commonly co-occuring with RDX in explosive mixtures (Sagi-Ben Moshe et al., 2009). RDX is instead partially converted biotically to reduced derivatives (hexahydro-1-nitroso-3,5-dinitro-1,3,5-triazine (MNX), hexahydro,1-3-dinitroso-5-nitro-1,3,5-trizaine (DNX), and hexahydro-1,3,5-trinitroso-1,3,5-triazine (TNX); which are also mobile in the environment (Sheremata et al., 2001; Sagi-Ben Moshe et al., 2009; Pennington et al., 2011). It is therefore critical to determine what role the biogeochemical characteristics of marine waters and sediments vs. terrestrial soils will play in the eventual fate of RDX and derivatives. Marine sediments differ from soils in several crucial ways that dictate the pathways and extent of the breakdown of organics (Hedges and Oades, 1997). Fine-grained, organic rich, marine sediments with well-established anaerobic zones facilitate in the removal of RDX from marine systems (Smith et al., 2013), yet the mechanism of removal, and the extent of mineralization remain unknown.

Isotopically labeled 'tracer' compounds can provide unique insight into the fate of contaminants. RDX mineralization rates are commonly estimated by monitoring the evolution of $^{14}CO_2$ from incubations containing radiolabeled [^{14}C]-RDX. This approach has been utilized to observe mineralization rates in laboratory incubations containing contaminated groundwater, white rot fungus, constructed wetlands, soils, municipal sludge, strong oxidants, bacterial isolates, and in aquatic systems (Best et al., 1998; Kwon et al., 2011; Sheremata and Hawari, 2000; Sheremata et al, 2001; Zoh et al., 2002; Price et al., 1998; Ronen et al., 2008; Hawari et al., 2000b; Beller 2002; Sikka et al., 1980; Montgomery et al., 2011; Montgomery et al., 2013). These studies have identified conditions that promote mineralization of the carbon (C)-containing triazine ring. Useful bioremediation guidance has resulted from these efforts, but the high N/C ratio in nitroamine explosives such as RDX (2:1) leaves the fate of the majority of the molecule unknown if only carbon mineralization is traced.

A much more limited dataset exists on nitrogen containing gaseous products of RDX mineralization, and no data to our knowledge exists for marine systems. The production of $^{15}N_2O$ from ^{15}N-[RDX] was observed in slurries with municipal anaerobic sludge (Hawari et al., 2000b), providing the first evidence of RDX-N mineralization of both the ring and nitro groups. N_2O has since been observed using this technique in aerobic incubations with white rot fungus (Sheremata and Hawari, 2000) and natural soils (Sheremata et al. 2001). N_2, however, has not been reported as an end product of RDX mineralization. The few studies that have monitored the evolution of N_2, through the use of triazine ring-labeled ^{15}N-[RDX] (Sheremata et al., 2001; Sheremata and Hawari, 2000), or controlled incubation headspaces (Bhushan et al., 2002a), have documented production of significant amounts of N_2O from RDX degradation without the observing production of N_2. However, N_2 and N_2O production resulting from RDX breakdown has not been evaluated in marine systems, where N_2O is unstable and typically rapidly denitrified

to N_2 in anaerobic sediment layers by denitrifying bacteria (Seitzinger et al., 2000; Hulth et al., 2005; Seitzinger et al., 2006; Devol, 2008).

Here, we document significant production of N_2 and N_2O from the denitrification of RDX ring-breakdown products ("RDX-Denitrification") in aquaria-scale marine mesocosms containing seawater and sediments from Long Island Sound. Nitro-group labeled ^{15}N-[RDX] was used as a substrate to quantify the evolution of dissolved $^{15}N_2$ and $^{15}N_2O$ over a period of 22 days. The experimental data, combined with a box model (the "RDX-DIN model") containing portions of the marine dissolved inorganic nitrogen (DIN) cycle and select RDX breakdown pathways was used to estimate mineralization rates of RDX in shallow coastal marine systems.

5.2. Materials and Methods

5.2.1 Experimental Design

The goal of the experimental setup was to mimic natural RDX biodegradation processes that occur in shallow-water marine systems at the sediment/water interface. A 150 l recirculating paired tank system connected to a common reservoir was used as described in Smith et al. (2013; Figure S-5.1). Sediments were collected from the subtidal waters of Long Island Sound (LIS), USA and added to 2- 30 gal aquariums in a layer ~7-8 cm deep. 25 cm of overlying LIS water was pumped through the system in an open loop configuration for 15 days after sediment addition to permit sediment acclimation to the experimental set up. After sediment redox gradients were re-established (15 days) the system was switched to a closed loop configuration and water recirculated among the 2 sediment-containing aquaria and a common re-mixing reservoir (Figure S-5.1). Sediment redox potential (E_o) was measured with a platinum electrode at 1 cm increments at four locations in the tank prior to the addition of RDX. Nitro group labeled ^{15}N–[RDX] (50 % ^{15}N of total N in RDX; 100 % ^{15}N in NO_2 groups) was synthesized by S. Fallis and T. Groshens at the Naval Air Warfare Center Weapons Division, Chemistry Division, China Lake, CA. The tracer was introduced as a single slug to the 150 liter system as a concentrated solution dissolved in 1ml acetone targeting a final mixed concentration of 1.0 mg l^{-1}; ~ <10% of the LC_{50} to aquatic organisms (Burton et al., 1994; Mukhi and Patino, 2008; Lotufo et al., 2010). The concentration of RDX and the isotopic distribution of $^{15}N_2$ were monitored in duplicate for a period of 22 days. $^{15}N_2O$ isotopic enrichments in this experiment were modeled (see "Model" section). A follow up experiment in larger tanks using the same RDX tracer, water, sediment, temperature, and salinity was conducted to provide measurements of $^{15}N_2O$ isotopic enrichments used to constrain the RDX-DIN model parameterization. Salinity and temperature ranged from 37.6 to 38.9 and 23-27ºC, respectively, over the course of the experiment**.**

5.2.2 Munitions Analysis

RDX was analyzed by High Performance Liquid Chromatography (HPLC). At each time point, 5 mls of seawater was dispensed into a 15 ml centrifuge tube containing 5ml of ACS grade methanol. The solution was shaken and filtered through a 0.2µm PTFE syringe-tip filter. 20µl was injected on an Agilent 1100/1200 series HPLC equipped with a Zorbax Eclipse C18 column

kept at 43^0C. Solvent flow was isocratic and consisted of 75% phosphate buffer (pH 6) and 25% Optima grade methanol. UV absorbance was monitored at 254 nm. Concentrations were quantified by comparison to an external 5-point calibration curve. RDX standards were obtained as a concentrated solution in acetone from Accustandard, and crystalline MNX, DNX, and TNX were synthesized by Ron Spanggord (Menlo Park, Ca). The precision of RDX concentration measurements in replicate tank samples ranged from 0.4 to 1.2 %. RDX concentrations are given as mg l^{-1} and total μmol in the system to facilitate both comparison to the literature and mass balance of N pools, respectively.

5.2.3 N_2 and N_2O Isotopic Analysis

Gas samples were collected using duplicate sets of 30 ml serum bottles that were sealed, pre-loaded with 100μl of 3M $NaHSO_4$ (preservation -Douglas et al., 2009), and evacuated with He for 15 minutes. 15 ml of overlying water from the tanks were pumped into each bottle using a peristaltic pump, gas impermeable tubing and a 23 gauge needle being careful not to entrain bubbles. Serums were allowed to equilibrate for at least 6 hours prior to analysis.

The ^{15}N isotopic composition of N_2 was measured via continuous flow isotope ratio mass spectrometry (IRMS) on a Thermo Delta V Plus. N_2 in equilibrated headspace samples was chromatographically separated from other major atmospheric gases prior to IRMS analyses using a modified Gas Bench interface equipped with a mol sieve 5A column and 250 μl sampling loop. Measured $^{15}N_2$ values were expressed in the delta notation ($\delta^{15}N_2 = R_{samp}/R_{std}$ -1 x1000), where R_{samp} and R_{std} are the ratios of $^{15}N/^{14}N$ in the sample and air standards, respectively. Measured $\delta\ ^{15}N_2$ values are normalized to air standards and expressed in units of per mil (‰). Analytical precision was typically better than 0.3 ‰.

The ^{15}N composition of N_2O was also measured via continuous flow IRMS interfaced to a modified Gas Bench (GB-IRMS). Dissolved gases in samples were He sparged and passed through a chemical soda lime trap to remove CO_2. N_2O was quantitatively cryo-trapped using liquid N. The trapped N_2O was then released and separated from any remaining trace CO_2 using a poraplot Q column, and then analyzed for ^{15}N-N_2O via IRMS. Low N_2O mass samples were spiked with unlabeled carrier N_2O. Subsequent $^{15}N_2O$ enrichments were calculated from the measured $^{15}N_2O$ and known N_2O carrier masses. Because of high levels of ^{15}N enrichment, $^{15}N_2O$ is reported as atom % excess ^{15}N (at. %). Precision of the $^{15}N_2O$ enrichments is on the order of 1-3 at. % against observed enrichments of 20-50 at%.

5.2.4 Gas Transfer

The value of the N_2 aeration coefficient was derived from an argon aeration coefficient measured from time series dissolved argon concentrations in the experimental tank following a slug addition of argon super saturated water (Douglas et al., 2009). The argon slug addition to the tank was done immediately prior to the RDX addition. Dissolved argon was measured via membrane inlet quadrupole mass spectrometry (MIMS; Figure S-5.2) and the argon aeration coefficient converted to a N_2 aeration coefficient through the Schmidt # ratio of the two gases (Wanninkof 1992).

An RDX transformation model was created based on previously described pathways (Hawari et al., 2000a), and the inclusion of denitrification pathways (Figure S-5.3). Rates of RDX breakdown to N_2O and to unmeasured ring products as well as all atmospheric exchanges were modeled using first order kinetics (for equations and assumptions see supplementary material). Ambient DIN (non-RDX derived DIN) conversion to N_2O, and N_2O conversion to N_2 via denitrification were modeled as zero order reactions with respect to DIN and N_2O concentrations due to the large size of the ambient DIN pool and organic carbon limitation of the final N_2O to N_2 reduction step, respectively. Gas exchange was modeled for both N_2O and N_2 using first order aeration coefficients and gas disequilibria for each gas each isotope as described in Eqn. S4. The full set of equations and assumptions of the model are included in the supplementary material, and kinetic orders and rates are given in Table S-5.1.

5.3. Results

5.3.1 RDX Concentrations and Removal Rates

Of the initial 800 μmol of RDX spiked into the system, 359 μmoles; ~ 44% remained after the 22 d period (Figure 5.1). The initial concentration of RDX was 1.13 mg l^{-1}, which exhibited first-order degradation to 0.50 mg l^{-1} over the course of the experiment. The first order rate constant (k = 0.037) translates to a half-life of 18.7 days, and is within the range of RDX removal rates observed for marine systems, freshwater, and groundwater (Smith et al., 2013). No reduced derivatives (TNX, DNX, MNX) were measured above the detection limit of the HPLC (~ 0.02 mg l^{-1}), and quantification methods for ring breakdown products were not performed.

5.3.2 $^{15}N_2$ Production from ^{15}N-[RDX]

We determined the evolution of $^{15}N_2$ from RDX by observing changes in $\delta^{15}N_2$ enrichments in overlying water and from calculated $^{15}N_2$ loss through evasion (Gas Transfer). $\delta^{15}N_2$ enrichment was observed in the 2nd water sample taken at 0.2 d (1.5 ‰; Table 5.1; Figure 5.1). ^{15}N enrichment increased to a maximum of 21.1 ‰ at 7 days, and decreased over the rest of the duration of the experiment to 13.4 ‰ after 22 days (Table 5.1; Figure 5.1). RDX conversion rates to N_2, taking into account both $^{15}N_2$ dissolved buildup and $^{15}N_2$ aeration (ΔN_2-RDX, Eq. S3) were 1.3 μmol d^{-1} at 0.2 d and increased to a maximum rate of 6.6 μmol d^{-1} at 7 days. Following the $\delta^{15}N$ pattern, rates decreased slowly to 1.2 μmol d^{-1} by day 15, and dropped below detection by 22 d (Table 5.1).

GB-IRMS analysis detected only the evolution of mass 29 ($^{14}N^{15}N$), with no significant change in mass 30 ($^{15}N^{15}N$). While we cannot rule out the production of any $^{15}N^{15}N$ without controlled headspace incubations (no ambient N_2), we assume each N_2 molecule consists of one N from the RDX nitro group and one N from the triazine ring based on previously documented N_2O production pathways (Sheremata and Hawari, 2000; Hawari et al., 2000b). Conversions of N_2 produced to RDX mineralized are performed assuming a ratio of 3:1 (N_2-N / RDX-N)

5.3.3 Gas Transfer

Experimentally determined aeration coefficients for Ar (k_{Ar}) ranged from 1.6 to 1.9 (x = 1.90 +/- 0.144 d^{-1}, n = 3) (Figure S-5.1). The resulting precision from the 3 individual runs (expressed as % RSD) is 8.4 %. Based on temperature and salinity variations in the mesocosm and the average Ar gas transfer rate, N_2 and N_2O gas transfer rates ranged from 1.6 (k_{N2}) and 1.6 to 1.7 d^{-1} (k_{N2O}), respectively.

5.3.4 $\delta^{15}N_2O$ and DIN Model Predictions

Results from the RDX-DIN model (Eqns. S5-S8) yielded good fits to the measured RDX and $\delta^{15}N_2$ values (Figure 5.1; Figure S-5.3). Overall, the model yielded similar estimates for the amount of $^{15}N_2$ production from RDX as the single-step calculations (Eqns S1-S4; Table 5.1). Modeled RDX loss, which includes mineralization and other pathways, was characterized by a total first order rate loss coefficient of 1.90 d^{-1}. Modeled N_2O enrichments predicted a 10-fold increase of N_2O concentrations from ambient concentrations when RDX was high and high ^{15}N at. % enrichments ranging from 30 to 40 % indicating a large amount of ^{15}N derived from RDX is transferred to the relatively small ambient dissolved N_2O inventory.

These levels of modeled increase in N_2O concentration and $^{15}N_2O$ enrichment were consistent in magnitude to those measured in the follow up ^{15}N-RDX experiment performed under similar conditions (at. % 14 to 37, Figure S-5.5). The model does not directly resolve pathways of RDX –N contribution to N_2O that may include both denitritration to nitrite (NO_2^-) with subsequent microbial reduction to N_2O (denit. path 2a, Figure S-5.3) vs. ring breakage with or without intermediate DNX, TNX or MNX (Hawari et al., 2000a). Nevertheless the modeled results indicate that under the experimental conditions and over the duration of the experiment, the amount of RDX-N conversion to N_2O and subsequently N_2 was 3.5 times larger than the natural sources of these biogenic gases.

Under the assumption that all $^{15}N_2O$ eventually proceeds to $^{15}N_2$, the yield of $^{15}N_2O$ lost to aeration is the key component for this inorganic N pool to be included in final mineralization rate estimates. The gas exchange component of the model predicts N_2O aeration rates account for 0.8 to 4.6 μmol RDX d^{-1} (Table 5.1), and the total μmol of RDX converted to N_2O and evaded to the atmosphere (50 μmol) was comparable to the total N_2 produced (43 μmol; Figure 5.2; Table 5.1).

5.4. Discussion

5.4.1 RDX Mineralization in the Ocean– Current Paradigm and Pathways

The coastal ocean, characterized by high rates of organic matter accumulation, remineralization , and N-limitation is a hotspot for N biogeochemical cycling (Hedges and Keil, 1995; Devol, 2008; Christensen et al., 1987). Montgomery et al. (2011, 2013) demonstrated with ^{14}C ring-labeled munitions that nitrogen limited coastal marine environments foster the microbially mediated processing and mineralization of nitrogen rich explosives such as TNT. However, the production of $^{14}CO_2$ provides limited mechanistic information for the fate of RDX, particularly because of the high N:C ratio of RDX (2:1), and the production of intermediates that contain no C.

The appearance of the nitro group ^{15}N label in the dissolved N_2 pool provides evidence for the mechanisms behind RDX removal. Sediments have been suggested as the primary location of RDX removal in the marine environment, specifically in deeper pore-waters where the respiration of organic matter can reduce O_2 levels and facilitate the anaerobic breakdown of RDX (Hawari et al., 2000a; Smith et al., 2013; Hawari et al., 2000b). A common reaction in this zone is denitrification which uses organic carbon to reduce N according to the pathway $NO_3^- \rightarrow NO_2^- \rightarrow N_2O \rightarrow N_2$ (Hattori, 1983). The use of oxidized N as a terminal electron acceptor in bacterial metabolism is a key N pathway in marine systems and a dominant mechanism for N_2 production and subsequent N removal in the ocean (Seitzinger et al., 2000; Hulth et al., 2005; Seitzinger et al., 2006; Christensen et al., 1987; Brezonik, 1997). The conditions in shallow coastal marine systems typical of contaminated systems, such as wetlands and estuaries, are particularly favorable to denitrification yielding some of the highest denitrification potential among natural systems.

All intermediate N species in the denitrification pathway can be generated within the cell, or can be supplied from an external source and enter the pathway to be reduced to N_2. With respect to RDX breakdown, this plasticity means that N_2 production may result from the denitrification of one or more of the intermediate compounds produced during RDX degradation. The complete pathway can be inferred based on previously hypothesized pathways of RDX breakdown under anaerobic conditions (Hawari et al., 2000a; Sheremata and Hawari, 2000). By identifying intermediates that overlap between denitrification and RDX biodegradation pathways, we can provide insight into the pathways of RDX removal and N_2 production in our simulated marine systems. These intermediates are likely N_2O and/ or NO_2^-, representing 2 distinct pathways of N_2 production from RDX (Figure 5.3).

N_2O has been observed as a major product of RDX-N mineralization in anaerobic incubations with municipal sludge (Hawari et al., 2000b; Halasz et al., 2002), and in aerobic incubations with the white rot fungus *Phanerochaete chrysosporium* (Sheremata and Hawari, 2000), and bacterial assemblages in natural soils (Sheremata et al., 2001). More recently, several anaerobic bacteria and aerobic fungi have since been identified in contaminated marine sediments that produce N_2O from RDX, including the bacteria *Halomonas*, *Marinobacter*, *Pseudoalteromonas* and *Bacillus* (Bhatt et al., 2005), and the fungi tentatively identified as *Rhodotorula, Bullera, Acremonium* and *Penicillium* (Bhatt et al., 2006).

The current paradigm of anaerobic RDX biodegradation is thought to follow one of two general paths. In the first (Figure 5.3, path b), the RDX ring is enzymatically cleaved to produce methylenedinitramine (MEDINA) and bis(hydroxymethyl)nitramine. These compounds have been observed to fully mineralize and produce N_2O through both abiotic and biotic processes (Hawari et al., 2000a; Hawari et al., 2000b; Hoffsommer et al., 1997). In the second (Figure 5.3, path a), nitro groups are sequentially reduced to form the derivatives MNX, DNX, and TNX. These compounds are further transformed through the production of unstable hydroxyl-amine derivatives, leading readily to ring cleavage products and N_2O (Hawari et al., 2000; McCormick et al., 1981; Crocker et al., 2006).

While the production of N_2O from RDX mineralization is well documented, the potential for production of NO_2^- and nitrate (NO_3^-) from RDX in marine systems is unclear, although denitrification of nitrate produced from RDX degradation has been previously observed in

groundwater (Beller et al., 2004). Bhushan et al. (2002a) suggested the enzymatic breakdown of reduced RDX derivatives to ring cleavage products proceeds via 3 separate pathways. One of these pathways involves an initial denitration step of MNX, DNX or TNX that produces NO_2^- under anaerobic conditions. They demonstrated the flavoenzyme diaphorase produced by *Clostridium Sp.* creates an RDX anion radical with an unpaired electron through an initial electron transfer (RDX*-), followed by denitration. There is also evidence NO_3^- may be produced to some extent through abiotic means, as it's a main product of certain abiotic RDX mineralization-based bioremediation strategies using UV light or hydroxide radicals (Bose et al., 1997a,b). Finally, Bhushan et al. (2002b) observed the production of ammonia (NH_3) after RDX had been reduced and converted to ring cleavage products by bacterial nitroreductase enzymes, which can be rapidly converted to NO_2^- and NO_3^- in oxic marine waters and sediments. These studies suggest multiple inorganic N products are possible from the breakdown of RDX that may enter the denitrification chain through redox processes.

The relative importance of pathways a and b (Figure 5.3) can be inferred from the production or absence of detectable MNX, DNX, and TNX, which are unique products in path a (Hawari et al., 2000; McCormick et al., 1981). Path a has typically been considered to occur under anaerobic conditions, as is evidence by the production of reduced RDX derivatives in anaerobic incubations with municipal sludge (Kwon et al., 2011; Halasz et al., 2002; McCormick et al., 1985; Shen et al., 1988; Shen et al., 1998) and bacteria isolates from soils (Kitts et al., 1994). However, MNX, DNX, and TNX have more recently observed during aerobic incubations with fungi (Sheremata and Hawari, 2000) and in topsoil (Sheremata et al., 2001). Similarly evidence of path b, or direct ring-cleavage as indicated by the absence of reduced RDX derivatives, has been detected in both aerobic and anaerobic groundwater (Bradley and Dinicola, 2005; Long et al., 2012).

The lack of detectable MNX, DNX, and TNX in our study suggests direct ring-cleavage of RDX is the dominant pathway of N_2O production in our mesocosms. However, the high detection limit of HPLC-UV (0.02 mg l^{-1}), taking into consideration that DNX and TNX are normally produced in trace amounts and MNX readily degrades to N_2O (Halasz et al., 2002), precludes confirmation. Additionally, E_o profiles indicate a redox gradient from +250 mv in the oxygenated water column to +100 mv at 3 cm sediment depth (Figure S-5.6). The complex interplay of aerobic and anaerobic environments in our system, combined with recent observations of both pathways occurring simultaneously in groundwater (Hatzinger and Fuller, 2014) suggests both RDX breakdown pathways were likely active.

5.4.2 New Insights

The complexity of the marine N cycle provides multiple pathways by which various RDX breakdown intermediates are oxidized or reduced. Nevertheless the measured appearance of ^{15}N in N_2 unequivocally connects RDX degradation to N_2 production through denitrification. By incorporating our experimental results with previous models of RDX degradation (Hawari et al., 2000a), we propose the most likely pathway for the observed N_2 formation (Figure 5.3; although annamox and condenitrification pathways of RDX-derived DIN are also plausible (Long et al., 2012). This mechanistic pathway suggests N_2O is not only formed from spontaneous ring breakdown via path a and path b (Figure 5.3) but also from NO_2^- and NO_3^- produced during bacterial denitration entering the denitrification pathway (Figure 5.3; denit. path

2a). Both of these N_2O pools go on to produce N_2 through denitrification (Figure 5.3; denit. path 1 and 2b, respectively).

RDX 'removal' in the environment is defined as total RDX conversion to any possible transformation product(s), including reduced derivatives, ring cleavage products, and inorganic gaseous and dissolved products. Here, we define RDX-denitrification as the total production of $^{15}N_2$ from nitro group labeled ^{15}N-[RDX] (Figure 5.3; denit. path 1 and 2b). RDX-denitrification was observed to account for almost a third (29%) of total RDX removal from the system, indicating it is a major pathway to be considered in marine contamination cases. Furthermore, this rate of denitrification of RDX is likely an underestimate, as N_2O produced from the denitrification of NO_2^- and NO_3^- (Figure 5.3; denit. Path 2a) and lost to the atmosphere was not included as it could not be distinguished from N_2O produced from spontaneous ring breakdown via paths a and b.

We approach estimating RDX mineralization rates by assuming denitrification proceeds to completion (all $^{15}N_2O$, $^{15}NO_2^-$, and $^{15}NO_3^-$ is converted to $^{15}N_2$; Seitzinger et al., 2006), and therefore add the inventory of $^{15}N_2O$ lost to the atmosphere (Figure S-5.3) to the inventory of $^{15}N_2$ both lost to the atmosphere (Figure S-5.3) and added or lost to the dissolved N_2 pool (Eqns. S3, S4). We estimate rates of RDX mineralization ranging from 0.8 to 10.3 μmol d^{-1}, and by the end of the experiment 11% of the spiked RDX had been mineralized and accounted for using our methods. Normalizing to total sediment mass in our mesocosm, we obtain similar estimates of mineralization (5.8 μg RDX kg^{-1} d^{-1}) as in Kahana Bay sediments (0 to 18 ug RDX kg^{-1} d^{-1}; Montgomery et al., 2011). However, C vs. N based mineralization estimates should be compared with caution, as they are partly based on the relative amounts of N_2O + N_2 and CO_2 formation after production of ring cleavage products in the final stage of mineralization. N_2O and CO_2 during anaerobic mineralization are formed from the decomposition of Methylenedinitramine (MEDINA) and formaldehyde (HCHO), respectively (Bhushan et al., 2002a; Halasz et al., 2002). While nitramines such as MEDINA are known to undergo spontaneous decomposition in water to produce N_2O (Hofsommer et al., 1997; Lamberton et al., 1949a,b; Urbanski, 1967), the conversion of formaldehyde to CO_2 requires additional biotransformation processes such as performed by acetogenic and methanogenic bacteria (Hawari et al., 2000a; Hawari et al., 2000b). This adds a potential rate-limiting step in the formation of CO_2 that doesn't affect N_2O production and by extension the reduction of N_2O to N_2 through denitrification.

Throughout the experiment, the mass of the ^{15}N spike compared to the mass of ^{15}N accounted for in dissolved RDX, and total N_2 or N_2O indicates the buildup of RDX-derived N in other pools. The sorption of RDX onto particle surfaces (in this case sediments and suspended particulates) is assumed to be minimal (Walsh et al., 2010; Sheremata et al., 2001; Pennington and Brannon, 2002). The majority of the missing ^{15}N is instead likely in organic and inorganic dissolved forms outside of our analytical window: particularly RDX ring cleavage products (i.e. MEDINA) and inorganic N species (NO_3^-, NO_2^-, NH_3). Additionally, stable isotopic probing has documented the incorporation of RDX-N into bacterial DNA and macromolecules in aquatic systems, including in marine environments (Hatzinger and Fuller, 2014; Roh et al., 2009).

It is unclear whether denitrifying bacteria in marine sediments will increase the rate of RDX mineralization (RDX removal coupled to denitrification), or instead promote the complete

removal of RDX-N by converting DIN produced from ring-cleavage to N_2O and N_2. Still, these results highlight the important role of sedimentary bacteria in RDX mineralization in marine systems, consistent with the recent finding that sulfate-reducing and methanogenic bacteria can incorporate RDX-N (Hatzinger and Fuller, 2014).

5.4.3 Future Research

While we unequivocally show the production of N_2 from nitro-labeled ^{15}N-RDX and suggest mechanisms for its formation, these results bring up several critical questions concerning the persistence of RDX and its derivatives in contaminated coastal marine systems.

1.) What are the relative amounts of inorganic N species ($^{15}N_2O$, $^{15}N_2$, $^{15}NO_3^-$, $^{15}NO_2^-$ and $^{15}NH_3$) formed during RDX mineralization, and how does this bias current mineralization rate estimates?

2.) What are the rate-limiting steps in the presented RDX mineralization pathways?

3.) Does denitrification serve to actually increase the removal rate of RDX in marine systems, or simply prevent the buildup of inorganic metabolites?

4.) How representative are these calculated RDX-N denitrification rates to what we would find *in situ* in contaminated coastal zones?

Specifically, these research questions highlight the assumptions involved in estimating mineralization rates of RDX in marine systems with complex N biogeochemical cycling. Future experiments should focus on the combined analysis of $^{15}N_2O$, $^{15}N_2$, $^{15}NO_3^-$, $^{15}NO_2^-$ and $^{15}NH_3$ along with RDX and derivatives to gain a greater understanding of the full mass balance of the system, and provide much needed insight into the partitioning of mineralized N species under different environmental conditions. This would serve to transcend the limited view we currently have on complete mineralization rates based on identifying only selected inorganic products.

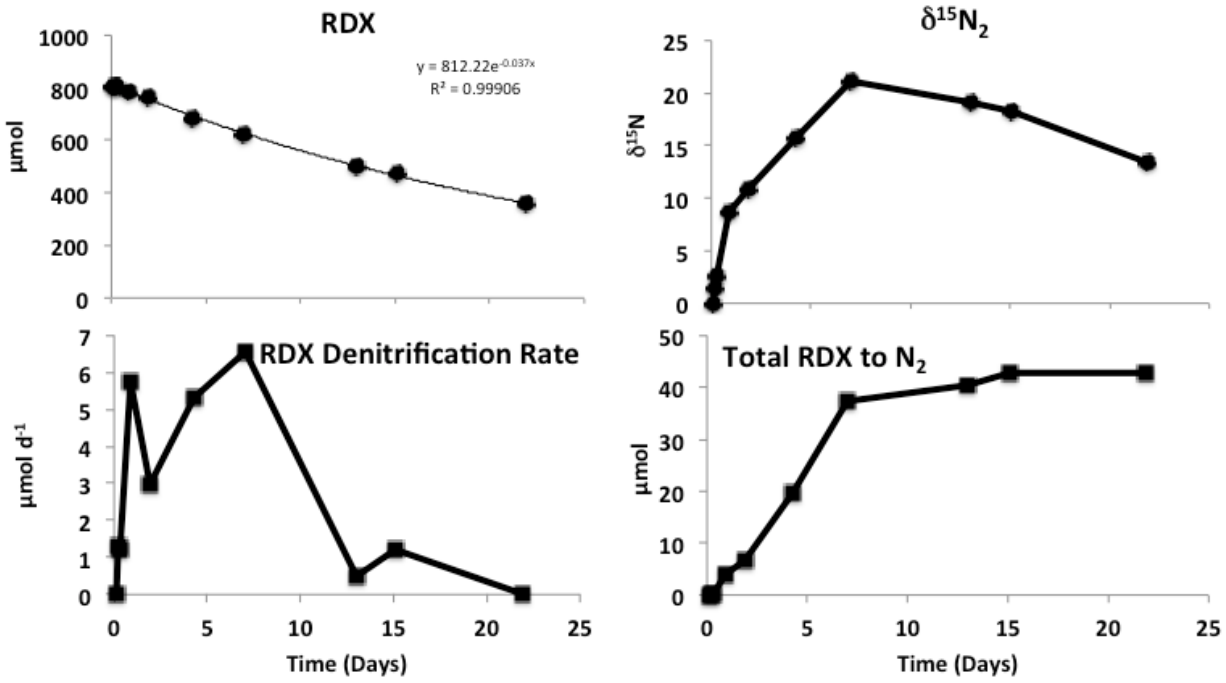

Figure 5.1 Graphical representation of data in Table 5.1. The production of $^{15}N_2$ from ^{15}N[RDX] accounts for up to almost a third (29%) of total RDX removal from the system, likely representing the dominant pathway of both RDX transformation and mineralization.

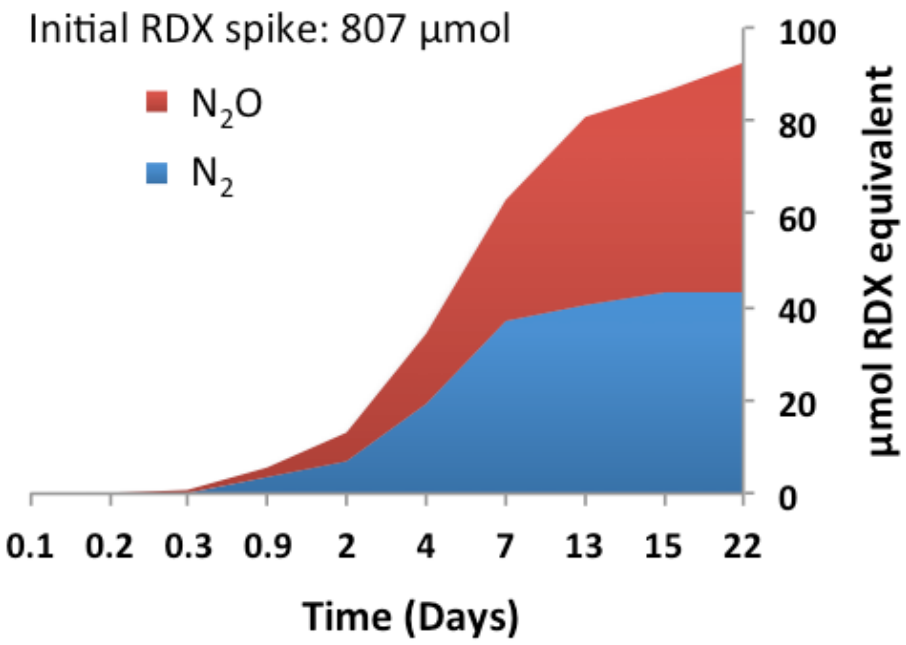

Figure 5.2. Yield of RDX accounted for in the production of ^{15}N labeled $^{15}N_2O$ (modeled) and ^{15}N (measured). RDX equivalents assume a 1:3 ratio of RDX to metabolites and include losses due to gas transfer.

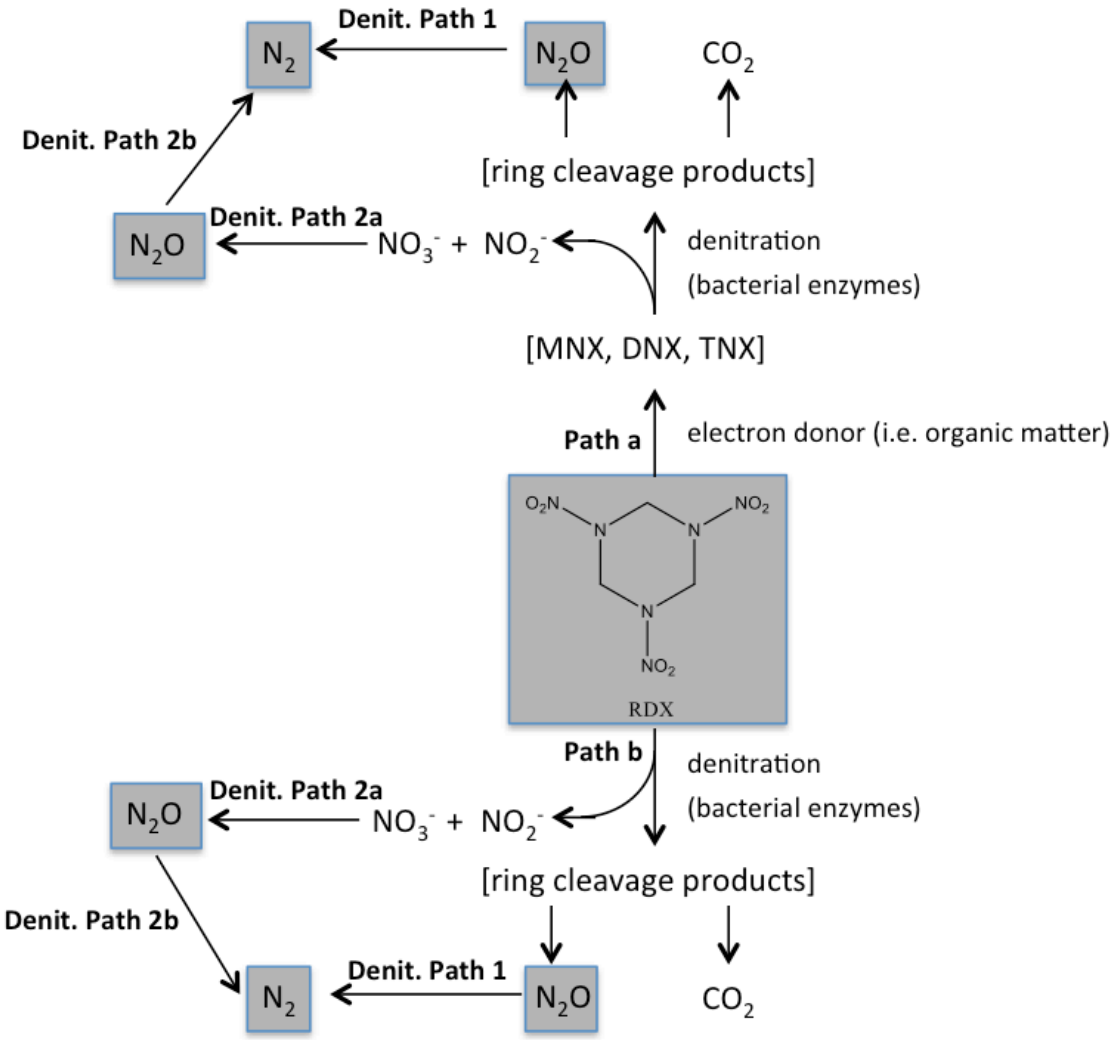

Figure 5.3. Proposed RDX anaerobic mineralization pathway including denitrification. Modified from Hawari et al. (2000a; Path a + b) and Bhushan et al. (2002a). Concentrations and ^{15}N enrichments for the shaded pools were explicitly modeled. Denit. Path 1 represents the conversion of N_2O produced from spontaneous ring combustion to N_2 via denitrifying bacteria in marine sediments. Denit. Path 2a + 2b represent the conversion of nitrite and nitrate produced from denitration to both N_2O and N_2 via the denitrification pathway.

Table 5.1. Estimated RDX denitrification and mineralization rates. Measured RDX quantities are presented as both concentrations (*mg l^{-1}*) and total abundance (*µmol*). RDX denitrification rates, in units of total RDX loss per day (*µmol d^{-1}*), are calculated as the sum of N_2 aeration and dissolved buildup (*RDX to N_2*). 'Instantaneous %' and 'cumulative %' express the relative yield of RDX removed that passed through denitrification. These percentages are "low end" estimates as they do not include N_2O produced from denit. path 2a. Mineralization rates are expressed as the sum of denitrification rates and modeled aeration rates of N_2O. *Modeled Rate.

Time	RDX		RDX to N_2 (Denitrification)					RDX Aerated as N_2O*		RDX Mineralization Rate and Extent		
Days	mg l^{-1}	µmol	$\delta^{15}N_2$	µmol d^{-1}	µmol	% instantaneous	% Cumulative	µmol d^{-1}	µmol	µmol d^{-1}	µmol	% of spike
0.1	1.13	807	0	0.00	0.00	-	-	0.8	0.0	0.8	0.0	0.0
0.2	1.13	807	1.5	1.3	0.26	-	-	1.4	0.1	2.7	0.4	0.0
0.3	1.13	807	2.6	1.2	0.38	-	-	2.8	0.2	4.0	0.6	0.1
0.9	1.10	786	8.6	5.8	3.8	16	18	4.6	1.9	10.3	5.8	0.7
2	1.07	764	10.9	3.0	6.8	13	16	3.5	6.5	6.5	13	1.6
4	0.96	683	15.7	5.3	20	16	16	4.0	15	9.3	35	4.3
7	0.87	622	21.1	6.6	37	29	20	2.5	26	9.0	63	7.8
13	0.71	504	19.1	0.5	40	2.6	13	1.5	40	2.1	81	10
15	0.66	472	18.2	1.2	43	7.8	13	0.9	44	2.1	87	11
22	0.50	359	13.4	0.00	43	0.0	10	2.3	50	2.3	93	11

Supplementary Material

$\delta^{15}N_2$ Corrections

$\delta^{15}N$-[N_2] values were corrected based on serum fractionation as observed with air saturated water (ASW) standards. The average value of 10 ASW standards was subtracted from each measured $\delta^{15}N$ value. Values were also corrected to an N_2 sample taken prior to dosing (T_0) to establish ^{15}N natural abundance values of N_2 in our tank system (0.29 ‰ after ASW correction). By applying this second correction to our $\delta^{15}N$-[N_2] values our pre-spike value is 0 ‰, and therefore any enrichment can be attributed to addition from the tracer.

RDX Denitrification Rate Calculations

The fractional amount of total RDX loss attributable to RDX mineralization coupled to denitrification was calculated for each sampling interval and cumulatively through the experiment. The instantaneous and cumulative fractions (Table 5.1) were calculated from equations #1, and 2, respectively.

$$(\Delta N_2\text{-}RDX_{(t,t-1)} / \Delta RDX_{(t,t-1)}) \quad \text{(S1)}$$

$$(\Delta N_2\text{-}RDX_{(t,t0)} / \Delta RDX_{(t,t0)}) \quad \text{(S2)}$$

The ΔN_2-RDX term is the change in the amount of N_2 derived from RDX (converted to moles of RDX) and ΔRDX is the total moles of RDX lost in that time interval. The ΔN_2-RDX was calculated from the change in RDX-derived ^{15}N in the dissolved N_2 pool ($\Delta^{15}N_2$), the gas transfer of excess ^{15}N ($GT^{15}N_2$) from dissolved N_2 to the atmosphere, and the ^{15}N mole fraction of the RDX ($X^{15}N$-RDX):

$$\Delta N_2\text{-}RDX = (\Delta^{15}N_2 + GT\ ^{15}N_2 / \Delta t) * X^{15}N\text{-}RDX^{-1} \quad \text{(S3)}$$

Where the GT $^{15}N_2$ rate was calculated as the product of the first order aeration coefficient for N_2 (k_{N2}) and the disequilibria between the measured dissolved $^{15}N_2$ and the predicted $^{15}N_2$ equilibrium as a function of temperature and salinity[63]:

$$GT\ ^{15}N_2 = k_{N2}\ (^{15}N_{2,measured} - {}^{15}N_{2,eq}) \quad \text{(S4)}$$

The value of the N_2 aeration coefficient was derived from an argon aeration coefficient as discussed in the main text ("Gas Transfer.")

Model-based $^{15}N_2O$

The ^{15}N tracer data were also used to model RDX mineralization within the context of the broader coastal marine N cycle using a multi-compartment time-stepping model (Figure 5.1, Figure S-5.1). The model provided estimates of RDX mineralization coupled N_2O production and ultimately to N_2 through denitrification. It provided a multi compartment mass balance constraint on the stepwise RDX-denitrification estimate derived from Eqns. 2 and 3. Several of the intermediate compounds identified in laboratory studies (Hawari et al., 2000) were

aggregated within the simplified modeling framework (Figure 5.1., Figure S-5.1). RDX loss was partitioned into mineralization that yielded nitrous oxide (Hawari et al., 2000; Hawari et al., 2000b) and other pathways that yielded unmeasured derivatives from ring breakdown (AEHA, 1985). In the model, N_2O produced from RDX mineralization was mixed with inputs of unlabeled N_2O produced from natural dissolved inorganic nitrogen (DIN) sources (e.g. nitrification and/or ambient $NO_2^- \rightarrow N_2O$ reduction), diluted by atmospheric exchange, and converted to N_2 via denitrifying bacteria (Figure S-5.1). Modeled N_2 was mass balanced between denitrification and atmospheric exchange. At each time step of the model, an individual N pool (N_t) mass balance was calculated with respect to total N mass, and individually for ^{14}N and ^{15}N. For the RDX, N_2O and N_2, the ^{14}N or ^{15}N isotopes (*N) are calculated by finite difference at each time step according to:

$$^{*}N_t = {}^{*}N_{t-1} + \Delta^{*}N \quad \text{and} \quad \Delta^{*}N = \Delta t \bullet \Sigma({}^{*}N_{in} - {}^{*}N_{out}) \qquad \text{(S5)}$$

*N denotes either ^{14}N or ^{15}N, and $^{*}N_{in,out's}$ are fluxes of $^{*}N$ into or out of each respective pool. The N fluxes of ^{14}N and ^{15}N are calculated at each time step independently and then recombined to yield the mole fraction ($X^{15}N$) or $\delta^{15}N$ value. Modeling of the individual isotopic species is done with the same governing equations applied to each isotope:

$$X^{15}N = [(\delta^{15}N/1000 + 1) \bullet 1/272] / \{1 + [(\delta^{15}N/1000 + 1) \bullet 1/272]\} \qquad \text{(S6)}$$

$$X^{14}N = 1 - X^{15}N \qquad \text{(S7)}$$

Where the total ^{15}N or ^{14}N mass inventory is the product of isotope-specific mole fraction ($X^{15}N$ or $X^{14}N$) and the pool size in N units. The $\delta^{15}N$ recalculated at each time step from the ^{15}N and ^{14}N masses at that time step is done from the $X^{15}N$ according to:

$$\delta^{15}N = \{272 \bullet X^{15}N / [1 - X^{15}N] - 1\} \bullet 1000 \qquad \text{(S8)}$$

Rates of RDX breakdown to N_2O and to unmeasured ring products as well as all atmospheric exchanges were modeled using first order kinetics. DIN conversion to N_2O and N_2O conversion to N_2 via denitrification were modeled as zero order reactions due to the large size of the ambient DIN pool and organic carbon limitation of the final N_2O to N_2 reduction step, respectively. Gas exchange was modeled for both N_2O and N_2 using first order aeration coefficients and gas disequilibria (Weiss, 1974) for each gas each isotope as described in Eqn. (S4).

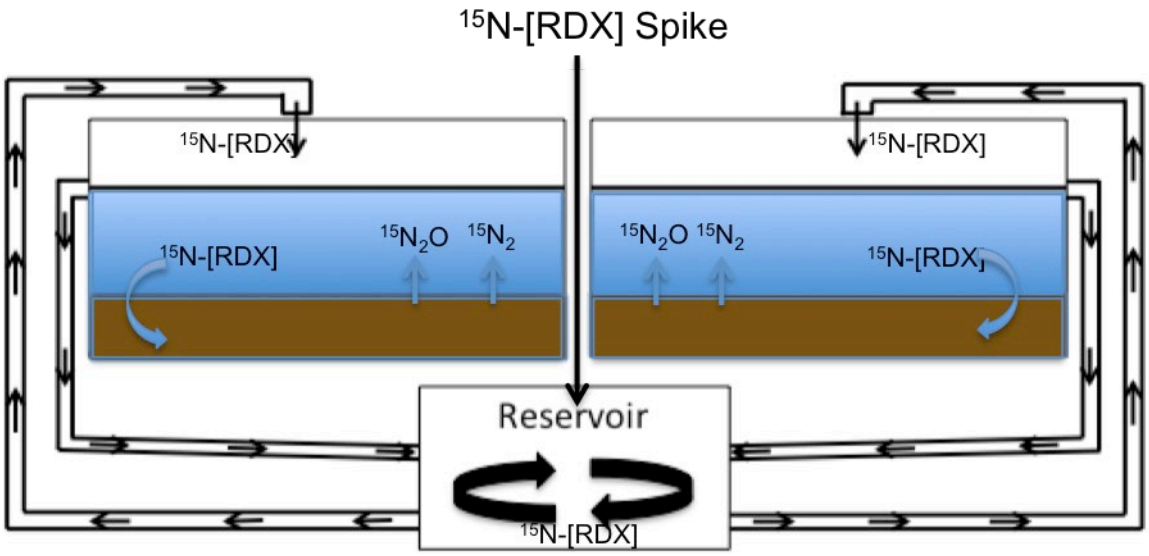

Supplementary Figure S-5.1. Conceptual model of the experimental design and dual-tank single-reservoir closed loop system.

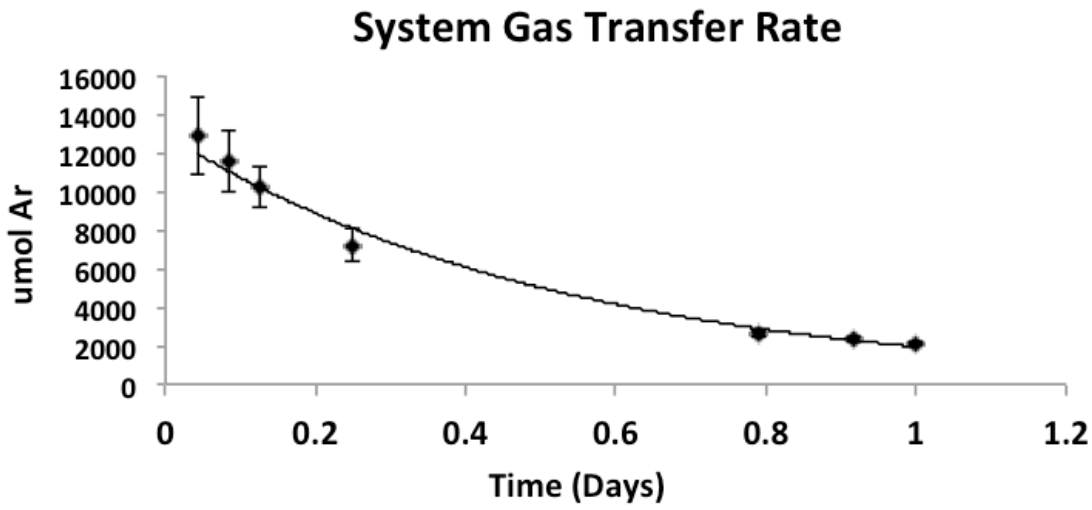

Supplementary Figure S-5.2. Experimentally determined argon gas transfer rates in the system. The equation of the trendline is $Y = 13000e^{-1.90}$, $R^2 = 0.99$. The average gas transfer rage of five experiments was 1.90 d^{-1}. This gas transfer rate was the basis for $^{15}N_2$ and $^{15}N_2O$ losses via aeration.

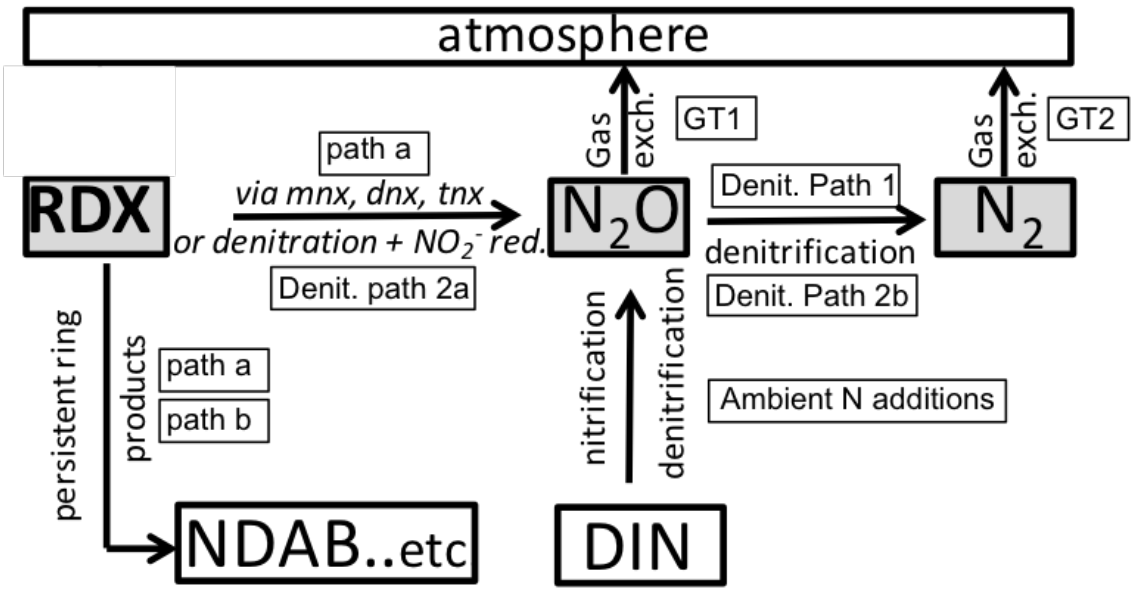

Supplementary Figure S-5.3. Simplified tracer model for RDX mineralization within the marine nitrogen cycle. Concentrations and ^{15}N enrichments for the shaded pools were explicitly modeled. Path a and b and denit. path 1, 2a, and 2b refer to Figure 5.3 in the main text. Also shown in the model are ambient N additions to the denitrification pathway and losses due to gas transfer (GT1; GT2).

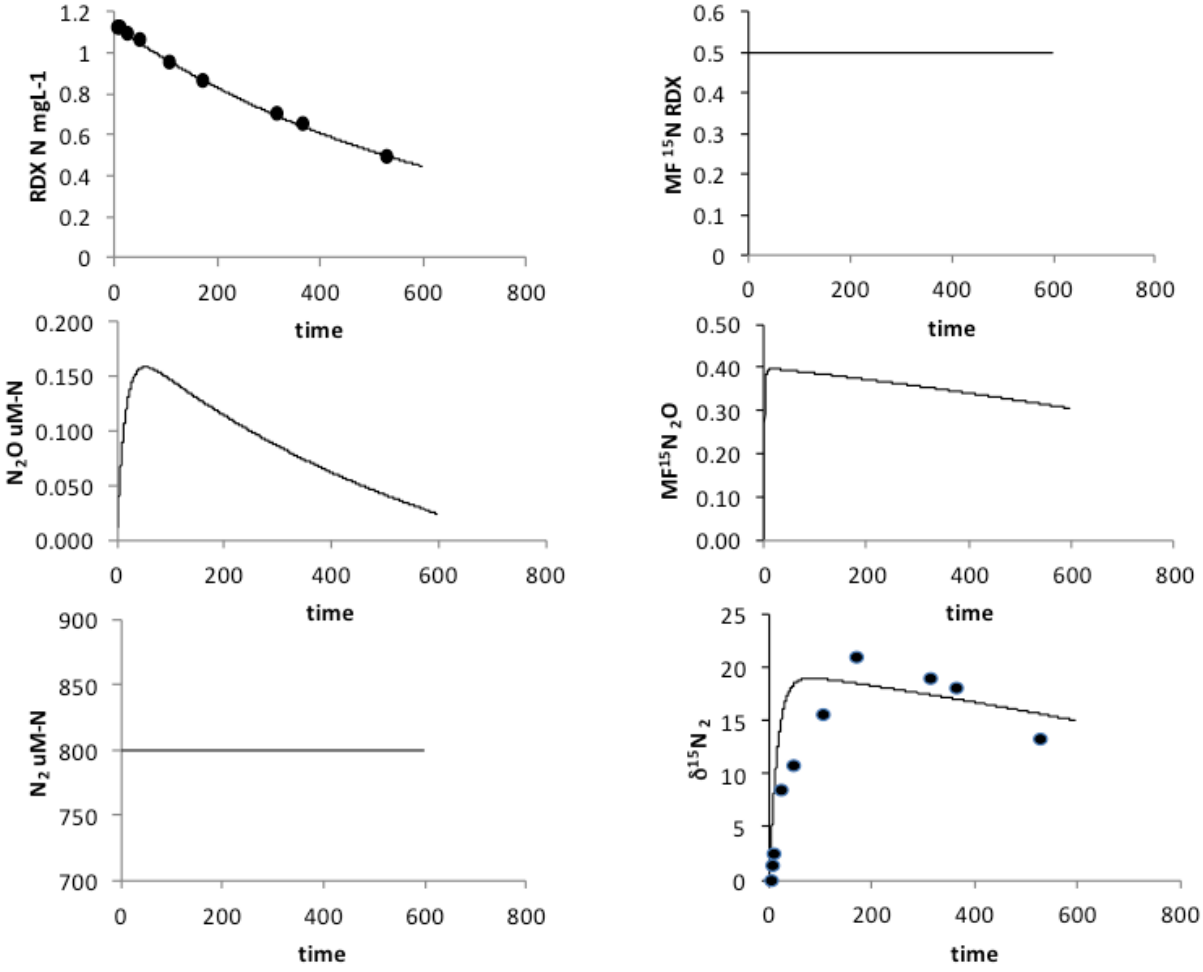

Supplementary Figure S-5.4. RDX - DIN Model Inputs and Results as a function of time. From the top left, clockwise: 1) RDX concentrations, 2) mol fraction (MF) of spiked RDX, 3) MF of $^{15}N_2O$ used to calculate N_2O derived from RDX-N, 4) isotopic enrichment in delta notation of dissolved N_2, 5) total dissolved N_2 concentration, including RDX-derived and ambient, and 6) Total μM of dissolved N_2O, including ambient and RDX-derived.

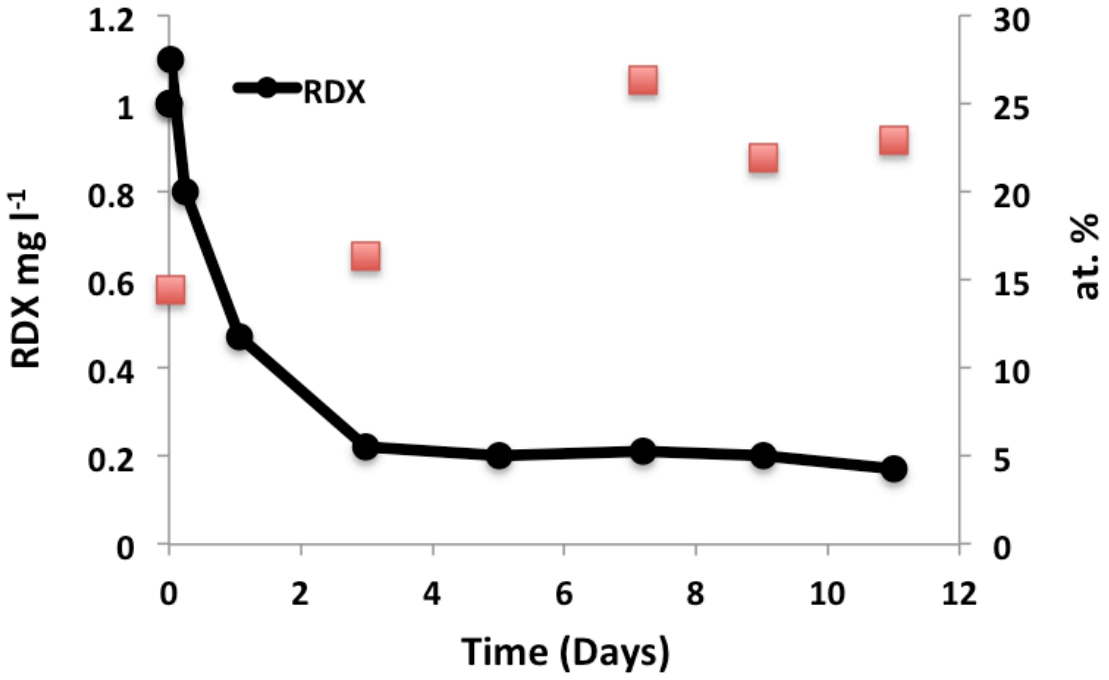

Supplementary Figure S-5.5. RDX concentrations (mg l^{-1}) and atom % excess $^{15}N_2O$ (at. %) in a subsequent 1000 l open mesocosm experiment (used to confirm model results).

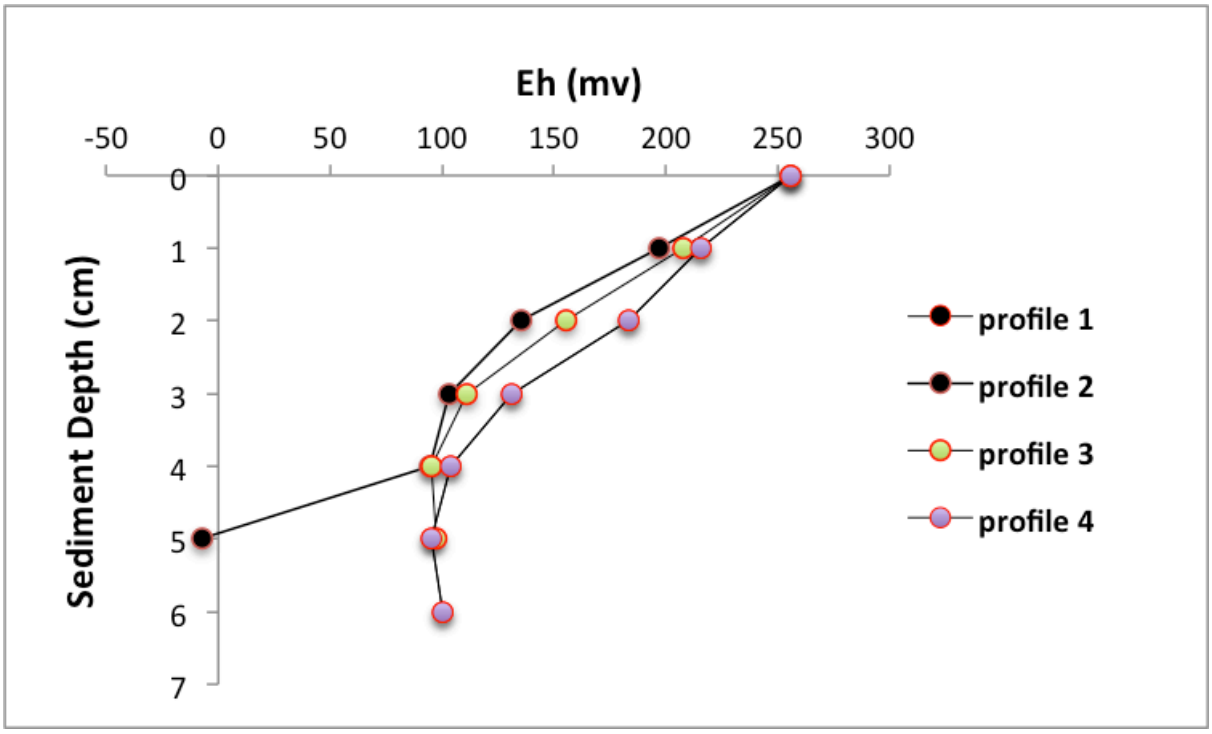

Supplementary Figure S-5.6. Aquaria redox conditions from 4 locations. Y-axis represents sediment depth (y = 0 represents water column values). Profiles 1 and 4 overlap.

Supplementary Table S-5.1- Kinetic pathways and rate coefficients in RDX-DIN model

Conversion	Kinetics	Rate Coeff. (hr^{-1})
RDX → N_2O	1st Order	0.00275
RDX → Unk. Ring Prod.	1st Order	0.005
Ambient DIN → N_2O	Zero Order	0.015
N_2O → N_2	Zero Order	0.0475

6.0. Tracing the Cycling and Fate of the Explosive 2,4,6-trinitrotoluene in Coastal Marine Systems with a Stable Isotopic Tracer, ^{15}N – [TNT]

This chapter was published, as follows:

Smith, R.W., Vlahos, P., Böhlke, J.K., Ariyarathna, T., Ballentine M., Cooper, C., Fallis, S., Groshens, T.J., and Tobias, C. 2015.Tracing the cycling and fate of the explosive 2,4,6-trinitrotoluene in coastal marine systems with a stable isotopic tracer, ^{15}N−[TNT]. Environmental Science and Technology, 49: 12223-12231.

Abstract

2,4,6-trinitrotoluene (TNT) has been used as a military explosive for over a hundred years. Contamination concerns have arisen as a result of manufacturing and use on a large scale, however despite decades of work addressing TNT contamination in the environment, its fate in marine ecosystems is not fully resolved. Here, we examine the cycling and fate of TNT in the coastal marine systems by spiking a ~ 120 L marine mesocosm with isotopically labeled TNT (^{15}N-[TNT]), simultaneously monitoring removal, transformation, mineralization, sorption, and biological uptake over a period of 16 days. Mesocosms contained seawater and sediments from Long Island Sound, and representative species of macroalgae, fish, shellfish, and bivalves. TNT degradation was rapid, and we observed accumulation of reduced transformation products dissolved in the water column and in pore waters, sorbed to sediments and suspended particulate matter (SPM), and in the tissues of the marine organisms. Bulk $\delta^{15}N$ analysis of sediments, SPM and tissues revealed large quantities of ^{15}N beyond that accounted for in identifiable derivatives. TNT-derived N was found in the dissolved inorganic N (DIN) pool, with isotopic enrichments as high as 20,000 ‰ in ammonium ($\delta^{15}NH_4+$), 14,682 ‰ in nitrate + nitrite ($\delta^{15}NO_x$), and 79 ‰ in dinitrogen gas ($\delta^{15}N_2$),with the highest $\delta^{15}NH_4+$ and $\delta^{15}N_2$ values in porewaters. Using multivariate statistical analysis and a ^{15}N mass balance approach, we identify the major transformation pathway as the deamination of TNT, promoted by sorption to SPM and oxic surface sediments. These results provide a mechanistic explanation behind the recent finding of increased TNT removal at marine turbidity fronts, and the documented increased removal observed in the presence of marine sediments.

6.1. Introduction

Large quantities of surplus and damaged munitions were dumped into the ocean by the Department of Defense (DoD) following WWI and WWII (USARDEC, 2001; CRS Report, 2007). The DoD reported 74 domestic and foreign dump sites, starting in 1918 and continuing until 1970 (USARDEC, 2001). Although the practice was banned in 1972 by Title I of the Marine Protection, Research, and Sanctuaries Act of 1972, known as the “Ocean Dumping Act” (33 U.S.C 1401, 1972), marine environments are still exposed to munitions as a result of training and weapons testing at military sites adjacent to coastal environments such as wetlands and estuaries. The DoD has responded with the Strategic Environmental Research and Development

Program's (SERDP) Munitions Response Program, including a focus on coastal marine environments (SERDP, 2010). Current research is primarily directed towards identifying the fate and transport of energetics compounds that are released into the marine environment from military munitions.

The explosive compound 2,4,6-Trinitrotoluene (TNT) was synthesized by German Chemist Julius Wilbrand in 1863 (Wilibrand, 1863), and first used as a military explosive in 1902 in German artillery shells (Brown, 1998). Currently, TNT is one of the most common explosives used in formulations for military munitions, produced in the U.S. on the order of 1 million kg annually (Harter, 1985). TNT has received attention as an environmental contaminant based on studies demonstrating its toxicity to aquatic and terrestrial organisms, and human monocytes (Sunahara et al., 1999; Talmage et al., 1999; Bruns-Nagel et al., 2000). In the marine environment, reported half-lives of TNT range from less than half a day in temperature estuarine waters in close proximity to fine-grained, organic carbon (OC)-rich sediments, to almost 2000 days in cold open ocean waters far removed from sediments (Brannon et al., 2005; Harrison and Vane, 2010; Smith et al., 2013a,b). The rapid removal of TNT in sediments may be responsible for the low concentrations of dissolved TNT in seawater near underwater UXOs and military munition dumpsites (MLA, 1996; DRDC, 2004). However, TNT is known to biotransform into organic derivatives rather than mineralize fully to inorganic C and N constituents due to the stability of the aromatic ring (Hawari et al., 2000). Additionally, recent work in estuarine waters demonstrated that mineralization and bacterial incorporation using ^{14}C labeled TNT were significant, but did not account for the majority of TNT disappearance (Montgomery et al., 2011), leaving the fate of the bulk of the TNT unknown.

Here, we provide a comprehensive assessment of the fate of TNT in a contaminated marine system, tracing its transformation, partitioning, and mineralization. We introduced isotopically labeled ^{15}N-[TNT] into a large aquarium-scale simulated coastal marine habitat (Smith et al., 2013b), and monitored the production of reduced TNT derivatives and the evolving isotopic compositions of both dissolved and particulate organic and inorganic N fractions, including nitrate and nitrite ($^{15}NO_x$), ammonium ($^{15}NH_4^+$), nitrogen gas ($^{15}N_2$), bulk sediments ($^{15}N_{sed}$), suspended particulate matter ($^{15}N_{SPM}$), and phototrophic and heterotrophic macrobiota ($^{15}N_{biota}$). Samples were routinely taken from surface and pore waters, as well as sediments and suspended particulates to provide constraints on the formation mechanisms of TNT metabolic products with respect to surface- and redox-mediated processes. Several species of marine plants and animals of environmental and economic interest to the US eastern coast were included in the mesocosm and monitored for ^{15}N enrichment of tissues and extractable munitions. Heterotrophic macrobiota included Eastern Oysters (*Crassostrea virginica*), Blue Mussels (*Mytilus edulis*), Winter Flounder (*pseudopleuronectes americanus*), mummichogs (*Fundulus heteroclitus*), Blue Crabs (*Callinectes sapidus*), European green crabs (*Carcinus maenas*), Hard Clams (*Mercenaria mercenaria*), and Periwinkles (*Littorina littorea*). Phototrophic macrobiota included Sea lettuce (*Ulva lactuca*) and Bladderwrack (*Fucus vesiculosus*). Multivariate statistical analyses were employed to identify major pathways controlling the fate of TNT.

6.2. Methods

6.2.1 Experimental Design

The goal of the experimental setup was to mimic natural coastal conditions as closely as possible in a laboratory setting, while still controlling for key boundary conditions. ^{15}N-[TNT] (fully labeled to 99.9 atom % ^{15}N) was added over a period of 16 days to 130 L (112 L water column, 18 L pore water) of Long Island Sound (LIS) estuarine seawater overlying a 7 cm deep bed of fine to medium-grained LIS sediment. The surface water: sediment: porewater ratio (V: V) was 8:2:1. The experimental set-up was described previously (Smith et al., 2013a,b).

The experiment was conducted in three phases, consisting of: (phase 1) a single TNT pulse followed by 5 days of monitoring; (phase 2) four days of continuous dosing to simulate *in situ* UXO leaching; (phase 3) termination of dosing and 7 days of monitoring (Figure S-6.1). The purpose of the initial single-pulse phase (phase 1) was to both simulate pulsed delivery of TNT to a naïve system, and to simplify estimation of a first order decay coefficient. Phase 2 (days 6-10) consisted of repeated spikes of TNT (6-7/day) to sustain a stable water column concentration. This phase simulated a scenario of continued exposure at a chronically contaminated site. Mass balance assessment of TNT fate was focused on day 4 of phase 2 (day 10 overall), after the system achieved a quasi-steady state with respect to TNT concentrations in the overlying water. Phase 3 was used to evaluate the fate of TNT after new additions ended, including re-evaluation of the decay constant. Co-occurring changes in the concentrations of TNT and TNT breakdown products throughout all 3 phases provided additional insight into transformation mechanisms.

6.2.2 Dissolved Explosives Analysis

Water column samples were analyzed for TNT and derivatives with an Agilent 1100/1200 Series High Performance Liquid Chromatograph with an Ultraviolet Detector set at 254 nm (HPLC-UV; Smith et al., 2013b; USEPA, 1994). Briefly, 5 ml of seawater were dispensed directly into 5 ml centrifuge tubes containing 5 mls of methanol, shaken for 1 min. and filtered through a 0.2μM PTFE syringe tip filter directly into a GC vial. Quantification was achieved with an external calibration containing all compounds of interest. In the water column, the following compounds were analyzed for by HPLC-UV: TNT, 2amino-dinitrotoluene (2a-DNT), 4amino-dinitrotoluene (4a-DNT), 1,3,5-trinitrobenzene (1,3,5-TNB), 1,3-Dinitrobenzene (1,3-DNB), Nitrobenzene (NB), 2,4-Dinitrotoluene (2,4-DNT), 2,6-Dinitrotoluene (2,6-DNT), 2-Nitrotoluene (2-NT), 3-Nitrotoluene (3-NT), 2-Nitrotoluene (4-NT), 4,4’,6,6’-tetranitro-2,2’-azoxytoluene (2,2’-Az), and 2,2’,6,6’-tetranitro-4,4’-azoxytoluene (4,4’-Az). Porewater samples were analyzed by HPLC-UV and no detectable peaks were observed. Detection limits were on the order of 0.02 mg L^{-1} for HPLC-UV, and therefore GC-ECD analysis was employed for porewater samples, with detection limits on the order of 0.0005 mg L^{-1}. Because of sample volume limitations, explosives were extracted from pore waters using a scaled-down version of the salting out technique in EPA 8330 (USEPA, 1994) and analyzed by Gas Chromatography with an Electron Capture Detector (GC-ECD; Agilent 6890; Pan et al., 2005). Compounds measured via this method included: TNT, 2a-DNT, 4a-DNT, 2,4-diaminonitrotoluene (2,4-DANT), and 2,6-diaminonitrotoluene (2,6-DANT). 2,4-DANT, 2,6-DANT were not measured by HPLC-UV despite available standards due to low retention on the column which resulted in

variable retention times. 2,4,6-triaminotoluene (TAT) was not analyzable with either HPLC or GC method.

6.2.3 Solid Phase Explosives Analysis

Suspended Particulate Matter (SPM) samples were taken in triplicate during each time point, and split for analysis of ^{15}N enrichment ($\delta^{15}N_{SPM}$) and extractable explosives concentrations. 250-300 ml of surface water were filtered with a peristaltic pump through pre-weighed combusted (450ºC) Whatman 25mm 0.7 um glass fiber filters (GF/F) at a low flow rate (~ 50ml/min). 1,2-dinitrobenezene (1,2-DNB: Accustandard, New Haven CT) was added as a recovery standard to lyophilized filters, and explosives were extracted by 1 hour of sonication in 5 mL acetonitrile. 3,4-dinitrotoluene (3,4-DNT: Accustandard, New Haven CT) was added prior to GC-ECD analysis to monitor detection efficiency. Precisions for TNT, 2α-DNT and 4α-DNT quantification via this method were 11.6 %, 9.4 %, and 6.3 % (% coefficient of variation: CV), respectively, based on the extraction of 6 replicate filters. Extraction efficiencies ranged from 77 – 97 %.

Macrobiota and sediment samples were homogenized, spiked with 0.01 mg L^{-1} of 3,4-dinitrotoluene (3,4-DNT; Accustandard) as a recovery standard, and 2 g of each was extracted with 10 mL of ACS-grade acetonitrile (ACN) by sonication for 1 hour followed by a clean-up extraction with 2 mL ACN. Samples were centrifuged, and the supernatant was removed and filtered through a 0.2 µm PTFE syringe tip filter for GC/ECD analysis. Extraction efficiencies averaged 80% for macrobiota and 82% for sediments

6.2.4 Bulk $\delta^{15}N$ Analysis

^{15}N enrichments were determined at each time point in bulk sediments, biological tissue of all macrobiota, and SPM via continuous flow elemental analyzer – isotope ratio mass spectrometry (EA-IRMS: Delta V, Thermofisher) at the University of Connecticut. Nitrogen isotope ratios are reported in δ notation as follows:

$$\delta^{15}N = [(R_{sample} - R_{STD})/R_{STD}] \quad (1)$$

where R_{STD} is the $^{15}N/^{14}N$ ratio of atmospheric nitrogen (1/272) and R_{sample} is the $^{15}N/^{14}N$ ratio of the sample. $\delta^{15}N$ values are reported in parts per thousand (‰), with analytical precision on the order of +/- 0.2 ‰. Duplicate samples replicated on the order of 9 – 16 % with respect to ‰ values. Weight percent organic carbon (%OC), weight percent total nitrogen (%TN), carbon to nitrogen molar ratios (C/N), and stable carbon isotope ratios ($\delta^{13}C$) were also determined.

6.2.5 Mineralization Products

Products representing mineralization of TNT functional groups (NO_2^-, NO_3^- , NH_4^+, N_2) were determined by making compound-specific $\delta^{15}N$ measurements of each pool, and applying the resulting mol fraction ^{15}N enrichments ($x^{15}N$) to the total mass of the analyte in each respective pool. $NO_2^- + NO_3^-$ and NH_4^+ concentrations were measured using the phenol hypochlorite and cadmium azo-dye methods, respectively. All 3 analytes were analyzed on the SmartChem 200 (Westco Scientific Instruments) automated nutrient analyzer. $\delta^{15}NO_x$ values were obtained via the denitrifier method using *Pseudomonas aureofaciens* (Sigman

et al., 2001; Casciotti et al., 2002) at the U.S. Geological Survey (USGS) in Reston, VA on surface water samples filtered through a 0.2µM PTFE filter and frozen. Analyses of dissolved ^{15}N-labeled TNT reagent by the bacterial method had apparent N yields less than 3 % of the TNT-N in the sample, with $\delta^{15}N$ values < 400 ‰, indicating negligible conversion of TNT to N_2O during the analytical procedure.

N_2 production and evasion rates were calculated as outlined in Smith et al. (2015a), with slight modifications. Briefly, duplicate gas samples were collected at each time point by pumping seawater into 30 ml serum bottles that had previously been sealed, pre-loaded with 750µl of 2M KOH (for preservation), and flushed with He for 15 minutes (Smith et al., 2006). After at least 6 hours of headspace equilibration, the isotopic composition of N_2 ($\delta^{15}N_2$) was measured via continuous flow isotope ratio mass spectrometry on a Thermo Delta V Plus with a Gas Bench interface (GB-IRMS). Analytical precision was typically better than 0.3 ‰. Dissolved N_2 ambient concentrations were assumed to be in equilibrium with the atmosphere and were calculated as a function of temperature and salinity (Weiss, 1970).

6.2.6 Data Analysis

Principal component analysis (PCA) was performed with XLstat 2012. In any given sediment sample, munitions under detection limit were set equal to ½ of the detection limit of the instrument. All values were mean normalized.

Equivalent yields of TNT found as ^{15}N in non-munition form were calculated assuming a stoichiometric ratio of 3:1 (^{15}N:TNT). While isotopic enrichments are reported in δ notation, $\delta^{15}N$ values are converted to $x^{15}N$ for all mass balance calculations according to the following equation:

$$x^{15}N = 1/[272/(\delta^{15}N+1)+1] \quad (2)$$

where $\delta^{15}N$ is defined as in Equation 1 (without a factor of 1000 ‰), and $x^{15}N$ is the excess mol fraction of ^{15}N.

6.3. Results

6.3.1 TNT

The initial water column TNT concentration in the tanks was 4.0 µmol L^{-1} (0.90 mg L^{-1}) (Figure S-6.2). TNT loss from the water column was immediate, with less than 3 % of the initial TNT spike present after 24 hours (Figure S-6.1). TNT loss followed a pattern of first order decay with a decay constant (k) of 3.83 day^{-1} ($R^2 = 0.89$), or a half-life of 0.18 days. On day 5, spiking re-commenced and was continued for four days. During phase 2 (hereafter referred to as "steady-state"), TNT concentrations based on 36 temporally spaced measurements were 3.40 +/- 0.31 µmol L^{-1} (0.80 +/- 0.20 mg L^{-1}).

The total amount of TNT in each pool (e.g. SPM, sed, biota) at each time point was calculated using the pool-specific TNT concentration and the total mass of each pool. At steady-state, TNT dissolved in the water column represented the largest yield of detectable TNT (93 %).

TNT was also found, in order from the highest to lowest absolute amounts: SPM > Phototrophic tissue > Shallow Sediments (0-2 cm) > Deep Sediments (2-4 cm) > Pore water > Heterotrophic tissue. (Figures 1, S3) However, total detectable TNT in all pools (including aqueous TNT) represented only 27 % of the total amount that had been introduced into the system by this time (Figure 6.1).

6.3.2 Derivatives

2-amino-dinitrotoluene (2α-DNT) and 4-amino-dinitrotoluene (4α-DNT) were detected in all dissolved and particulate pools, with the exception of no measurable 2α-DNT in 2-4 cm sediments (Figure 6.2). None of the other analyzed TNT derivatives were detected in any pools. In the water column, 2α-DNT and 4α-DNT were detectable within 1 d, and reached concentrations of 0.09 and 0.57 μmol L^{-1} (0.02 and 0.11 mg l^{-1}), respectively, after the initial spike before falling below the limit of detection at day 6 (Figure S-6.2). At steady-state, the sum of derivatives was about 70% of the TNT concentration, with 2α-DNT and 4α-DNT concentrations reaching values of 0.49 and 2.1 μmol L^{-1}, respectively (0.10 and 0.42 mg l^{-1}). In phase 3, after TNT spiking ceased, both derivatives slowly increased in concentration until the end of the experiment 6 days later.

At steady state near the end of Phase 2, dissolved 2α-DNT and 4α-DNT in the water column represented the largest pool of detectable reduced TNT derivatives; similar to what was observed for TNT partitioning between sediment and overlying water (Figure 6.2). However, a larger fraction of the derivatives was partitioned into other pools (SPM + sed+ biota): 8 % and 6% for 4α-DNT and 2α-DNT, respectively, in comparison to 2 % for TNT. In particular, 2α-DNT and 4α-DNT partitioned less into SPM, and were extractable in larger amounts (relative to total abundance in the system) from heterotrophic biomass. The concentrations of TNT, 2α-DNT, and 4α-DNT in sediment porewaters were highly variable, relative to temporal differences in other fractions.

6.3.3 Remineralization Products

^{15}N isotopic enrichment was observed in all DIN pools, including NO_2^-+NO_3^- (NO_x), NH_4^+, and N_2 (Table 6.1). $\delta^{15}NH_4^+$ and $\delta^{15}NO_x$ values at the end of phase 2 were much higher (20,000 and 48,000 ‰, respectively) than $\delta^{15}N_2$ (6.5 ‰). When converted to μmol ^{15}N-TNT equivalents, based on both δ values and ambient DIN concentrations, these data indicate each DIN pool represents a relatively similar amount of remineralized TNT (Figure S-6.3), with NH_4^+ being the largest pool. Throughout the course of the experiment, the quantity of TNT-derived N found as remineralization products ranged from 1.1 to 7.1 % of the total yield of TNT-N added to the system (Table 6.1). This includes, at any one time-point, the combined standing stock of dissolved $^{15}NO_2^-$, $^{15}NO_3^-$, $^{15}NH_4^+$, $^{15}N_2$, and $^{15}N_2$ lost due to evasion to the atmosphere. At the end of the experiment, over 95 % of $^{15}N_2$ formed was lost to the atmosphere, based on gas transfer calculations (Figure S-6.4).

6.3.4 Solid Phases

Significant isotopic enrichment was observed in all particulate pools throughout the duration of the experiment (Table S-6.1). $\delta^{15}N_{SPM}$ values increased from 3.5 ‰ before the initial

TNT spike to a range of 7,344 – 16,758 ‰ during the experiment (avg = 11,957 +/- 5,462 ‰), with no discernable trends in the data (Table S-6.1). $\delta^{15}N$ of 0-2 cm surface sediments ($\delta^{15}N_{sed0-2}$) increased from a pre-spike value of 10.1 ‰ to a range of 110 – 3,792 ‰, with the highest values occurring at the end of the experiment. $\delta^{15}N$ of deeper sediments (2-4 cm; ($\delta^{15}N_{sed2-4}$) also increased to peak values on the last day ranging from 64 – 1,035 ‰. $\delta^{15}N_{biota}$ values were highly variable with time and species. For simplicity, these results were summed for both phototrophs (macroalgae) and heterotrophs (all other macrobiota) for the multivariate analysis. Individual results for each species are shown in Table S-6.2.

6.4. Discussion

6.4.1 Mass Balance

The distribution of tracer ^{15}N mass into various pools at steady-state, in order from largest to smallest, were: ΣTNT in the water column > $^{15}N_{unidentified}$ in phototrophic macrobiota> $^{15}N_{unidentified}$ in sediments > ^{15}N in remineralization products (NH_4^+, N_2, NO_X) > $^{15}N_{unidentified}$ in heterotrophic macrobiota tissue > ΣTNT in phototrophic macrobiota > ΣTNT in pore water > ΣTNT in 0-4 cm sediments > ΣTNT in SPM > ΣTNT in heterotrophic macrobiota. ΣTNT is the sum of TNT, 2a-DNT and 4a-DNT, and $^{15}N_{unidentified}$ represents the bulk quantity of ^{15}N in each solid phase minus the sum of ^{15}N in extractable compounds that were analyzed (Figure 6.1, S-6.3). The total amount of ^{15}N accounted for in all pools, relative to the total yield of ^{15}N introduced to the system as TNT ($^{15}N_{added}$), decreased over the course of the experiment. After 1 day, nearly 80% of $^{15}N_{added}$ was accounted for, decreasing to a low of 17% after 11 days. At all sampling times after day 1, 'missing ^{15}N' (hereafter referred to as $^{15}N_{missing}$, or the total ^{15}N added to the system minus ^{15}N in all measured pools during the sampling period) represented the largest pool of ^{15}N mass, despite the comprehensive analysis of possible ^{15}N sinks in this study. Here, we discuss new insights gained into TNT transformation, remineralization, and partitioning processes in the marine environment through the observed distribution of ^{15}N.

6.4.2 Transformation

The rapid removal of TNT from the system is consistent with previous studies demonstrating short half-lives in seawater in the presence of sediments (Smith et al., 2013b). The primary pathway of TNT removal in the environment has been attributed to bacterial transformation, promoted primarily by the relative reactivity of the nitro ($-NO_2$) functional groups in comparison to the relative stability of the aromatic ring (Hawari et al., 2000; Spain et al., 2000). Here, only two TNT derivatives, 2α-DNT and 4α-DNT were produced in measurable quantities. Many other potential derivatives were analyzed for and not observed, including 1,3,5-TNB, 2,4-DNT, 2,6-DNT, 2,4-DANT, 2,6-DANT, 1,3-DNB, NB, 2-NT, 3-NT, 4-NT, 4,4;'-AZ, and 2,2'-AZ. At steady state, and considering all pools, TNT and the sum of measured derivatives (4α- + 2α-DNT) accounted for nearly equivalent amounts of total ^{15}N in the system (7.2 % and 6.8 %, respectively), with 4α-DNT present in larger amounts than 2α-DNT (Figure 6.2).

At steady state, continuous additions of ^{15}N-[TNT] produced increasingly larger quantities of $^{15}N_{missing}$ despite stable yields of ^{15}N in detectable pools. We suggest these

relationships indicate the build-up of one or more unidentified TNT transformation products that represent the ultimate fate of TNT in our system over the 16 day period. In order to constrain potential formation pathways of the unidentified transformation products, we employed PCA on the 16 d time-series with all pools of ^{15}N included as metrics (Figure 6.3). Measurements that group together in the PCA plot are influenced by the same underlying factors. PC1 reflects the degree of TNT processing, and possibly the duration of the experiment, with fresh TNT added to the water column plotting in the far left quadrant, and transformation and remineralization products in the far right quadrant. PC2 has sediment and pore water measurements separated from suspended particulate matter measurements, suggesting aerobic vs. anaerobic pathways are the controlling factors.

$^{15}N_{added}$ and $^{15}N_{missing}$ formed a distinct cluster with concentrations of 2α-DNT and 4α-DNT in the water column. Linear correlation analysis of the sum 2α- and 4α-DNT vs. $^{15}N_{missing}$ reveals a strong, significant linear correlation (Figure 6.1; $R^2 = 0.93$, $p < 0.001$). The primary TNT transformation route thus passes through these intermediates. The reduction of TNT nitro to amine ($-NH_2$) groups is the most well documented transformation pathway in both aerobic and anaerobic environments, producing a number of possible reduced derivatives beyond 4α-DNT and 2α-DNT, primarily 2,4-DANT, 2,6-DANT, and TAT (Spain et al., 2000; McCormick et al., 1976; Hawari et al., 1998; Elovitz and Weber, 1999; Juhasz and Naidu, 2007; Esteve-Nunez and Ramos, 1998). While we lack data from the water column due to the limitations of the HPLC-UV method, 2,4-DANT and 2,6-DANT were not detected in pore waters or in SPM, sediment, and macrobiota extractions. TAT formation requires redox values below -200 mV (Funk et al., 1993; Hofstetter et al., 1999) compared to the values of +100mV typically found in deeper sediment layers of our system (Smith et al., 2015). Many studies have noted the production of these compounds only in small quantities, or their complete absence, for example in *Pseudomonas* cultures (Esteve-Nunez and Ramos, 1998). Several studies that observe the formation of TAT report further degradation to unidentified transformation products on the order of a few days (Hawari et al., 1998; Pruess and Rieger, 1995; Duque et al., 1997). We therefore rule out TAT, 2,4-DANT and 2,6-DANT as large contributors to the unidentified derivative pool, although we were not able to determine if they were intermediates in the pathway in question. Also, the lack of measureable 1,3,5-TNB suggests phototransformation is not a major pathway, and azoxytoluenes, produced from the reaction of reduced TNT products in the presence of oxygen (Haidour and Ramos, 1996; Fiorella and Spain, 1997), were not observed in our system despite the right conditions being present.

Here, we observed significant isotopic enrichment of the DIN pool, with $^{15}NH_4^+$ being the largest component (Table 6.1). Furthermore, the production of $^{15}NH_4^+$ correlated linearly with the sum of 2α-DNT and 4α-DNT separately in both pore waters ($R^2 = 0.59$) and the water column ($R^2 = 0.70$) (Figure S-6.5). We therefore suggest deamination of the amine functional groups in 2α-DNT and 4α-DNT is the pathway linking the observed compounds to unidentified transformation products. Esteve-Nunez and Ramos (1998) demonstrated that some bacteria favor denitration over the reduction pathway, anaerobically utilizing TNT as a sole C and N source. Denitration and/or deamination has been further supported by the observation of N-free TNT transformation products such as 4-hydroxybenzaldehyde, 4-hydroxybenzoic acid, p-cresol, methyl phloroglucinol, and toluene (Funk et al., 1993; Esteve-Nunez and Ramos, 1998; Boopathy and Kulpa, 1992; Boopathy and Kulpa, 1993; Lewis et al., 1997).

Deamination can produce a large suite of products depending on the fate of the other two nitro functional groups and the methyl group. The lack of measureable quantities of 2,4-DNT, 2,6-DNT, 2-NT, 3-NT, and 4-NT suggests the deaminated end-products contain at least one amine functional group, and/or has a modified or removed $-CH_3$ group. The absence of 1,3-DNB and NB in our analysis provides further constraints on the identity of the end-product, by ruling them out as possible end-products.

10,482 μmol of ^{15}N was "missing" at day 10 (73% of $^{15}N_{added}$) when the system best represented steady state conditions, compared to the total 185 μmol of ^{15}N found as DIN (NH_4^+, NO_x^-, and N_2, including N_2 lost by exchange with air/headspace up to this time point). This would seem to suggest that deaminated products were not quantitatively important with respect to missing ^{15}N. However, macroalgae ('phototrophic biomass') contained the largest quantity of identifiable ^{15}N in the system (after water column TNT), much larger than found in heterotrophic biomass. Macroalgae assimilate and store large quantities of NH_4^+ and NO_3^-, and may have kept concentrations of TNT-N mineralization products low in the water column. This hypothesis is supported by the PCA cluster representing the incorporation of ^{15}N by macrobiota ($^{15}N_{biota}$) and concentrations of ^{15}N labeled DIN (Figure 6.3). If we assume that the higher yield of ^{15}N in macroalgae versus heterotrophic biomass was entirely the result of ^{15}N-labeled DIN uptake, an additional 1,376 μmol of ^{15}N may have entered the N-cycle through deamination. If 2 functional groups, on average, were deaminated, then unidentified compound(s) could represent 6 % of $^{15}N_{missing}$. However, if only 1 amino group was deaminated, then unidentified compound(s) could represent 26% of $^{15}N_{missing}$.

6.4.3 Partitioning

TNT and its derivatives are particle-reactive compounds, with high affinities for sorption onto soils and sediments (Elovitz and Weber, 1999; Pennington and Patrick, 1990; Sheremata et al., 1999). Here, we observed sorption of TNT and 2α- and 4α-DNT to both SPM and sediments (Figure 6.2, S-6.6). The amount of TNT sorbed to these pools represented 0.8% of the total added at steady-state, and 2α-DNT and 4α-DNT represented another 2.7 % and 1.8 %, respectively, of the total TNT added. This is consistent with studies demonstrating sorption affinity of TNT transformation products increases with reduction of nitro groups to amine groups (Sheremata et al., 1999).

Mass normalized concentrations of TNT, 2α-DNT, and 4α-DNT sorbed to SPM were consistently 3-4 orders of magnitude larger than for sediments. For TNT, these differences were not accounted for in the high water column to pore water concentration ratio (1 to 2 orders of magnitude higher concentrations in the water column). $\delta^{13}C$ data indicate SPM consisted primarily of re-suspended sediments, and therefore the focusing of TNT onto SPM over sediments is likely related to redox effects or differences in the composition of microbes in the water column vs. sediments.

To summarize the partitioning of the TNT derived ^{15}N tracer, most of the ^{15}N introduced to our seawater + sediment mesocosms in the form of ^{15}N-[TNT] was not accounted for as TNT, 2α-DNT, 4α-DNT, ^{15}N labeled DIN, or as bulk ^{15}N in sediments, SPM, and the tissues of macrobiota. Furthermore, large quantities of tracer ^{15}N in sediments, SPM, and macrobiota could not be identified as munitions compounds or derivatives within the solid samples. The

relative size of this $^{15}N_{unidentified}$ pool varied largely between solid phase fractions (Figure S-6.7). In heterotrophic biomass, the sum of ^{15}N in extractable TNT, 2a-DNT, and 4a-DNT as a fraction of total ^{15}N (calculated directly from $\delta^{15}N$ and % TN) averaged 0.75 %, the lowest of all fractions. Phototrophic biomass contained similarly low percentages of munitions, which averaged 4.5% of the total ^{15}N pool. Sediments contained slightly higher relative yields, averaging 8.5%. SPM contained by far the highest relative yield of recognizable munitions, with over 25% of the ^{15}N pool found in TNT and derivatives. $^{15}N_{unidentified}$ pools were 1-2 orders of magnitude more concentrated on SPM than on sediments, similar to the concentration ratio of TNT in the water column vs. porewater. We suggest this $^{15}N_{unidentified}$ pool may be related to TNT N incorporation into the macromolecular material of surface-associated bacteria, such as DNA, proteins, and/or lipids (Gallagher et al., 2010; Carpenter et al. 1978). Additionally, this pool may represent sorption of the deaminated TNT derivative.

6.4.4 The Fate of TNT in Marine Systems

Tracing the fate of TNT with ^{15}N places new constraints on TNT cycling generally, and in coastal marine systems specifically. We provided several lines of evidence suggesting that the deamination of 2α-DNT and 4α-DNT produces an unidentified transformation product (or suite of products) in large quantities. The yield of ^{15}N contained in this pool, and the continual accumulation of this pool at steady-state, suggests this derivative was the ultimate fate of TNT in our system. Constraints provided here should focus future research towards the discovery of its identity.

This transformation process produced NH_4^+ in large quantities, which was further converted to NO_2^-, NO_3^-, and N_2 by nitrifying and denitrifying microbial communities present in the system (Ward, 2007). Denitrification of N produced from explosives breakdown was demonstrated for RDX in similar experimental systems (Smith et al., 2015). For TNT the N_2 produced can be solely attributed to deamination, NH_4^+ oxidation and subsequent NO_x reduction to N_2, rather than alternate pathways suggested for RDX[24]. Accounting for ^{15}N labeled DIN removal by macroalgae, 10% of TNT-N was deaminated at steady-state, representing mineralization of TNT functional groups. However, unlike ring C mineralization reported by Montgomery et al. (2011), the mineralization of TNT functional groups did not constitute complete removal of the TNT molecule from the system, as the aromatic ring contains only C.

This study provides support for the importance of SPM in TNT processing (Montgomery et al., 2011). SPM had several characteristics indicating its importance in TNT transformation pathways: 1) concentrations of TNT and derivatives sorbed to SPM were several orders of magnitude higher than in sediments, 2) sorbed compound concentrations on SPM (TNT_{SPM}, 2α-DNT_{SPM}, 4α-DNT_{SPM}) fall into a distinct "aerobic" cluster on the PCA plot (Figure 6.3), and 3) SPM concentrations and instantaneous TNT removal rates exhibit similar trends (Figure S8). We suggest SPM strongly sorbs TNT, increasing its bioavailability (Robertson and Jjemba, 2005) and promoting its transformation to deaminated products that are not routinely measured. This process was likely mirrored by oxic surface sediments, which have previously been shown to play an important role in TNT processing (Smith et al., 2013a,b). Their role, however, was likely masked in our analysis due to the shallow depth of the oxic zone (Smith et al., 2015).

In coastal marine systems, oxic surface sediments, and SPM derived from coastal runoff and resuspended sediments can be expected to influence the rate and mechanism of TNT

processing. These results provide a mechanistic explanation behind the recently observed increased removal of TNT in a marine environment at a turbidity front (Montgomery et al., 2011), and should serve as a platform for future research into the fate of TNT in the coastal ocean.

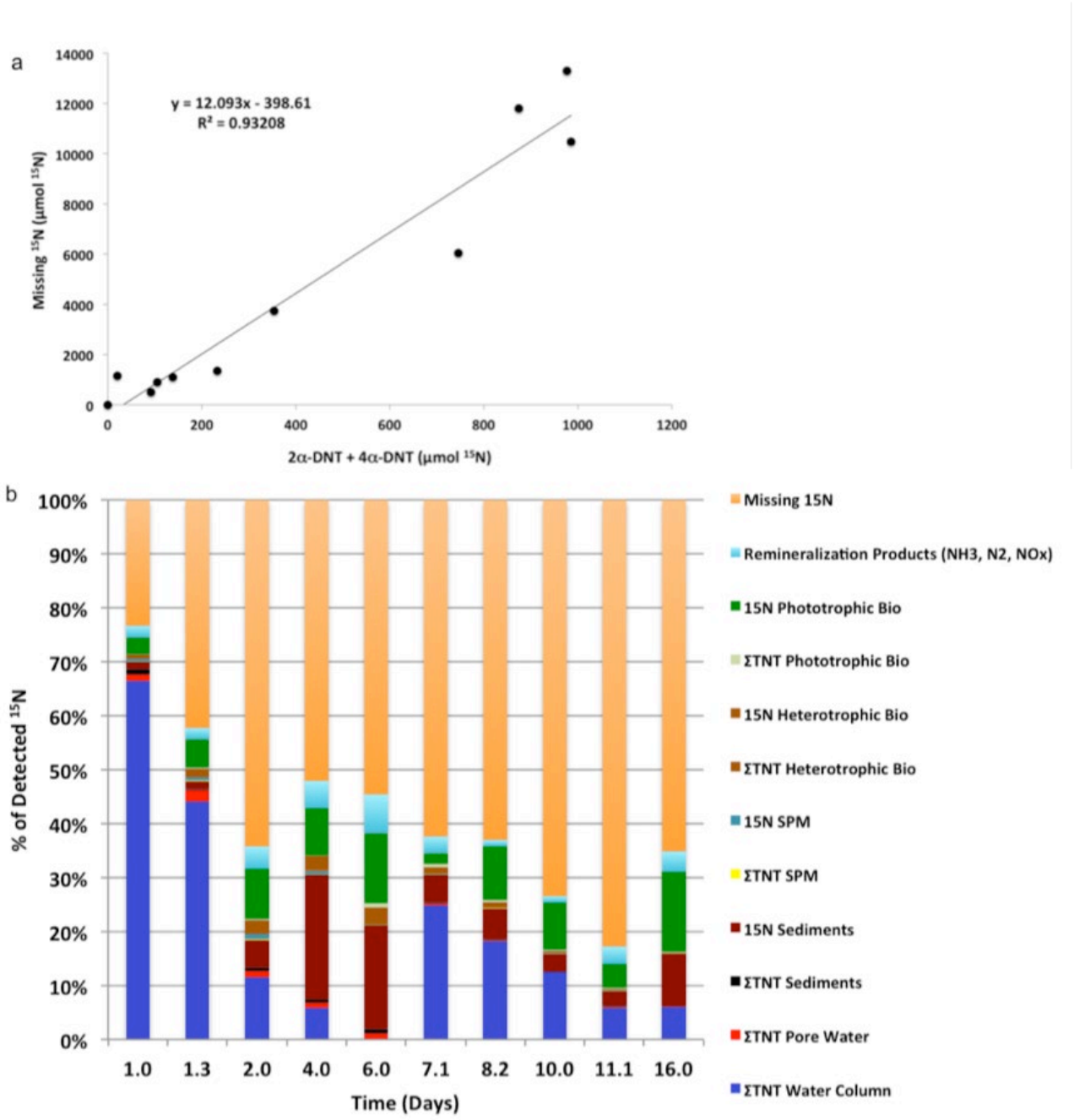

Figure 6.1. Fraction of ^{15}N added to the system in each detected pool. A) the yield of missing ^{15}N linearly correlates with 2a-DNT and 4a-DNT concentrations. B) full ^{15}N mass balance. ΣTNT = [TNT + 2a-DNT + 4a-DNT]. ^{15}N (i.e. '^{15}N SPM' in legend) = total^{15}N from bulk analysis minus ^{15}N in extractable compounds.

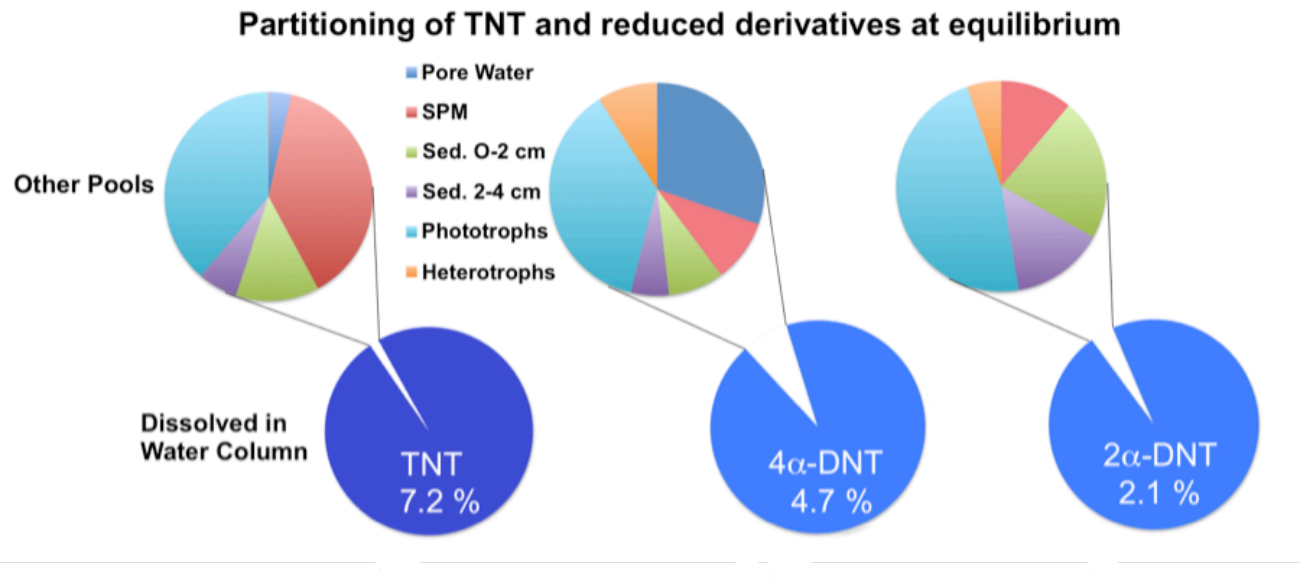

Figure 6.2. TNT and derivative partitioning at steady state (after 4 days of constant TNT concentration in surface water). Percentages represent the fraction of the total TNT added to the system that was represented by each compound.

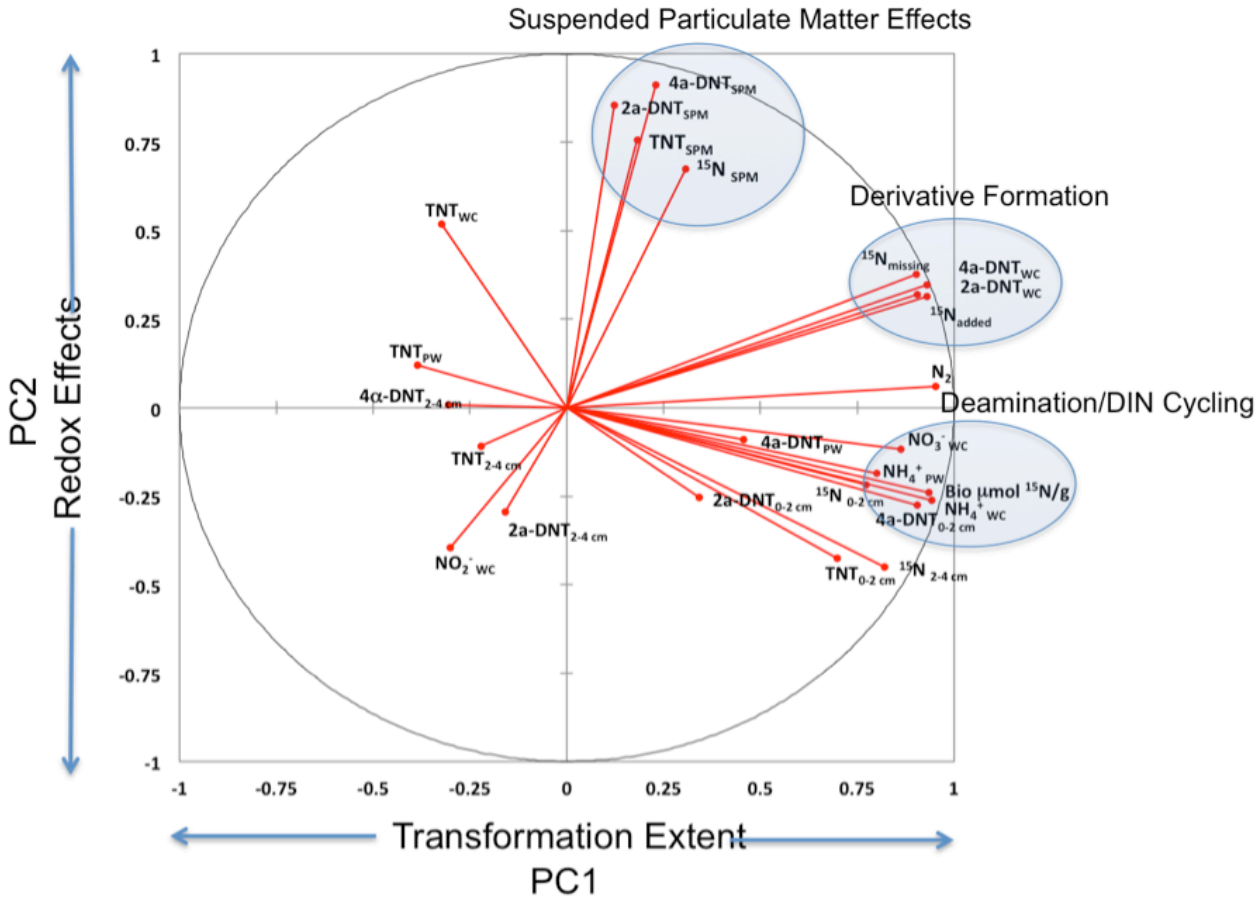

Figure 6.3. PCA provides insight into the cycling of TNT and TNT-derived N. The 3 boxes highlight correlated pools of ^{15}N and identify the main routes of TNT transformation in our study

Table 6.1. DIN production from TNT. Total ^{15}N yields are given as the sum of water column and pore water values for $\delta^{15}NH_4^+$, although not for $\delta^{15}N_2$ due to a lack of measurements and gas transfer estimates from porewaters. $\delta^{15}NO_x$ was measured in the water column only.

Time	δ^{15}N Water Column			δ^{15}N Pore Water		µmol ^{15}N excess			µmol TNT equivalent			µmol spiked	%TNT as DIN
Days	NH_4^+	No_x	N_2	NH_4^+	N_2	NH_4^+	No_x	N_2	NH_4^+	No_x	N_2	TNT	%
0.0	12.9	0	-0.9	12.9	-	0	0	0.0	0	0	0	0	0.0
1.0	243	217	5.5	4058	-	39	6.5	2.8	13	2.2	0.9	705	2.3
1.3	341	473	5.8	33.7	-	26	17	2.1	8.8	5.5	0.7	702	2.1
2.0	653	738	6.5	76.6	-	53	33	3.6	18	11	1.2	702	4.3
4.0	967	663	0.5	1885	-	64	37	2.7	21	12	0.9	702	4.9
6.0	6988	604	0.7	3441	-	97	45	4.2	32	15	1.4	702	6.9
7.1	-	1600	6.1	6586	-	121	59	7.1	40	20	2.4	1997	3.1
8.2	-	130787	3.0	171	-	84	37	6.5	28	12	2.2	3199	1.3
10	93449	433514	4.8	2244	-	149	94	9.9	50	31	3.3	5358	1.6
11	-	114490	3.0	8270	76.0	495	41	10	165	14	3.4	5358	3.4
16	10108	17965	2.5	19927	79.5	518	56	14	173	19	4.6	5358	3.7

Supplementary Material

Supplementary Methods

Sampling and Sample Prep

Biota samples (5 min. rinse) and TSS filters (30 ml) were immediately rinsed with tracer free seawater to remove dissolved and weakly sorbed munitions and ^{15}N from tissue surfaces. Biota, sediment, and TSS filters were all frozen immediately after sampling and lyophilized prior to analysis. Biota samples were homogenized using a Tissue Master 125 (Omni International). Sediments were homogenized with a mortar and Pestle. TSS filters were sliced into fine pieces with razorblades.

Mixed standards containing all analytes of interest were sonicated alongside TSS filters to monitor for thermal degradation, which we did not observe. 2 Filters were chosen for re-extraction (T7 and T10) to obtain an independent measurement of extraction efficiency. An additional 1-4 % of TNT, 11-18 % of 4a-DNT, and 10-20 % of 2a-DNT were obtained from the second round of sonication, indicating extraction efficiencies obtained with 1,2-DNB are reasonable in magnitude.

Controls

No control tanks were carried out in tandem with the tank system in the study: however, conditions were kept as closely to those in Smith et al. (2013) as possible. For example, as in that previous study the following parameters were identical: 1) tank system, 2) sediment source as in tanks SED_{FG}, 3) water temperature within 1-2ºC using a chiller bath, 4) Long Island Sound coastal seawater, and 4) water volumes and sediment masses. The new aspects to the current experimental design are the addition of tracer ^{15}N-[TNT] and marine organisms. Therefore, with a certain degree of confidence we can compare aspects of our labeled study to the behavior of non-labeled TNT in these previous experiments.

Labeled TNT Doses

TNT was delivered to the tank reservoirs concentrated in acetone (34 mg/ml). In low concentrations acetone is not toxic to marine life, and it impacts the closed system to a smaller degree than adding larger quantities of seawater containing dissolved TNT throughout the experiment, due to the constant changes in dissolved carbon and nutrients this would cause. Also, TNT breakdown rates were actually observed to increase over the course of our experiment, mitigating acetone toxicity concerns to the active microbial community.

TNT Concentrations

Discrete TNT points during this phase are represented as the average of several measured points since the last full sampling period. Several TNT measurements (4-6) were made between each sampling period in order to constrain the degradation rate of TNT and the amount of spike necessary. Weighted concentrations ranged from 0.81 to 1.3 mg L^{-1}. While shorter-term variations in TNT concentrations between spikes are of concern from a kinetic point of view, reduced derivative concentrations did not vary on this time scale suggesting we may have approximated equilibrium conditions.

Missing Data Points

Missing data points in any given fraction represent a significant problem precluding observation of the change in mass balance over time. Linear interpolation was used for missing data points that were part of an obvious trend in the data, while an average value of all measured time points was used when an obvious trend was not present. While each individually interpolated or averaged point may be misleading, overall it will result in reduced anomalies in the mass balance, as a missing data point will influence all other fractions % of the total.

Statistics

Simple regression analyses were performed using Sigma Plot, Inc. (Version 11.0). Means are reported with a 95% confidence interval and differences between means were established using unpaired *t*-tests (Sokal and Rohlf, 1995). One-way analysis of variance (ANOVA) was performed using Sigma Plot Inc., (Version 11). An *F*max test was used prior to ANOVA and regression analyses to check for homogeneity of variances. This test uses the ratio of the maximum and minimum variances and then compares the ratio with the cumulative probability distribution of *F*max to determine homogeneity of variances (Sokal and Rohlf, 1995).

Mineralization Products

%AT excess ^{15}N values were applied to NH_3 measurements made on the Smartchem as opposed to filter N masses in order to avoid bias from incomplete diffusions.

Supplementary Figures

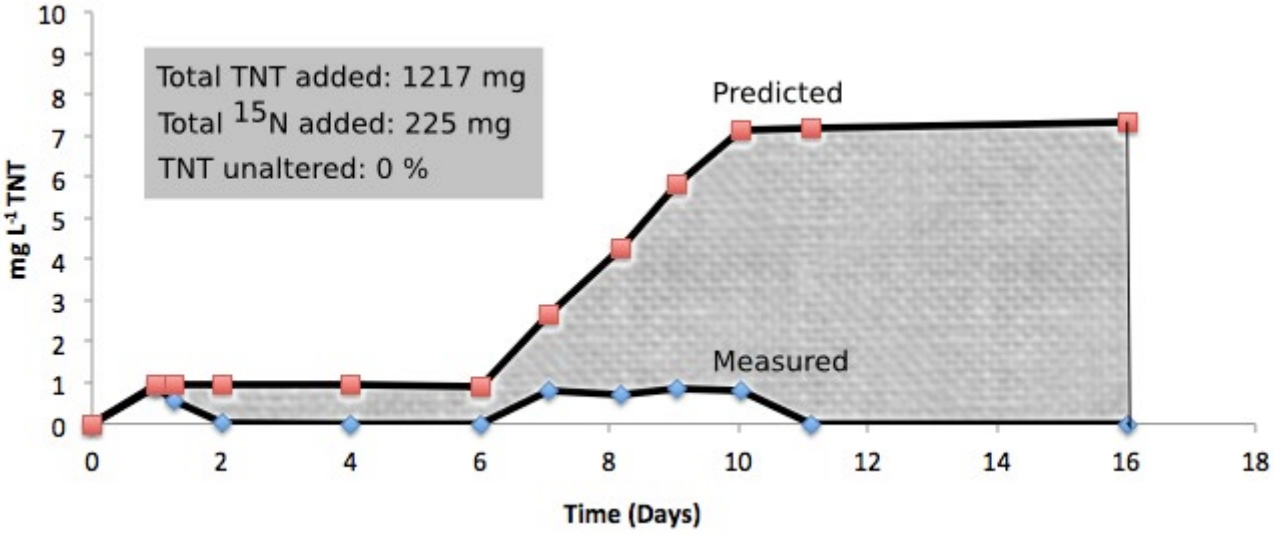

Supplementary Figure S-6.1. Observed concentration of TNT in the experimental mesocosm compared to predicted concentrations if TNT addition was conservative. The grey region represents the mass of TNT (or TNT derived nitrogen) that must be accounted as other derivatives or in other fractions to close the mass balance.

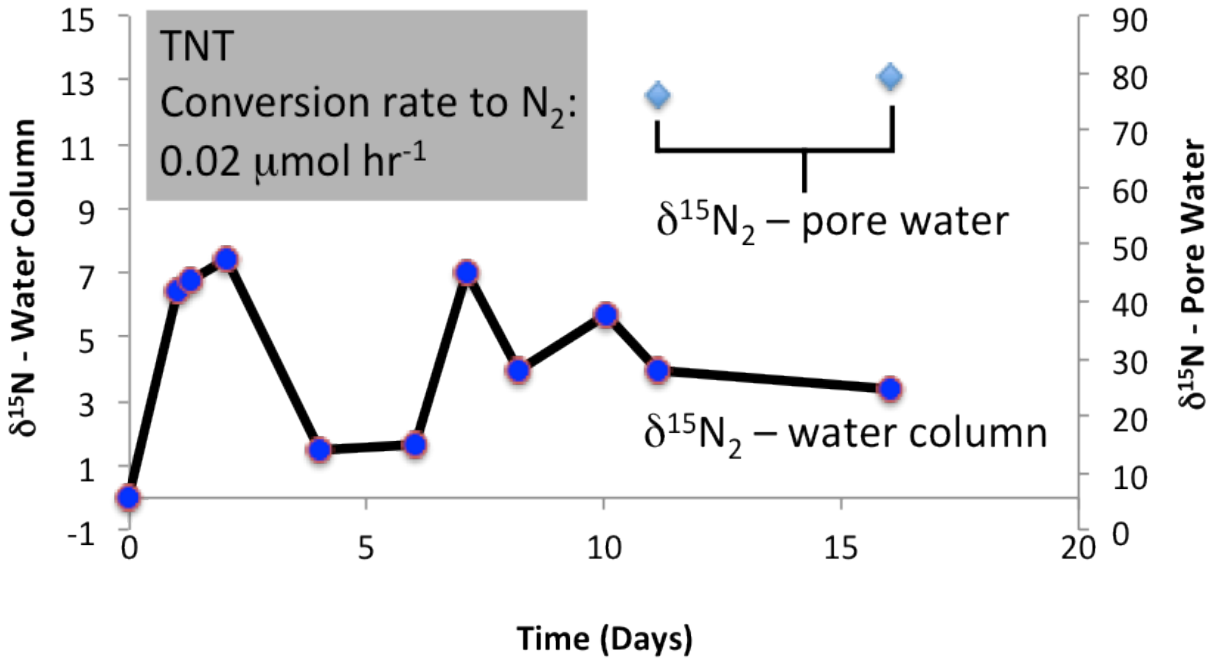

Supplementary Figure S-6.2. Isotopic enrichments of N_2 in the water column and extracted from pore water.

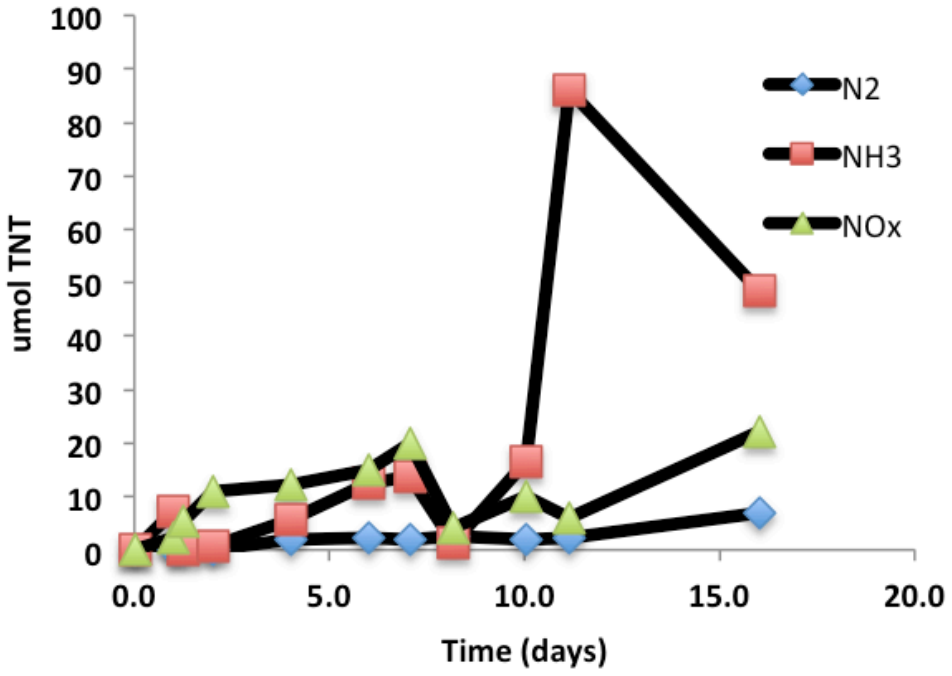

Supplementary Figure S-6.3. – µmol equivalents of TNT found as remineralization products.

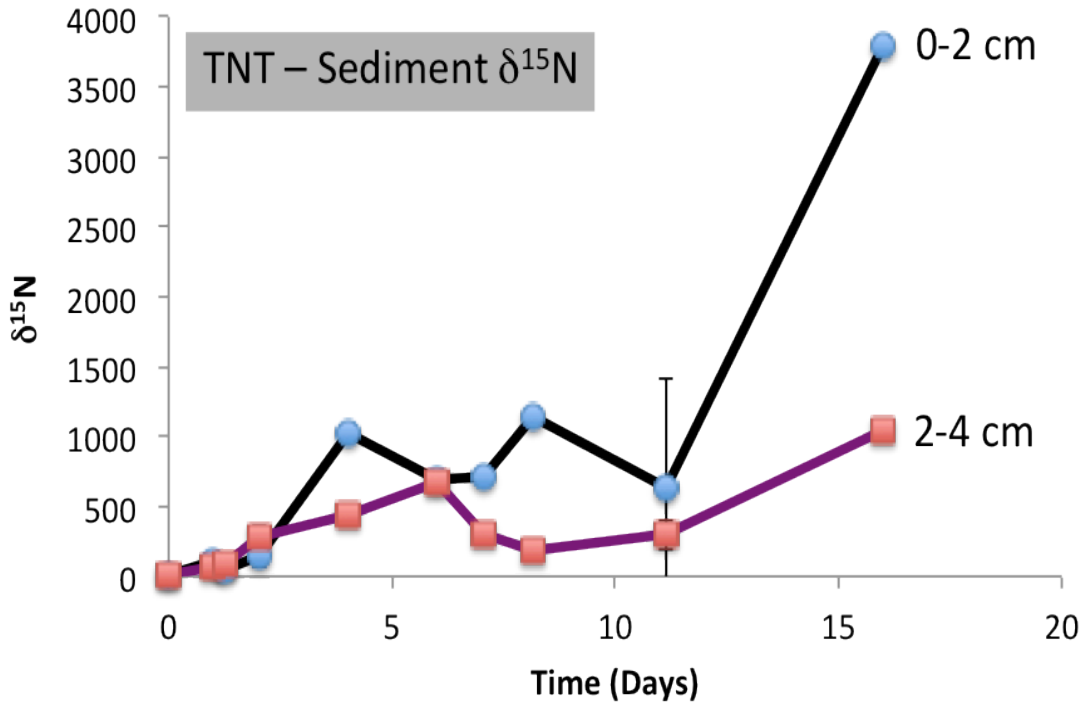

Supplementary Figure S-6.4. N isotopic enrichment of 0-2 and 2-4 cm sediment layers

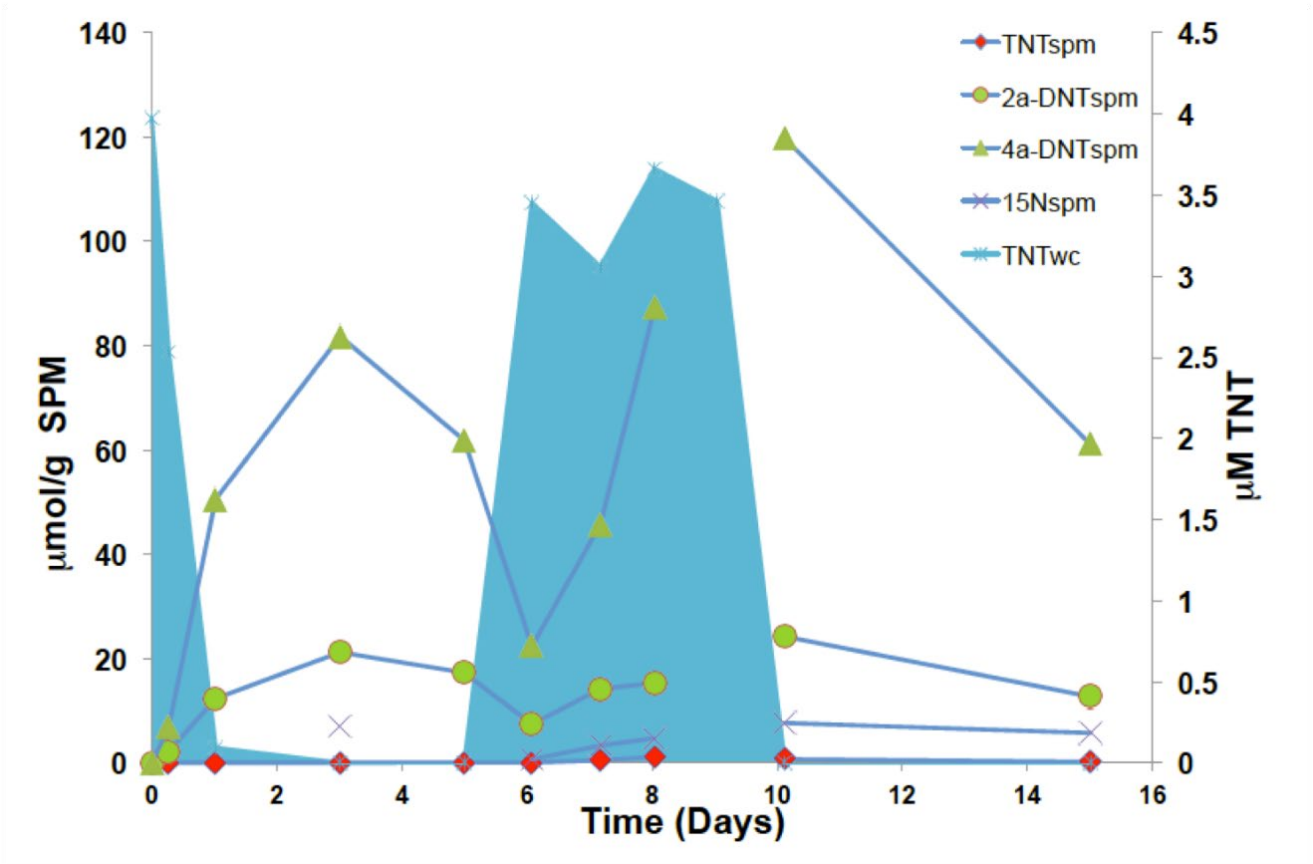

Supplementary Figure S-6.5. Concentrations of extractable munitions from SPM. The blue area represents the concentration of TNT in the tanks.

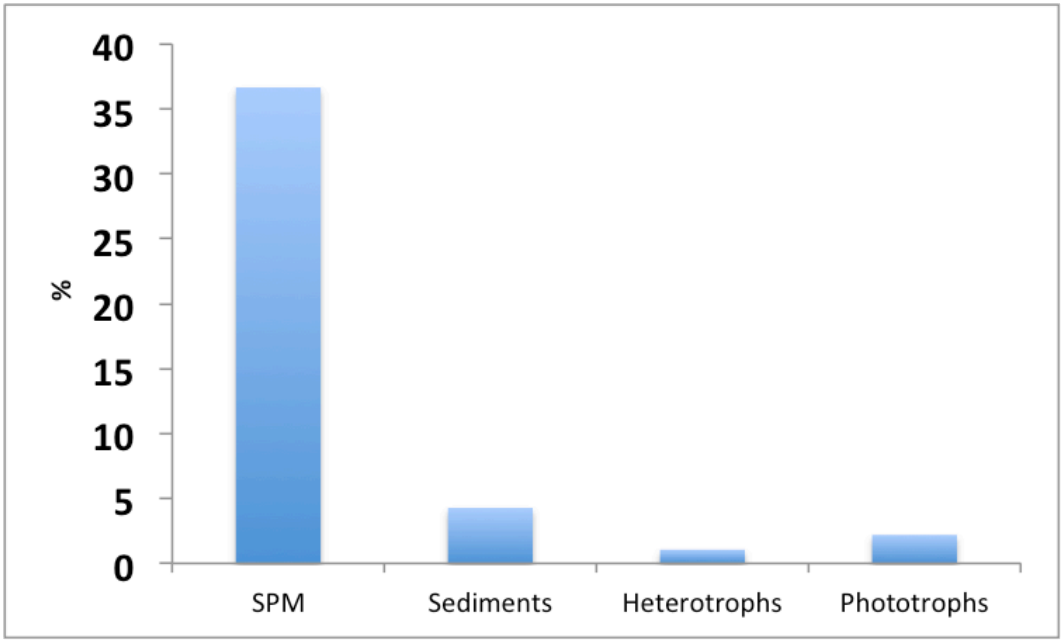

Supplementary Figure S-6.6. Percentages of ^{15}N in each fraction found in identifiable compounds (TNT, 2a-DNT, 4a-DNT).

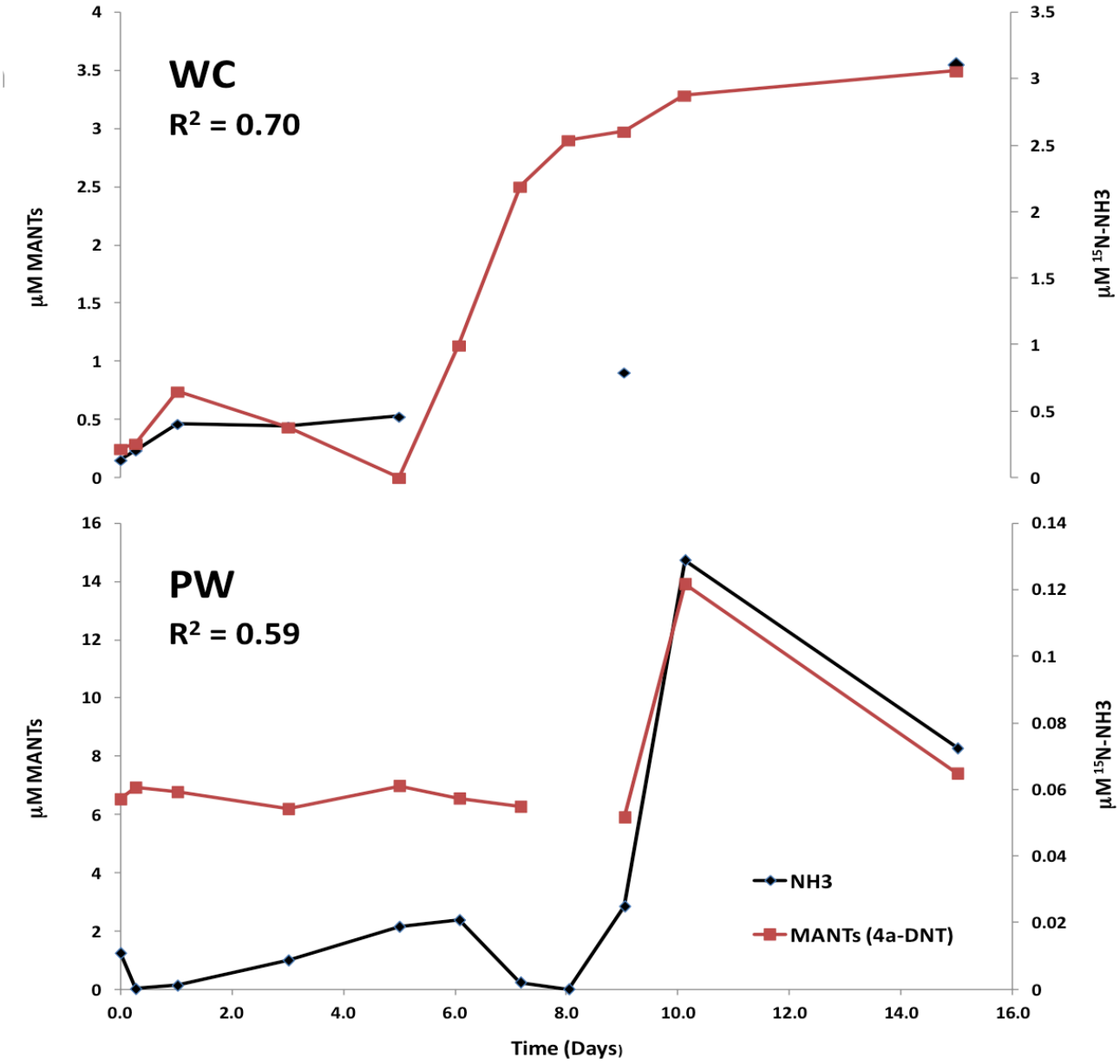

Supplementary Figure S-6.7. Correlation between $^{15}NH_3$ and 2a-DNT + 4a-DNT concentrations.

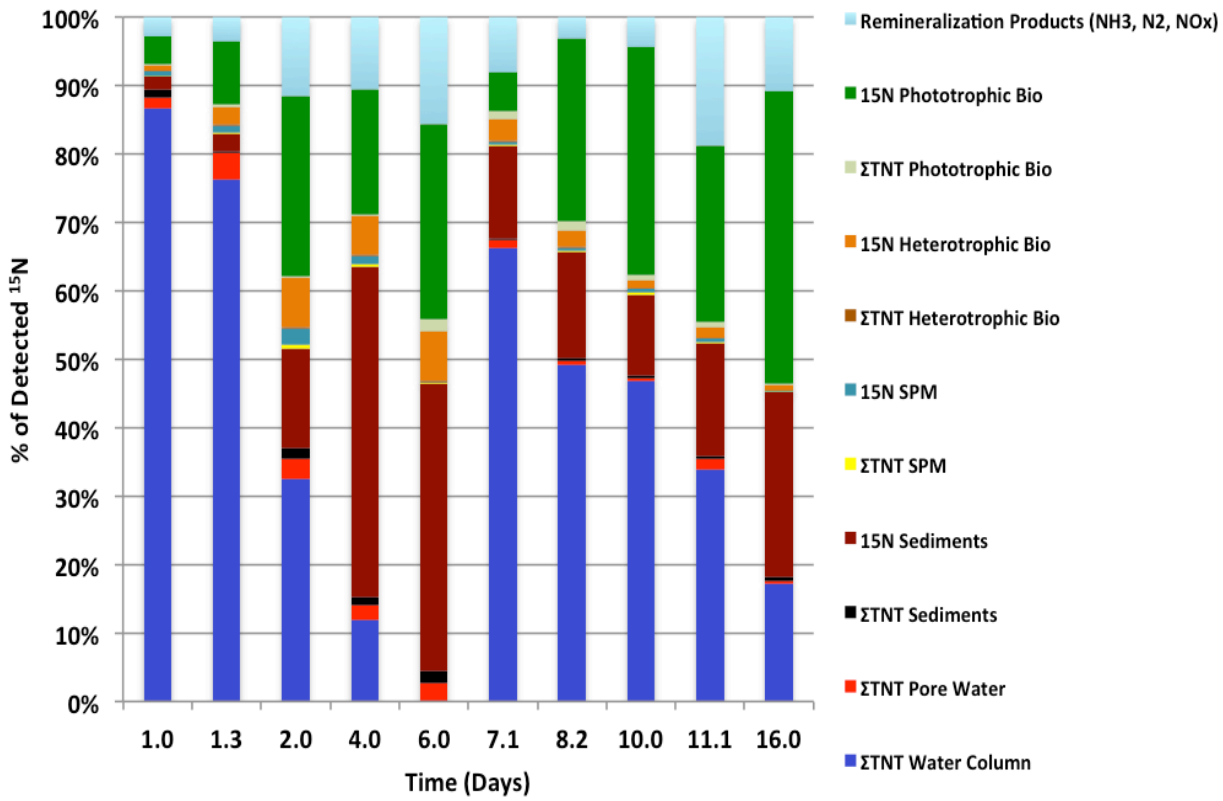

Supplementary Figure S-6.8. ^{15}N mass balance (missing ^{15}N not shown for clarity).

7.0. Comparative Study of Biodegradation and Metabolism of hexahydro-1,3,5-trinitro-1,3,5-triazine in Three Coastal Habitats Using a Stable Isotopic Tracer, ^{15}N-RDX

This chapter was published, as follows:

Ariyarathna, T. 2016. Sorption and Metabolism of Explosives in Sediment of Coastal Marine Ecosystems. PhD Dissertation, Chapter 5, University of Connecticut.

Abstract

It has been estimated that there are hundreds of explosive-contaminated marine sites all over the world and managing these contaminated sites is an international challenge. The demand for data on the sorption, biodegradation and mineralization of trinitrotriazine (RDX) in coastal ecosystems is the impetus for this study. Stable nitrogen (^{15}N) isotope labeled RDX was used to track its processing in three coastal ecosystem types. Mesocosm experiments representing subtidal vegetated, subtidal non-vegetated, and intertidal marsh ecosystems were conducted and a steady state supply of RDX was maintained in the systems throughout 17-day experiments. Sediment, pore-water and overlying water samples were analyzed for RDX and transformation products including nitroso-triazines and dissolved inorganic nitrogen (DIN) pools including ammonium, nitrate, nitrite, nitrous oxide and nitrogen gases that contained the ^{15}N tracer. 50%, 44% and 25% of supplied RDX were transformed in intertidal marsh, subtidal vegetated and subtidal non-vegetated mesocosms respectively. RDX was biodegraded to nitroso-derivatives (MNX, DNX and TNX) via reduction (2% - 3% of system sequestrated RDX) and further breakdown formed inorganic nitrogen as mineralization products (50% - 72% of system sequestrated RDX) in coastal marine ecosystems. RDX was mineralized to N_2O (primarily) and N_2 (secondarily) through a series of intermediates (47% - 70% of system sequestrated RDX) and escaped to the atmosphere. Degradation and mineralization of RDX were favored by lowered redox potential and available microbial assemblage in surface sediment of the ecosystem. Subtidal vegetated and intertidal marsh ecosystems containing fine grained, organic carbon rich sediment where significant anaerobic respiration prevailed (presence of H_2S) showed notably higher mineralization of RDX. Subtidal non-vegetated ecosystem with organic carbon poor sediment where moderate anaerobic respiration prevailed (presence of Fe^{+2}) conditions showed the least mineralization and highest persistence of RDX in the system compared to the subtidal vegetated and intertidal marsh mesocosms. Partitioning of RDX and degradation products onto particulates was a negligible process in the overall mass balance of the systems (2% - 4%) and sorption onto the sediment decreased from intertidal marsh, subtidal vegetated to subtidal non-vegetated systems based on the available organic carbon content and grain size of the sediment. The fate of RDX quantitatively differed in different coastal marine habitats based on prevailing sediment redox condition in the ecosystem.

7.1. Introduction

The explosive compound, Hexahydo-1,3,5-trinitro-1,3,5-triazine (RDX) is utilized globally, mainly as a military munition since the second world war. Contamination of soil, surface water, groundwater, wetlands and coastal ecosystems with RDX has become a global environmental issue (Pichtel, 2012). RDX has been found to be toxic to aquatic (Ballentine et al., 2016) and terrestrial species (Hawari et al., 2000), and a carcinogen to humans (Pichtel 2012). The US coast has been significantly exposed to munitions via disposal of unexploded ordnances (MacDonald et al., 2009; Kalderis et al., 2011) while military training and weapon testing add an additional source.

Based on the physico-chemical properties of RDX, it has been found that RDX is less soluble in water (Kalderis et al., 2011) and persistent in surface water bodies where aerobic conditions prevail (Felt et al., 2009). Different removal strategies have been proposed for RDX (An et al., 2014) based on the characteristic properties of RDX (Kalderis et al., 2011; Ariyarathna et al., 2016) and geochemical variables in the system (Halasz and Hawari, 2011; Gregory et al., 2004). Sorption has not been identified as an effective removal mechanism of RDX from water due to its relatively low K_{OW} value (Ariyarathna et al., 2016).

RDX tends to degrade biotically (Juhasz and Naidu, 2007; Sheremata and Hawari, 2000) and abiotically (Ariyarathna et al., 2016) forming various transformation products in aquatic systems. Abiotic degradation is comparatively less favorable than microbial degradation of RDX (Ariyarathna et al., 2017) and the role sediments play in enhancing biotic degradation of RDX depends on sediment properties including organic carbon content, texture, microbial population and redox conditions (Ariyarathna et al., 2016; Gregory et al., 2004).

The degradation of RDX occurs via a chain of nitroso compounds, Hexahyro-1-nitroso-3,5-dinitro-1,3,5-triazine (MNX), Hexahyro-1,3-dinitroso-5-nitro-1,3,5-triazine (DNX), and Hexahyro-1,3,5-trinitroso-1,3,5-nitro-1,3,5-triazine (TNX) and has been widely documented in the literature, under both hypoxic and/or anoxic conditions (Ariyarathna et al., 2016; Halasz and Hawari, 2011; Smith et al., 2015a). Ring cleavage and complete mineralization are also reported for RDX (Halasz and Hawari, 2011; Sheremata and Hawari, 2000; Smith et al., 2015a). For instance, it has been identified that the cleavage of either N- NO_2 or C-H bonds in RDX produces unstable intermediates (with ring C-N bonds of 2 kcal/mol) leading to rapid ring cleavage. Therefore, any successful initial enzymatic attack on RDX can initiate degradation resulting in ring cleavage (Hawari et al., 2000). Nitrites, nitrates and ammonium resulting via denitration (Halasz and Hawari, 2011; Ariyarathna et al., 2017; Smith et al., 2015a) can be used as nitrogen sources by microorganisms (Beller, 2002; Montgomery et al., 2013), and N_2O and N_2 are formed as the ultimate mineralization products, mainly in low oxygen conditions (Sheremata and Hawari, 2000; Smith et al., 2015a; Hawari et al., 2000; Best et al., 1999; Kwon et al., 2011). Therefore, hypoxic/anoxic degradation and mineralization of RDX has been commonly observed in the literature coupled with microbial populations from soil, sediment and sewage sludge (Sheremata and Hawari, 2000; Montgomery et al., 2013; Ronen et al., 2008), under nitrate-reducing (Freedmen and Sutherland, 1998), iron-reducing (Gregory et al., 2004), and sulfate reducing conditions (Hawari et al., 2000; Boopathy et al., 1998). Although, biodegradation pathways of RDX have been studied to a certain extent, most studies have been conducted using specific microbial cultures in controlled laboratory conditions (Sheremata and Hawari, 2000; Beller, 2002; Ronen et al., 2008;

Sheremata et al., 2001). However, research in natural environmental conditions with different geochemical parameters and complex bacterial assemblages may yield considerable differences in the transformation of RDX in terms of breakdown products (quality and quantity), compound removal rates, biodegradation and mineralization efficiencies etc.

Vegetated marine ecosystems generally contain organic carbon rich, fine grain textured sediments while non-vegetated ecosystems contain organic carbon poor, coarse grain textured sediments (Cammen, 1982). Microbial populations habituated in vegetated and non-vegetated marine ecosystems vary in terms of types of microbes and microbial population size, depending on the available resources in systems (Cammen, 1982). Prevailing sediment redox potentials in these systems are quite different and all these factors affect sorption, degradation and mineralization of RDX in coastal marine ecosystems. Furthermore, intertidal marsh ecosystems experience tidal variation which alters the geochemistry of water and sediment, redox conditions and microbial populations in the system during high tide and low tide cycles (Zheng et al., 2016).

The objective of this research is to reveal the differences and compare the fate and metabolism of RDX in different nitrogen limited coastal marine habitats by tracking the transformation of RDX in different pools of the ecosystem including well aerated surface water and hypoxic/anoxic sediment using ^{15}N isotope labelled RDX as a tracer. Such a comparison has not been performed to date. This utilizes an integrated mass balancing approach with a stable ^{15}N isotope tracer which facilitates tracking a number of the RDX pathways that remove bioavailable, dissolved RDX from the ecosystem. Resulting outcomes from above mentioned comprehensive analysis of fate and metabolism of RDX helps to determine the most suitable remediation techniques for different coastal marine systems. This study also benefits future efforts related to the investigations and characterization of munition contaminated coastal sites since it identifies variations in removal rates and pathways.

7.2. Methods

7.2.1 Experimental Design, Sampling Plan and Techniques

Three experimental set-ups representing different coastal marine ecosystems, non-vegetated, subtidal vegetated and intertidal marsh were constructed in Rankin Seawater facility, University of Connecticut, Avery Point in order to compare fate and metabolism of RDX in different coastal marine habitats.

7.2.2 Non-vegetated Mesocosm

1000 L fiberglass experimental tank was connected to a reservoir tank filled with raw seawater from Long Island Sound (30 PSU) and loaded with an 8cm deep layer of sandy, low organic carbon (OC) containing sediment (0.2 % OC) collected from a subtidal habitat in Long Island Sound (LIS) (latitude: 41^0 19′ 13″ N and longitude: 72^0 2′ 59″ W) (Figure 1). Raw sea water was pumped to the experimental tank continuously from the reservoir tank under flow through conditions over two weeks to achieve stabilized redox conditions in sediment and then, experimental tank was loaded with macroalgae, epifaunal, bivalve and fish species typical of that habitat. The tank was aerated using air stones and overlying water was well mixed using pumps,

and total water volume was 686 L. The system was reconfigured to recirculation mode, and the seawater inflow rate was adjusted to 3.29 mL s^{-1} over the course of the experiment (17 days). ^{15}N labelled RDX (99 At% ^{15}N with respect to nitro groups) dissolved in methanol was introduced into the experimental tank as a pulse of concentrated stock (20.4 mL) to achieve initial target RDX concentrations of 1 mgL^{-1}, followed by continuous addition at a rate of 0.07 mL min^{-1} - 0.08 mL min^{-1} to target a conservatively mixed steady state RDX concentration of 0.5 mgL^{-1} throughout the experiment. The water residence time in the tank was 2.5 days. Figure 7.1 presents a schematic diagram of non-vegetated mesocosm (1: reservoir tank; 2: overlying water in experimental tank; 3: sediment layer).

Time series samples (total 9 sampling time points) of overlying water, porewater, suspended particulate matter (SPM) sediment and biota were taken from the tanks over the course of the experiment including two time points with triplicate samples. Overlying water was drawn using a peristaltic pump at a rate of 50 mL min^{-1} and filtered through Whatman 25 mm, 0.7 μm glass fiber filters (GF/F). Suspended particulate matter (SPM) was sampled by filtering 250−300 mL of overlying water through pre-weighed combusted (450 °C) GF/F filters, and split for analysis of bulk ^{15}N enrichment ($\delta^{15}N$ SPM) and extractable explosives concentrations. Porewater was using a $1/16^{th}$ in inch stainless steel tube inserted into the sediment layer, attached to a peristaltic pump. Porewater was collected at a slow pumping rate of 2.5 mL min^{-1} and filtered through polyethersulfone - 0.2 μM (0.2 μM PES) syringe tip filters. Sediment cores with a diameter of 2.6 cm were obtained and sliced at 2cm intervals prior to the analysis.

7.2.3 Subtidal Vegetated (eel grass) Mesocosm

The experimental setup was constructed similarly to the non-vegetated mesocosm except it contained fine grained, organic carbon rich sediment collected from Mumford Cove, LIS (latitude: 41^0 19′ 15″ and longitude: 72^0 0′ 24″) and sods of eel grass (Zostera marina) collected from LIS were transplanted in the sediment (Figure 7.2). In terms of sea water pumping, compound introduction, maintaining specific concentrations in the system, and sampling were performed identically to the non-vegetated system over an 18 day-experimental time duration. Porewater sampling techniques was adjusted due to the clogging issues of fine sediment particles in sampling tube. At each time point, porewater was extracted by centrifuging sediment slices obtained from above and below the oxic-anoxic interface of the sediment. Figure 7.2 presents a schematic diagram of subtidal vegetated mesocosm (1: reservoir tank; 2: overlying water in experimental tank; 3: sediment layer; 4: vegetation layer of eel grass).

7.2.4 Intertidal Marsh Mesocosm

The intertidal marsh mesocosm was constructed using two connected 1000 L tanks (reservoir and mesocosm) and the mesocosm tank was filled with fine grained, high organic carbon containing, compacted peaty sediment (15cm thickness) collected from Stonington, LIS (latitude: 41^0 20′ 5″ and longitude: 71^0 54′ 10″) (Figure 3). Intact sods of marsh grasses (*Spartina alterniflora*) were transplanted in the sediments of the mesocosm tanks and stocked with biota (macroalgae, epifaunal, bivalve and fish species). Raw sea water was pumped into the reservoir tank with a rate of 5.22 mL sec^{-1}. Pumps, timers, and float switches were used to exchange water back and forth between the reservoir and mesocosm tanks every 6 hours to simulate a flooding/draining tidal cycle

with a 1 foot tidal range. Water in the reservoir tank was mixed with a pump while the reservoir tank and mesocosm were sufficiently well mixed by the exchange of water between both tanks using a pump. Both tanks were aerated using air stones and the system was maintained at steady state conditions. ^{15}N labelled RDX (99 At% ^{15}N respect to nitro groups) was introduced into the reservoir tank using an initial slug dissolved in acetone to achieve an RDX concentration of 1 mgL^{-1} followed by continuous addition of RDX at a rate of 0.064 mL min^{-1} to achieve a 0.5 mgL^{-1} steady state concentration of RDX in the system. Figure 7.3 presents a schematic diagram of intertidal marsh mesocosm (1: reservoir tank; 2: Mixing tank; 3: surface water in experimental tank; 4: sediment layer; 5: vegetation layer of marsh grass).

Time series of overlying water, porewater and sediment samples were taken using similar techniques used in the non-vegetated mesocosm over an experimental duration of 17 days including 5 time points with triplicates (total of 10 sampling times). Overlying water and sediment samples were taken when the water level has reached its maximum height (high tide) in the mesocosm. Sediment cores of 8cm were sliced into 2cm intervals for the analysis. Porewater samples were taken when the water level had saturated the sediment surface (flood tide) and when it reached its maximum height (high tide). Flood tide samples were taken only from shallow depths of sediment (2cm from sediment surface) while high tide samples were obtained as a profile of two depths (2cm and 4cm from sediment surface). pH, dissolved oxygen, hydrogen sulfide profiles of sediment were obtained using the microsensors during both flood tide and high tide at each sampling point from three static wells permanently constructed in the sediment in order to avoid breakage of the microsensors.

7.2.5 System Characterization

Physical parameters of the systems including temperature and salinity were measured using a YSI probe (YSI 556 MPS) over the course of the experiments. Both overlying water and porewaters were analyzed for nutrients (ammonium, total nitrate and nitrite (NO_x)) using a Smartchem nutrient analyzer (Westco-W12623) following cadmium azo-dye and phenol hypochlorite methods (Smith and Bogren, 2001), respectively. 3 mL of filtered (0.2 µM PES) porewater were directly introduced to the reagents to minimize exposure to atmospheric oxygen and analyzed using the ferrozine method (Stookey, 1970) and methylene blue method (Cline, 1969) for dissolved ferrous and hydrogen sulfide respectively by UV/Vis spectrophotometry (Hitachi-U-30110). The redox potential of sediment was measured using a platinum electrode (Paleo Terra, Amsterdam) relative to an Ag/AgCl reference electrode (Fisher Scientific). In-situ profiles of dissolved oxygen, hydrogen sulfide and pH profiles in sediment were obtained using a Unisense DO, H_2S and pH microsensors (OX-50, H_2S-50, pH-50 micron). Sediment was characterized for TOC, total nitrogen (TN) and total elemental sulfur (S) using a Perkin Elmer elemental analyzer (NA 1500; Hedges and Stern, 1984). Sediment texture was determined using a mechanical sieve analyzer with a set of sieves from 0.063 mm to 2.0 mm.

7.2.6 Explosive Analysis

RDX and its reduced degradation products, including, MNX, DNX and TNX, were analyzed in both overlying water and porewater samples. A modified salting-out method (Miyares and Jenkins, 1990) adapted for smaller sample sizes was used for extraction of munition compounds

from aqueous samples following methods described in Ariyarathna et al. (2015). An average recovery of 99.1 ± 0.5% was obtained for known amounts of 1, 2-dinitrobenzene (1,2-DNB) in water extractions. Water extracts were analyzed using gas chromatography (GC)/electron-capture detection (ECD) following the methods described by Ariyarathna et al. (2015); 3, 4-dinitrotoluene (3,4-DNT) was added to each extract prior to injection to monitor detection efficiency. Explosive analysis was performed with an Agilent GC/ECD equipped with an HP-DB5 column (30 m x 320 µm, 0.25-µm; Agilent). Quantification was based on an external calibration curve of available standard munitions RDX, MNX, DNX and TNX. (AccuStandard, New Haven, CT). The average reporting limit for all compounds was 7.8 ng mL^{-1}. Sediment samples were homogenized and 2g of each was extracted with 10mL of ACS-grade acetonitrile (ACN) following the method described by Ariyarathna et al. (2015) and Smith et al. (2015b). 3,4-dinitrotoluene (3,4-DNT; Accustandard) was spiked as a recovery standard and extraction efficiencies averaged as 82%. Sediment extractions were analyzed for explosives (RDX, MNX, DNX and TNX) using gas chromatography (GC)/electron-capture detection (ECD) as mentioned above.

7.2.7 Bulk δ^{15}N Analysis

Freeze dried sediment and SPM samples were analyzed using a continuous flow elemental analyzer – isotope ratio mass spectrometry (EA-IRMS: Delta V, Thermofisher) at the University of Connecticut for bulk ^{15}N enrichments. Nitrogen isotope ratios are reported in δ notation as follows:

$$\delta^{15}N = [(R_{sample} - R_{STD})/R_{STD}] \quad (1)$$

where R_{STD} is the $^{15}N/^{14}N$ ratio of atmospheric nitrogen and R_{sample} is the $^{15}N/^{14}N$ ratio of the sample. δ^{15} N values are reported in parts per mil (‰) and external calibration was done using glutamic acid standards USGS 40 and USGS 41. The delta values were converted to mole fractions ($X^{15}N$) and excess ^{15}N tracer derived from the RDX was calculated from mole fractions and total N mass according to (Equation 2).

$$^{15}N \text{ mols Excess} = N \text{ mols} * (X^{15}N_t - X^{15}N_{t0}) \quad (2)$$

For Eqn. 2, the total N mass, and mole fractions of ^{15}N at time t ($X^{15}N_t$) and time 0 ($X^{15}N_{t0}$) were obtained from an elemental analyzer – isotope ratio mass spectrometry EA-IRMS (Delta V, Thermofisher). Analytical precision for sediment and SPM samples was 10% and 14% respectively (% coefficient of variance, CV).

7.2.8 Mineralization Product Analysis

The mineralization products, $^{15}NH_4^+$, total $^{15}NO_2^-$ and $^{15}NO_3^-$ ($^{15}NO_X$), $^{15}N_2$ and $^{15}N_2O$ in the aqueous phase (surface water and porewater), were quantified using IRMS techniques. Filtered (0.2 µM PES), frozen water samples (from subtidal non-vegetated and intertidal marsh mesocosms) and sediment (from subtidal vegetated) were extracted for NH_4^+ following the methods from Holmes et al. (1998). Ammonium extraction from sediment was done using a 2M KCl solution. δ^{15}N isotopic enrichment of ammonium extractions were obtained using a continuous flow EA-IRMS. Extraction efficiency was between 95-105% based on the recovery of NH_4NO_3 standards and analytical precision is 25% (percent coefficient of variance, CV).

Moles of $^{15}NH_4^+$ were calculated using NH_4^+ concentrations and mole fractions of ^{15}N ($X^{15}N_t$ and $X^{15}N_{t0}$) obtained from EA-IRMS (Equation 3).

$$^{15}NH_4^+ \text{ mols Excess} = NH_4^+ \text{ mols} * (X^{15}N_t - X^{15}N_{t0}) \quad (3)$$

$\delta^{15}NO_X$ values of overlying and porewater were obtained via the denitrifier method using *Pseudomonas aureofaciens* (Smith et al., 2015b) at the US Geological Survey (USGS) in Reston, VA on water samples filtered through a 0.2µM PES filters and frozen. Moles of $^{15}NO_X$ were calculated using NO_X concentration and the mole fractions of ^{15}N ($X^{15}N_t$ and $X^{15}N_{t0}$) obtained from isothermal GC-IRMS (Equation 4).

$$^{15}NO_X \text{ mols Excess} = NO_X \text{ mols} * (X^{15}N_t - X^{15}N_{t0}) \quad (4)$$

Gas samples were collected at each time point by pumping unfiltered water into 30 mL and 60 mL serum bottles for N_2 and N_2O respectively that had previously been sealed, pre-loaded with 3M $NaHSO_4$ (for preservation), and flushed with He for 12 minutes (Smith et al., 2015a). Following sample collection, At least after 6 hours of headspace equilibration, the isotopic composition of N_2 and N_2O ($\delta^{15}N$-N_2 and $\delta^{15}N$-N_2O) was measured. $^{15}N_2$ in water samples was determined using continuous flow isotope ratio mass spectrometry (IRMS) on a Thermo Delta V Plus with a Gas Bench interface (GB-IRMS). Dissolved ambient N_2 concentrations were assumed to be in equilibrium with the atmosphere and were calculated as a function of temperature and salinity (Weiss, 1970). $^{15}N_2O$ in water samples was measured via continuous flow IRMS interfaced to a modified Gas Bench. Dissolved gases in samples were He sparged and passed through a chemical soda lime trap to remove CO_2. N_2O was quantitatively cryo-trapped using liquid N. The trapped N_2O was then released and separated from any remaining trace CO_2 using a poraplot Q column, and then analyzed for $^{15}N_2O$ via IRMS. Dissolved N_2O concentrations were obtained from GC-ECD and analytical precision of the analysis is 3% (% coefficient of variance, CV). Evasion rates for $^{15}N_2$ and $^{15}N_2O$ were calculated from excess ^{15}N masses of each gas and gas transfer coefficients measured following known gas tracer additions (SF_6) using the method described in (Smith et al., 2015a).

7.2.9 Data Analysis

A mass balancing approach was based on ^{15}N equivalents in masses of each analyzed N-containing parent and derivative pools and illustrated in following equations (Equation 5).

$$^{15}N\text{-}RDX_{system} = {}^{15}N\text{-}\sum RDX_{\text{surface water}} + {}^{15}N\text{-}\sum RDX_{\text{porewater}} + {}^{15}N\text{-}\sum RDX_{\text{sediment}} + {}^{15}N\text{-}\sum RDX_{\text{biota}} + {}^{15}N_{SPM} + {}^{15}N\text{-}NH_4^+{}_{\text{dissolved}} + {}^{15}N\text{-}NO_{X\ \text{dissolved}} + {}^{15}N\text{-}N_2 + {}^{15}N\text{-}N_2O + \text{unidentified } {}^{15}N\text{-compounds in the system} \quad (5)$$

where, ^{15}N-RDX_{system} represents system sequestrated ^{15}N-RDX based on rates (cumulative influx of ^{15}N-RDX into the system – cumulative outflux from the system) and the remaining terms represent ^{15}N measured in different RDX-derived metabolites in overlying water, porewater, sediment, bio-tissues and SPM. The aqueous terms are adjusted for outflow, and the gas terms are adjusted (included) outflow and evasion to the atmosphere. ∑ RDX represents RDX and measurable derivatives including MNX, DNX and TNX.

Removal kinetics of munitions were analyzed determining removal rate constants (Equation 6) and half-lives (Equation 7) using the following equations.

$$\ln [C_i] = -kt + \ln [C_i]_{t=0} \quad (6)$$

$$t_{1/2} = \ln 2 / k \quad (7)$$

where t is time (hr) and k is the first order removal rate constant (hr^{-1}).

7.3 Results

7.3.1 Characterization and Mass balance of the Ecosystem

Measured physical and chemical parameters those describe the variations among mesocosms are shown in Table 7.1. System sequestrated ^{15}N-RDX (cumulative input of RDX into the system - cumulative output of RDX from the system; Figure 7.4) was found in different compartments of the mesocosm including dissolved fractions in surface water and porewater, sorbed fractions in sediment, particulate organic matter and biota, and gaseous fractions that escaped to the atmosphere. Loss of RDX (cumulative input of RDX into the system - cumulative output of RDX from the system - total RDX stored in surface water, porewater and sediment) at the end of the experiment in subtidal non-vegetated, subtidal vegetated and intertidal marsh mesocosms were 25%, 44% and 50% respectively (Table 7.2). First order removal rate constants of RDX from overlying waters were 0.029 hr^{-1}, 0.066 hr^{-1}, and 0.095 hr^{-1} in non-vegetated, vegetated and marsh, respectively. Half-lives of RDX decreased in the order of non-vegetated (24 days), vegetated (11 days) and marsh mesocosms (7 days; Table 7.2).

Amount of RDX stayed in water is higher in subtidal non-vegetated mesocosm (25%), compared to the subtidal vegetated (10%) and intertidal marsh (6%) mesocosms. ^{15}N-RDX was partitioned onto particulates in the ecosystem (sediment and SPM) and higher in intertidal marsh mesocosm (4%) than vegetated (3%) and non-vegetated (2%) mesocosms. Nitroso-derivatives did not show significant variation in between mesocosms: non-vegetated (3%), vegetated (2%) and marsh (2%). The distribution of tracer ^{15}N mass into various pools in mesocosms in terms of the amount of RDX stays in water, amount of derivatives and mineralization products in water, and the amount of RDX derived ^{15}N partitioned onto solids at end of the experiment is shown as a cumulative mass balance in Figure 7.5. Subtidal vegetated (68%) and intertidal marsh (72%) ecosystems showed notably higher mineralization of RDX forming dissolved inorganic nitrogen (ammonia, nitrates, nitrous oxide and nitrogen gases). Subtidal non-vegetated ecosystem showed the least mineralization (50%). Nitrous oxide was the prominent mineralization product of RDX for all the treatments (95-96% of total mineralization) that escaped to the atmosphere (Figure 7.6). Highest amount of ^{15}N gas production (N_2O and N_2) was found in marsh mesocosm, followed by vegetated silt, and finally the low organic non-vegetated sandy mesocosm.

7.3.2 Transformation

RDX transformation products, nitroso-triazines (MNX, DNX and TNX) were present in both surface water and porewater throughout the experimental duration in all three mesocosms

(Table S-7.1). The amount of total detected nitroso-triazines in surface water stayed relatively constant during the experiment and concentration ranges did not show significant variations among ecosystems (Figure 7.7). Total detected nitroso-triazines in porewater decreased with the time in all three treatments and highest porewater concentrations were found in the intertidal marsh mesocosm (Figure 7.7C). The ratio of total detected nitroso-triazines in porewater to surface water on day 17 in non-vegetated, vegetated and marsh mesocosms were 14, 7 and 24 respectively. Rapid transformation of RDX was observed in coastal marine mesocosms showing the highest total detected nitroso-triazines in surface water after 6 hr of spiking and at 24 hr for porewater.

7.3.3 Partitioning

Partitioning of ^{15}N-RDX onto particulates (sediment and SPM) followed similar trends in all the studied coastal mesocosms showing rapid increase in sorbed ^{15}N-RDX onto particulates followed by a drop and then, remaining constant during the remainder of the experiment (Figure 7.8). Sorption of ^{15}N-∑RDX (^{15}N from RDX and derivatives) onto SPM (1.31 - 344 nmol/g SPM) showed higher values than those values sorbed onto surface sediment (1.18 – 96.3 nmol/g sed) in coastal marine mesocosms (Figure 7.8). But, sediment became a better sink for ^{15}N-∑RDX than SPM because depth integrated total sediment mass in the mesocosms was huge compared to SPM. Sorption of ^{15}N-∑RDX onto SPM was highest in the non-vegetated mesocosm (8.22 – 344 nmol/g SPM) while it was lowest in the subtidal vegetated mesocosm (1.31 – 89.2 nmol/g SPM). ^{15}N-∑RDX values found in SPM of intertidal marsh mesocosm ranged from 53.9 nmol/g SPM to 244 nmol/g SPM during the experiment (Figure 7.8A). Bulk ^{15}N-∑RDX found in surface sediment decreased in the order of intertidal marsh, subtidal vegetated and subtidal non-vegetated showing value ranges of 14.8 - 96.3 nmol/g sed, 1.30 – 31.7 nmol/g sed and 0.32 – 25.5 nmol/g sed respectively (Figure 7.8B). The highest RDX amount in sediment (6 - 40% of bulk ^{15}N in sediment) was found at the beginning of the experiment in all the three mesocosms and decreased with time, disappearing by the end of the experiment in subtidal vegetated and intertidal marsh mesocosms (Figure S-7.1). Nitroso-triazines were identifiable in surface sediment of coastal marine mesocosms with ratios of RDX to total nitroso-triazines were 4.5, 0.5 and 3.1 in non-vegetated, vegetated and marsh mesocosms respectively. The highest DNX amount in sediment (10% of bulk ^{15}N in sediment) was found in the non-vegetated system after 6 hours of spiking while TNX appeared at a slower rate with time. TNX was formed as the main nitroso-derivative in both subtidal vegetated and intertidal marsh mesocosms (Figure S-7.1).

7.3.4 Mineralization

Mineralization in terms of detected inorganic nitrogen was identified as the main fate of RDX in all the three coastal marine ecosystems: subtidal non-vegetated, subtidal vegetated and intertidal marsh mesocosms. Figure 7.5 shows the contribution of different mineralization products ($^{15}NH_4^+$, $^{15}NO_x$, $^{15}N_2$ and $^{15}N_2O$) to the total mineralization. N_2O was produced as the prominent mineralization product of RDX, but $^{15}N_2O$ contribution to the total mineralization did not significantly vary among non-vegetated (84% - 96%), vegetated (71% - 96%) and marsh (76% - 95%) mesocosms. $^{15}NO_x$ peaked at the very first sampling time point (6 hr after spiking) and gradually decreased approaching steady state concentrations in all three mesocosms. The ranges of percentages of $^{15}NO_X$ out of total mineralization were found as 14% - 2%, 29% - 3% and 23% - 2% in non-vegetated, vegetated and marsh mesocosms respectively. Although $^{15}NH_4^+$ (1%) and

$^{15}N_2$ (2%) were detected in the mesocosms, they did not significantly contribute to the total mineralization in coastal mesocosms. Ammonium production from RDX in porewater was higher than in surface water and ratios of standing stock $^{15}NH_4^+$ in sediment porewater to surface water were 5, 50 and 10 in non-vegetated, vegetated and marsh mesocosms respectively. Porewater $^{15}NH_4^+$ production was highest in subtidal vegetated mesocosm among three studied coastal mesocosms (Table 7.3). $^{15}N_2O$ production was significantly higher (30 times) than $^{15}N_2$ production (Figure 7.5). Time series N_2O production and the mole fraction of $^{15}N_2O$ are shown in figure 9. Mole factions of $^{15}N_2O$ in non-vegetated and marsh mesocosms varied within the range of 0.4 to 0.5 while they are 0.3 to 0.4 in vegetated mesocosm.

7.3.5 Depth Influence on Fate of RDX in Intertidal Marsh Mesocosm

Table 7.3 shows the time series concentrations of bulk ^{15}N in sediment, $^{15}NH_4^+$, $^{15}N_2$ and $^{15}N_2O$ at depth 1 (0-2cm) and depth 2 (2-4cm) of peaty sediment in intertidal marsh mesocosm. All the measured ^{15}N-RDX pools (bulk ^{15}N in sediment, $^{15}NH_4^+$, $^{15}N_2$ and $^{15}N_2O$) in deeper (2-4cm) level sediment showed quantitatively lower values compared to those values in shallow (0-2cm) level sediment, although, the time series trends followed the same patterns as they appeared in shallow sediment (Table 7.3). The ratio of bulk ^{15}N values in shallow sediment to deeper sediment varied within the range of 1.4 to 6.4 during the experiment of 16 days. Measured dissolved inorganic nitrogen (DIN) containing mineralization products, $^{15}NH_4^+$, $^{15}N_2$ and $^{15}N_2O$ showed average ratios of shallow to deeper level concentrations in porewater during the experiment as 1.6, 1.8 and 6.3 respectively.

7.4. Discussion

7.4.1 Behavior of RDX in Mesocosms

Depending on the differences in redox potential and available resources, different microbial populations including nitrate-reducers, iron-reducers and sulfate-reducers were involved in RDX transformation in coastal marine mesocosms (Halasz and Hawari, 2011). The least loss of RDX was seen in subtidal non-vegetated mesocosm containing sandy sediment with low organic carbon content that only permitted nitrate and iron reduction in the sediment. The subtidal vegetated and intertidal marsh mesocosms had higher organic carbon that supported nitrate, iron and even sulfate reduction that may have contributed to higher loss of RDX than the non-vegetated system (Delaune and Reddy, 2005). Further, the high RDX loss in the marsh could have been facilitated by tidally driven downward advection of water into the sediment. The shortest half-life of RDX in surface water was found in intertidal marsh. The non-vegetated mesocosm had the longest half-life and the highest persistence of RDX in surface water in the system. RDX loss mainly resulted from degradation and mineralization of RDX in sediment while sorption onto particulates was not a significant process.

The use of ^{15}N enabled a much more complete assessment of the fate and transport of RDX in coastal marine ecosystems. A mass balancing approach based on sequestrated ^{15}N-RDX into the systems illustrated that 80% - 84% of the ^{15}N contained in RDX that processed in the mesocosm was recovered in the measured pools. Subtidal vegetated and intertidal marsh ecosystems showed a notably higher mineralization of RDX to inorganic nitrogen, since prevailing reduced redox condition forming H_2S from SO_4^{2-} in organic carbon rich sediment

donated a surplus of electrons for reductive anaerobic mineralization of RDX (Smith et al., 2015a). The subtidal non-vegetated ecosystem showed the least mineralization and highest persistence of RDX compared to the subtidal vegetated and intertidal marsh mesocosms, since it had low organic carbon containing sediment which only permitted iron reduction in the sediment (Boopathy et al., 1998). Partitioning onto particulates, sediment and suspended organic matter and degradation of RDX into nitroso-triazines did not contribute significantly to the ecosystem-wide ultimate fate of RDX in coastal marine mesocosms.

7.4.2 Transformation of RDX to Derivatives

Total detected nitroso-triazines remained constant in surface water without a significant quantitative variation in the production of nitroso derivatives among three marine ecosystems, since further breakdown to dissolved inorganic nitrogen was less favorable in aerated conditions (Khan et al., 2012). The total detected nitroso-triazine amount was higher in porewater than in surface water of all the three mesocosms, so that sediment played an important role in the transformation of RDX (Smith et al., 2013). Enhanced mineralization of nitroso derivatives in hypoxic surface sediments (Smith et al., 2015a) resulted in a decreasing pattern of total detected nitroso-triazines in porewaters of all the three mesocosms with time. The lowest total nitroso-triazine production was found in subtidal vegetated ecosystems where the lowest redox potential persisted among three mesocosms, confirming further breakdown of nitroso products under low oxygen conditions by anaerobic microorganisms (eg: *Clostridium* sp., *Shewanella halifaxensis*) to use as a nitrogen and energy source (Halasz and Hawari, 2011).

7.4.3 Partitioning

Due to the relatively low hydrophobicity in terms of log Kow, the structure of RDX and its derivatives, passive partitioning onto sediment and SPM did not constitute a major pathway in the fate of RDX (Ariyarathna et al., 2016). However, RDX and RDX-derived metabolite partitioning into the particulate pools (sediment, SPM) in subtidal non-vegetated, vegetated and intertidal marsh mesocosms showed significant differences among treatments based on sediment characteristics (Ariyarathna et al., 2016). Generally, RDX and derivatives rapidly sorbed onto the particulates. Both SPM and sediment (Ariyarathna et al., 2016), attained steady state conditions of bulk ^{15}N from RDX and derivatives (^{15}N-$\sum$RDX) in particulates towards the end of the experiment and it might be a result of similar sorption and desorption rates. The least ^{15}N-$\sum$ RDX in SPM was found in the subtidal vegetated system where partitioned RDX might be degraded to nitroso-derivatives under lower redox potentials and transferred to the dissolved fraction in surface water. Well aerated surface water in non-vegetated mesocosms did not provide favorable conditions for biodegradation (Hawari et al., 2000) allowing higher partitioned ^{15}N-$\sum$ RDX amount to stay in SPM as a sorbed fraction. However, partitioning of RDX and derivatives was significantly enhanced by the elevated organic carbon content and finer grain size of peaty sediments in the intertidal marsh system while considerably lower bulk ^{15}N-$\sum$ RDX values in deeper sediment confirmed the low vertical diffusion of RDX and its derivatives in peaty sediment of the intertidal marsh mesocosm. Lower organic carbon and clay fraction containing sandy sediment in the subtidal non-vegetated mesocosm is not a favorable zone for partitioning of RDX and derivatives (Ariyarathna et al., 2016). Marine microbial assemblages (e.g. *Shewanella halifaxensis, Clostridium sp*.) may have contributed to degradation of RDX under oxygen limited conditions (Anke et al., 2003), especially, in the subtidal vegetated ecosystem, with the lowest

RDX amount detected in sediment at all stages of the experiment. Since sandy sediment which only permitted iron reduction in the non-vegetated mesocosm was not a favorable zone for biodegradation, RDX persisted in the sediment to a certain extent even after the two-week time duration. Anaerobic biodegradation under lower redox potential which permitted sulfate reduction (Boopathy et al., 1998; Boopathy et al., 1997) in subtidal vegetated and intertidal marsh mesocosms resulted TNX as the main identifiable ^{15}N containing compound in sediment. Unidentified ^{15}N in sediment might reside as non-measured derivatives such as MEDINA (Anke et al., 2003) or as microbially incorporated ^{15}N.

7.4.4 Mineralization

Mineralization of RDX in terms of inorganic nitrogen production ($^{15}NO_X$, $^{15}NH_4^+$, $^{15}N_2$ and $^{15}N_2O$ gases) played an important role in the fate of RDX in marine mesocosms and among the other inorganic nitrogen products, gaseous mineralization product, $^{15}N_2O$ formation was favored by the available microbes and prevailing environmental conditions in all the three marine ecosystems (Smith et al., 2015a). $^{15}N_2O$ was produced under lower redox potential which permitted nitrate, iron and sulfate reduction in surface sediment (Halasz and Hawari, 2011) via breakdown of Methylenedinitramine (MEDINA), an anaerobic ring cleavage product formed via denitration of RDX followed by hydroxylation (Halasz and Hawari, 2011). Mole fraction of $^{15}N_2O$ (~ 0.5) produced in this study also revealed that triazine ring in RDX opened up to form $^{15}N_2O$ which was consisted of one isotopically labelled ^{15}N atom coming from nitro group and another unlabelled ^{14}N atom coming from the ring of RDX. It might be the primary pathway of formation of $^{15}N_2O$ which was then readily diffused through the water column and escaped to the atmosphere (Smith et al., 2015a). Besides the decomposition of MEDINA, mono or poly-denitration of RDX and nitroso-triazines including MNX, DNX and TNX were also secondarily involved in the formation of $^{15}N_2O$ by denitrification of cleaved $^{15}NO_X$ from nitroso-triazines that acted as an intermediate mineralization product. Mineralization of RDX producing $^{15}N_2O$ significantly elevated in organic carbon rich subtidal vegetated and intertidal marsh mesocosms those showed anaerobic respiration forming H_2S via sulfate reduction (Felt et al., 2009). Although, there was a possibility of formation of $^{15}N_2$ from denitrification of $^{15}N_2O$ under anaerobic conditions (Smith et al., 2015a), it was a negligible mineralization pathway of RDX quantitatively in all the studied marine coastal mesocosms relative to $^{15}N_2O$ production. $^{15}NO_X$ is identified as the second highest mineralization product of RDX and it was rapidly formed in surface water via denitration and denitrosation (Halasz and Hawari, 2011) in all the three marine ecosystems. Denitration of RDX was augmented by reduced redox conditions (Smith et al., 2015a) resulting in the highest and lowest $^{15}NO_X$ productions found in subtidal vegetated and non-vegetated mesocosms respectively. $^{15}NO_X$ was not a stable mineralization product of RDX though it might be rapidly consumed via biological uptake (Ballentine et al., 2016) or acted as an intermediate during the process of forming $^{15}N_2O$ via denitrification in the systems (Smith et al., 2015a). Formation of MEDINA has been identified as a common $^{15}NH_4^+$ releasing process from RDX under low oxygen conditions (Halasz and Hawari, 2011), consistent with the elevated $^{15}NH_4^+$ in sediment porewaters versus surface water in subtidal non-vegetated, vegetated and intertidal marsh mesocosms here. All mesocosm sediments had requisite redox character to support nitrate reduction ammonium formation (Freedman and Sutherland, 1998). Despite the appearance of tracer in multiple DIN pools, $^{15}N_2O$ formation from RDX, followed by evasion to the atmosphere was the most significant mineralization pathway.

7.5. Conclusions

Tracing the fate of RDX with ^{15}N provided a descriptive picture of partitioning, degradation and mineralization of RDX in coastal marine ecosystems. The fate of RDX in marine coastal ecosystems including subtidal non-vegetated, subtidal vegetated, intertidal marsh varied depending on different sediment characteristics and prevailing redox conditions. Persistence of RDX in the system decreased in the order of subtidal non-vegetated, subtidal vegetated and intertidal marsh mesocosms based on half-lives of RDX in the systems. Here, we conclude that 50%, 44% and 25% losses of RDX were reported in contaminated intertidal marsh, subtidal vegetated and subtidal non-vegetated coastal marine habitats respectively. The majority of the RDX lost was accounted for by mineralization to 15N2O with subsequent venting of N2O to the atmosphere. Prevailing redox condition based on organic carbon content of sediment in the ecosystem was the key factor for natural attenuation of RDX in contaminated coastal marine habitats.

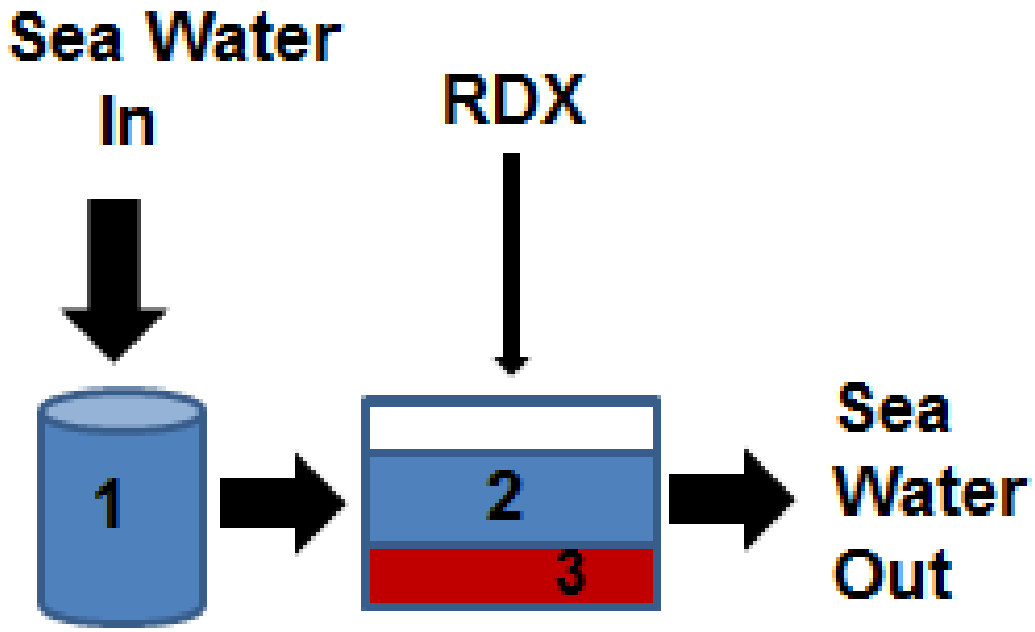

Figure 7.1. Schematic diagram of non-vegetated mesocosm (1: reservoir tank; 2: overlying water in experimental tank; 3: sediment layer).

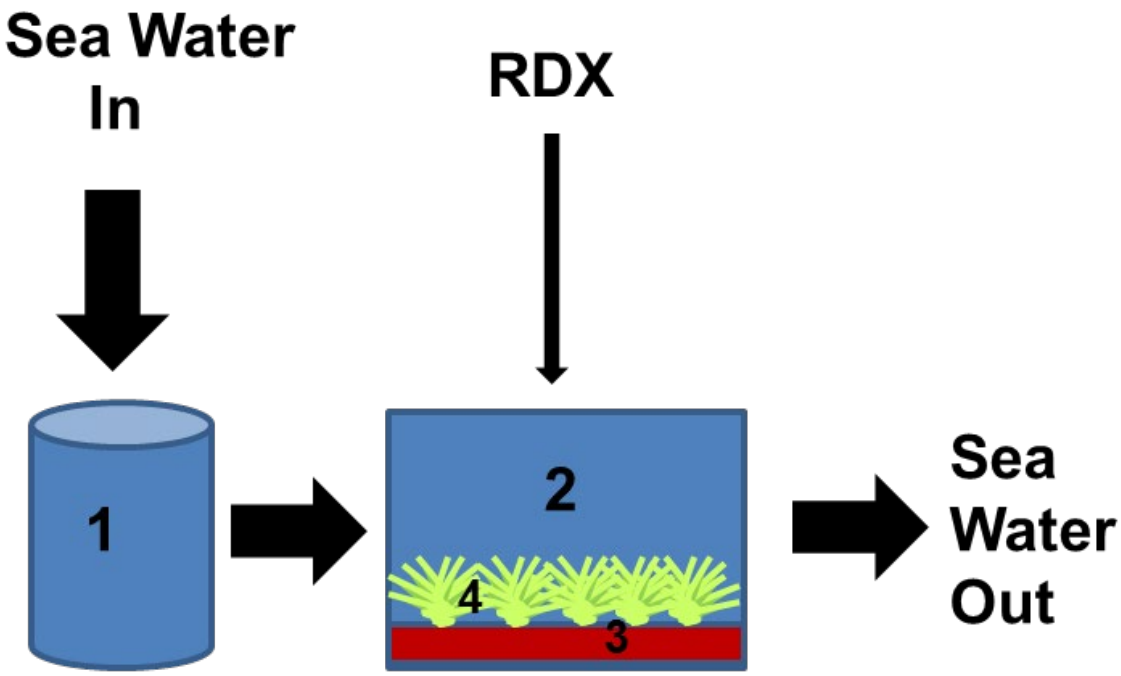

Figure 7.2. Schematic diagram of subtidal vegetated mesocosm (1: reservoir tank; 2: overlying water in experimental tank; 3: sediment layer; 4: vegetation layer of eel grass).

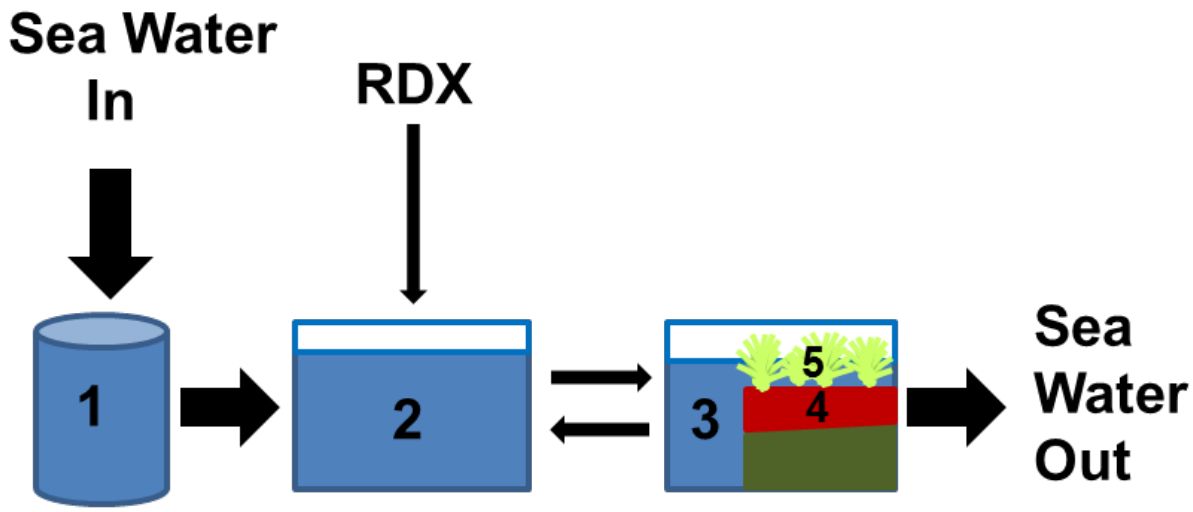

Figure 7.3. Schematic diagram of intertidal marsh mesocosm (1: reservoir tank; 2: Mixing tank; 3: surface water in experimental tank; 4: sediment layer; 5: vegetation layer of marsh grass).

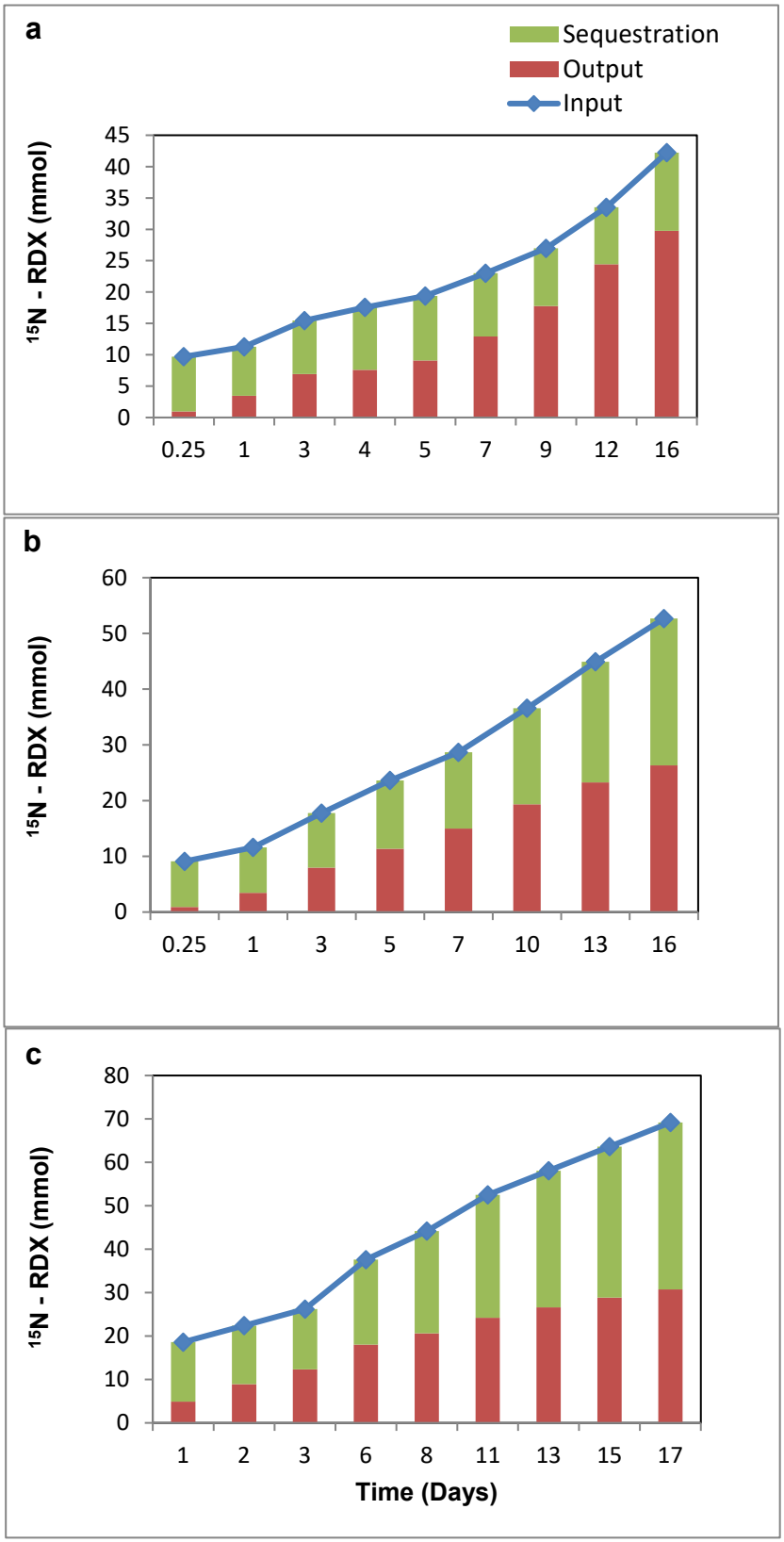

Figure 7.4. Time series system sequestration (cumulative influx – cumulative outflux) of ^{15}N-RDX in a) subtidal non-vegetated b) subtidal vegetated c) intertidal marsh.

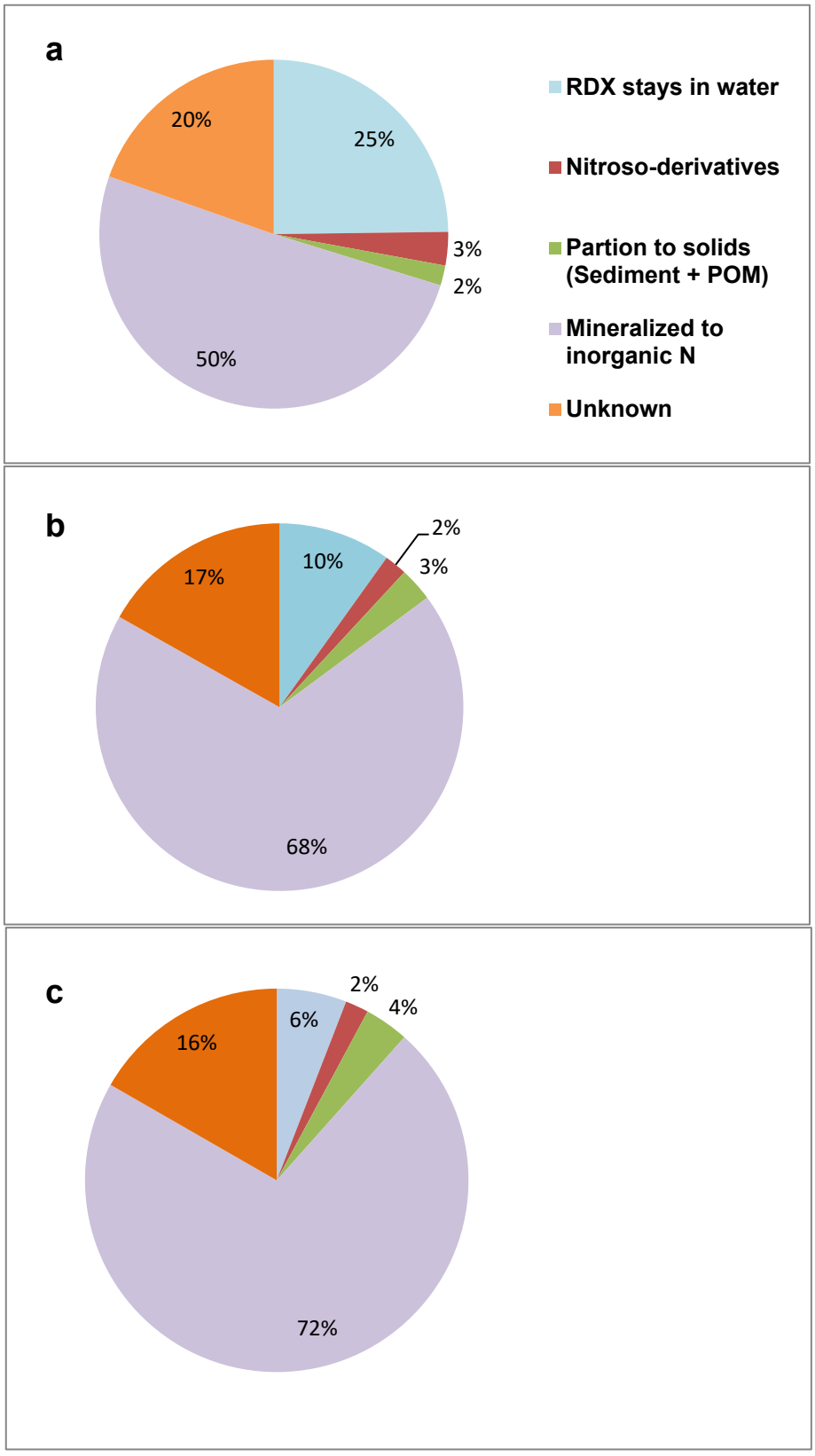

Figure 7.5. ^{15}N cumulative mass balance of system sequestrated ^{15}N-RDX on the last day of the experiment in a) subtidal non-vegetated b) subtidal vegetated c) intertidal marsh.

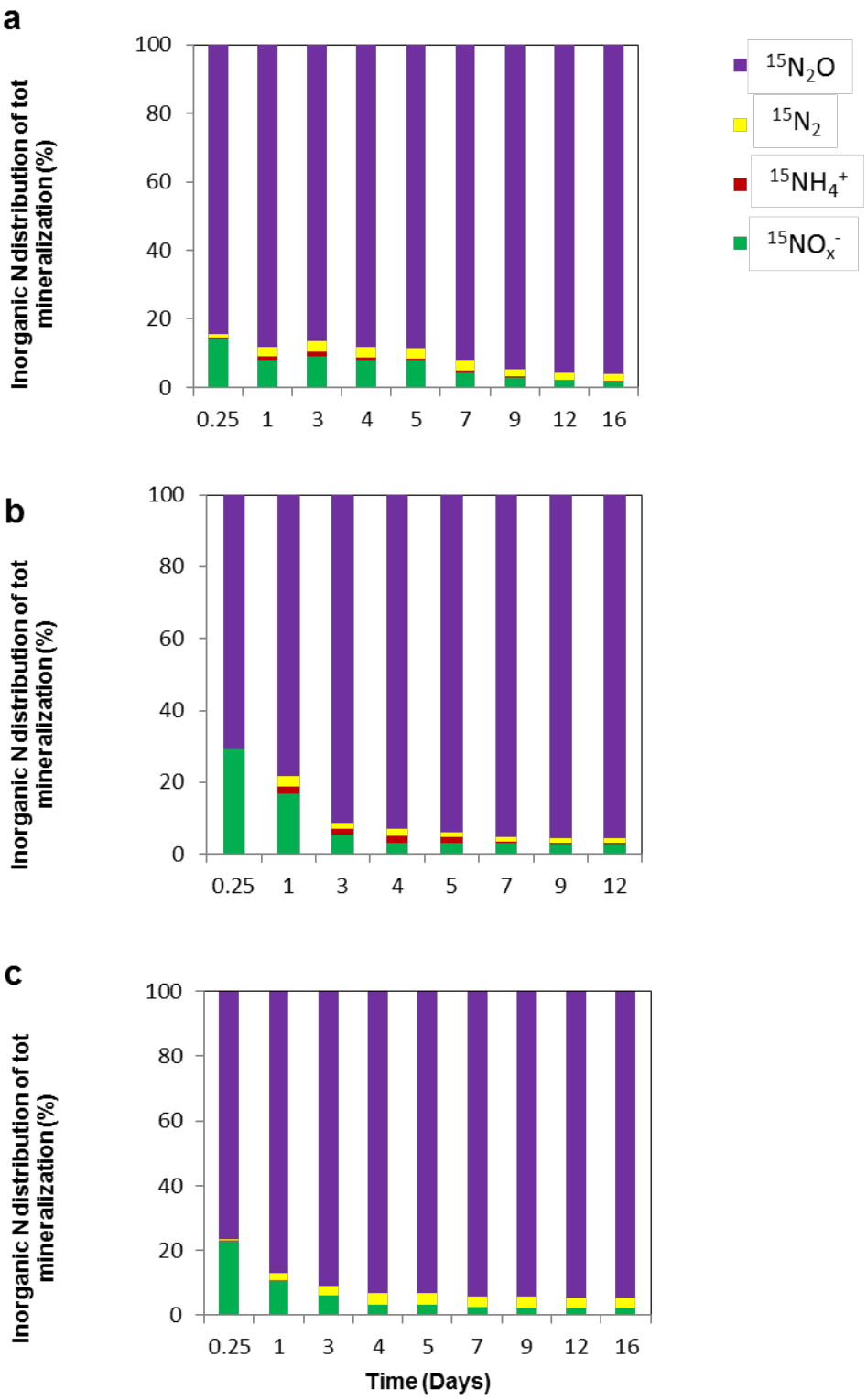

Figure 7.6. Time series distribution of inorganic nitrogen (dissolved and evaded) of total mineralization in a) subtidal non-vegetated b) subtidal vegetated c) intertidal marsh.

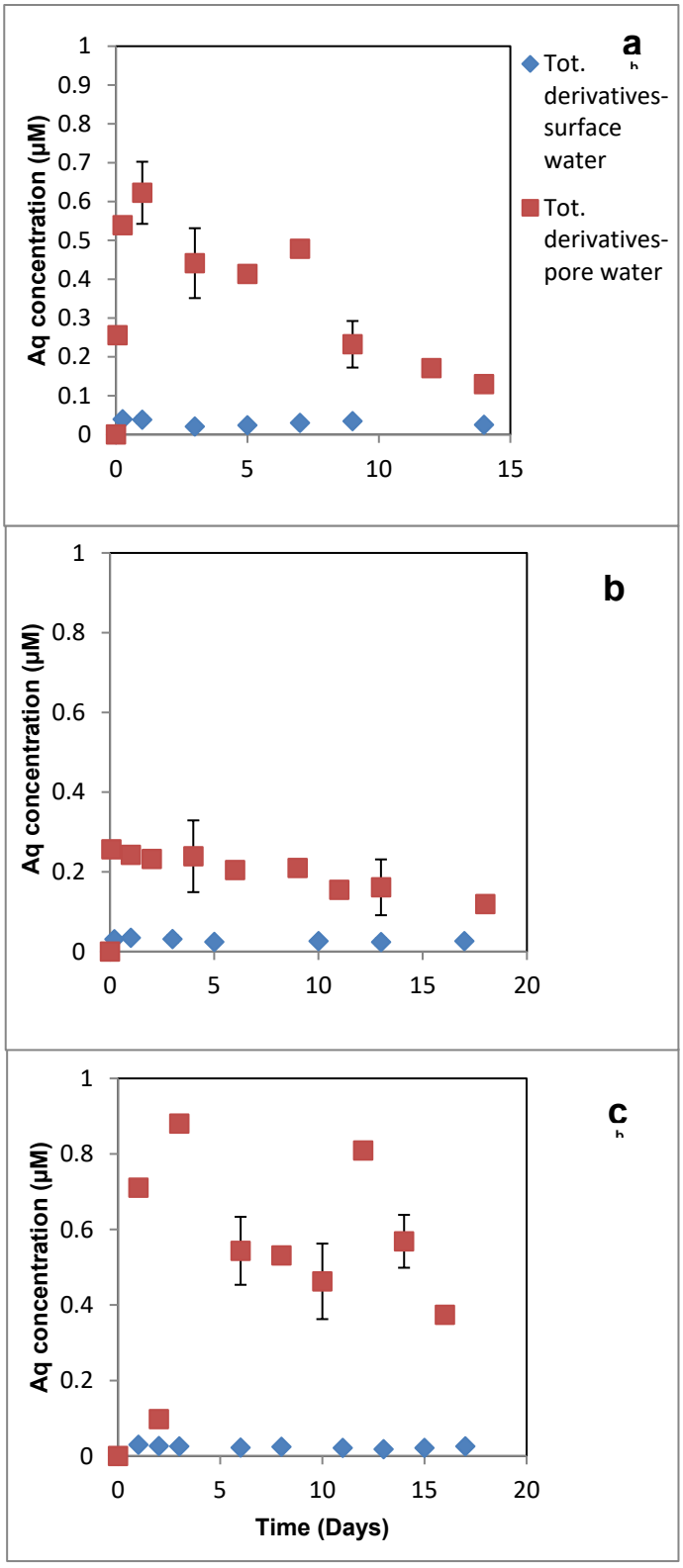

Figure 7.7. Time series total aqueous derivative concentrations (sum of MNX, DNX and TNX) in a) subtidal non-vegetated b) subtidal vegetated c) intertidal marsh.

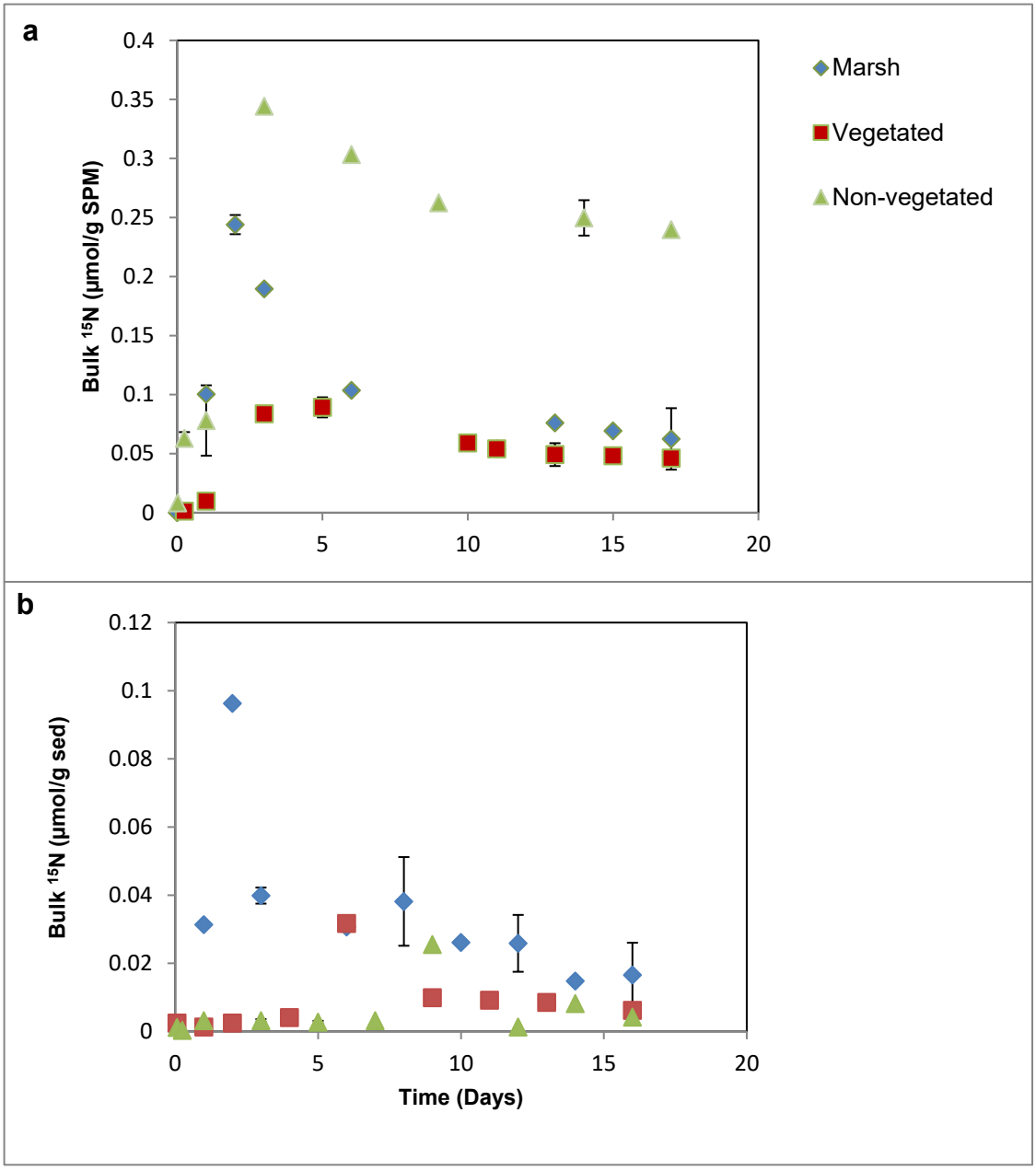

Figure 7.8. Time series bulk ^{15}N in a) SPM b) sediment in coastal marine mesocosms: subtidal non-vegetated, subtidal vegetated and intertidal marsh; Error bars represent standard deviations and are included only to the time points when sampling was done in triplicates.

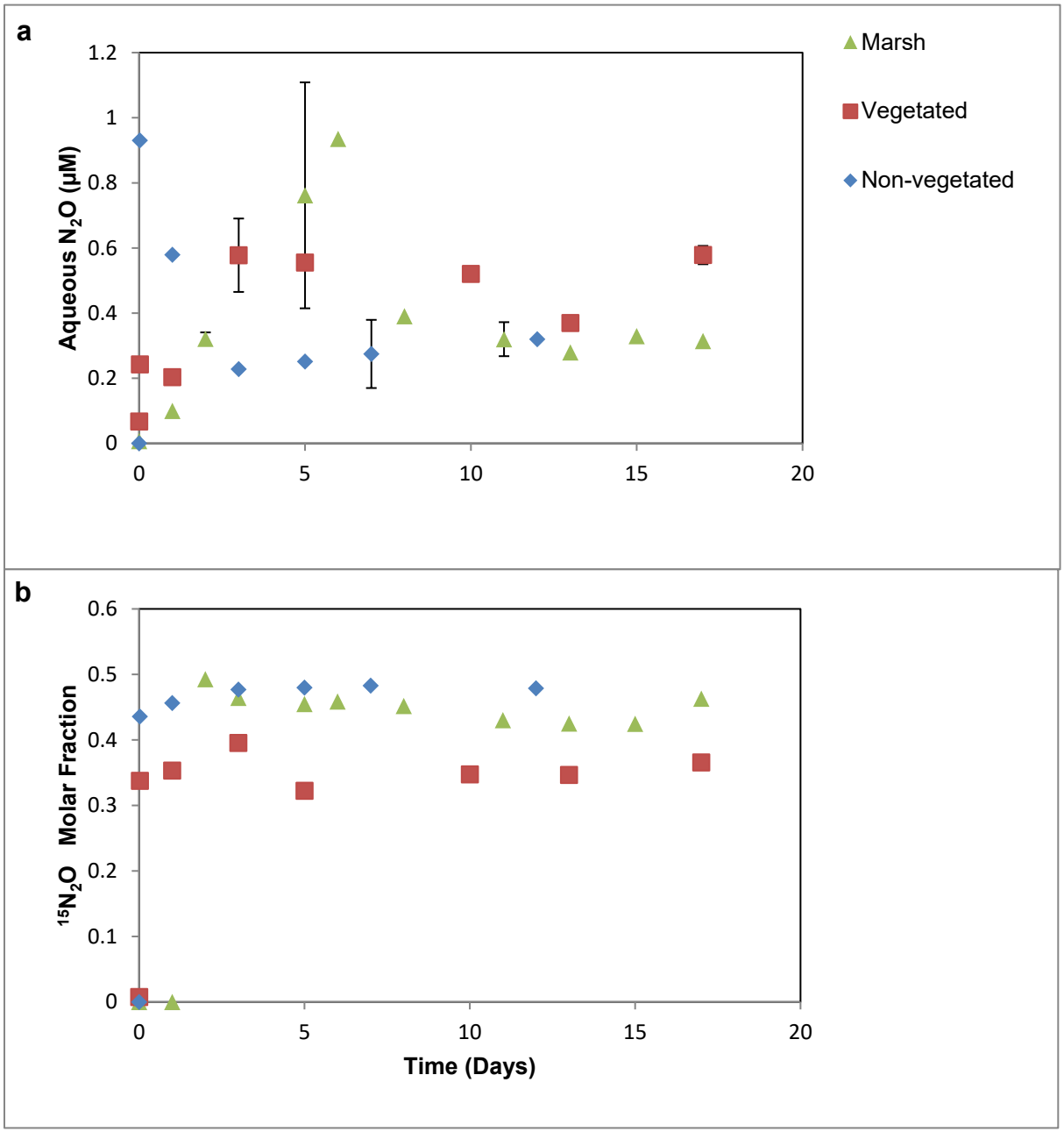

Figure 7.9. Time series a) concentration of surface water N_2O b) mole fraction of surface water $^{15}N_2O$ in coastal marine mesocosms: subtidal non-vegetated, subtidal vegetated and intertidal marsh.

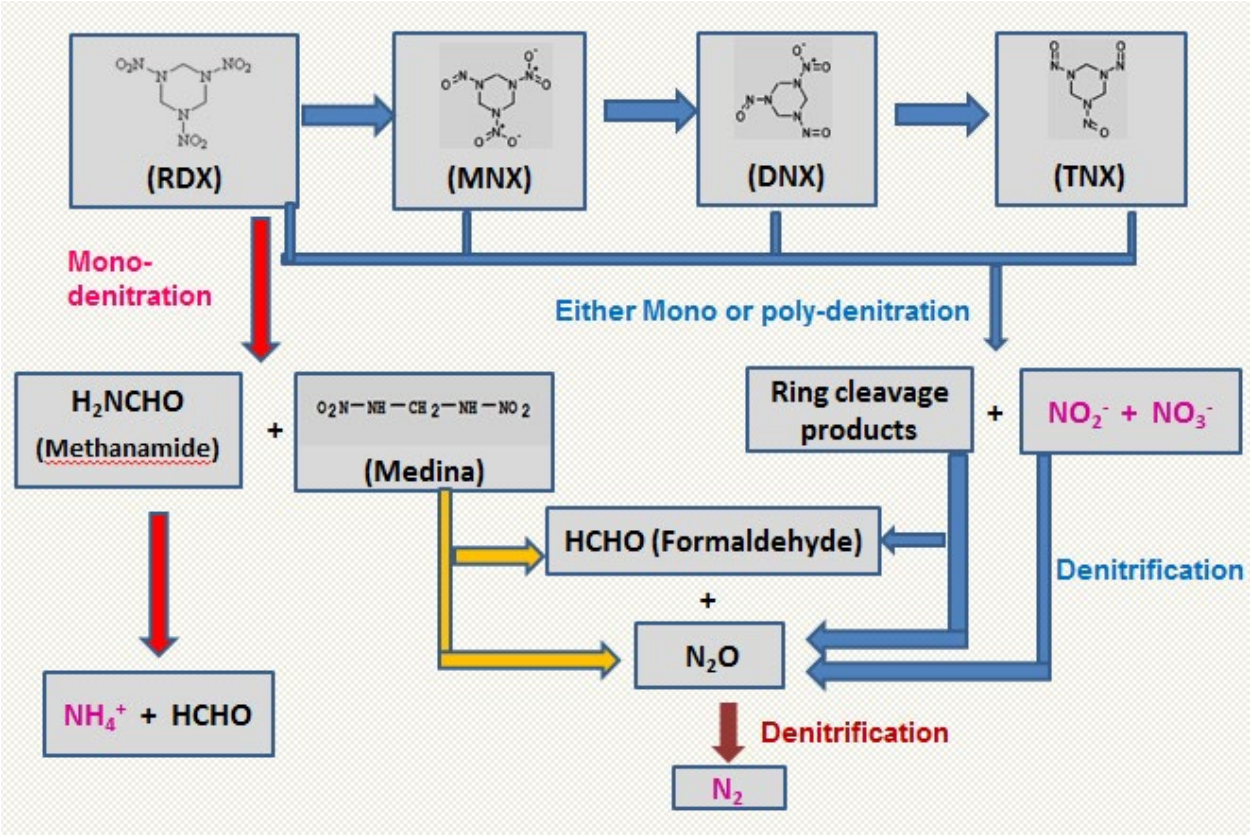

Figure 7.10. Proposed transformation pathways of RDX in hypoxic surface sediment in coastal marine habitats.

Table 7.1. Physical and chemical properties in subtidal non-vegetated, subtidal vegetated and intertidal marsh mesocosms.

Medium	Parameter	Mesocosm Type		
		Subtidal non-vegetated	**Subtidal vegetated**	**Intertidal marsh**
Porewater: 0-2cm	Redox (mV)	(-265) – (-306)	(-440) – (-450)	(-317) - (-325)
	Fe^{+2} (µM)	1.0 - 17	BD	6.8 - 430
	H_2S (µM)	BD	222 - 686	58 - 412
	Ammonium (µM)	12 - 44	47.7 - 128	11.5 – 73.9
Sediment: 0-2cm	Sand (%)	97	40	-
	Silt and Clay (%)	3	60	-
	Density (g cm^{-3})	2.01	1.42	0.51
	TOC (mg/g sed)	1.23	27.5	34.4
	TN (mg/g sed)	0.15	2.84	13.7
	S (mg/g sed)	0.22	5.2	10.2

BD = below detection

Table 7.2. Removal rate constants, half-lives and loss percentage (%) of RDX in mesocosms.

Treatment	RDX		
	Removal rate constant (day^{-1})	Half-life (days)	Loss (%)
Subtidal non-vegetated	0.029	24	76
Subtidal vegetated	0.066	11	90
Intertidal Marsh	0.095	7	94

Loss percentage of RDX corresponds to the end of the experiment.

Table 7.3. Time series concentrations of different ^{15}N-RDX pools at depth 1 (0-2 cm) and depth 2 (2-4 cm) in intertidal marsh mesocosm.

Time (days)	Bulk ^{15}N (μmol/g sed)		$^{15}NH_4^+$ (nM)		$^{15}N_2$ (nM)		$^{15}N_2O$ (nM)	
	D1	D2	D1	D 2	D1	D 2	D1	D 2
1	31.4	4.90	54.7	54.5	56.7	18.5	733	322
2	96.2	40.0	112	91.9	491	301	1800	1071
3	29.6	5.69	70.6	70.7	198	160	787	210
6	30.7	16.8	51.9	51.7	271	207	316	317
8	38.2	27.9	9.74	9.47	31	30.8	433	108
10	26.1	17.6	37.3	25.2	67.1	47.4	202	123
12	25.9	7.24	24.3	23.7	96.8	49.2	318	50.1
14	14.8	7.26	82.8	16.7	157	43.6	552	105
16	16.6	7.29	44.7	28.6	82.4	60.7	416	13.7

D1 = Depth 1 (0-2cm); D 2 = Depth 2 (2-4cm)

Supplementary Material

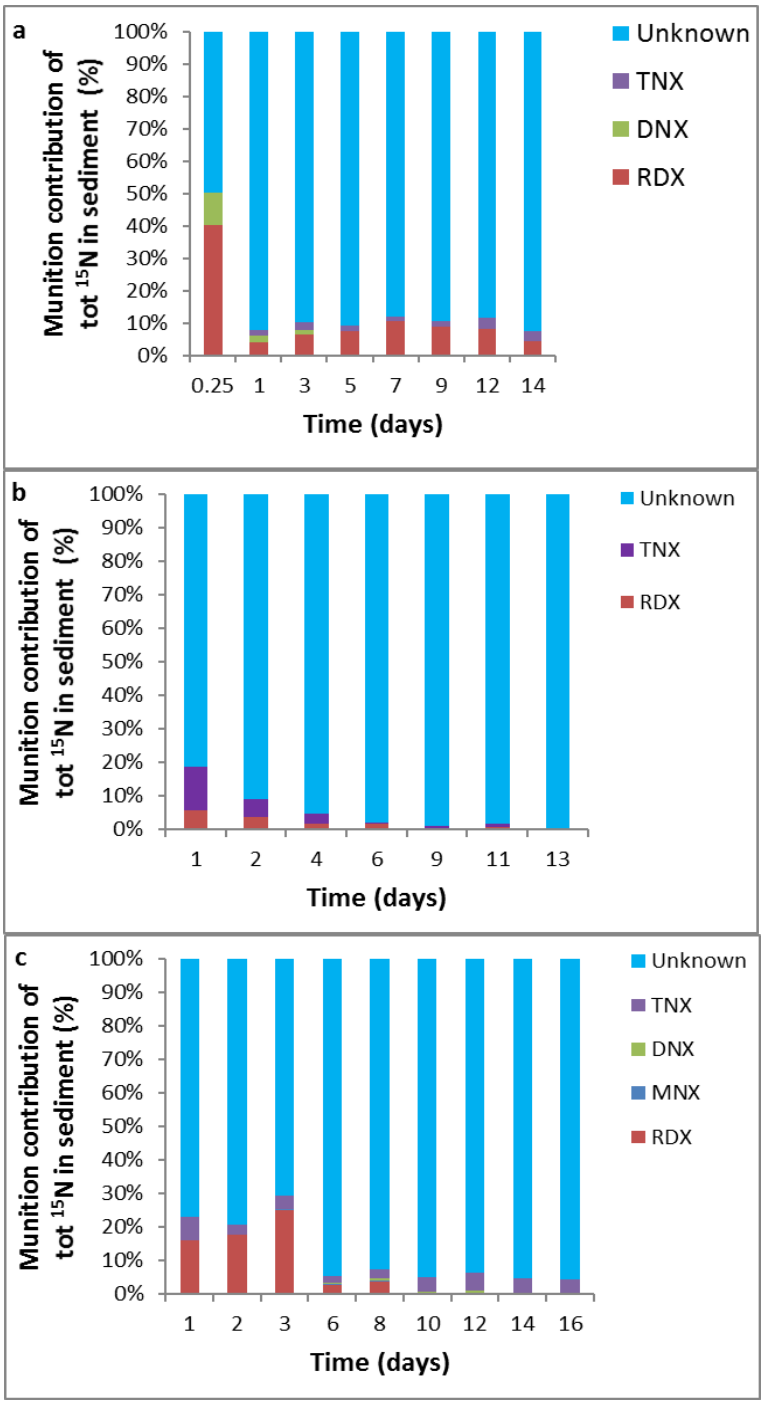

Supplementary Figure S-7.1. Time series of munition contribution to total ^{15}N in sediment in coastal marine mesocosms: subtidal non-vegetated, subtidal vegetated and intertidal marsh.

Supplementary Table S-7.1a. Subdivision of time series aqueous concentrations of munitions in a) surface water b) porewater in subtidal non-vegetated, vegetated and intertidal marsh mesocosms.

a)

Mesocosm type	Time (Days)	Surface water (µM)			
		RDX	MNX	DNX	TNX
Subtidal non-vegetated	0.25	4.95	0.027	BD	0.012
	1	4.45	0.026	BD	0.012
	3	1.49	0.008	BD	0.013
	5	1.43	0.009	BD	0.015
	7	2.60	0.017	BD	0.013
	9	3.00	0.019	BD	0.016
	14	1.81	0.010	BD	0.015
Subtidal vegetated	0.21	4.26	0.017	BD	0.014
	1	4.03	0.021	BD	0.014
	3	2.59	0.015	BD	0.016
	5	2.40	0.013	BD	0.011
	10	1.83	0.011	BD	0.015
	13	1.64	0.009	BD	0.015
	17	1.45	0.009	BD	0.017
Intertidal marsh	1	3.56	0.016	0.003	0.011
	2	2.89	0.013	0.003	0.010
	3	2.47	0.012	0.003	0.010
	6	0.96	0.006	0.006	0.010
	8	1.00	0.007	0.005	0.013
	11	0.82	0.004	BD	0.012
	13	0.89	0.005	BD	0.013
	15	0.81	0.006	BD	0.015
	17	0.72	0.006	BD	0.020

BD = below detection

Supplementary Table S-7.1b. Subdivision of time series aqueous concentrations of munitions in a) surface water b) porewater in subtidal non-vegetated, vegetated and intertidal marsh mesocosms.

b)

Mesocosm type	Time (Days)	Porewater (μM)			
		RDX	MNX	DNX	TNX
Subtidal non-vegetated	0.063	0.138	0.135	0.070	0.051
	0.25	2.89	0.356	0.114	0.069
	1	3.59	0.351	0.177	0.094
	3	1.04	0.153	0.183	0.105
	5	1.22	0.121	0.195	0.097
	7	1.56	0.155	0.215	0.109
	9	0.86	0.070	0.100	0.063
	12	1.77	0.044	0.073	0.054
	14	0.10	0.032	0.060	0.038
Subtidal vegetated	0.0623	0.127	0.045	0.010	0.112
	1	0.130	0.044	0.097	0.102
	2	0.110	0.042	0.093	0.097
	4	0.100	0.041	0.095	0.103
	6	0.239	0.036	0.084	0.084
	9	0.085	0.044	0.095	0.071
	11	0.169	0.044	0.076	0.036
	13	0.100	0.043	0.087	0.032
	18	BD	0.042	0.052	0.026
Intertidal marsh	1	1.75	0.216	0.237	0.257
	2	1.68	BD	0.040	0.058
	3	0.364	0.271	0.295	0.314
	6	0.294	0.259	0.284	BD
	8	0.206	0.298	0.228	0.312
	10	0.241	0.221	0.242	BD
	12	0.301	0.284	0.309	0.324
	14	0.301	0.272	0.297	BD
	16	0.208	0.033	0.231	0.338

BD = below detection

8.0. Bioconcentration of TNT and RDX in Coastal Marine Biota

This chapter was published, as follows:

Ballentine, M., Tobias, C., Vlahos, P., Smith, R., & Cooper, C. (2015). Bioconcentration of TNT and RDX in coastal marine biota. Archives of Environmental Contamination and Toxicology, 68, 718-728.

Abstract

The bioconcentration factor (BCF) was measured for 2,4,6-trinitrotoluene (TNT) and hexahydro-1,3,5-trinitro-1,3,5-triazine (RDX) in seven different marine species of varying trophic levels. Time series and concentration gradient treatments were used for water column and tissue concentrations of TNT, RDX, and their environmentally important derivatives 2-amino-4,6-dintrotoluene (2-ADNT) and 4-amino-2,6-dinitrotoluene (4-ADNT). BCF values ranged from 0.0031 to 484.5 mL g^{-1} for TNT and 0.023 to 54.83 mL g^{-1} for RDX. The use of log K_{ow} value as an indicator was evaluated by adding marine data from this study to previously published data. For the munitions in this study, log K_{ow} value was a good indicator in the marine environment. The initial uptake and elimination rates of TNT and RDX for *Fucus vesiculosus* were 1.79 and 0.24 h^{-1} for TNT and 0.50 and 0.0035 h^{-1} for RDX respectively. Biotransformation was observed in all biota for both TNT and RDX. Biotransformation of TNT favored 4-ADNT over 2-ADNT at ratios of 2:1 for *Fucus vesiculosus* and 3:1 for *Mytilus edulis*. Although RDX derivatives were measureable, the ratios of RDX derivatives were variable with no detectable trend. Previous approaches for measuring BCF in freshwater systems compare favorably with these experiments with marine biota, yet significant gaps on the ultimate fate of munitions within the biota exist that may be overcome with the use stable isotope labeled munitions substrates.

8.1 Introduction

Munitions have been released to the environment through detonation, manufacturing, disposal, and leakage of underwater military munitions (UWMMs; Harrison and Vane, 2010; Hovatter et al., 1997; Talmage et al., 1999). The United States alone has >50 coastal military sites. Documented contamination in soils, aquatic sediments, surface and groundwaters has been reported (Best et al. 1999; Pennington and Brannon 2002). Disposal of UWMMs into the oceans has been practiced since the Second World War (Darrach et al., 1998; Sunahara et al., 2009), but contamination levels and biological accumulation in marine systems is neither well documented nor understood (Clausen et al., 2004; Rosen and Lotufo, 2007; Lotufo et al., 2009). For example, low concentrations of munitions detected in marine sediments (Darrach et al., 1998; Ek et al. 2006) have been linked to increase mortality to *Nitocra spinipes*, a marine copepod,

whereas no significant impact was found for either *M. edulis* (blue mussel) or *Platichtys flesus* (European flounder; Ek et al., 2006).

The munitions most likely to be of concern in marine environments are 2,4,6 trinitrotoluene (TNT), hexahydro-1,3,5-trinitro-1,3,5-triazine (RDX), and octahydro-1,3,5,7-tetranitro-1,3,5,7-tetrazocine (HMX; Lotufo et al., 2010). TNT readily undergoes microbial-mediated transformations along with abiotic processing to produce the mono amino products 2-amino-4,6-dintrotoluene (2-ADNT) and 4-amino-2,6-dinitrotoluene (4-ADNT), but breakdown products of RDX are not often observed (Pennington and Brannon, 2002; Smith et al., 2013; Monteil-Rivera et al., 2009). TNT and RDX along with their derivatives are United States Environmental Protection Agency (USEPA) priority pollutants. Toxicity of TNT and its two major degradation products, 2-ADNT and 4-ADNT, along with RDX have been reported for several aquatic and terrestrial species (Lotufo et al., 2001, 2010; Nipper et al., 2009; Talmage et al., 1999; Yoo et al., 2006). However, the bioconcentration of TNT and RDX in coastal marine biota is not well studied (Lotufo et al., 2009; Talmage et al., 1999).

Bioconcentration factor (BCF) is the most common indicator for the tendency of a substance to partition to exposed biota (Meylan et al., 1999). The BCF value is a ratio of the concentration of the compound in the biota tissue to the concentration of the compound in the surrounding seawater. BCF values can be experimentally derived, as in this study, or they can be estimated from the regression equations of the general form (Meylan et al., 1999):

$$\log BCF = a \log K_{ow} + b \quad (1)$$

where K_{ow} is the octanol/water partition coefficient, and terms a and b are empirically derived constants for a wide variety of compounds. Meylan et al. (1999) derived a = 0.86 and b = -0.39 for nonionic compounds with a Log K_{ow} in the range of 1-7 (Meylan et al., 1999). Lotufo et al. (2009) similarly derived an equation relating K_{ow} to BCF from a review of published works for a variety of munition compounds and species (a = 0.53 and b = -0.23) and found that the majority of BCF values for munitions in their study were dramatically lower than the predicted values using Meylan et al. (1999) values (Lotufo et al., 2009). The equation relating BCF to K_{ow} for munitions reported by Lotufo et al. (2009) contains values derived from a relatively small number of primarily freshwater species and only one marine fish. Increasing the range of species evaluated by Lotufo et al. (2009) to include the following marine biota would be valuable for further study of munitions effects on marine organisms and food webs.

The BCF values of coastal marine biota with respect to munitions compounds are not well known. The majority of experiments completed for munitions are toxicity studies that were performed using terrestrial and freshwater organisms with very few BCF studies completed for marine species (Rosen and Lotufo, 2007; Lotufo et al., 2009, 2010; Ek et al., 2006; Ownby et al., 2005). Expanding munitions BCF characterization to a broader collection of marine organisms is an important first step for constraining reasonable assessments of ecological and human health risks in marine settings associated with these compounds. The objectives of this study were threefold: (1) to experimentally determine minimum approach steady-state BCF values for TNT, RDX, and their derivatives in marine biota across a range of trophic levels similar to studies summarized in Lotufo et al. (2009); (2) to assess metabolism of munitions in organisms that contribute to BCF values; and (3) to assess these experimentally derived values in the context of other approaches for estimating BCF values.

8.2. Methods

8.2.1 Experimental Design

In total, one phytoplankton species (*Tetraselmis impellucida*), two macroalgae species (*Fucus vesiculosus* and *Ulva lactuca*), two epifaunal species (*Hemigrapsus sanguineus* and *Littorina littorea*), and two bivalve species (*Crassostrea virginica* and *Mytilus edulis*) were used in TNT- and RDX-exposure experiments. The species were chosen to represent several trophic levels of a coastal marine ecosystem.

Two experimental approaches were used to expose organism to the munitions compounds; each designed to address a specific objective. The first approach consisted of exposures to multiple concentrations (concentration gradient) to calculate BCF values. The second approach used a single addition followed by rapid time series sampling to calculate initial uptake and elimination rates and determine metabolism of munitions within the organism.

8.2.2 BCF Values

The experiments designed to estimate BCF were based on modifications of Rosen and Lotufo (2007). Multiple 18-liter glass aquaria were established with each containing three individuals of a single species. Each aquarium then had an addition of different munitions concentrations (Table 8.1). All organisms were sampled once after a 24 hour exposure period. This concentration gradient approach was performed on *F. vesiculosus* (macroalgae), *U. lactuca* (macroalgae), *H. sanguineus* (green crab), *L. littorea* (periwinkle), *C. virginica* (eastern oyster), and *M. edulis* (blue mussel), as well as on the phytoplankton *T. impellucida*, where the incubation was performed in culture flasks instead of aquaria. *T. impellucida* had munitions added in 250 mL Corning culturing flasks (Cole-Parmer, USA) and were held in an 18°C temperature- and light-controlled room. *T. impellucida* was gifted by Gary Wikfors from a pure stock grown in the National Oceanic and Atmospheric Administration laboratory (Milford, Connecticut, USA). All biota, with the exception of *T. impellucida,* were collected from eastern Long Island Sound Connecticut and held in flow through seawater tanks sourced from Long Island Sound before experimentation.

8.2.3 Rates and Munitions Biotransformation

The experiments designed to quantify munitions biotransformation consisted of a concentrated single addition of the munitions TNT and RDX dissolved together in methanol (~0.05 percent of total aqueous volume, Table 2.1) into 75 liter glass aquaria containing several individuals of a single species. Aqueous and biota sampling occurred 1 h after the initial spike and then once every 24 h for 168 h for *M. edulis*. For *F. vesiculosus,* aqueous and biotic sampling occurred at 15, 30 min, 1, 4, 24, 48 h, and finally at 120 h. The initial uptake rates are defined for this experiment as the increase of munitions in biota from the time of the spike until the concentration in the tissue reached a maximum and started to decrease. Initial uptake rates were calculated using plots of log concentration versus time during the first few time points during which the water concentration was relatively constant and matched requirements of a "constant" concentration exposure according to American Society for Testing and Materials (ASTM) E1022-94 (2013). This is method differs from Cruz-Uribe et al. (2007) and Makris et al. (2007) where uptake rates were modeled using removal rates of munitions from water. The

elimination rates in this study were calculated using plots of log concentration versus time plots starting at the time point with the highest concentration of munitions until the end of the experiment. The elimination rate in this study differed from Lotufo and Lydy (2005) and Rosen and Lotufo (2007) who calculated depuration rates from a decrease in tissue munitions concentrations in organisms that had been exposed but subsequently moved to munitions-free water (ASTM E1022-94 ,2003). Two organisms, the bivalve *M. edulis* and the macroalgae *F. vesiculosus,* were used in this experiment, both of which, according to existing literature, are believed to possibly represent disparate magnitudes of storage versus processing of munitions (Cruz-Uribe et al., 2007; Makris et al., 2007; Rosen and Lotufo, 2007; Vila et al., 2007).

Seawater for all experiments (~30 ppt) was supplied from Long Island Sound and was sand-filtered before addition to the tanks. Temperature, salinity, and dissolved oxygen in the tanks were monitored with an YSI 556 MPS multiparameter instrument (YSI Inc., Yellow Springs, OH) during the experiments. All treatments, except for *T. impellucida*, were exposed to ambient light conditions and room temperatures (16° to 18°C). These ambient conditions were previously shown to have minimal photo degradation effect on the munitions during the time period of the experiments (Smith et al. 2013). *T. impellucida* were kept in a climate-controlled environmental room with a constant temperature of 18°C and a 12-hour light-to-dark cycle.

8.2.4 Sampling and Analysis

Water and biota collected from the experimental aquaria were analyzed for TNT, 2A-DNT, 4A-DNT, RDX, hexahydro-1,3,5-trinitroso-1,3,5-triazine (TNX), hexahydro-5-nitro-1,3-dinitroso-1,3,5-triazine (DNX), and hexahydro-3,5-dinitro-1-nitroso-1,3,5-triazine (MNX). For water samples, all experiments, except those with *F. vesiculosus*, 5-mL seawater samples were taken and immediately added to 5 mL of high-performance liquid chromatography (HPLC)-grade methanol, shaken, and filtered using 0.45-µm polytetrafluoroethylene (PTFE) syringe-tip filters. Samples were then analyzed by HPLC using USEPA method 8330 (USEPA 1994) as modified by Smith et al. (2013).

To accommodate smaller sampling volumes, water samples for *F. vesiculosus* incubations used a modified "salting out" technique adapted from (Miyares and Jenkins, 1990). The change in water-sampling method was introduced to detect munition at lower concentrations. Two mL of seawater sample were added to 1.3 grams of NaCl and shaken. American Chemical Society (ACS)-grade acetonitrile, 1.5 mL, was added then shaken for 5 min. Once the acetonitrile separated from the seawater, the acetonitrile was siphoned off using a 10-mL syringe. The process was repeated two more times using 1 mL of the ACS-grade acetonitrile. Final extract, 1 mL, was then placed into a chromatography vial and run using the gas chromatographer (GC)/electron-capture detector (ECD) with the same method detailed later in the text.

For biota samples, immediately after harvesting the biota were rinsed for 5 min with clean filtered seawater to remove dissolved and weakly sorbed munitions from the tissue surfaces. In the case of *T. impellucida*, the growth media was filtered to collect the species, and then the filters were rinsed with clean filtered seawater. The shells of *M. edulis, H. sanguineus, C. virginica, and L. littorea* were opened before being rinsed. Once rinsed, tissues were removed, freeze-dried, and weighed. The *H. sanguineus* eggs were found attached to the crab before the experiment and were left in place. The entire sample (crab and eggs) was frozen, and

then the eggs were removed from the crabs before the freeze-drying step. The eggs were then prepared the same as all other samples. Samples were then extracted using methods modified from (Conder et al., 2004). ACS-grade acetonitrile, 10 mL, was added to the samples and homogenized using a Tissue Master 125 (Omni International, Kennesaw, GA). Homogenates were then spiked with 0.01 mg L^{-1} of aldrin as an internal standard. The homogenate was sonicated for 1 h and then centrifuged for 10 min at 10,000 rpms. The supernatant was removed and filtered through 0.22-µm PTFE syringe-tip filter.

GC/ECD analysis on the extracts was performed according to methods described by Pan et al. (2005). One microliter of the solution was injected into an Agilent GC/ECD equipped with a HP-DB5 column (30 m x 320 µm, 0.25 µm; Agilent). A pulsed splitless liner was used with helium as the carrier gas at a flow rate of 11.9 mL min^{-1}. The oven temperature was maintained at 90°C with two ramps: ramp 1 at 10.9 min to 200°C held for 1.5 min and ramp 2 at 14.2 min to 250°C held for 1.9 min. Quantification was based on an external calibration curve of available standard munitions TNT, 2-ADNT, 4-ADNT, RDX, MNX, DNX, and TNX (Accustandard, New Haven, Connecticut, USA). The reporting limit for all compounds was 0.7 ng mL^{-1} because this is the lowest point on the calibration curve, and recoveries of munitions from tissue samples were 82 ± 15 %.

8.3. Results

8.3.1 Aqueous Concentrations

For the single addition time series experiments (*F. vesiculosus* and *M. edulis*), TNT decreased over the incubation period with a loss of 93% in the *F. vesiculosus* treatment and 70% in the *M. edulis* treatment by the 120- and 168-hour mark, respectively (Figure 8.1a, b). RDX concentrations remained relatively constant through both incubations. During the course of the incubation, RDX breakdown products TNX, DNX, and MNX were not detected, but TNT derivatives 4-ADNT and 2-ADNT were measurable and increased during the exposure (Figure 8.1a, b). By the end of the incubation, 4-ADNT and 2-ADNT reached concentrations of 0.29 mg L^{-1} and 0.15 mg L^{-1} for the *F. vesiculosus* treatment (Figure 8.1a) , and 0.29 mg L^{-1} and 0.10 mg L^{-1} for the *M. edulis* (Figure 8.1b), i.e., 21 and 18% of the initial TNT concentration, respectively. The ratio of 4-ADNT to 2-ADNT in the water was initially measured at 15 min at 1:1 increasing to 2:1 over the incubation for the *F. vesiculosus* and 2.3:1 to 2.8:1 for *M. edulis*.

Aqueous concentrations of munitions in the 24-hour concentration gradient experiments varied little from the initial spike concentration (Table 8.1). Initial munitions concentrations were compromised before analysis, but repeat experiments indicated good fidelity between measured initial concentrations, target concentrations, and TNT and RDX concentrations over the 24 hour duration (Table 8.1).

8.3.2 Tissue Concentrations

No mortality or sublethal effects were observed in any of the experiments. Extractable munitions concentrations were normalized to organism gram dry weight (g dw) to account for differences in size. For the single-addition time series experiment, the *F. vesiculosus* TNT

uptake rate was 3.5 times faster than that for RDX. TNT concentrations in *F. vesiculosus* followed a pattern of initial uptake followed by a decrease until they reach a constant value of approximately 0.1 µg TNT g dw^{-1} (Figure 8.2a). 4-ADNT and 2-ADNT increased rapidly to reach a peak value after 1 h of 2 µg 4-ADNT g dw^{-1} and 1.4 µg 2-ADNT gdw^{-1}, respectively. TNT derivatives were measured at greater values then TNT in *F. vesiculosus* tissue at every time point. At the final time point of 120 h, 4-ADNT was 10 times more concentrated in tissue than TNT, and 2-ADNT was 5 times greater. The ratio of 4-ADNT to 2-ADNT increased with time to a maximum ratio of 2.7 to 1. RDX, however, experienced an initial uptake without any subsequent decrease in concentration in the tissue and remained constant (Figure 8.2b). There were no derivatives of RDX in *F. vesiculosus.* The initial uptake of TNT and RDX were calculated for *F. vesiculosus* from plots of log concentration versus time (Table 8.2). Although the TNT concentration in the water was added as a single addition, the first 4 h the concentration remained within 24% of the initial concentration, thereby permitting a calculation of uptake rates according to ASTM E1022-94 (2013). Only RDX-elimination rates (Table 8.2) were calculated for *M. edulis* because there were not enough data points to calculate initial uptake rates and because the TNT concentration decreased too quickly to permit calculation of TNT-elimination rates according to ASTM E1022-94 (2013). The single-addition time series for *M. edulis*, however, showed quick uptake of TNT within the first hour of exposure and then a near constant amount of TNT and derivatives (Figure 8.2c, d) even though the water concentration continued to decrease. 4-ADNT was the dominant TNT derivative with concentrations that were constantly 2 to 3 times higher than measured TNT. The ratio of 4-ADNT to 2-ADNT in *M. edulis* increases from 1.4:1 to 2:1 over the time series. Rapid incorporation of RDX into tissues during the first hour was followed by a decrease to a lower constant value of approximately 5 µg RDX g dw^{-1} (Figure 8.2d). Only trace RDX derivative concentrations were measured. MNX and TNX were 5-10 times less than the RDX with the ratio of MNX to TNX ranging from 0.5:1 to 2:1. The ratios for the RDX derivatives were variable with no clear trend over the time series.

In the concentration gradient experiments, the 24-hour TNT tissue concentrations varied between species by one order of magnitude for any given concentration though tissue concentrations in all species increased with higher aqueous concentrations. The variability in tissue concentrations measured among replicates was dependent on species type. For example, differences as low as 4% were measured in *M. edulis*, whereas tissue concentrations varied ≥89% in *C. virginica.* With the exception of *H. sanguineus*, all species showed a large amount of TNT derivatives relative to TNT (Table 8.3). *H. sanguineus* and its eggs contained ≥15 times more TNT than derivatives. Ratios of 4-ADNT to 2-ADNT in all species had a narrow range from 1.1:1 to 2.1:1, respectively (Table 8.3). The *H. sanguineus eggs* contained 9 times the amount of 4-ADNT than 2-ADNT. Ratios of RDX and its derivatives in tissue varied greatly between and within species. In *Crassostrea virginica* for example, RDX would range from 27 to 83% the sum total of RDX and derivatives. DNX (and no MNX) was detected in two species, *H. sanguineus* eggs and *L. littorea.* MNX was detected in all other species tissues tested.

8.3.3 BCF Determination

Measured concentrations and subsequent BCF values calculated are reported for parent explosives and the sum of parent explosives and their primary derivative products ∑TNT or ∑RDX (Table 8.4), where the ∑TNT = TNT + 2-ADNT + 4-ADNT and ∑RDX = RDX + DNX + MNX + TNX. BCF values were calculated in two ways from the concentration gradient data as

follows: (1) Linear regressions were used to express BCF value as a ratio of munitions with the concentration of munitions in tissue in the numerator divided by the denominator of the concentration of munitions in the seawater (Figure 8.3) or (2) a portion of the RDX and ∑RDX - BCF values from the concentration gradient experiments were calculated using single point values instead of linear regressions. In this case, single time point BCF values were derived by dividing the tissue munitions concentrations by the aqueous munitions concentrations for a given time point. These single time point BCF values were then averaged to yield a single species-specific BCF estimate (Table 8.4). This approach was used when the tissue concentration did not yield a significant linear regression as a function of aqueous concentration. BCF values were used to calculate the ∑RDX BCF values in all species except *F. vesiculosus, M. edulis, H. sanguineus,* and *H. sanguineus* eggs (Table 8.4). This approach was not used for any TNT BCF values. The BCF values for TNT and RDX ranged over several orders of magnitude (Table 8.4). The lipid rich *H. sanguineus* eggs had the highest BCF for ∑TNT at 484.5 mL g^{-1}, whereas *U. lactuca* had the lowest value at 0.40 mL g^{-1}. For the ∑RDX, *T. impellucida* had the largest BCF value at 54.83 mL g^{-1} and *U. lactuca* the lowest at 0.21 mL g^{-1}.

8.4. Discussion

8.4.1 Rates

Overall, the measured initial uptake rates for TNT and RDX fell within published uptake values for fresh and marine biota (Lotufo and Lydy, 2005; Makris et al., 2007; Rosen and Lotufo, 2007). In the time series experiments, the initial uptake rates were a function of compound type but not organism type. The parent compounds TNT and RDX showed a rapid initial uptake in tissues of *M. edulis* and *F. vesiculosus* within the first hour. This result is more consistent with the different chemical properties of the munitions controlling uptake rather than some species-specific to difference in organisms. This result is surprising given the dissimilarities between *M. edulis* and *F. vesiculosus* tissues with respect to C:N ratios, lipid content, differences in metabolism, and behavior (Jones and Harwood, 1992; Smaal and Vonck, 1997; Thompson and Bayne, 1974; Yates and Peckol, 1993). Elimination rates of RDX differed substantially between *M. edulis* and *F. vesiculosus*. Like previous reports, RDX elimination rates measured in this marine study were faster than those reported for aquatic organisms (Conder et al., 2004; Lotufo and Lydy, 2005; Rosen and Lotufo, 2007). The slower elimination rate of RDX in *F. vesiculosus* could be caused by intracellular storage of RDX being a more important factor than biotransformation of the compound in the tissue similar to reports in agronomic plants (Vila et al., 2007). RDX elimination rates measured were similar to TNT elimination rates found by Cruz-Uribe et al. (2007) using three species of marine macroalgae. *M. edulis* does not seem to have a storage mechanism for RDX. Instead the rates for uptake and elimination quickly yielded an apparent steady-state concentration of RDX within the *M. edulis* (Figure 8.2d). The appearance rate for TNT derivatives reported in Table 8.2 is the rate that TNT derivatives initially appear and then increase over the time series. Appearance rate in this experiment could include the internal biotransformation of TNT to its derivatives and/or production of derivatives in the water that are repartitioned. Half-lives reported (Table 8.2) reflect the balance among uptake, breakdown, and elimination rates.

8.4.2 Biotransformation

The time series experiments showed measureable amounts of 4-ADNT and 2-ADNT detected within the first hour in both water and tissue depending on organism and compound. TNT transformation in the water column within this first hour was likely bacterially mediated. Photodegradation was discounted by both a control and by previous experiments (Smith et al., 2013) wherein the control tank (water only) showed a loss of only 27% of the parent munitions in the water. Ratios of the TNT derivatives in tissues shifted over time. Initially, *F. vesiculosus* tissue had the same 1:1 ratio of 4-ADNT to 2-ADNT as did the water column. Over the time series, biotransformation occurred within the organism, and the ratio increased as high as 3:1 in the *F. vesiculosus* tissue, whereas the water column shifted to a 2:1 ratio. Similarly, in the *M. edulis* treatment, the ratio of 4-ADNT to 2-ADNT did increase in both the tissue and the water column over the time series. The ratio in the water increased from 2:1 to 3:1, whereas the ratio in the tissue also increased from 1.5:1 to 2:1, respectively. For both *M. edulis* and *F. vesiculosus*, the lower TNT derivatives ratio in tissue relative to the water indicate that TNT biotransformed within the organisms, and this is consistent with similar reports (Lotufo et al. 2009). The ratios of 4-ADNT to 2-ADNT for all the biota exposed to an addition of munitions show a non-organism specific preferential biotransformation pathway to 4-ADNT (Table 8.3).

For both the *F. vesiculosus* and *M. edulis* treatments, the water column had no detectable RDX derivatives indicating little breakdown, microbial or otherwise, in the aqueous phase. The high RDX and lack of derivatives measured in *F. vesiculosus* may reflect uptake and storage, with little biotransformation, as observed in vascular plants (Vila et al., 2007). In contrast, *M. edulis* tissue was found to contain RDX derivatives. Because there were no RDX derivatives in the water, the RDX derivatives detected in *M. edulis* tissues were due to internal biotransformation. MNX and TNX were found in *M. edulis* tissue at a ratio ranging from 0.5:1 to 2:1, respectively. The lack of DNX in the tissue might suggest that the production of DNX from MNX is a rate-limiting step in the breakdown of RDX. The relatively small amounts of MNX, DNX, and TNX compared with those of RDX also suggest that the biota do not readily breakdown RDX on these time scales although the capacity for detoxifying enzymes' ability to process all these compounds has been documented (Cho et al., 2008; Kitts et al., 2000; Levine et al., 1990; Macek et al., 2000). For RDX, despite increasing knowledge of transformation pathways in groundwaters and sediments, clear mechanisms of derivative production from RDX in biota remains unresolved.

8.4.3 BCF Values

BCF values calculated fall within ranges of published experimental values for a variety of freshwater and limited number of saltwater species (Belden et al. 2005; Lotufo and Lydy 2005; Ownby et al. 2005; Yoo et al. 2006). The majority of the BCF values reported in this study are within one order of magnitude of each other (Table 8.4), and are all lower than BCF of 1000, which is typically considered the threshold above which high bioaccumulation potential should be significant (Singh, 2013). The *H. sanguineus* eggs were found to have a much higher BCF for TNT than whole biota. Furthermore, the similarity of the ∑TNT (484.5 mL g^{-1}) and TNT (466.4 mL g^{-1}) BCF values, along with the ratio of TNT to 2-ADNT and 4-ADNT (Table 8.3), indicate that biotransformation of TNT in eggs was much less than the extent in the biota. This greater egg BCF value is likely due to greater lipid content and is consistent with a greater K_{ow} of TNT

than that of RDX. Greater amounts of TNT also are found in the viscera of fish that contain relative more lipid content than other parts of the organism (Lotufo, 2011). The greater lipid content and possible missing biotransformation framework of the eggs could be of ecological interest since the BCF is greater. The toxicological effects of the TNT on the eggs were not evaluated here, but they might be important for egg development and to organisms that eat the eggs. Although the BCF values measured in this study are greater than other BCF values reported for terrestrial and aquatic organisms, they remain <1,000 and are not considered to be indicative of high bioaccumulation potential (Singh, 2013).

Here we calculated BCF values for parent and parent plus derivatives based on direct analysis of these compounds, but there are a variety of approaches used to determine the BCF value that must be clear when comparing BCF estimates. The BCF can be calculated with only the extractable parent compound, the sum of parent and derivatives, or from extractable (or total) radioactivity following exposure to a radiolabeled parent compound. BCF values calculated from the radiotracer approach have been shown to be greater because ^{14}C tissues measurement includes both the label attributable to parent compound plus the derivatives but also any of the labelled C that may have been metabolized and retained (Belden et al., 2005; Lotufo, 2011; Ownby et al., 2005). The fraction metabolized and retained in tissues, however, no longer represents the potential for bioconcentration and/or extant toxicity. Our results provide evidence of compound breakdown within the organisms, and our BCF values are indeed lower than those reported based on a radiotracer. The approach of directly measuring parent compound along with derivatives would give a better, or at least a more conservative, measure of true BCF value.

8.4.4 Kow

BCF values derived experimentally, including those reported in this study, are normally lower than those predicted from log K_{ow} values (Figure 8.4; Ownby et al., 2005). Variations in estimated BCF values using log K_{ow} values may result from differences in life stages, metabolism, and lipid content (Jones and Harwood, 1992; Smaal and Vonck, 1997; Thompson and Bayne, 1974; Yates and Peckol, 1993). However, these variations in predicted BCF value for TNT and RDX do not seem significant because all estimates, including their variances, are several orders of magnitude lower than BCF values that would indicate bioaccumulation. The dashed-dotted lines on figure 2.4 represents a ± factor of 10 uncertainty about the linear best fit line of the log K_{ow} equation. The majority of BCF values previously reported and added from this study fall within those boundaries with the only outlier being the eggs measured in this study. When values from this study are added to those from previous studies that studied mainly freshwater species, the linear fit relating BCF value to log K_{ow} value does not substantially change (Lotufo et al., 2009). Therefore, it remains that the log K_{ow} value is a reasonable predictor of the BCF value for these munitions compounds in marine organisms.

8.5. Conclusion

Results from the time series and concentration gradient experiments support four major findings: (1) the rapid initial uptake of RDX into tissues is consistent with rates reported for marine and freshwater species; (2) TNT and RDX are transformed into multiple derivatives within biota; (3) BCF values are low and do not indicate a high potential for bioconcentration;

(4) the use of existing log K_{ow} formulas as predictor of munitions BCF value is reasonable for coastal marine organisms.

BCF values found in this study were low for both TNT and RDX in marine coastal biota. These low BCF values suggest that for TNT, RDX, and their derivatives have a similarly low bioaccumulation potential. Initial uptake and elimination rates calculated in this study also fall within previously published values of both marine and non-marine biota. The use of log K_{ow} value as a predictor of BCF values works well as well for marine biota as it does for fresh and terrestrial biota. The ultimate fate of munitions is still not well known in marine systems, and further experiments particularly using ^{15}N- or ^{13}C-labeled munitions, might shed some light on the metabolic pathways and the fate of the munitions that do make it into the biota. Further research in the fate of munitions within more realistic systems must be performed to fully evaluate and understand the fate and process involved with TNT and RDX in coastal marine environments.

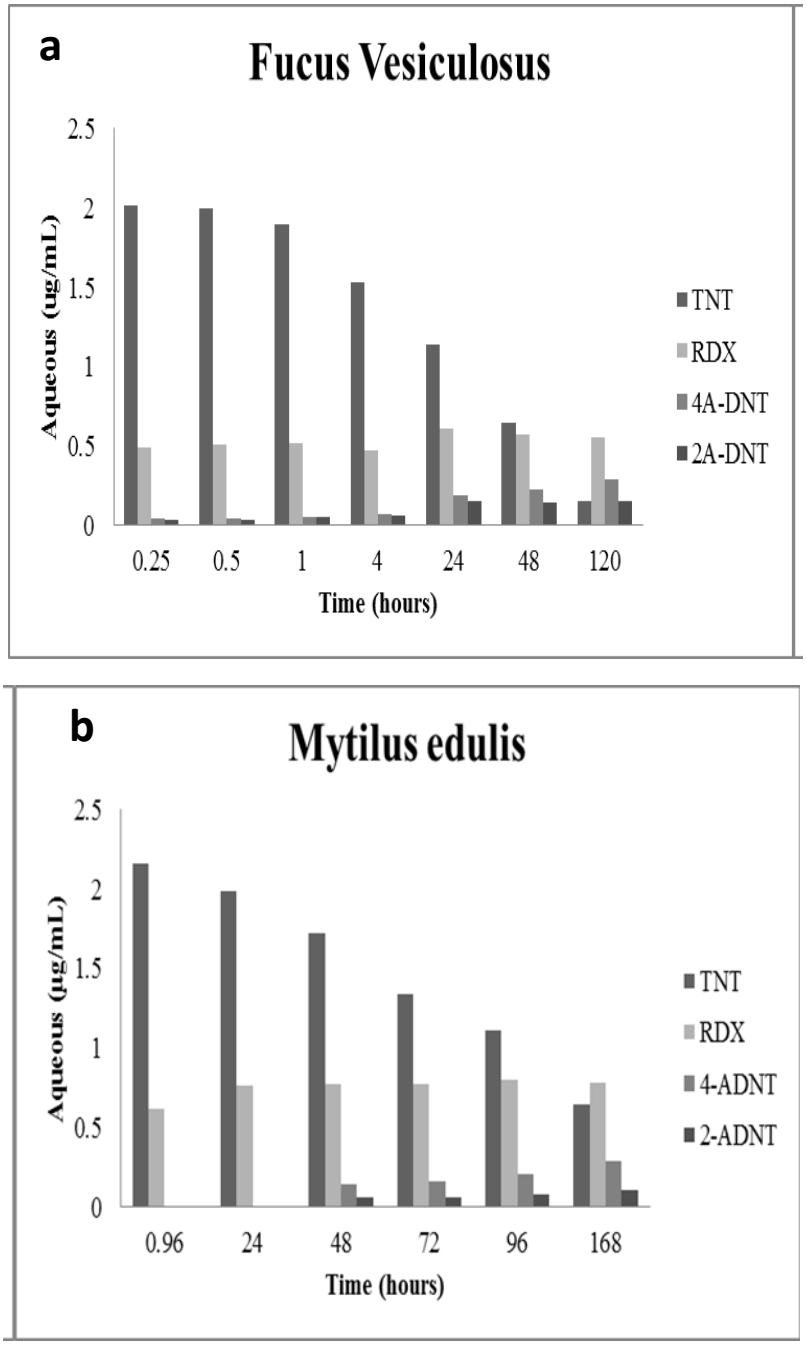

Figure 8.1. Aqueous munition concentrations for single dose time series treatment. Panels a and b represent separate aquaria that were dosed with a mixture of TNT and RDX.

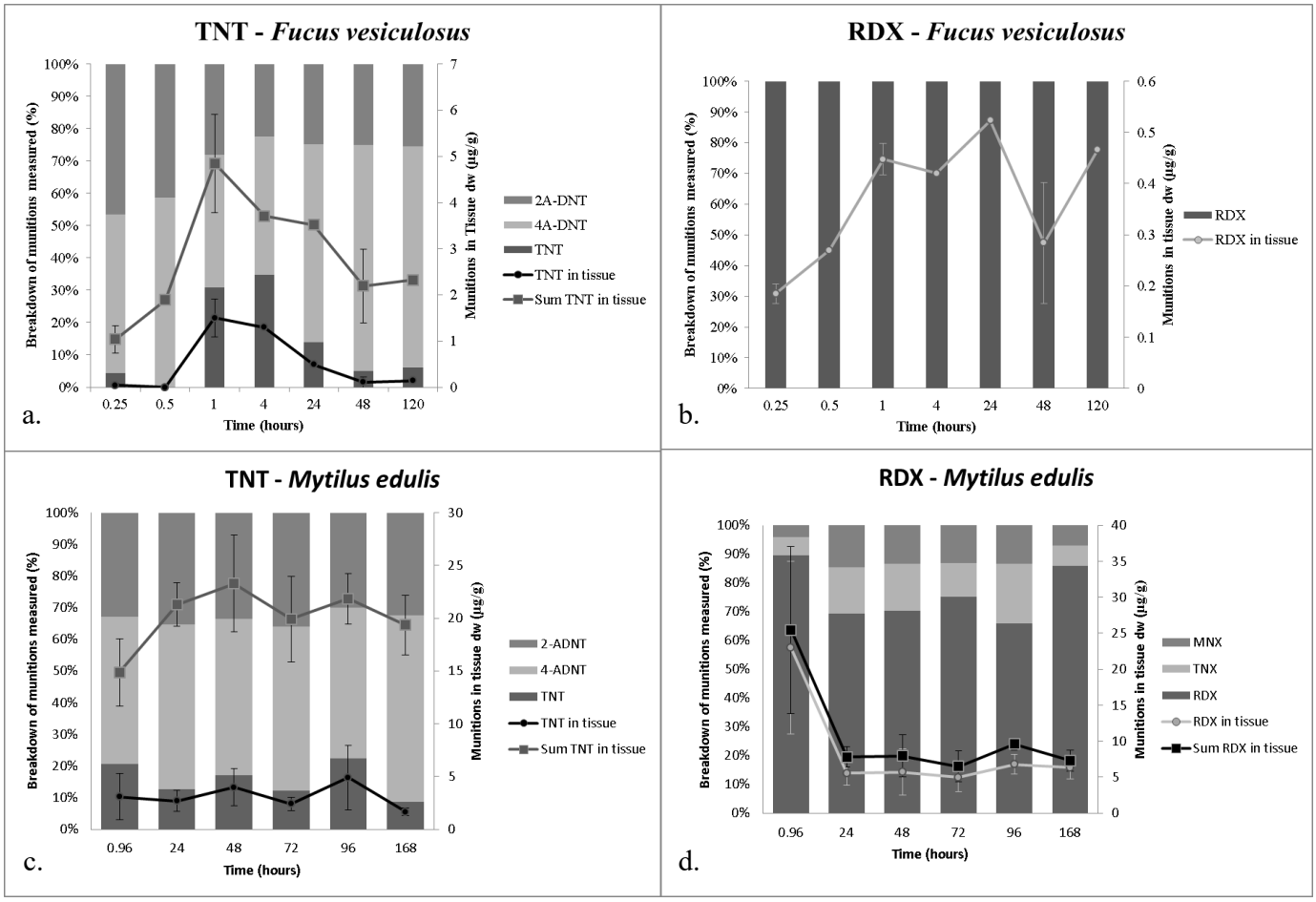

Figure 8.2. Tissue concentrations for single dose time series treatment. Solid line shows extractable parent explosive for both parent explosive and ∑ of the parent explosive as detailed in Table 4. Values with error bars consist of the average of 3 separate individual samples (n=3) while points without are single samples (n=1). The bar graph shows the breakdown percent of parent compound and derivatives measured for *Fucus vesiculosus* and *Mytilus edulis*.

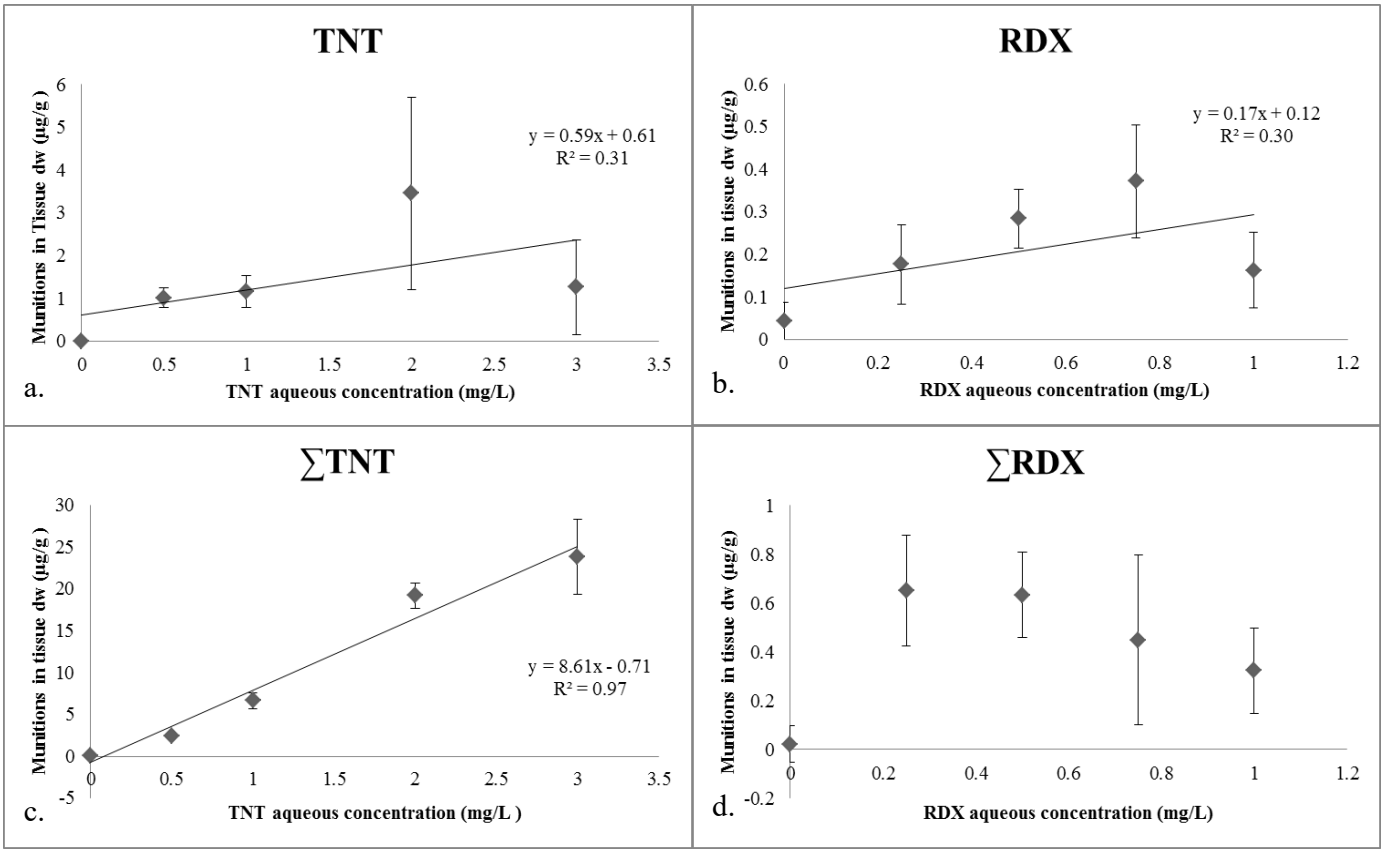

Figure 8.3. Example derivation of BCF from the concentration gradient experiments: *Crassostrea virginica*. Each value consists of the average of 3 separate individual specimens (n=3). The solid lines are best fit regressions. ∑TNT and ∑RDX values consist of sum of parent compound and the respective derivatives. BCFs derived from these plots for all organisms are summarized in Table 4.

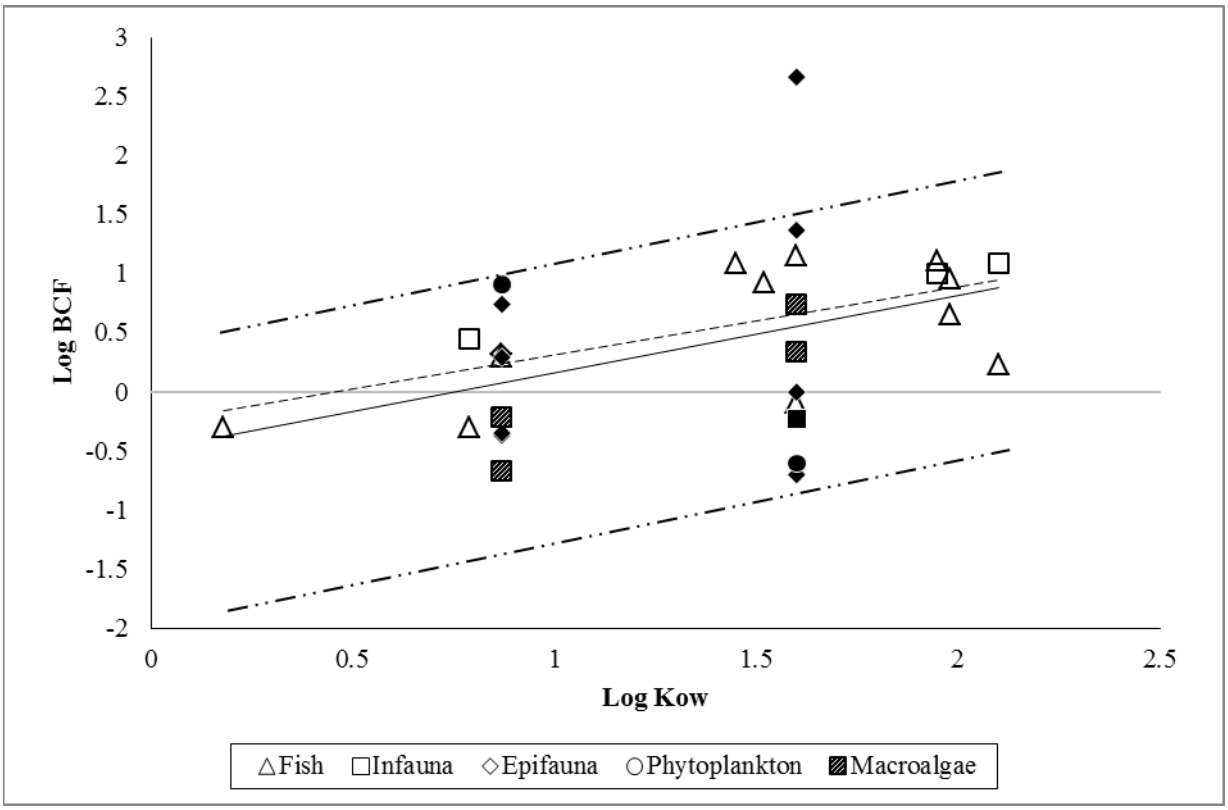

Figure 8.4. Log BCF vs. Log Kow regression. The solid filled markers and all macroalgae values are from this study. Empty markers are from previously published values. The solid line is a best fit regression line with previous and this study's values (log BCF = 0.66 log Kow – 0.49, r2 = 0.19). The 2 dotted-dashed lines are lines that have the same slope as the solid line and represent one order of magnitude difference from the best fit linear regression. The dotted best fit regression is from previously summary of data by Sunahara et. al. (2009) where log BCF = 0.53 log Kow – 0.23, $r^2 = 0.37$).

Table 8.5. Concentration gradient experiment aqueous spike concentrations. *A selection of water samples was lost due to error. Precision experiments were run and completed in replicate to test the amount of munitions after 24 hours. The combinations of precision experimental and actual measured values are reported with standard deviations between precision and BCF water values.

Tank #	TNT (mg/L)	Measured (mg/L)*	RDX (mg/L)	Measured (mg/L)*
1	3	2.82 ± 0.17	1	1.01 ± 0.09
2	2	1.92 ± 0.21	0.75	0.71 ± 0.09
3	1	1.14 ± 0.04	0.5	0.52 ± 0.06
4	0.5	0.54 ± 0.07	0.25	0.24 ± 0.02
5	0	0	0	0

Table 8.6. Time series experiment calculated rates. Initial uptake, elimination, and appearance rates were calculated using a plot of Log concentration vs. time. Appearance rate for this experiment is defined as the rate at which 4-ADNT and 2-ADNT increased over the time series. Not determined values (ND) were due to the lack of data points within the first hour. Values in parentheses are coefficients of determination.

Initial uptake rate (hours^{-1})	***Fucus vesiculosus***	***Mytilus edulis***
TNT	1.79 (0.67)	ND
RDX	0.50 (0.99)	ND
Elimination rate (hours^{-1})		
RDX	0.0035 (0.45)	0.013 (0.73)
Half-life (hours)		
RDX	198.6	53.3
Appearance rate (hours^{-1})		
4-ADNT	0.75 (0.93)	ND
2-ADNT	0.58 (0.98)	ND

Table 8.7. Ratios of TNT and derivatives. Concentration gradient ratio values are calculated by taking the average of the species in all of the separate aquaria (n=12).

Species	Ratio of TNT to derivatives	Ratio of 4-ADNT to 2-ADNT	Ratio of ∑TNT to 4-ADNT	Ratio of ∑TNT to 2-ADNT
Tetraselmis impellucida	0.17 ± 0.11	1.1 ± 0.40	0.81 ± 0.16	0.79 ± 0.40
Fucus vesiculosus	0.03 ± 0.02	2.1 ± 0.15	1.51 ± 0.04	3.22 ± 0.17
Ulva lactuca	0.12 ± 0.08	2.1 ± 0.41	1.69 ± 0.23	3.44 ± 0.25
Hemigrapsus sanguineus	4.1 ± 0.59	1.7 ± 0.50	8.35 ± 1.76	13.58 ± 1.73
Hemigrapsus sanguineus eggs	15.5 ± 8.24	9.4 ± 4.29	18.7 ± 9.03	164 ± 91.8
Crassostrea virginica	0.29 ± 0.23	1.5 ± 0.10	3.25 ± 0.46	2.14 ± 0.45
Littorina littorea	0.07 ± 0.05	1.1 ± 0.09	2.15 ± 0.34	2.17 ± 0.11

Table 8.8. TNT and RDX Bioconcentration factors (BCF). BCF values are given the units mL g-1. ∑TNT = (TNT + 4-ADNT + 2-ADNT). ∑RDX = (RDX + MNX + TNX + DNX) when detected. BCF values indicated by an (*) were not calculated with a best fit line but as an average of single point values. Values in parentheses are coefficients of determination.

Species	Common Name	TNT	∑TNT	RDX	∑RDX
Tetraselmis impellucida	PLY 429	0.25 (0.02)	1.53 (0.66)	8.15 (0.42)	54.83 ± 26.85*
Fucus vesiculosus	Bladder wrack	0.0031 (0.60)	1.85 (0.99)	0.73 (0.65)	0.68 (0.84)
Ulva lactuca	Sea lettuce	0.0056 (0.071)	0.40 (0.70)	0.023 (0.32)	0.21 ± 0.12*
Hemigrapsus sanguineus	Asian shore crab	23.51 (0.61)	28.1 (0.61)	1.97 (0.64)	2.29 (0.56)
Hemigrapsus sanguineus	Asian shore crab external eggs	466.4 (0.92)	484.5 (0.93)	5.55 (0.91)	5.29 (0.67)
Crassostrea virginica	Eastern oyster	0.59 (0.31)	8.61 (0.97)	0.21 (0.44)	2.42 ± 1.76*
Mytilus edulis	Blue mussel	1.0 (0.80)	14.2 (0.98)	0.43 (0.59)	0.33 (0.28)
Littorina littorea	Common periwinkle	0.20 (0.89)	12.30 (0.99)	0.45 (0.82)	4.03 ± 2.01*

9.0. Uptake and Fate of hexahydro-1,3,5-trinitro-1,3,5-triazine (RDX) in Coastal Marine Biota Determined Using a Stable Isotopic Tracer, ^{15}N-[RDX]

This chapter was published, as follows:

Ballentine, M., Ariyarathna, T., Smith, R. W., Cooper, C., Vlahos, P., Fallis, S., Groshens, T., Tobias, C. (2016). Uptake and fate of hexahydro-1, 3, 5-trinitro-1, 3, 5-triazine (RDX) in coastal marine biota determined using a stable isotopic tracer, 15 N–[RDX]. Chemosphere, 153: 28-38.

Abstract

Hexahydro-1,3,5-trinitro-1,3,5-triazine (RDX) is globally one of the most commonly used military explosives and an environmental contaminant. ^{15}N labelled RDX was added into a mesocosm containing 9 different coastal marine species in a time series experiment to quantify the uptake of RDX and assess the RDX derived ^{15}N retention into biota tissue. The ^{15}N attributed to munitions compounds reached steady state concentrations ranging from 0.04 to 0.67 μg ^{15}N g dw^{-1}, the bulk ^{15}N tissue concentration for all species was 1-2 orders of magnitude higher suggesting a common mechanism or pathway of RDX biotransformation and retention of ^{15}N. A toxicokinetic model was created that described the ^{15}N uptake, elimination, and transformation rates. While modeled uptake rates were within previous published values, elimination rates were several orders of magnitude smaller than previous studies ranging from 0.05 to 0.7 days^{-1}. These small elimination rates were offset by high rates of retention of ^{15}N previously not measured. Bioconcentration factors and related aqueous:organism ratios and tracer calculated using different tracer and non-tracer methods and yielded a broad range of values (0.35-101.6 mL g^{-1}) that were largely method dependent. Despite the method-derived variability, all values were general low and consistent with little bioaccumulation potential. The use of ^{15}N labelled RDX in this study indicates four possible explanations for the observed distribution of compounds and tracer; each with unique potential implications for possible toxicological impacts in the coastal marine environment.

9.1. Introduction

Hexahydro-1,3,5-trinitro-1,3,5-triazine (RDX) is a cyclic nitramine military explosive that has been extensively used since World War II (Darrach et al., 1998; Roh et al., 2009). The global use of RDX has resulted in its introduction into the environment through detonation, production, storage, disposal, and leakage of underwater military munitions (Harrison and Vane, 2010; Hovatter et al., 1997; Jenkins et al., 2006; Talmage et al., 1999). RDX is a contaminant in terrestrial (Pennington and Brannon, 2002) and marine (Darrach et al., 1998) ecosystems and has been shown to be persistent (Smith et al., 2013). Toxicological studies have been reported for terrestrial (Simini et al. 2003), freshwater (Bentley et al., 1977; Mukhi et al., 2005; Mukhi and Patiño, 2008; Steevens et al., 2002), and marine systems (Lotufo et al., 2001, 2010; Nipper et al.,

2001; Rosen and Lotufo, 2007a). The presence of RDX is likely to be of concern in marine environments due to RDX being a possible human carcinogen and a convulsant (Sweeney et al., 2012). Yet, marine systems have not been fully characterized for contamination levels and biological accumulation, nor is the ecological fate of RDX fully understood (Rosen and Lotufo, 2007b; Lotufo et al., 2009).

Direct uptake and bioconcentration for several species of marine coastal biota have been measured directly and show that RDX has a very small bioconcentration potential (Ballentine et al., 2015; Lotufo et al., 2010; Rosen and Lotufo, 2007b). Similarly low bioconcentration potential can also be predicted for coastal marine systems using octanol/water-partitioning coefficient of RDX (log K_{ow} = 0.87; Burken and Schnoor, 1998). The use of carbon isotopes incorporated into RDX as tracers (Lotufo et al., 2009) has shown that a greater amount of RDX is taken up into tissues relative to measures based on direct uptake or predicted from log K_{ow} values. This larger amount of RDX uptake observed in carbon isotope tracer studies is often attributed to munitions transformations to non-extractable compounds (Lotufo et al., 2009). The non-extractable compounds formed are assumed to be solvent-resistant or possibly tissue bound but surmised to be RDX, RDX derivatives, and/or adducts. The use of the stable nitrogen isotope as a tracer has been used in a variety of marine systems for examining uptake/cycling of dissolved inorganic nitrogen (DIN; Tobias et al., 2001, Holmes et al., 2000), and has potential utility for study of RDX uptake. The RDX ring is broken in several possible biotic pathways (Crocker et al., 2006; Pennington and Brannon, 2002) allowing for the possibility of more nitrogen containing products being bound as non-extractable derivatives, adducts, or incorporated into tissue. The use of ^{15}N labeled RDX may show greater sensitivity compared with uptake studies that only use non-labeled RDX or carbon labelled RDX since there is twice the amount of nitrogen in a RDX molecule relative to carbon.

Past studies using bacteria (Annamaria et al., 2010; Bhatt et al., 2006; Van Aken et al., 2004), fungi (Bhatt et al., 2006), terrestrial (Just and Schnoor, 2004; Thompson et al., 2005), and freshwater biota (Houston and Lotufo, 2005) have used ^{18}O and ^{14}C labeled RDX to primarily show biodegradation or mineralization of RDX. Our study builds upon a few select studies that track the fate of munitions compounds in complex multi-compartmental experiments (Rosen and Lotufo, 2010; Lotufo et al., 2001) by the addition of ^{15}N as a tracer. By comparing total amounts of RDX plus the metabolites to total amounts RDX-derived ^{15}N tracer in organisms we can assess gross uptake and retention of compound. The use of ^{15}N allows for the tracking of breakdown of the RDX and its main derivatives and identify amounts of these compounds transformed and retained in tissues in forms other than RDX and its primary nitroso metabolites (MNX, DNX, and TNX). The objective of this study was to quantify RDX uptake in 9 different coastal marine species, and assess RDX-derived nitrogen retention in the organism using ^{15}N nitro-labeled RDX in an aquaria scale simulation of a coastal marine ecosystem where other competing RDX degradation pathways are operating (mineralization). ^{15}N mass balance modeling was used to evaluate the uptake, transformation, retention, and elimination of biota.

9.2. Methods

9.2.1 Experimental Design

Two 70 L glass aquaria containing seawater and sandy sediments from Long Island Sound, Connecticut, USA were connected to a common recirculating glass aquarium reservoir. The sandy sediments were collected from a single site and were primarily consisted of medium sand (50%) and coarse sand (33%) with the remaining percentage consisting of smaller particles. The sediments used had a density of 2.02 g mL^{-1}, porosity of 40%, total organic carbon and total nitrogen of 1.233 mg g sed^{-1} and 0.176 mg g sed^{-1} respectively. The experimental aquaria design was similar to aquaria setup from Smith et al. (2013). Sediments were collected from a nearby subtidal habitat in Long Island Sound (LIS) and added to the aquaria to an average depth of 10 cm. Seawater was then added from LIS. The system was allowed to stabilize over a period of two weeks with flow through water from the LIS. 24 h before the start of the experiment the system was switched to recirculation mode and biota was added. In total, two macroalgae species (*Fucus vesiculosus* and *Ulva lactuca*), two epifaunal species (*Littorina littorea* and *Carcinus maenas*), three bivalve species (*Crassostrea virginica*, *Mytilus edulis*, and *Mercenaria mercenaria*), and two fish species (*Pseudopleuronectes americanus* and *Fundulus heteroclitus*) were used. ^{15}N nitro labelled-RDX (^{15}N-RDX) was synthesized by S. Fallis and T. Groshens at the Naval Air Warfare Center Weapons Division, Chemistry Division, China Lake, CA and was added to the reservoir in single 1 mL addition of methanol for an initial target tank RDX concentration of 0.4 mg L^{-1}, and then added throughout the time series experiment with the use of a peristaltic pump to target steady state at a rate of 0.037 mL min^{-1}. The pump rate was designed to maintain a steady state RDX at the same initial concentration of 0.4 mg L^{-1} based on measured rates of RDX removed measured in preliminary experiments. Water and biota collected from the experimental aquaria were analyzed for RDX, hexahydro-1,3,5-trinitroso-1,3,5-triazine (TNX), hexahydro-5-nitro-1,3-dinitroso-1,3,5-triazine (DNX), and hexahydro-3,5-dinitro-1-nitroso-1,3,5-triazine (MNX).

9.2.2 Aqueous Sampling

Time series (21 days) water column aqueous munition samples (2 mL) were taken from the experimental tank and placed in 15 mL centrifuge tubes at each time point (days 7, 14, and 21 n=3). Water samples measured for munitions used a modified "salting out" technique adapted from Miyares and Jenkins (1990) and used by Ballentine et al. (2015). Briefly, the 2 mL of sample were added to 1.3 g of NaCl and shaken. American Chemical Society (ACS) – grade acetonitrile, 1.5 mL, was then added and shaken for 5 min. The separated acetonitrile was removed and the process was repeated two more times using 1 mL of ACS-grade acetonitrile. The final extract was then placed into a gas chromatography vial and run using a gas chromatograph (GC) equipped with an electron-capture detector (ECD) as detailed in Ballentine et al. (2015).

9.2.3 Biota Sampling

Biota samples were removed from the experimental aquaria then immediately rinsed for 5 min with clean filtered seawater to remove dissolved and weakly sorbed munitions compounds from the tissue surfaces. The shells of *L. littorea, C. virginica*, *M. edulis*, and *M. mercenaria* were opened before being rinsed. *C. maenas* eggs were removed prior to freeze drying and

separated into their own sample vials then freeze-dried. Once rinsed, tissues were removed, freeze-dried, and weighed. Freeze-dried samples were homogenized using a mortar and pestle and then separated into a fraction for measuring munitions compounds concentrations in the tissue and a fraction for bulk ^{15}N isotope. Samples analyzed for munitions compounds concentrations were extracted using methods modified from Conder et al. (2004). ACS-grade acetonitrile, 10 mL, was added to the samples and then sonicated for 1 h. The homogenate was then centrifuged for 10 min at 10,000 rpm. The supernatant was removed, filtered through 0.22-µm PTFE syringe-tip filter, and 0.01 mg L^{-1} of 3,4-dinitrobenzene (3,4-DNB) as an recovery standard. GC/ECD analysis was conducted with the same method as the water samples (Ballentine et al., 2015). Quantification was based on an external calibration curve of standard munitions RDX, MNX, DNX, and TNX (AccuStandard, New Haven, Connecticut, USA). The recoveries of munitions from tissue samples (n=3) ranged between 42 and 138% with a mean of 97% and standard deviation of 21% with a reporting limit for all compounds of 0.7 ng mL^{-1}. To account for various sizes of organisms extractable munitions concentrations were normalized to organism dry weight (g dw). In addition to munitions concentrations, biota were analyzed for total ^{15}N tracer.

9.2.4 ^{15}N Analysis

Total ^{15}N in all solid samples (sediments, biota tissues, and suspended particulate matter) were analyzed by elemental analyzer – isotope ratio mass spectrometry (EA/IRMS: Delta V, Thermofisher). Samples were freeze-dried and weighed into tin capsules. Sufficient sample mass was used to achieve 40-80 µg N for isotope analyses. Isotope values were normalized with a 2-endpoint correction using United States Geological Survey reference materials L-glutamic acid (USGS40 and USGS41) accompanying each analytical batch and also served as check standards for drift correction. Analytical precision on ^{15}N measurements was 0.3 per mil which is equivalent to approximately 1/5000th of one percent excess ^{15}N. ^{15}N enrichments were reported in $\delta^{15}N$ using equation 1:

$$\delta^{15}N = (R_{sample} / R_{standard} - 1) \cdot 1000 \quad [1]$$

where R_{sample} is the $^{15}N/^{14}N$ ratio of the sample and $R_{standard}$ is the $^{15}N/^{14}N$ ratio of atmospheric nitrogen. All $\delta^{15}N$ values are reported as per mil (‰) with an EA/IRMS sensitivity of 0.3‰.

9.2.5 Nitrogen Isotope Modeling

The model mass balanced ^{15}N tracer. For the model, the munitions compounds concentrations measured in the biota and aqueous samples were converted to units of µg ^{15}N g dw^{-1}. The units were derived from the molar munitions compounds concentrations (both biota and aqueous samples) times the molar stoichiometry between munitions and ^{15}N tracer (1:3). This conversion was done to enable direct comparison (and unit compatibility) with bulk measurements of ^{15}N in tissue provided by the corrected EA-IRMS values.

Uptake and elimination rates of labeled nitrogen (^{15}N) derived from RDX were determined from a three compartment box model (Figure 9.1) consisting of the ^{15}N attributable to tissue parent compound (C_p), the ^{15}N attributable tissue metabolites (C_m), and the ^{15}N in tissue, not accounted for either the parent nor metabolite (C_m). MATLAB R2013b by Mathworks was the software used to construct the three box model used. This model was modified from a

simpler two box model (Lydy et al., 2000) that directly modeled concentrations of only the parent and metabolite. The root mean square error (RMSE) is a common and well used statistical method to calculate how well the model fits experimental data and was calculated for the ^{15}N three box model (Chai and Draxler, 2014; Table 9.1) Box 1 (Figure 9.1; C_p) of the model was fit to the experimental data with Equation 2:

$$\frac{dC_p}{dt} = (k_u \cdot C_w) - \left(k_{ep} \cdot C_p\right) - \left(k_m \cdot C_p\right) - (k_{pN} \cdot C_p) \quad [2]$$

where C_w = concentration of ^{15}N in water (µg N mL^{-1}) derived from aqueous RDX concentration, C_p = concentration of labeled nitrogen isotope attributed to the parent compound in the biota (µg N g dw^{-1}), k_u = uptake clearance coefficient (mL g^{-1} d^{-1}), k_{ep} = elimination rate constant (d^{-1}), k_m = uptake rate constant nitrogen derived from RDX (d^{-1}), k_{pN} = nitrogen incorporation rate constant from parent compound (d^{-1}), and t = time (d). Box 2 (Figure 9.1; C_m) of the model is the ^{15}N derived from RDX metabolites fit to experimental data with Equation 3:

$$\frac{dC_m}{dt} = \left(k_m \cdot C_p\right) - (k_{em} \cdot C_m) - (k_{mN} \cdot C_m) \quad [3]$$

where C_m = concentration of labeled nitrogen attributed to metabolized derivatives in the biota (µg N g dw^{-1}), k_{em} = metabolite derived nitrogen elimination rate constant (d^{-1}), and k_{mN} = nitrogen incorporation rate constant from metabolites (d^{-1}). Box 3 (Figure 9.1) is the ^{15}N not attributed to RDX or the derivatives MNX, TNX, or DNX. Box 3 (Figure 9.1; C_N) of the model was fit to experimental data using Equation 4.

$$\frac{dC_N}{dt} = (k_{mN} \cdot C_m) + \left(k_{pN} \cdot C_p\right) + (k_{DN} \cdot C_{DIN}) - (k_{eN} \cdot C_N) \quad [4]$$

C_N = concentration of total labeled nitrogen in the biota (µg N g dw^{-1}), C_{DIN} = concentration of nitrogen from DIN (µg N mL^{-1}), k_{eN} = nitrogen elimination rate constant (d^{-1}), and k_{DN} = uptake of nitrogen from aqueous medium rate constant (d^{-1}). The rate constant k_{DN} is only included for the macroalgae due to the ability to directly uptake DIN from the water column. The model equations (3.2-3.4) were simultaneously fit to experimental data for the concentrations of munitions and ^{15}N-DIN in the system (Figure 9.1).

In addition to providing the gross rate of exchange between boxes within the organism and with its environment, the model output was also used to calculate bioconcentration factors (BCFs) for comparison to other approaches. BCFs were calculated four ways, three of which were similar to other studies for comparison to other species (Belden et al., 2005; Lotufo et al., 2010; Nuutinen et al., 2003). The first method (BCF_m) used concentrations of munitions in tissue and water (Eqn. 5; ASTM E1022-94, 2013). The next three methods represent a deviation from the standard ASTM E1022-94 (2013) definition of a BCF and represent a more specific partitioning ratio. The second method (BCF_T), used concentrations of total ^{15}N in tissue and water (Eqn. 6) similar to Belden et al. (2005b) who used ^{14}C. The third method (BCF_{kow}) used the log K_{ow} of RDX in Equation 7 derived by Meylan et al. (1999). The forth approach was model derived and used the uptake coefficients and elimination rates including k_{eN} (Eqn. 8). This approach has previously not been used to calculate BCF and collectively includes the uptake and elimination of RDX and all of its derivatives.

$$BCF_m = \frac{C_p}{C_w} \quad [5]$$

$$BCF_T = \frac{C_{15p}}{C_{15w}} \quad [6]$$

$$BCF_{kow} = log_{BCF} = 0.86 \cdot log_{K_{ow}} - 0.39 \quad [7]$$

$$BCF_R = \frac{k_u}{k_{ep} + k_{em} + k_{eN}} \quad [8]$$

9.3. Results

9.3.1 Aqueous Concentrations

Over the 21 day incubation period RDX decreased by 31% below the target concentration of 0.4 mg L^{-1} (Fig. 3.2) with a new RDX quasi-steady state concentration of 0.25 ± 0.04 mg L^{-1} achieved by day 9. The temporal changes in nitroso derivative concentrations differed from RDX. The derivatives measured reached a steady state 2 days before RDX on day 7. The derivatives declined in concentration late in the experiment when RDX had a slight increase (Figure 9.2). TNX peaked on day 9 at 0.028 ± 0.005 mg L^{-1} until decreasing to an average concentration of 0.013 ± 0.001 mg L^{-1} for days 16 through 21. MNX maintained a concentration of 0.012 ± 0.002 mg L^{-1} for the first 14 days after which MNX could no longer be detected. DNX was not measured in the water column during the 21 day incubation period.

During the 14 days that MNX remained in the water column, TNX and MNX had an average ratio of 2.35 to 1 with respect to each other. The measured derivatives never had a combined concentration greater than RDX. The ratio of RDX to TNX and MNX combined started at 13 to 1 and decreased over the 14 days when MNX was no longer measured to a ratio of 5 to 1. As TNX and MNX degraded and RDX remained steady, the ratio increased to 21 to 1.

9.3.2 Tissue Concentrations – Munitions and ^{15}N

$^{15}N_R$ (^{15}N attributed to RDX) and $^{15}N_D$ (^{15}N attributed to MNX + TNX + DNX) were measured in all species. The concentration of $^{15}N_D$ did not exceeded that of $^{15}N_R$ at any time point. Total bulk ^{15}N retained in biota was measured at an average of 1 order of magnitude greater than both $^{15}N_R$ and $^{15}N_D$ in all species (Figure 9.3). Although certain species retained a greater amount of total ^{15}N than other species, there was no distinguishable pattern between uptake and retention of total ^{15}N. The $^{15}N_R$ and $^{15}N_D$ reached steady states typically by day 1, which was much faster than the rate at which total ^{15}N in each species attained steady state.

9.3.3 Primary Producers

Both autotrophic species had a rapid initial uptake of munitions and reached a steady state of $^{15}N_R$ on day 1. *F. vesiculosus* obtained a measured steady state of 0.09 ± 0.03 µg $^{15}N_R$ g dw^{-1} while *U. lactuca* reached a steady state of 0.17 ± 0.8 µg $^{15}N_R$ g dw^{-1} (Figure 9.3). The $^{15}N_D$ ratio to $^{15}N_R$ in *U. lactuca* ranged from 0.6 – 6.5 to 1. No clear pattern of the ratios of $^{15}N_D$ to

$^{15}N_R$ was apparent. In both macroalgae species the total µg ^{15}N g dw^{-1} measured was 1-2 orders of magnitude greater than both $^{15}N_D$ and $^{15}N_R$ combined (Figure 9.3). MNX, DNX, and TNX were not detected in *F. vesiculosus* tissue. TNX was detected throughout the incubation for *U. lactuca* with MNX only detected in the first 2 days. The total ^{15}N in the macroalgae also reach a steady state much later than the $^{15}N_R$ (Figure 9.3). *U. lactuca* ^{15}N value on day 21 increases beyond the steady state. The total ^{15}N in *U. lactuca* reached a peak value twice as high as *F. vesiculosus.*

9.3.4 Epifauna

L. littorea reached a steady state of 0.12 ± 0.06 µg $^{15}N_R$ g dw^{-1} after day 5 while *C. maenas* steady state value of 0.04 ± 0.01 µg $^{15}N_R$ g dw^{-1} was obtained on day 7 (Figure 9.3). Derivative to RDX ratios showed no clear pattern for either epifaunal species. The $^{15}N_D$ measured values in *L. littorea* are very similar to the $^{15}N_R$ values for *L. littorea*. *C. maenas* ratio of $^{15}N_D$ to $^{15}N_R$ ranged from 0.2 – 2.4 to 1. There were 2 *C. maenas* egg samples analyzed. $^{15}N_R$ in the *C. maenas* eggs measured 0.14 ± 0.01 µg $^{15}N_R$ g dw^{-1}. The ratio of $^{15}N_D$ to $^{15}N_R$ for *C. maenas* eggs was 0.26 to 1. MNX was found in both epifaunal species while DNX was found only in *L. littorea* and TNX was only found in *C. maenas*. The epifaunal species had an initial uptake of ^{15}N that then increased to a steady state. The total ^{15}N in *L. littorea* reached a steady state value 5 times higher than the ^{15}N in *C. maenas.* Total ^{15}N for *C. maenas* eggs was 2 orders of magnitudes greater than $^{15}N_D$ and $^{15}N_R$ combined for all other *C. maenas* tissues.

9.3.5 Bivalves

C. virginica tissue concentrations of $^{15}N_R$ were highly variable between time points and within triplicates likely reflecting the variable amount of active pumping observed between individuals. An average concentration of 0.26 ± 0.30 µg $^{15}N_R$ g dw^{-1} was reached after day 2 of the incubation (Figure 9.3). Both *M. edulis* and *M. mercenaria* reached steady state values of 0.44 ± 0.21 µg $^{15}N_R$ g dw^{-1} and 0.05 ± 0.03 µg $^{15}N_R$ g dw^{-1} respectively. MNX was measured in both *C. virginica* and *M. mercenaria* throughout the incubation. DNX was found only at the day 1 time point in *C. virginica* and *M. edulis*. Measured concentrations of all the derivatives were found only at the day 1 time point in *M. edulis* after which no other derivatives were measured in *M. edulis*. Total ^{15}N was measured 2 orders of magnitude greater than $^{15}N_D$ and $^{15}N_R$ for *M. edulis* and *M. mercenaria* while the total ^{15}N measured in *C. virginica* was measured 1 order of magnitude greater than that of $^{15}N_D$ and $^{15}N_R$ combined. ^{15}N did reach a steady state in *C. virginica* on day 3 of the incubation at a value of 7.6 ± 2.4 µg ^{15}N g dw^{-1} (Figure 9.3). The total ^{15}N measured in *M. edulis* measured twice the concentration than that measured in *M. mercenaria* and *C. virginica*.

9.3.6 Fish

$^{15}N_D$ for *P. americanus* had an average steady state value reached after 1 day of 0.37 ± 0.15 µg $^{15}N_D$ g dw^{-1}. $^{15}N_R$ reached a steady state for *P. americanus* after day 1 with a value of 0.67 ± 0.29 µg $^{15}N_R$ g dw^{-1}. Due to unidentifiable interference with the GC /ECD analysis tissue concentrations of $^{15}N_D$ and $^{15}N_R$ for *F. heteroclitus* were not able to be determined. MNX, DNX, and TNX were measured in *P. americanus*. DNX and TNX were measured values were sporadic. On average the total ^{15}N measured in *P. americanus* was 1 order of magnitude greater

than that of $^{15}N_D$ and $^{15}N_R$ combined over the time series. *F. heteroclitus* total ^{15}N reached a steady state after 1 day of an average value of 7.6 ± 1.3 μg ^{15}N g dw^{-1}.

9.3.7 Total ^{15}N Distribution Across Biota

The species can be divided into two groups with respect to uptake and retention of total ^{15}N. The first group (*M. edulis, P. americanus, L. littorea, F. vesiculosus, U. lactuca*, and *F. heteroclitus*) had double the average amount of uptake and retention of ^{15}N normalized to mass throughout the experiment than the second group (Figure 9.4). While the second group (*C. virginica, C. maenas*, and *M. mercenaria*) only retained half the amount of ^{15}N normalized to mass (Figure 9.4). *U. lactuca* and *L. littorea* contributed the largest percent of ^{15}N attributed to the biota with 17 ± 9 % and 16 ± 4% respectively (Figure 9.4). *C. maenas* contributed the lowest amount of ^{15}N retained with 6 ± 1% of the total ^{15}N retained by all species. The contribution to the total ^{15}N in each species remained at a steady state starting at day 1 with the exception of a transient spike of ^{15}N measured in *P. americanus* at day 14 (Figure 9.4).

After the initial incorporation of ^{15}N tracer into biota between day 0 and 1, the ^{15}N found in the biota decreased over time. On day 1 the ^{15}N in the biota only accounted for 8% of the total ^{15}N added to the system initially in the form of ^{15}N-RDX (Figure 9.5). At the end of the experiment on day 21 the biota accounted for only 4% of the total ^{15}N added to the system. Of the small 8% of the ^{15}N accounted for by the biota, the combined $^{15}N_D$ and $^{15}N_R$ percent found in all species tissues was 11% at day 1. The contribution of $^{15}N_D$ and $^{15}N_R$ to the total ^{15}N in the biota steadily decreases over the time series to a final value of 1% (Figure 9.5). Majority of the ^{15}N measured in the biota were unknown retained pools of ^{15}N and is much larger than the $^{15}N_R$ and $^{15}N_D$.

9.3.8 Modeling

The RDX uptake (k_u) varied up to 10 fold among the different species. *M. edulis* had the largest k_u at 38.2 mL g^{-1} day^{-1} while *F. Vesiculosus* had the slowest at 2.3 mL g^{-1} day^{-1} (Table 9.1). There was no pattern to the modeled k_u for the various species with respect to organism group, trophic position, or niche. The two macroalgae species showed markedly different k_u from each other, spanning the whole range of k_u seen across species. The bivalves showed similar k_u rates, ranging from 6 to 36; about the same amount as the periphyton supported *L. littorea* and higher than the infaunal filter feeding *M. mercenaria*. *C. maenas* had among the lowest k_u values and there were similar values between *P. americanus* and *F. heteroclitus* despite their benthic vs pelagic positions. The rate constants for elimination of RDX (k_{ep}) for each species were similar with values ranging from 0.2 to 0.7 $days^{-1}$. The modeled values for k_m varied greatly between some species, ranging from 0 to 5 $days^{-1}$ and mainly reflecting large differences in metabolite concentrations among biota. In comparison to the other parameters, k_{pN} and k_{mN} were much larger. Modeled values for k_{pN} ranged from 1.6 to 7 $days^{-1}$ while k_{mN} ranged from 0 to 3 $days^{-1}$ (Table 9.1). Uptake of RDX derived N mineralized through the DIN pool (k_{DN}) values were small and only existed for three of the species: *F. Vesiculosus*, *U. lactuca*, and *L. littorea*.

BCFs were calculated with 4 different methods. Variation in BCF values were more dependent upon how the BCF was calculated rather than organism type. (1) The BCF calculated with the concentrations of parent munitions (BCF_m) using equation 3.5 were low. (2) The BCF

based on total ^{15}N (BCF_T) was calculated by using the total ^{15}N concentrations (Eqn. 3.6) were on average 2 orders of magnitude greater than BCF_m values (Table 9.1). (3) The BCF_R calculated from the model fell between BCF_m and BCF_T values. (4) Finally, a BCF_{kow} calculated from the Log K_{ow} of RDX is shown in Table 9.1 for comparison (Meylan et al., 1999).

9.4. Discussion

Results from the ^{15}N RDX experiments and modeling support two major findings: (1) RDX was transformed into multiple derivatives, with subsequent ^{15}N retention in the organism; (2) ^{15}N toxicokinetic parameters and BCFs values calculated using ^{15}N labeled RDX, MNX, TNX, and DNX were larger and more variable than previous studies have indicated.

9.4.1 RDX Uptake and Transformations in Biota

RDX has been shown to be degraded by bacteria (Bhatt et al., 2005; Hawari et al., 2000; Vila et al., 2007) and fungi (Bhatt et al., 2006; Sheremata and Hawari, 2000), and taken up into freshwater fish (Belden et al., 2005b) and terrestrial biota (Just and Schnoor, 2004; Sarrazin et al., 2009; Vila et al., 2007), but few studies have discussed the fate of RDX in coastal marine biota or generally the fate of RDX in macrobiota after uptake. The previous use of ^{14}C and ^{15}N labeled RDX in aerobic bacterial or fungal studies have been useful in demonstrating mineralization to CO_2 and DIN (NO_x, and N_2O; Fournier et al., 2002; Sheremata and Hawari, 2000; Thompson et al., 2005). While many previous toxicological studies have focused on uptake rates, removal rates, and BCF values of RDX, MNX, TNX, and DNX in single organism simplified experiments, but as presented in a few previous similar studies (Rosen and Lotufo, 2005, 2010) the environmental uptake of RDX into organisms operates within a host of other transformation and degradation pathways. Here we created experimental conditions whereby both microbial breakdown pathways could operate side by side with macrobiotic uptake and transformations. This study shows that the ^{15}N derived from RDX was found in biota in much larger concentrations than could be attributed to munitions compounds and the ^{15}N concentration should be considered conservative estimates because only the nitro groups were labeled on the RDX and not the ring N. In this study, the amount of total ^{15}N in biota was 1-2 orders of magnitudes greater than can be accounted for by measureable tissue RDX indicating that a significant amount of the RDX taken up into the biota is being processed into various nitrogen retention pathways.

Despite rapidly attaining a quasi-steady state (maximum but variable concentrations) for RDX and its main derivatives, the munitions derived N was transformed more slowly within the organisms and then retained in the larger total bulk N pool of each organism. This process was evidenced by the slowly increasing total ^{15}N enrichment that required days to weeks before the ^{15}N enrichment leveled to a steady state (Figure 9.3). The difference in trajectory and pattern between ^{15}N attributed to RDX and total ^{15}N along with the small percentage attributable to RDX (Figure 9.5) can be seen in all the biota in this study. This result suggests that the mechanisms or pathways responsible for these patterns may be common across biota types.

The data suggests that there are four possible explanations for the difference in pattern between ^{15}N attributed to RDX and total ^{15}N uptake in the biota. (A) The first possible explanation is that the RDX was mineralized to DIN externally in the environment and taken up by macrobiota as DIN. Autotrophs can readily take up DIN, and the model showed that the

uptake of DIN (k_{DN}; Table 9.1) was needed to appropriately model the total ^{15}N trajectories in the autotrophs (*F. vesiculosus and U. lactuca*) and the one species heavily grazing on autotrophic periphyton (*L. littorea*). While autotrophic uptake of DIN is common, heterotrophs cannot directly assimilate DIN. Therefore such a pathway cannot explain the ^{15}N subsidy in heterotrophs, and the model validated that k_{DN} for heterotrophs were nonexistent. (B) The second possible explanation is that RDX was rapidly partitioned into the biota and then transformed and retained in tissue as unknown free breakdown products of RDX. Peak MNX, DNX, and TNX concentrations as well as the rate of change in those concentrations varied widely across species. The highly variable patterns of metabolite composition and concentration trajectories between organisms suggest that organism-specific transformations were important determinants of net tissue metabolite concentrations. It may also be indicative of the multiple different biodegradation pathways that produce secondary ^{15}N containing metabolites beyond MNX, TNX, and DNX. Several pathways have been documented for fungi and prokaryotes, and some have been attributed to the action of cytochrome P450 (Seth-Smith et al., 2008). Similar reactions may also be operating in macrobiota (Bhatt et al., 2006; Crocker et al., 2006). Cytochrome P450 belongs to a protein family that is highly evolutionarily conserved and is found in different types of both prokaryotic (Seth-Smith et al., 2008) and eukaryotic cells (Bhushan et al., 2003). The P450 protein has been shown to produce RDX metabolites (nitrite, 4-Nitro-2,4-diazabutanal, formaldehyde, and ammonium) by consuming RDX and NADPH in rabbit liver cells (Bhushan et al., 2003) and evidence of nitro formation includes the possibility of macrobiota acting as partial mineralizers. Similar metabolites have been measured via *Rhodococcus sp.* mediated metabolism of RDX with similar mechanisms proposed (Hawari et al. 2002). P450 has also been reported to biodegrade RDX derivatives MNX and TNX to similar metabolites in rabbit cells (Halasz et al., 2012). In this study, because the tissues were not extracted prior to bulk ^{15}N analyses, and derivatives other than the MNX, DNX, and TNX were not measured in the extracted fraction, any free derivative other than MNX, DNX, and TNX would be counted in the bulk ^{15}N measurement. Interestingly, because some of the nitroso breakdown pathways include denitration steps, it leaves open the possibility that macrobiota may also contribute to mineralization of RDX to DIN. (C) The third possible explanation is that further breakdown of the nitroso derivatives led to compounds that quickly formed adducts that are bound to specific tissue types. Bound adducts have been proposed in ^{14}C labelled munitions experiments as an unextractable fraction and used to explain discrepancies between the measurable amount of munitions and the radio isotope label (Belden et al., 2011). As indicated by the model, (k_{pN} and k_{mN}) the ^{15}N was biotransformed into other compounds other than the three main RDX derivatives MNX, DNX, and TNX and both explanations B and C are supported by these models results. While these secondary products could take numerous forms (Crocker et al., 2006), they were nonetheless retained within the organism otherwise would not have appeared as a ^{15}N subsidy in the bulk EA analysis. (D) Finally a less likely but possible fourth explanation remains that the RDX is fully mineralized within macrobiota and the mineralized ^{15}N tracer is used in the biosynthesis of tissues. Several nitroso breakdown pathways yield variable oxidation state inorganic N compounds (Fournier et al., 2002). Although it is unclear if those reactions operate within macrobiota, and we do not propose a specific mechanism, this possibility cannot be wholly discounted.

RDX as a potential toxicant in marine biota depends on which pathway caused the discrepancy between the ^{15}N accounted for in RDX and the much larger amount of bulk ^{15}N-RDX. If the RDX is mineralized, either externally or internally, (options A and D) and then

incorporated into tissue through natural biosynthesis pathways, then RDX is most likely not a large concern for organisms coastal marine environment. Similar pathways to A and D with low toxicological effect have been documented (Nipper et al. 2009). However if intra-organism transformations lead to derivative production other than MNX, DNX, and TNX and those products are either in the "free" state or as adducts (options C and D) and are more toxic than RDX or the nitroso derivatives then RDX could be of greater concern. RDX in general is associated with low toxicity, which leads to the inference that and "free" or adduct breakdown products do not substantially contribute to acute toxicological effects. However any long-term effect, particularly associated with production of adducts with DNA remain unknown.

9.4.2 Model Toxicokinetics and BCFs

Distribution and movement of RDX, RDX derivatives, and ^{15}N were accurately described using the first order equations (Eqns. 2-4). The expansion of previously published models (Lydy et al., 2000; Nuutinen et al., 2003) allowed for a better understanding of the fate of RDX by tracking the biodegradation and metabolism of RDX derived N. The rates and rate constants reported in Table 9.1 are not markedly different across species though some patterns do emerge. The modeled k_u values derived from the model fall within the few reported values published (Belden et al., 2005a; Lotufo et al., 2009). The similarities between our k_u and previous published values is expected since the k_u is controlled by the physical partitioning of the RDX molecule into tissue rather than active assimilation. However stark differences arose in other terms in our model due to the inclusion of modeling the bulk ^{15}N tracer. The modeled elimination k_{ep} values derived here are smaller by 1-2 orders of magnitude than previously reported k_e values (Belden et al., 2005a; Lotufo et al., 2009). The difference in the k_{ep} values reported here is offset by the higher retention of ^{15}N (k_{pN} and k_{mN}) in this study's tracer model. The k_{pN} and k_{mN} are one order of magnitude larger than the elimination values k_{ep} and k_{em}. Since k_{pN} and k_{ep} pull from the same ^{15}N pool (Figure 9.1) the ^{15}N is not being removed but retained by the organism. With k_{pN} and k_{mN} being so much larger than the elimination values for the those pools, the need to account for the total ^{15}N led to the low k_{eN} and $^{15}N_R$ values for biota suggests that ^{15}N is retained in tissue and not just removed as previous studies indicate.

The model provided an additional way to estimate BCF and for this study, we had a total of 4 options to estimate a BCF. (1) The ratio of the steady state concentration of tissue concentration divided by the aqueous munitions concentration (BCF_m, Eqn. 5). (2) The use of total ^{15}N values attributed to RDX (BCF_T, Eqn. 6). (3) The use of Log K_{ow} values as a proxy for BCF (Eqn. 7). (4) Finally, the modeled derived rate balance was used to calculate a BCF (BCF_R, Eqn. 8). Generally our BCF values compared favorably to other reports for aquatic organisms derived with similar methods (Lotufo et al., 2009). BCFs calculated in previous studies have shown that BCF calculated with only the parent compound (BCF_m) are typically lower than estimates using Log K_{ow} values (BCF_{Kow}; Lotufo et al., 2009). Similarly BCFs calculated with total isotopes inventory (BCF_T) also yield a BCF much higher than estimates using Log K_{ow} as summarized by Lotufo et al (2009). Most toxicological studies have either used Log K_{ow} or BCF_m method. Either of these methods work well for studies that need to know only how much of the parent compound is in the species tissues for a given aqueous concentration. However, if the parent and derivatives are important (such as when breakdown products might have high toxicity) then a more complete BCF using total reactivity (BCF_T) should be utilized as it indicates other potentially unmeasured metabolites, adducts, or other compounds of similar

toxicological relevance provided options B and/or C are dominant. Alternatively, if the BCF_T reflects tracer that has been liberated through mineralization and subsequent incorporation of N into tissue (options A and D), it may be a better indication of processing than as an indicator of the partitioning of an intact compound with some presumed toxicity.

Similar to other studies, the BCF_R calculated here from the modeled rate constants gave a larger BCF values relative to BCF_m method, but it was smaller than the BCF_T. The BCF_R as defined by Eqn. 8 functions as an aggregated BCF of RDX, its derivatives, and adducts assuming options B and C are the principle cause. Under these scenarios the BCF_R is not a unique metric for only the parent compound and/or its measured derivatives but instead captures all compounds derived from RDX that may retain some toxic properties, and reflects the balance between uptake, elimination, and transformations of RDX. The value that is calculated for the BCF_R reflects the transformations and eliminations that the ^{15}N model captures and that the more simple BCF_m method does not take into account. If options A or D are correct from the previous section, then k_{eN} would need to be removed from Eqn. 8, because the accumulation of ^{15}N in DIN does not include tracer associated with derivatives. This adjusted BCF_R would still adequately characterize ratio of uptake to retention of RDX plus all metabolites.

Our model can accurately describe not only the experimental BCF_m but also the subsequent processing the RDX post uptake as it is transformed and subsequently retained by the organism. Even though our model can both track ^{15}N movement in the organism and accurately estimate BCFs that could be used for toxicological studies, the model cannot eliminate the possibility of some unknown derivatives or partial breakdown products with adducts. Resolving these questions should be part of future work since it would help better define the fate of RDX after uptake and useful for assessing the RDX effects on coastal biota.

9.5. Conclusions

The multi organism ^{15}N tracer experiment identified uptake, conversion of RDX into its primary derivatives, and retention of nitroso derived N into the macrobiota. The biota reached a steady state with respect to both RDX and ^{15}N although at much different rates. The different rate of retention of ^{15}N indicates that RDX is continually metabolized and the nitrogen was retained into tissue. While the rates to steady state varied, the larger ^{15}N bulk then ^{15}N attributed to RDX indicated that there are common pathways or mechanism to the biotransformation and retention of ^{15}N. The identification of the ^{15}N breakdown products is paramount of importance to knowing whether the unknown large ^{15}N subsidy measured in tissue is harmful. ^{15}N was instrumental in identifying the fact that much more compound was taken up and processed even though we don't exactly know how. The use of ^{15}N constrains more traditional analytical chemistry approaches in this regard. The disadvantage of ^{15}N beyond additional cost and instrumental overhead is that N can be widely distributed among many pools, some associated with uptake and some not. It is sometimes difficult to isotopically characterize some specific compounds that are formed. The lack of compound identification can lead to large percentages of unknown in the ^{15}N tissue mass balance. The large percentages of unknown in ^{15}N tissue mass balance is both a boon (in that it can identify missing and possibly important processes seen here) and a difficulty because the optimum utility of the tracer often relies on analysis of many different N containing fractions. The value of using ^{15}N labeled munitions, as with many techniques, depends on whether it can yield information that cannot be derived through other

means. For this study, it clearly did. Bioconcentration factors were calculated with 4 different methods. The different BCF methods add variety to the current published methods to allow for a more accurate measurement of BCF for different systems. Toxicokinetic modeling of the ^{15}N tracer, RDX, and derivatives revealed a more complete picture of the fate of the RDX. The new model was a good fit to experimental data and has the ability to estimate the amount of ^{15}N incorporated into a variety of coastal marine biota. The model simultaneously modeled the ^{15}N and calculated toxicological relevant BCF values by introducing a new ^{15}N rate term. Future works should include identification of the unknown breakdown products and adducts. ^{15}N labeled compounds can offer many insights to transport and fate studies and should be used in follow up studies specifically in other environments (aquatic and terrestrial), other nitrogen containing compounds, and identifying the unknown breakdown products formed.

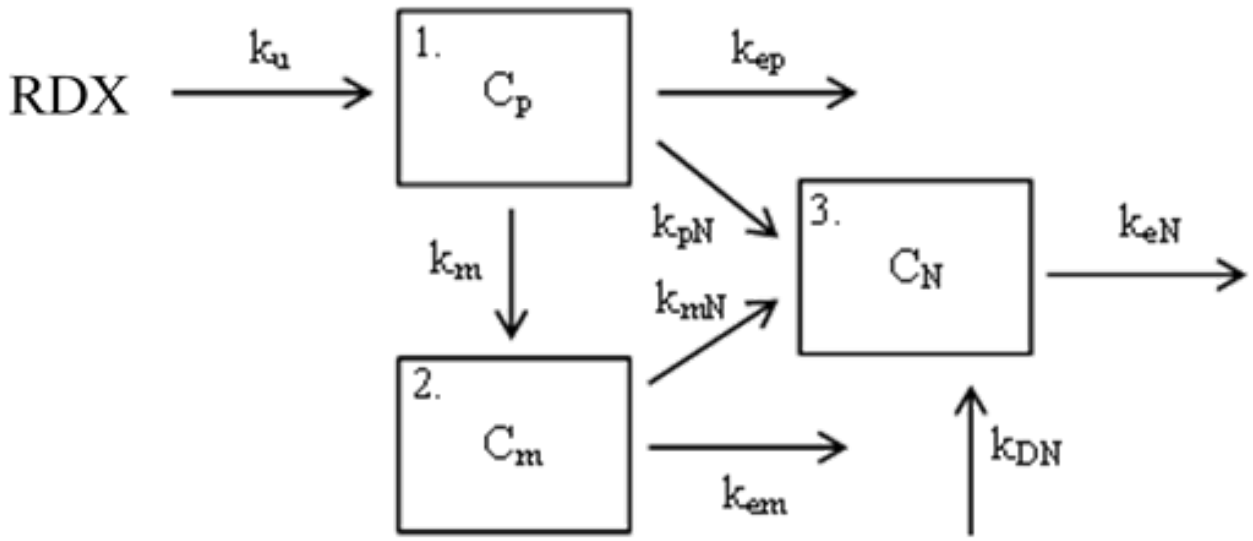

Figure 9.1. ^{15}N tracer three box model: Model structure representing uptake and movement of ^{15}N derived from within an organism. Box 1 is ^{15}N that attributed to RDX. Box 2 is the ^{15}N attributed to the sum of the nitroso derivatives (ie. metabolites TNX, DNX, and MNX). Box 3 represents the total ^{15}N in the organism not represented in box 1 or box 2.

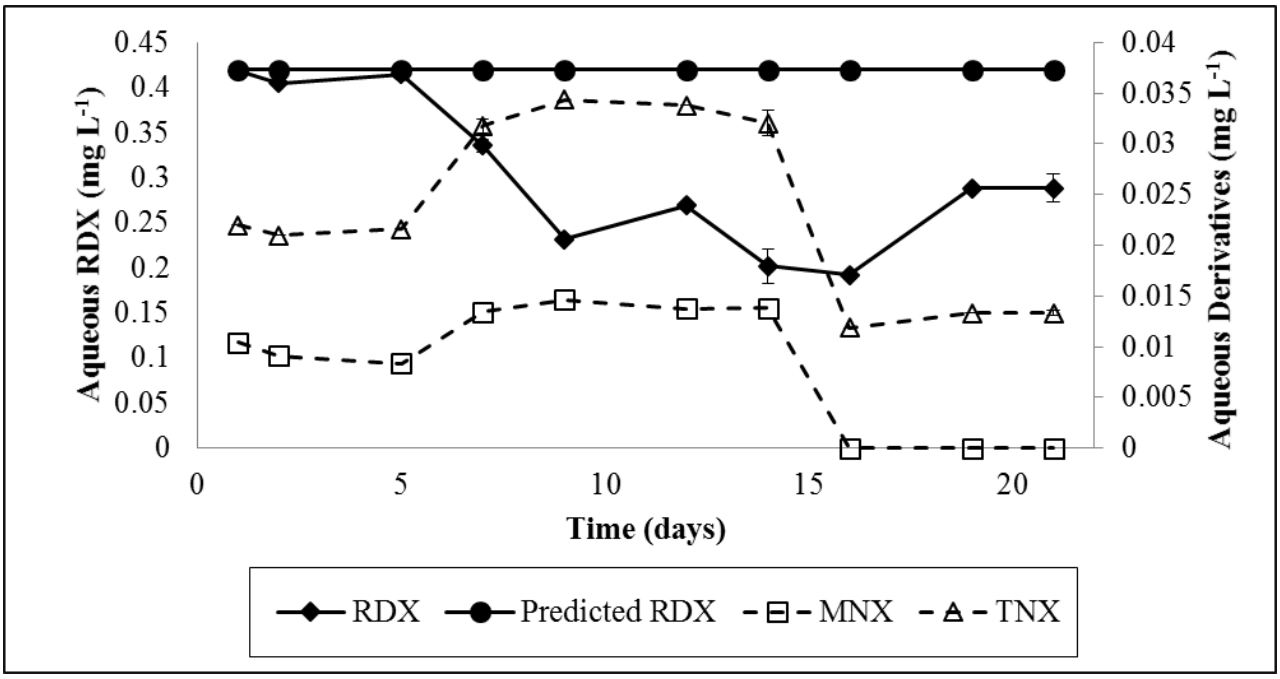

Figure 9.2. Aqueous munitions concentration: Time series experimental aqueous data for munitions. Error bars are standard deviation (N=3). Predicted RDX concentrations were calculated from the initial spike and pumping rate of RDX into the experimental setup. DNX was not detected.

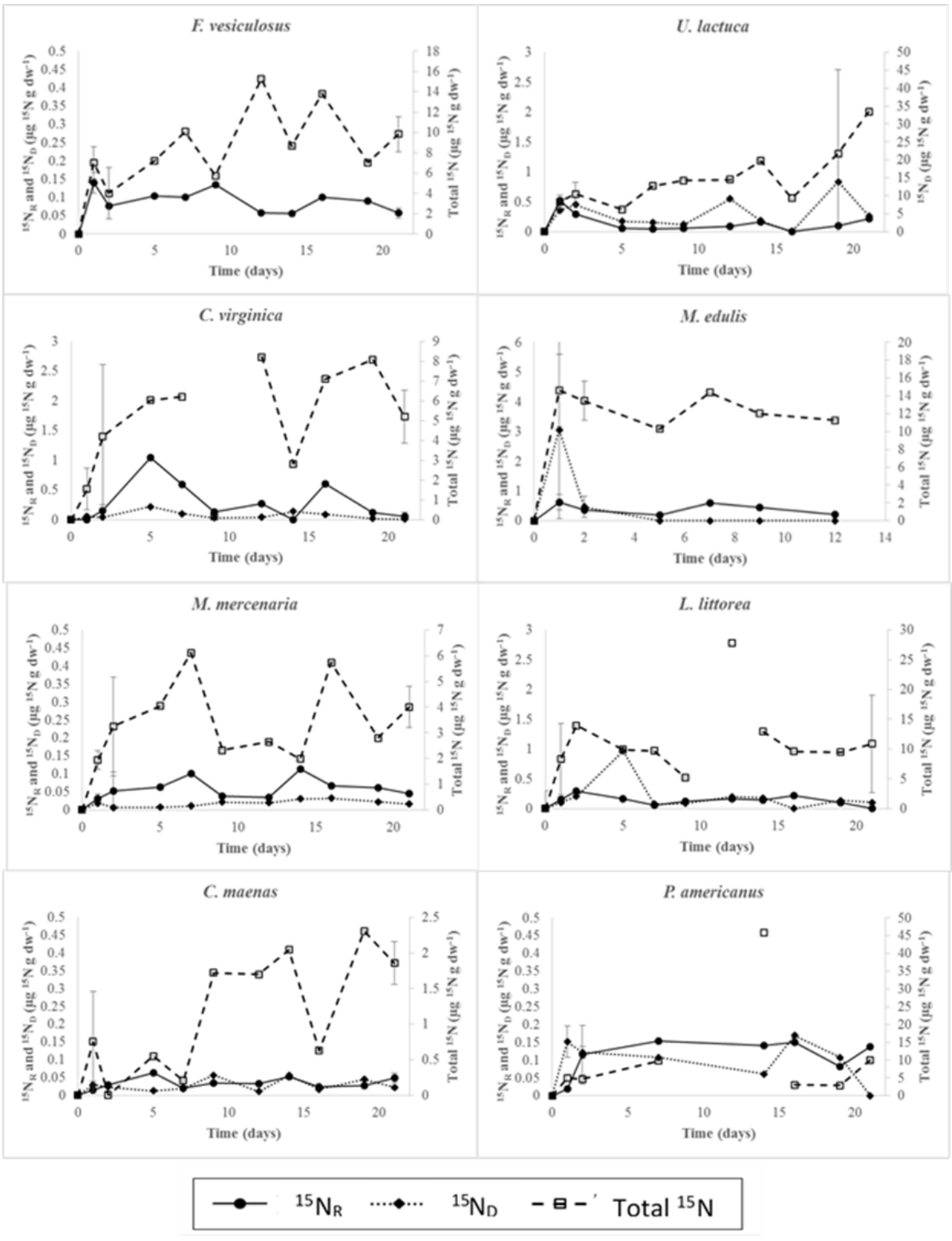

Figure 9.3. ^{15}N concentrations in biota tissue: Time series experimental biota data for munitions represented in ^{15}N units. $^{15}N_R$ and $^{15}N_D$ use the right axis while total ^{15}N uses the left axis. *F. heteroclitus* is not presented as data for $^{15}N_R$ and $^{15}N_D$ were lost.

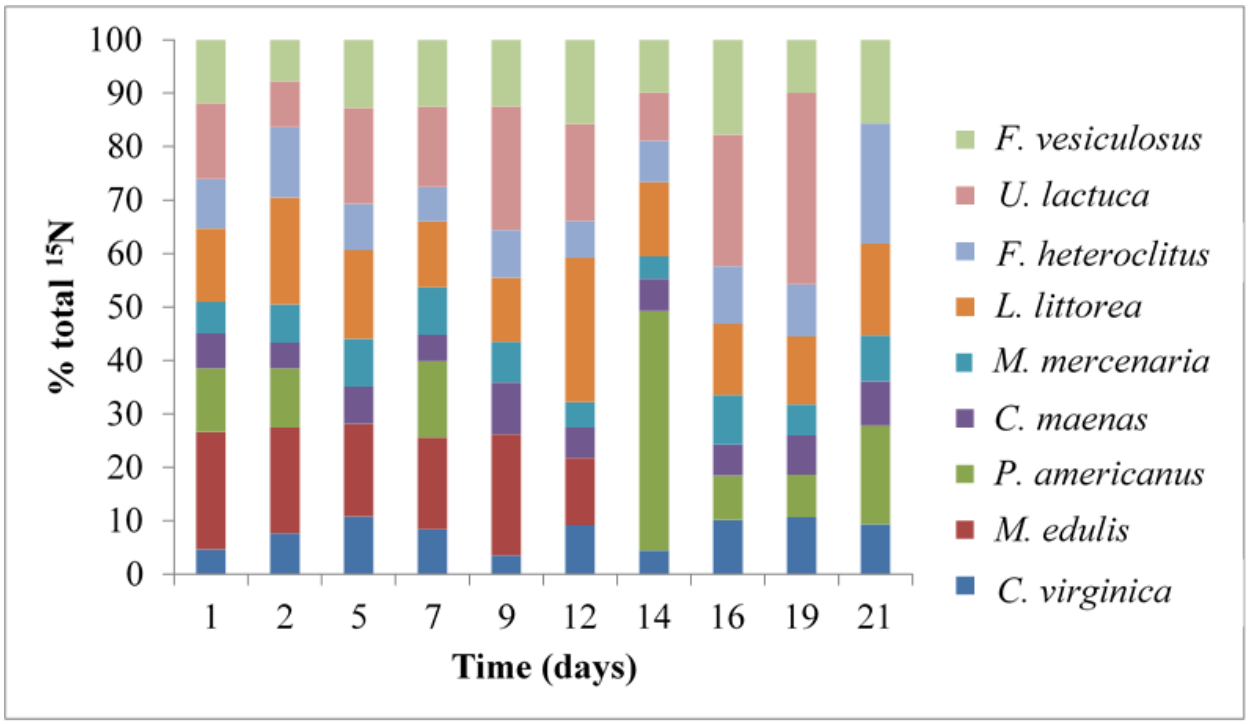

Figure 9.4. ^{15}N in biota normalized to mass: Total ^{15}N measured in all species was normalized to total mass for each species. *M. edulis* died off after day 12. All *U. lactuca* samples were removed after day 19.

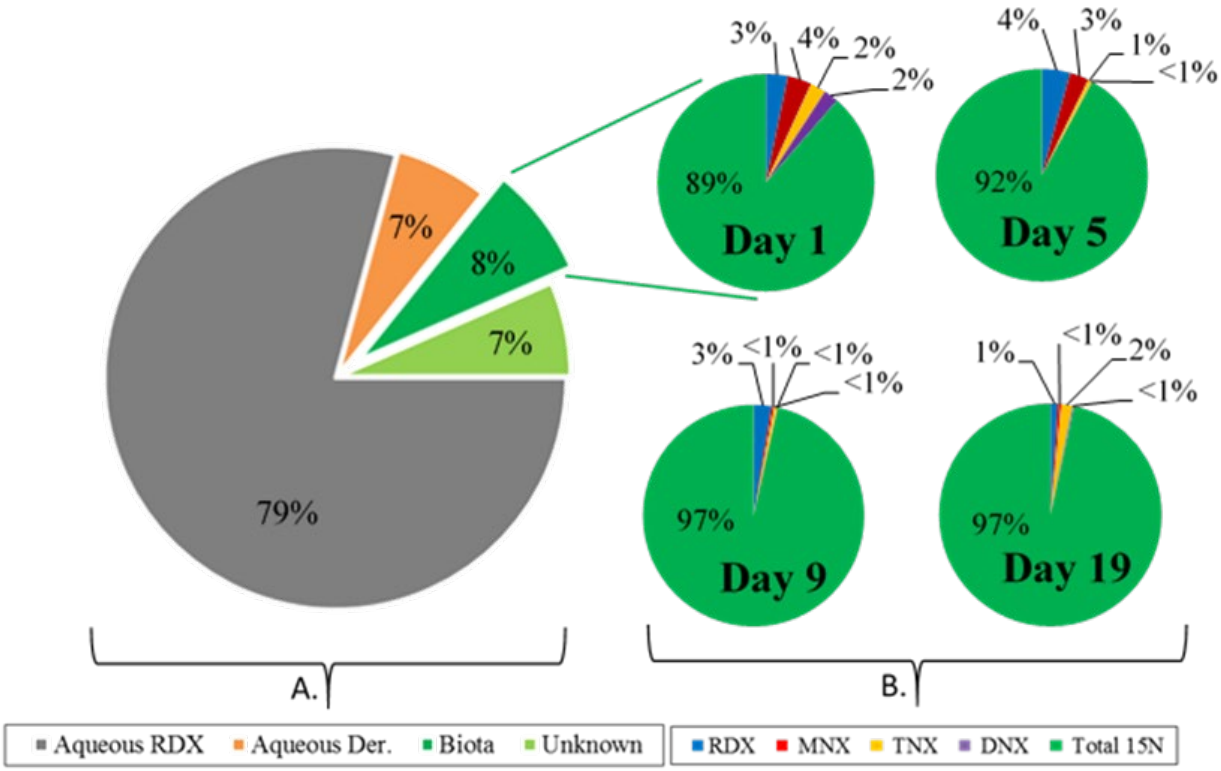

Figure 9.5. Partitioning of total ^{15}N: Total ^{15}N is represented in percentages. Pie chart A represents the total ^{15}N added to the experimental setup. The 'unknown' fraction is calculated by difference and could include sediment-bound munitions, mineralization products in sediments or aqueous phases, and other possible RDX derivatives not measured in this study. B shows how much of the ^{15}N found in biota can be accounted for as munitions species measured in tissues.

Table 9.1: Modeled rates and bioconcentration factors (BCFs): Uptake coefficients and rates for ^{15}N were modeled for each species individually using equations #'s 2-4. k_u = uptake clearance coefficient, k_{ep} = elimination rate constant, k_m = derivative uptake rate constant, k_{em} = metabolite elimination rate constant, k_{pN} = incorporation rate constant from parent compound, k_{mN} = nitrogen incorporation rate constant from metabolites, k_{eN} = nitrogen elimination rate constant, and k_{DN} = nitrogen uptake rate constant from DIN. BCF rates were calculated three ways. BCF_m was calculated using parent munitions concentrations, BCF_T was calculated using total ^{15}N measured in tissue, and BCF_R was calculated using modeled rates. BCF_{kow} values were previously reported in Lotufo et al. (2009) and represent the BCF values empirically derived from the Log K_{ow} of RDX. Root mean square error (RMSE) were calculated between the ^{15}N model data and the experimental values for each time point.

	F. vesiculosus	*U. lactuca*	*M. edulis*	*M. mercenaria*	*C. virginica*	*L. littorea*	*C. maenas*	*P. americanus*	*F. heteroclitus*
k_u (mL g^{-1} day^{-1})	2.3	36.4	38.2	6.9	21.7	25	2.5	12.3	11.9
k_{ep} (days $^{-1}$)	0.05	0.5	0.4	0.5	0.2	0.5	0.7	0.03	0.5
k_m (days $^{-1}$)	0	5	0.8	1	1.5	1.5	0.4	3.5	2.5
k_{em} (days $^{-1}$)	0	0.5	0.5	0.5	0.5	0.5	0.04	0.4	0.5
k_{pN} (days $^{-1}$)	1.6	4	3.5	7	6	7	3	3	3
k_{mN} (days^{-1})	0	3	2	2	2	2	0.8	3	2
k_{eN} (days $^{-1}$)	0.02	0.072	0.11	0.04	0.12	0.11	0.0047	0.022	0.04
k_{DN} (days $^{-1}$)	0.085	0.04	0	0	0	0.05	0	0	0
BCF_m (mL g^{-1})	0.57 (0.23)	5.90 (3.96)	4.36 (3.12)	1.44 (0.24)	1.21 (1.14)	3.37 (3.15)	0.35 (0.15)	1.67 (0.53)	N/A
BCF_T (mL g^{-1})	66.3 (12.7)	101.6 (51.6)	12.3 (7.42)	17.4 (7.50)	42.1 (10.2)	67.4 (24.8)	8.54 (3.16)	68.7 (74.7)	34.6 (23.0)
BCF_R (mL g^{-1})	32.9	33.9	37.8	6.6	26.5	22.5	3.3	27.2	11.4
BCF_{kow} (mL g^{-1})	2.3	2.3	2.3	2.3	2.3	2.3	2.3	2.3	2.3
RMSE (µg ^{15}N g dw^{-1})	1.3×10^{-2}	1.5×10^{-6}	1.6×10^{-6}	1.9×10^{-5}	2.0×10^{-3}	7.0×10^{-2}	6.0×10^{-3}	8.0×10^{-4}	2.0×10^{-3}

10.0. Biotic Uptake and Retention of hexahydro-1,3,5-trinitro-1,3,5-triazine (RDX) Derived Nitrogen Measured in Three Simulated Coastal Habitats

This chapter was published, as follows:

Ballentine, M., Ariyarathna, T., Smith, R. W., Cooper, C., Vlahos, P., Fallis, S., Groshens, T., Tobias, C. (2016). Biotic uptake and retention of hexahydro-1,3,5-trinitro-1,3,5-triazine (RDX) derived nitrogen measured in three simulated coastal habitats. Environmental Toxicology and Chemistry, In Review.

Abstract

Hexahydro-1,3,5-trinitro-1,3,5-triazine (RDX) is one of the most commonly used munitions of the past century and remains an environmental contaminant of concern though little is known about its fate in coastal systems. ^{15}N nitro-labeled RDX was added to three marine mesocosm types, each simulating a different coastal environment. Uptake, retention, and transformation of the RDX and nitrogen derived from RDX was quantified in 13 different species. The amount of ^{15}N tracer in the organisms attributable to RDX and its primary derivatives MNX, DNX, and TNX was small (< 0.1 μg ^{15}N g dw^{-1}). It varied significantly between species in the same habitat, and was similar among the same species across different habitats. The tissue ^{15}N tracer concentrations associated with intact RDX were 1-2 orders of magnitude lower for all 13 species than the total ^{15}N measured in the biotic tissue indicating that the majority of the RDX uptake was biotransformed internally. There was limited correlation between aqueous RDX concentrations and RDX tissue concentrations suggesting that post uptake transformations are as important as aqueous RDX concentrations in setting tissue RDX levels. Extrapolating mesocosm results to ecosystem scales revealed that RDX retention in biota and macrobiotic processing scaled linearly with expected species biomass with "hot spots" of high retention and/or transformation in marsh macrophyte roots, and select filter feeding and oligochaete species.

10.1 Introduction

The explosive hexahydro-1,3,5-trinitro-1,3,5-triazine (RDX) is one of the most commonly used munitions of the past century (Darrach et al., 1998) and has caused the contamination of aquatic, terrestrial (Pennington & Brannon, 2002), and marine environments (Darrach et al., 1998). RDX can enter the marine environment through unexploded ordnance (UXOs), munitions disposed of at sea, nearshore storage, and ongoing training exercises (Harrison & Vane, 2010; Hovatter et al., 1997; Jenkins et al., 2006; Talmage et al., 1999). Most studies of RDX have mainly focused on biodegradation pathways (aerobic and anaerobic;

Pennington & Brannon, 2002) and toxicological effects on aquatic (Bentley et al., 1977; Mukhi et al., 2005; Mukhi & Patiño, 2008; Steevens et al., 2002) and terrestrial (Simini et al., 2003) biota. Potentially high costs to remediate RDX contamination *in situ* serves as good motivation to research the fate of this and other of munitions in the marine settings (USA GAO, 2003).

Most studies of biological effects of RDX have been done in short duration benchtop experiments using single species (Lotufo et al., 2010; Rosen & Lotufo, 2007). These studies resulted in very low uptake, retention, and toxicity of the parent compound, however these studies were of relatively short duration and isolated the species from their natural environments. This limitation can be overcome by using larger marine mesocosms that more closely simulate the complexities of marine systems. In this study, the uptake and retention of RDX is subject to competing uptake and mineralization pathways (Crocker et al., 2006), trophic interaction (Lotufo et al., 2009), and intra-organism turnover (Ballentine et al., 2016); all of which affect RDX water column concentrations, physical and chemical partitioning, and uptake. Closely mimicking the natural environments over an extended period of time permits a more realistic picture of RDX and breakdown product distribution among ecosystem compartments. The mesocosms types used in this study represent three common shallow marine ecotypes: bare sand, silty vegetated sediment (eel grass), and an intertidal salt marsh. Each consists of different sediment types, levels of organic matter, and redox environments allowing for the possibility of different environmental interactions with RDX that could affect the uptake and retention of RDX within the biota.

The current literature suggests that aqueous concentration (Ballentine et al., 2015), partition coefficients (Belden et al., 2005), and lifestyles (e.g. benthic, pelagic, filter feeder) of the biota all play a role in biotic uptake, processing, and storage of munitions. For RDX, aqueous concentration is a good predictor of tissue concentrations, with ranges of bioconcentration factors (BCFs) for RDX indicating uptake is primarily through rapid physical partitioning (Ballentine et al., 2016; Lotufo et al., 2009), rather than bioaccumulation. Trophic level and/or organism lifestyle may account for interspecies differences. Large differences in uptake and bioconcentration have been found between autotrophs and heterotrophs derived from significant differential breakdown and storage of RDX (and its breakdown products) in autotrophs, particularly vascular macrophytes (Vila et al., 2007). Different marine settings are likely to impact aqueous concentrations, which are the net result of load and RDX mineralization, the species composition/interactions, and in turn set availability of RDX for further uptake.

The use of RDX labelled with the stable nitrogen isotope (^{15}N) allows for the tracking of nitrogen derived from RDX and thus its uptake and processing. Stable isotopes have been used previously for toxicological (Rosen & Lotufo, 2005), bioconcentration (Houston & Lotufo, 2005), and biodegradation studies (Annamaria et al., 2010; Smith et al., 2015; Van Aken et al., 2004). The objective of this study was to compare the biotic uptake and retention of RDX derived nitrogen using ^{15}N nitro-labeled RDX in 13 different marine species of varying trophic levels and lifestyles. Patterns of biotic processing were compared across three common marine ecosystems in simulated mesocosms.

10.2. Materials and Methods

10.2.1 Experimental Design

Three experiments using 1000L mesocosms were conducted. Each experiment simulated one of three coastal ecosystems; sand, vegetated silt, and intertidal salt marsh. All experiments were conducted as steady state constant source RDX additions. These habitat types were selected to span the range of organic matter (OM) and redox conditions; two factors known to influence RDX processing. Two different designs were used in the construction of the mesocosms (Figure 10.1). A single tank design was used for the sand and silt experiments. A two tank design was used for marsh experiment. For the sand and silt experiments, sediment (20 cm deep) was added first from coastal Long Island Sound (LIS). For the marsh experiment, *S. alterniflora* and associated sediment were added as intact sods. Water from LIS was then pumped through all mesocosms for an equilibrium period of 7 days. Following the equilibration period, macrobiota common to each habitat type (Table 10.1) were added and the system was switched to recirculation mode for a 24 hour acclimation period after which the addition of the ^{15}N RDX tracer commenced.

10.2.2 Mesocosm Setup 1 – Sand and Silt Experiments

For the single tank design (Figure 10.1A) that was used for two of the three mesocosms (sand and silt), raw seawater from LIS was pumped (Figure 10.1A) through a coarse mesh filter to remove large particulates. Seawater was added to the experimental tank from this reservoir (Figure 10.1A) using a peristaltic pump at an average rate of 180 mL min^{-1}. The turnover time of the seawater was 2.5 days in the experiment which was kept well mixed and aerated using 3 submersible pumps. ^{15}N nitro labeled-RDX (^{15}N-RDX) was added to the experimental tank in a single 20.4 mL addition of methanol for an initial target tank RDX concentration of 1.0 mg L^{-1}, and then metered in throughout the time series experiment with the use of a peristaltic pump at a rate of 0.07 mL min^{-1} and 0.08 mL min^{-1} for sand and silt respectively. This analyte pump rate was set to maintain a steady state concentration between 0.5 and 1.0 mg L^{-1} based on seawater turnover time and previously measured rates of RDX removal (Smith et al., 2013).

10.2.3 Mesocosm Setup 2 – Marsh Experiment

For the dual tank design (Figure 10.1B) used in the intertidal marsh mesocosm (marsh) raw LIS seawater was pumped through the coarse filter into a tidal mixing tank (Figure 10.1B) at a rate of 312 mL min^{-1} to produce a seawater turnover rate of 2.5 days. Tidal oscillations in water level was achieved using a combination of float switches and timers to move water between the tidal mixing and experimental tanks inducing marsh wetting and drying periods. Water between the tidal mixing and experimental tanks was constantly exchanged to insure a homogenous water mass using 2 submersible pumps at a rate of 1,900 mL min^{-1}. ^{15}N-RDX was initially added to the tidal mixing tank in a single addition of 39 mL of methanol to bring the concentration of the entire system to 1.0 mg L^{-1}. After the initial single addition, the ^{15}N-RDX was metered into the tidal mixing tank using a peristaltic pump at a rate of 0.07 mL min^{-1} to reach an estimated ^{15}N-RDX aqueous concentration of between 0.5 and 1.0 mg L^{-1}. Time series samples were collected over 15 days for aqueous RDX, RDX biota concentrations, and total ^{15}N tracer.

During the experiments, biota were allowed free range of the mesocosm and could interact with the exception of *Carcinus maenas* and *Alitta virens*. Both *C. maenas* and *A. virens* were in cages with removable lids for sampling. Additionally, the *A. virens* cage did not have a bottom allowing for *A. virens* interaction with the sediments. Each mesocosm was placed in a water bath and the experimental seawater temperature was kept between 19 and 21°C. A canopy was placed over the top of the experimental tanks to limit the exposure of the experimental tank to sunlight.

10.2.4 Aqueous Sampling

Time series water column aqueous RDX samples (2 mL) were taken from the experimental tanks (Figure 10.1A,B) and the tidal mixing tank (Figure 10.1B). Water samples were measured for RDX, MNX, DNX, and TNX used a modified "salting out" technique adapted from Miyares and Jenkins (1990) and used by Ballentine et al. (2015). Briefly, the 2 mL of sample were added to 1.3 g of NaCl and shaken. American Chemical Society (ACS) – grade acetonitrile, 1.5 mL, was then added and shaken for 5 min. The separated acetonitrile was removed and the process was repeated two more times using 1 mL of ACS-grade acetonitrile. The final extract was then analyzed and run using a gas chromatograph (GC) equipped with an electron-capture detector (ECD) as detailed in Ballentine et al. (2015).

10.2.5 Biota Sampling

Time series biota samples (Table 10.1) were removed from the experimental tank from both mesocosm setups then immediately rinsed for 5 min with clean filtered seawater to remove dissolved and weakly sorbed munitions from the tissue surfaces. The shells of *L. littorea, C. virginica*, *M. edulis*, *G. demissa*, and *M. mercenaria* were opened before being rinsed. *Z. marina* and *S. alterniflora* samples were separated into shoot and rhizome (*Z. marina*) or roots (S. alterniflora) after the rinse and were handled as separate samples. *S. alterniflora* and *G. demissa* were taken at both low and high tide. Once rinsed, tissues were removed, freeze-dried, and weighed. Freeze-dried samples were homogenized using a mortar and pestle and then separated into a fraction for measuring munitions concentrations in the tissue and a fraction for bulk ^{15}N isotope. Samples analyzed for munitions concentrations were extracted using methods modified from Conder et al. (2004). ACS-grade acetonitrile, 10 mL, was added to the samples and then sonicated for 1 hour. The homogenate was then centrifuged for 10 min at 10,000 rpm. The supernatant was removed, filtered through 0.22-µm PTFE syringe-tip filter, and 0.01 mg L^{-1} of 3,4-dinitrobenzene (3,4-DNB) as a recovery standard. GC/ECD analysis was conducted with the same method as the water samples (Ballentine et al., 2015). Quantification was based on an external calibration curve of standard munitions RDX, MNX, DNX, and TNX (AccuStandard, New Haven, Connecticut, USA). The recoveries of munitions from tissue samples (n=3) ranged between 70 and 98% with a mean of 90% and standard deviation of 7% with a reporting limit for all compounds of 0.7 ng mL^{-1}. To account for various sizes of organisms extractable munitions concentrations were normalized to organism dry weight (g dw). In addition to munitions concentrations, biota were analyzed for total ^{15}N tracer.

10.2.6 ^{15}N Analysis

Total ^{15}N in all solid samples were analyzed by elemental analyzer – isotope ratio mass spectrometry (EA/IRMS: Delta V, Thermofisher). Samples were freeze-dried and weighed into

tin capsules. Sufficient sample mass was used to achieve 40-80 µg N for isotope analysis. Isotope values were normalized with a 2-endpoint correction using United States Geological Survey reference materials L-glutamic acid (USGS40 and USGS41) accompanying each analytical batch and also served as check standards for drift correction. Analytical precision on ^{15}N measurements was 0.3 per mil which is equivalent to approximately 1/9,000th of one percent excess ^{15}N. The µg ^{15}N g dw^{-1} was calculated by combining the ^{15}N mole fraction excess that was given from the EA/IRMS with the N content for each sample.

3. Results

10.3.1 Aqueous Munitions

The measured inputs and outflow of RDX in each experiment was used to calculate a predicted RDX aqueous concentration assuming no reactive losses. In all three experiments aqueous RDX (RDX_{aq}) concentrations decreased from starting concentrations and remained below concentrations predicted by conservative mixing (Figure 10.2). The silt and marsh experiments reached RDX_{aq} steady state concentrations of 0.50 ± 0.07 mg L^{-1} on day 3 (Figure 10.2B) and 0.22 ± 0.04 mg L^{-1} on day 2 (Figure 10.2C) respectively. The sand experiment did not reach an aqueous RDX steady state concentration (Figure 10.2A) due to pumping irregularities. MNX and TNX were detected in all three experiments at concentrations 2 to 3 orders of magnitude lower than that of RDX_{aq} concentrations. DNX was detected sporadically and only within the first 9 days of the experiment at 3 orders of magnitude lower than RDX_{aq} concentrations. The difference between the predicted and measured aqueous concentrations indicated an RDX loss of 25%, 44%, and 50% in the sand, silt, and marsh experiment respectively. The total ^{15}N recovered in the biota accounted for a small percentage of the mass of RDX ^{15}N lost from the aqueous phase and was equivalent to 1.4, 0.5, and 0.01 percent in the sand, silt, and marsh mesocosms respectively.

10.3.2 Tissue Concentrations – Munitions and ^{15}N

For comparison to bulk ^{15}N tracer measured in biota, munitions concentrations measured in tissue were converted into ^{15}N units (µg ^{15}N g dw^{-1}) using the molar ratio of labeled ^{15}N to the whole RDX molecule (3:1). This conversion yielded the amount of ^{15}N tracer in tissues that could be attributed to intact RDX ($^{15}N_R$). A similar conversion was made for MNX + TNX + DNX to yield a measure of the amount of ^{15}N in tissues that could be attributed to these intact species ($^{15}N_D$). Total ^{15}N concentrations measured in the biota tissue by EA-IRMS will be heretofore be referred to as $^{15}N_T$. The time weighted mean for $^{15}N_R$ and $^{15}N_T$ was calculated and used for comparisons between species and experiments. Comparisons were done using a statistical t test assuming unequal variances and assessed at the $p \leq 0.05$ level. Finally, the fraction of $^{15}N_T$ attributed to $^{15}N_R$ ($f^{15}N$) in the biotic tissue was calculated for each species.

10.3.3 Autotrophs

The $^{15}N_R$ in the tissues were similar for each of the autotrophic species (*F. vesiculosus*, *U. lactuca*, *Z. marina*, and *S. alterniflora*) across the different mesocosms as the $^{15}N_R$ increased quickly and remained relatively constant throughout the experiment. With the exception of *S.*

alterniflora root samples with mean $^{15}N_R$ of 0.53 ± 0.15 µg $^{15}N_R$ g dw^{-1}, all other autotrophic $^{15}N_R$ ranged from 0.03 to 0.13 µg $^{15}N_R$ g dw^{-1}. *S. alterniflora* root and shoot $^{15}N_R$ showed no difference between high and low tide. The root $^{15}N_R$ were as much as one order of magnitude greater and significantly different ($p < 0.01$) than the shoot $^{15}N_R$ (Figure 10.3). All other comparison between autotrophs in the same mesocosm or across different mesocosms experiments did not show significant difference for $^{15}N_R$. $^{15}N_D$ was not detected for any autotrophic species. While autotrophic $^{15}N_R$ was low and fairly consistent across species and mesocosms, $^{15}N_T$ was not.

Mean autotrophic $^{15}N_T$ was dissimilar between species and some habitats. *F. vesiculosus* was the only autotrophic species that was in more than one mesocosm experiment and the $^{15}N_T$ was 2 orders of magnitude greater in the sand than the silt and was significantly different ($p < 0.001$) between the two mesocosms (Figure 10.3). The autotrophs (*F. vesiculosus* and *U. lactuca*) in the sand mesocosm had greater mean $^{15}N_T$ than all other autotrophs in the silt and marsh mesocosm experiments by a factor of 10 (Figure 10.3). The $^{15}N_T$ in *F. vesiculosus* was large and significantly different than *U. lactuca* (sand) and *Z. marina* shoot (silt; $p <$ of 0.01). All other mean $^{15}N_T$ values among autotroph species were not significantly different. *U. lactuca* had the largest mean $^{15}N_T$ of all species across all experiments. This ^{15}N, ultimately derived from RDX, was equivalent to 0.1% of total N in *U. lactuca* tissue.

The fraction of total ^{15}N attributable to RDX ($f^{15}N$) was smallest for the autotrophs in the sand experiment with values less than 2% (Figure 10.3). *F. vesiculosus* $f^{15}N$ increased to 23% in the silt experiment 4 times higher than *Z. marina* $f^{15}N$ fractions. The highest $f^{15}N$ of all autotrophs was *S. alterniflora* root samples at 44%, indicating large amounts of uptake with little internal RDX processing relative to its storage (Figure 10.3).

10.3.4 Epifauna

The mean $^{15}N_R$ for the epifauna species varied from 0.06 to 0.24 µg $^{15}N_R$ g dw^{-1} with one notable exception, *C. virginica* had a mean $^{15}N_R$ of 0.80 µg $^{15}N_R$ g dw^{-1} in the silt experiment. *M. edulis*, *L. littorea*, and *C. maenas* were used in all three mesocosm experiments. Both *M. edulis* and *L. littorea* have similar mean $^{15}N_R$ across the mesocosms types of 0.11 ± 0.03 and 0.18 ± 0.02 µg $^{15}N_R$ g dw^{-1} respectively (Figure 10.4). *C. maenas* $^{15}N_R$ declined from sand to silt to marsh with mean $^{15}N_R$ values of 0.25 ± 0.05, 0.14 ± 0.05, and 0.04 ± 0.01 µg $^{15}N_R$ g dw^{-1} respectively. Interesting, only *M. edulis* and *L. littorea* had a significant difference when comparing between their mean $^{15}N_R$ in the silt mesocosm ($p < 0.001$) and *C. maenas* and *G. demissa* ($p < 0.05$) had a similar significant difference in the marsh mesocosm. While many of the epifaunal species showed similar $^{15}N_R$, the $^{15}N_T$ was more variable.

The $^{15}N_T$ differed among the species and within the same species between mesocosm experiments by over 1 order of magnitude (Figure 10.4). *M. edulis* mean $^{15}N_T$ was significantly higher ($p < 0.05$) in the silt mesocosm (18 ± 4.6 µg $^{15}N_T$ g dw^{-1}) than in the sand (3.5 ± 0.9 µg $^{15}N_T$ g dw^{-1}) and marsh (3.3 ± 0.5 µg $^{15}N_T$ g dw^{-1}; Fig. 4). Although the *L. littorea* mean $^{15}N_T$ was higher in the sand mesocosm (5.4 ± 1.3 µg $^{15}N_T$ g dw^{-1}) than the silt and marsh mesocosms there was no significant difference in the $^{15}N_T$ mean values (Figure 10.4). *C. maenas* $^{15}N_T$ varied significantly ($p < 0.01$) between mesocosms with concentrations ranging from 0.3 ± 0.2 µg $^{15}N_T$ g dw^{-1} in the marsh to 1.5 ± 0.3 µg $^{15}N_T$ g dw^{-1} in the silt mesocosm. *C. maenas* (sand and marsh) mean $^{15}N_T$ was higher than other epifaunal species ($p < 0.05$). Within the silt mesocosm,

M. edulis mean $^{15}N_T$ was higher than both *L. littorea* ($p < 0.01$) and *C. maenas* ($p < 0.01$). The epifaunal $f^{15}N$ values were similar in magnitude to autotrophs and ranged from 3% to 12% with only a few exceptions (Figure 10.4). *C. maenas* (sand) had the highest $f^{15}N$ of 31% and *M. edulis* (silt) had the lowest $f^{15}N$ of 0.3%.

10.3.5 Infauna

Both infaunal species (*M. mercenaria* and *A. virens*) were used in more than one mesocosm type (sand and silt mesocosm) and $^{15}N_R$ varied between 0.02 and 0.63 μg $^{15}N_R$ g dw^{-1}. *M. mercenaria* and *A. virens* mean $^{15}N_R$ between the sand and silt mesocosm were similar (Figure 10.5) and were not significantly different. When the mean $^{15}N_R$ values for both infaunal species were compared within the same mesocosm, the silt experiment infaunal species $^{15}N_R$ values varied significantly ($p < 0.01$) even though *A. virens* had a high concentration in both the sand (0.23 ± 0.17 μg $^{15}N_R$ g dw^{-1}) and the silt (0.63 ± 0.50 μg $^{15}N_R$ g dw^{-1}) mesocosms (Figure 10.5). Mean infaunal $^{15}N_T$ values for *M. mercenaria* and *A. virens* were 10 – 20 fold significantly higher for the mean $^{15}N_R$ in both the sand and silt mesocosms. The $^{15}N_T$ ranged from 1.4 to 6.0 μg $^{15}N_T$ g dw^{-1} and *A. virens* exceeded *M. mercenaria* ($p < 0.001$) by a factor of 3 in the sand, while *M. mercenaria* $^{15}N_T$ exceeded *A. virens* ($p < 0.001$) by a factor of 3.5 in the silt experiment. The infaunal $f^{15}N$ values were all below 4% with the exception of *A. virens* (silt) that had among the highest $f^{15}N$ measured suggestive of high RDX uptake coupled with little post-uptake processing and retention of N-bearing transformation products. This value was similar to the autotroph *S. alterniflora* root (marsh) at 44% (Figure 10.5).

10.3.6 Fish

Fish species $^{15}N_R$, $^{15}N_T$, and $f^{15}N$ were each roughly 2 times higher than both the epifauna and infaunal species in the sand and marsh mesocosms, while in the silt mesocosm the fish species had $^{15}N_R$ and $^{15}N_T$ values roughly 2 times less than the epifaunal and infaunal species. *F. heteroclitus* (pelagic) was used in all three experiments, while *P. americanus* (benthic) was used only in the sand and silt experiments. *F. heteroclitus* mean $^{15}N_R$ showed no significant difference between experiments with for the sand, silt, and marsh of ranging between 0.23 – 0.41 μg $^{15}N_R$ g dw^{-1} respectively (Figure 10.5). Similarly, there was no significant difference in the $^{15}N_R$ of *P. americanus* between the sand and silt experiments. Between species, only the silt mesocosm had a significant difference between *F. heteroclitus* and *P. americanus* $^{15}N_R$ ($p < 0.01$) even though *F. heteroclitus* $^{15}N_R$ exceeded that of *P. americanus* in both mesocosm types (Figure 10.5). There was no significant difference between the silt and sand mean $^{15}N_T$ concentrations for *F. heteroclitus* but the *P. americanus* mean $^{15}N_T$ was higher in the sand (6.0 ± 0.24 μg $^{15}N_T$ g dw^{-1}) relative to the silt (0.38 ± 0.15 μg $^{15}N_T$ g dw^{-1} ; $p < 0.001$; Fig. 5). No differences in $^{15}N_T$ between the two species was measured regardless of mesocosm type. The $f^{15}N$ in fishes were less than 6% in the sand and marsh mesocosms. But both species showed higher $f^{15}N$ values (17 – 20%) in the silt experiment (Figure 10.5).

10.3.7 Tissue Concentration Correlation to Aqueous RDX

The time series changes in aqueous RDX concentration in the mesocosms coupled with past evidence that tissue RDX rapidly responds to aqueous RDX concentration (Ballentine et al., 2016; Lotufo et al., 2009) permitted examination of the relationship between $^{15}N_R$, $^{15}N_T$, and the aqueous RDX concentration over the course of the experiments. Stepwise linear regressions

between $^{15}N_R$ and RDX_{aq} and $^{15}N_T$ and RDX_{aq} were performed by species and by mesocosm type. For $^{15}N_R$ across all mesocosms the RDX_{aq} concentration explained more than 50% of the variance in $^{15}N_R$ for only 5 species correlations out of 26. All of those occurred in the sand mesocosm where RDX loss (presumably from mineralization) was smallest. Only two species (*P. americanus* and *F. vesiculosus*) had coefficients of determinations (r^2) above 0.65, while the majority of the species had r^2 of 0.40 and below (Table 10.2). When the mean of all coefficients of determination for each mesocosm were calculated, the $^{15}N_R$ variance attributable to RDX_{aq} (average r^2 of all species regressions) showed a decreasing trend from sand > silt > marsh.

For $^{15}N_T$ there were only 4 correlations where the RDX_{aq} explained more than 50% of the variance in $^{15}N_T$ over time (Table 10.2). These occurred in the sand and silt mesocosms with none in the marsh mesocosm. The low species-specific r^2 were most often below 0.3 (Table 4.2). Unlike the cross mesocosm regressions for $^{15}N_R$, the average $^{15}N_T$ r^2 did not show any significant patterns between mesocosms (Table 10.2).

10.4. Discussion

Results from the ^{15}N RDX multi mesocosm experiments support three major findings: (1) the habitat type controlled RDX_{aq}, but RDX_{aq} only partially explained variance found in biota concentrations particularly in more OM rich environments; (2) $^{15}N_R$ concentrations in biota was always less than $^{15}N_T$ concentrations indicating much more internal processing of RDX post-uptake rather than retention of intact RDX; (3) the balance between retention of intact RDX and processing/throughput of RDX by macrobiota at the ecosystem scale is generally a function of ecosystem productivity (biomass), but some species represent hotspots of RDX uptake/processing that is disproportionately large relative to their species-specific population biomass.

10.4.1 Mesocosm Control of Available RDX

Yields of RDX loss (predicted RDX_{aq} – measured RDX_{aq}; Figure 10.2) in the three mesocosms was consistent with recent studies that found that aqueous RDX removal from seawater is in large part a function of sediment type (Ariyarathna et al., 2017; Smith et al., 2013). The differential loss of RDX and associated ^{15}N tracer relative to conservative mixing was the lowest in the sand mesocosm and highest in the marsh. Expressed as a percent of RDX loading 25%, 44%, and 50% was lost in sand, silt, and marsh respectively (Figure 10.2).

This pattern of loss occurred likely as the result of higher RDX mineralization in the presence of higher concentration of sedimentary OM in the silt and marsh mesocosms (Sheremata et al., 2001). Further the presence of sharp redox gradients typical of vegetated sediments subtidal *Z. marina* and intertidal *S. alterniflora*, provides a suitable environment for aerobic and anaerobic mineralization pathways for RDX in close proximity. Unlike many past studies of RDX processing (Belden et al., 2005; Rosen & Lotufo, 2005), these mesocosm studies included varied biota as a potential sink for the ^{15}N-RDX. But the $^{15}N_T$ macrobiota values, when scaled to the total biomass in each of the mesocosms were not the cause of the differential RDX losses in the mesocosms. Macrobiota accounted for only small percentages of the observed total RDX ^{15}N loss from the aqueous phase (Sand 1.4%, Silt 0.5%, and Intertidal marsh 0.01%).

Variations in $^{15}N_R$ and $^{15}N_T$ among the three mesocosms was likely a function of RDX mineralization rates, which regulated the amount of RDX_{aq} available for biota to uptake. Yet RDX_{aq} was not the sole determinant of either $^{15}N_R$ or $^{15}N_T$. The use of habitat appropriate fauna in each mesocosm type prevents a full crosswise comparison, but for the species common to all mesocosms and some pairwise comparisons indicate that correlations for the fish, non-filter feeding epifauna, and infauna vary widely across mesocosm type suggesting a significant environmental effect on both $^{15}N_R$ and $^{15}N_T$ aside from just RDX_{aq}. If $^{15}N_R$ was controlled solely by rapid partitioning of RDX_{aq} to tissues, and $^{15}N_T$ was controlled solely by $^{15}N_R$, then both $^{15}N_R$ and $^{15}N_T$ should, as BCF would predict, be highly correlated to RDX_{aq}. It was not. Based on controlled BCFs experiments (Ballentine et al., 2015), we would expect RDX_{aq} to be a better predictor of the variance in $^{15}N_R$ in the sand vs silt vs marsh, and we observed this in the mesocosms as evidenced by the distribution of the average coefficients of determination for linear regressions of $^{15}N_R$ vs. RDX_{aq} across mesocosm type (Table 10.2). Competing reactions for RDX within each system (e.g. mineralization) would be expected to increase from sand to silt to marsh, and this expectation is evidenced by the higher RDX_{aq} losses measured along this gradient. The mineralization of significant quantities of RDX could account for why RDX_{aq} is not a good predictor of $^{15}N_R$ or $^{15}N_T$ particularly in the high OM silt and marsh environments. Alternatively, higher amounts of intra-organism processing (Lotufo et al., 2009), lowering $^{15}N_R$, may be more efficient in the higher productivity silt and marsh mesocosms. If this is the mechanism behind the disconnect between RDX_{aq} and $^{15}N_R$ then such processing must be followed by elimination otherwise $^{15}N_T$ would be inversely related to $^{15}N_R$ across habitat types, which it is not. For $^{15}N_T$, there was no clear relationship to the RDX_{aq} within or across habitats. The role of intraorganism processing of RDX (affecting $^{15}N_R$) and the ultimate elimination of transformation products (affecting $^{15}N_T$) may be central to setting both $^{15}N_R$ and $^{15}N_T$. RDX biotransformation and breakdown pathways studies in microbiota have been shown to be complex and to vary (Crocker et al., 2006), yet RDX transformation pathways in eukaryotes and specifically in macrobiota are presently ill-defined. If this explanation is correct, the data in Table 10.2 suggest that these removal mechanisms are of equal to or similar importance as uptake constants (e.g. BCFs) *in situ*.

10.4.2 RDX Uptake, Processing, and Retention of Tracer in Biota

All $^{15}N_R$ values in heterotrophs, regardless of species type, lifestyle, trophic position, or experiment were small relative to $^{15}N_T$ (Figures 10.3, 10.4, and 10.5). These mesocosm-scale observations mimic similar findings from lab experiments that were summarized by Lotufo et al. (2009). Time averaged $^{15}N_R$ for nearly all heterotrophic species regardless of experiments was close to 0.1 μg $^{15}N_R$ g dw^{-1}. Low RDX tissue concentrations are consistent with other reports for this relatively polar compound (Belden et al., 2005; Lotufo et al., 2009). Average heterotroph $^{15}N_T$ was generally close to 5.0 μg $^{15}N_T$ g dw^{-1} and the resulting $f^{15}N$ for heterotrophs were also low (< 20%) for all but two species (*C. maenas* and *A. virens*). The high $^{15}N_T$ indicated that a substantial amount of the RDX, internally processed, was retained in some unknown form. A striking difference from this study and others using RDX (Sunahara et al., 2009) is the lack of $^{15}N_D$ measured in any species throughout the time series other than a few small concentrations at random time points. This result suggested that biotransformation pathways did not lead to MNX, TNX, and DNX accumulation in any significant concentrations that could have had toxicological impacts on the biota.

Because heterotrophs are unable to take up $DI^{15}N$ released from ^{15}N-RDX mineralization (Smith et al., 2015), a precondition for high $^{15}N_T$ is high rates of encounter with ^{15}N-RDX. The amount of RDX encountered could be inferred from RDX_{aq} but not entirely depending on the mechanism of exposure. RDX_{aq} was only a poor to marginal proxy for $^{15}N_T$ for most species (Table 10.2). The amount of exposure to RDX is likely as/more important than the RDX_{aq} concentration. *M. edulis* and *C. virginica* (among the highest $^{15}N_T$ for heterotrophs) both cycle through large amounts of seawater in the process of filter feeding allowing for a greater exposure of RDX_{aq} to tissues. Moreover, *M. edulis* had the larger mean $^{15}N_T$ in the silt experiment that was mostly due enhanced exposure to the resuspension of silt containing RDX, and/or enhanced filter feeding on elevated particulate organic matter (POM) in that experiment. Similarly higher $^{15}N_T$ in *L. littorea,* likely resulted from grazing of tank biofilms that were sites of RDX processing (Fournier et al., 2004; Thompson et al., 2005). Every species had a much larger mean $^{15}N_T$ than $^{15}N_R$ and a $f^{15}N$ typically < 20% indicating the RDX was being taken up and the biotransformed internally instead being retained unaltered. The total heterotrophic $^{15}N_T$ is small relative to the RDX loss in the mesocosm. The processing of the RDX is possibly still important for each individual organism, helping to set tissue RDX concentrations and the possibility that other biotransformation products containing tracer (inert or potentially toxic) may accumulate.

Autotrophs contrast with the heterotrophs in two important respects: some species are known to take up and store RDX intact (Thompson et al., 1999), and because they can assimilate DIN directly there is the potential for acquiring ^{15}N tracer that had originally been derived from RDX but was liberated as $DI^{15}N$ during mineralization. This ^{15}N uptake would increase $^{15}N_T$ values. An example of the direct uptake and storage of RDX by an autotroph was the large $f^{15}N$ (40%) by *S. alterniflora* root, yet the RDX was processed during translocation to the shoots as evident by a factor of 3 drop in the $f^{15}N$ in the *S. alterniflora* shoots. The high mean $f^{15}N$ for *S. alterniflora* root could also be due to a greater uptake of RDX as the sediments were recharged with a pulse of new RDX at each high tide. But unlike the high amount of RDX storage found in shoots/leaves of poplar trees (Thompson et al., 1999), RDX appears to be processed during translocation from roots to shoots in *S. alterniflora*. In contrast, *Z. marina* had little intact RDX storage, either as a result of low uptake or fast processing, in roots and shoots which both showed low $f^{15}N$ values.

Some autotrophs, particularly macroalgae, have the ability to uptake DIN from the water column in excess of what is needed to maintain their N:P cellular ratio (Sterner and Hessen, 1994; Stelzer and Lamberti, 2001). This 'luxury uptake' of DIN may have included ^{15}N-DIN originating from RDX_{aq} via mineralization (Smith et al., 2015). The autotrophs, including the smallest $f^{15}N$ reported in *U. lactuca*, had smaller $f^{15}N$ values than the heterotrophs (Figure 10.3). Interestingly, autotrophic $^{15}N_T$ concentrations decreased with mesocosm transition from sand to silt to tidal marsh as overall natural DIN availability increased, but $^{15}N_T$ results should be interpreted cautiously for macroalgae in settings where mineralization might be high and luxury uptake possible.

Generally, the autotrophic species compared closely to the heterotrophs in that the $^{15}N_R$ and $^{15}N_T$ values were relatively similar (Figures 10.3, 10.4, and 10.5). Similar to the heterotrophic species no matter the experiment, $^{15}N_R$ values in autotrophs were much less than $^{15}N_T$ indicating the all species processed more RDX relative to RDX retention in tissue.

10.4.3 Scaling to the Ecosystems Level

The mesocosms represent an intermediate step to scale from laboratory studies to intact ecosystems. Because $^{15}N_R$ was similar among species, the total amount of RDX within an ecosystem should be dependent on solely the amount of biomass (e.g. total RDX m^{-2} = $^{15}N_R$ x g biota m^{-2}), and the amount of RDX in any given species population will be a function of total population biomass. Similarities in $^{15}N_R$ between species despite disparate growth rates, lifestyles, and trophic position suggest that these factors are less important than total ecosystem biomass for determining a collective steady state inventory of RDX in all biota. The mesocosm results coupled with typical biomass estimates of each species in coastal habitats show that higher productivity species (in terms of biomass) correspond to higher $^{15}N_R$ and $^{15}N_T$ m^{-2} (Figure 10.6A,B) at the ecosystem level. The biomass effect on total RDX is generally linear across species and habitat type suggesting high productivity ecosystems (i.e. more biomass) will store more RDX in biota (Figure 10.6, Tables 10.3 and 10.4). Because the largest standing stocks are typically autotrophs, these populations would be expected to harbor the most RDX mass within an ecosystem (Figure 10.6, Table 10.3). While the mesocosm $^{15}N_T$ results show that the total RDX in biota is low relative to RDX load and RDX loss, it is important to examine how RDX and RDX transformations in biota would be distributed throughout the ecosystem. There are notable exceptions to the general linear effect of biomass on RDX storage and processing. *S. alterniflora* roots, the filter feeder *C. virginica*, and the infaunal polychaete *A. virens* all contain anomalously high ecosystem level RDX ($^{15}N_R$) retention relative to their typical population biomass. These hotspots for storage may reflect active uptake (*S. alterniflora*) and/or high aqueous or sediment throughput/exposure as a function of feeding (*C. virginica* and *A. virens*). The results for *S. alterniflora* are similar to those seen in phytoremediation studies (Best et al., 1997; Just & Schnoor, 2004) but the mesocosm results (low shoot $f^{15}N$) show the RDX in *S. alterniflora* is processed during translocation to shoots so the root storage of RDX is transient and a first step to further transformation. Typically macrobiota has been viewed as an ecological risk receptor. The high $^{15}N_T$ and low $f^{15}N$ values suggest they play an active role in transformation, but this transformation is not uniform among species. At the ecosystem level, a similar analysis of the biomass scaling for RDX transformation (derived from $^{15}N_T$), revealed the filter feeder *M. edulis* and the macroalgae *F. vesiculosus* and *U. lactuca* as ecosystem compartments that disproportionately take up RDX, transform it internally, and retain the N-bearing transformation products (Table 10.4). *F. vesiculosus* and *U. lactuca* may also be active hotspots for processing although this conclusion should be considered cautiously due to a potential for luxury uptake effects on $^{15}N_T$.

The extrapolation of the mesocosm experiment results provided three metrics to gauge the role of different ecosystem compartments with respect to RDX. High $^{15}N_R$, low $^{15}N_T$, and high $f^{15}N$ identify primarily reservoirs for unaltered RDX. These compartments include *S. alterniflora* root, *A. virens*, and C. maenas (Figures 10.3, 10.4, and 10.5; Table 10.3 and 10.4). Low $^{15}N_R$, high $^{15}N_T$, and low $f^{15}N$ consist of zones where internal transformations supersede storage and there is a disproportionate amount of macrobiotic processing of RDX. These compartments include *F. vesiculosus*, *U. lactuca*, and *S. alterniflora* shoots. These metrics may also apply to macroalgae that have utilized N liberated through mineralization of RDX. Finally, compartments with high $^{15}N_R$, high $^{15}N_T$, and low $f^{15}N$ would be the most active transformers in the ecosystem; representing high uptake and extensive processing. The translocation of RDX

from *S. alterniflora* roots to *S. alterniflora* shoots reflects this transition from high $^{15}N_R$, low $^{15}N_T$, high $f^{15}N$ to low $^{15}N_R$, high $^{15}N_T$, low $f^{15}N$ compartment.

10.5. Conclusions

The amount of tissue bound ^{15}N tracer attributed to RDX constituted a small amount of total RDX loss in all marine mesocosms. Tissue ^{15}N levels varied by an average factor of 8 between species in the same habitat, and were similar among the same species across different habitats. For all biota, the tissue ^{15}N tracer concentrations associated with intact RDX were at least 1 order of magnitude lower than the total ^{15}N measured in biotic tissue indicating that the majority of the RDX uptake was biotransformed internally. Aqueous RDX concentration was only a modest predictor of tissue RDX and total ^{15}N tracer derived from RDX. This observation coupled with the low fraction of total ^{15}N attributable to RDX suggests that post uptake biotransformation is equally important as gross uptake for setting tissue concentrations *in situ*. While the use of ^{15}N as a tracer for RDX showed a large amount of biotransformation in comparison to intact storage, the exact products formed are not known and warrants further study. Ecosystem level extrapolation of mesocosm results yielded a linear relationship between total biomass and RDX per area across species with hot spots for retention and/or transformation existing in marsh macrophytes roots, and select filter feeding and oligochaete species.

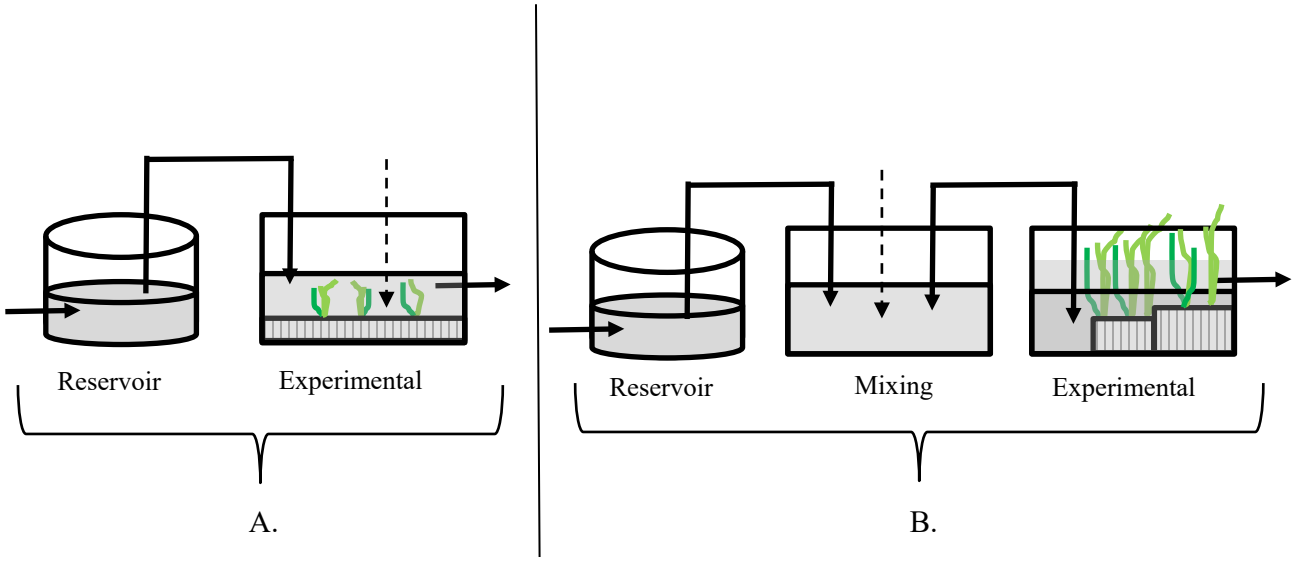

Figure 10.1. Experimental Tank Setups A. Single experimental tank setup (sand and silt). Shaded areas are seawater. Arrows indicate direction of seawater flow. B. Two experimental tank setup (marsh). Double headed arrows indicate flow of seawater in both directions. The dotted line for the seawater indicates the high tide water level while the solid line indicates low tide level. The single arrowed dotted line indicates were ^{15}N-RDX was added. Lined rectangles indicate the location of sediments.

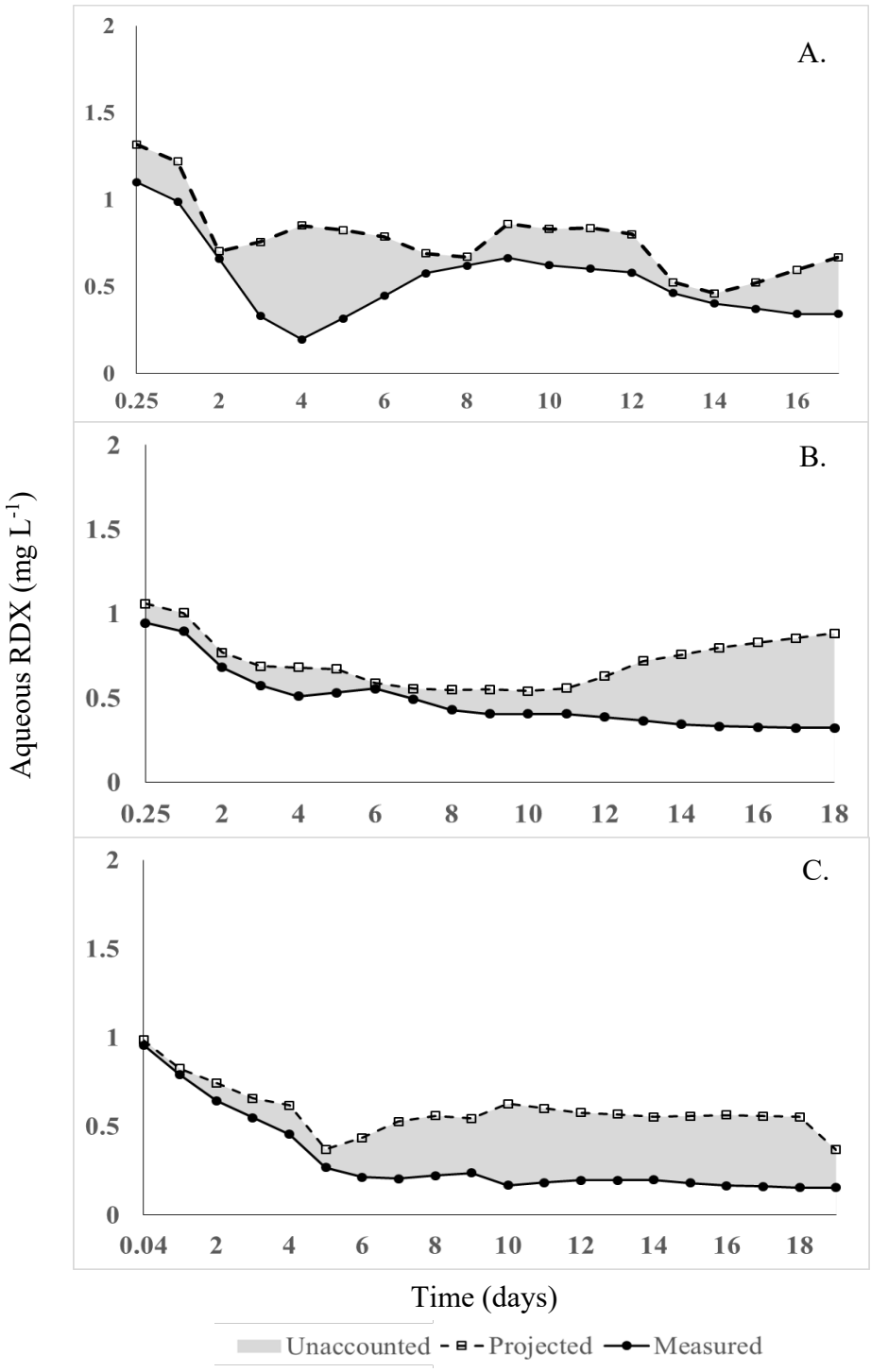

Figure 10.2. Aqueous RDX Concentrations. Solid lines are the measured aqueous RDX (RDX_{aq}) concentrations. The dashed line is the predicted aqueous RDX concentrations based on conservative mixing of RDX tracer with water volumes/inputs. Shaded area is the lost (missing) RDX. A. Sand mesocosm B. Silt mesocosm C. Tidal marsh mesocosm.

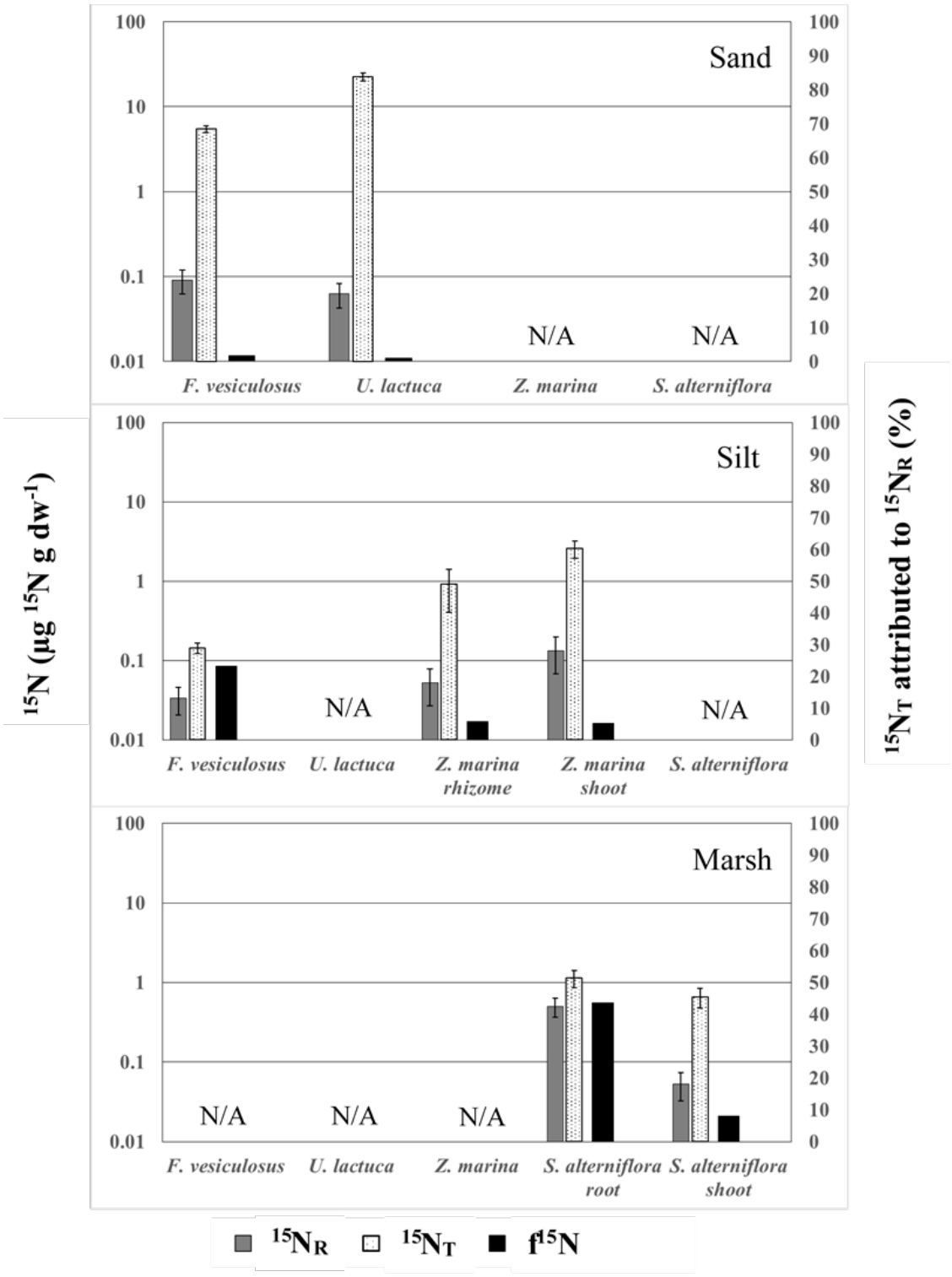

Figure 10.3. Autotrophic ^{15}N concentrations. Temporal mean (se) ^{15}N tracer autotrophic tissue concentrations for each mesocosm (Sand, Silt, and Marsh). $^{15}N_R$ and $^{15}N_T$ tissue are represented by the gray and hatched bars. The solid black bar ($f^{15}N$) represents the percent of $^{15}N_T$ that can be attributed to $^{15}N_R$. N/A denotes organisms that were not used.

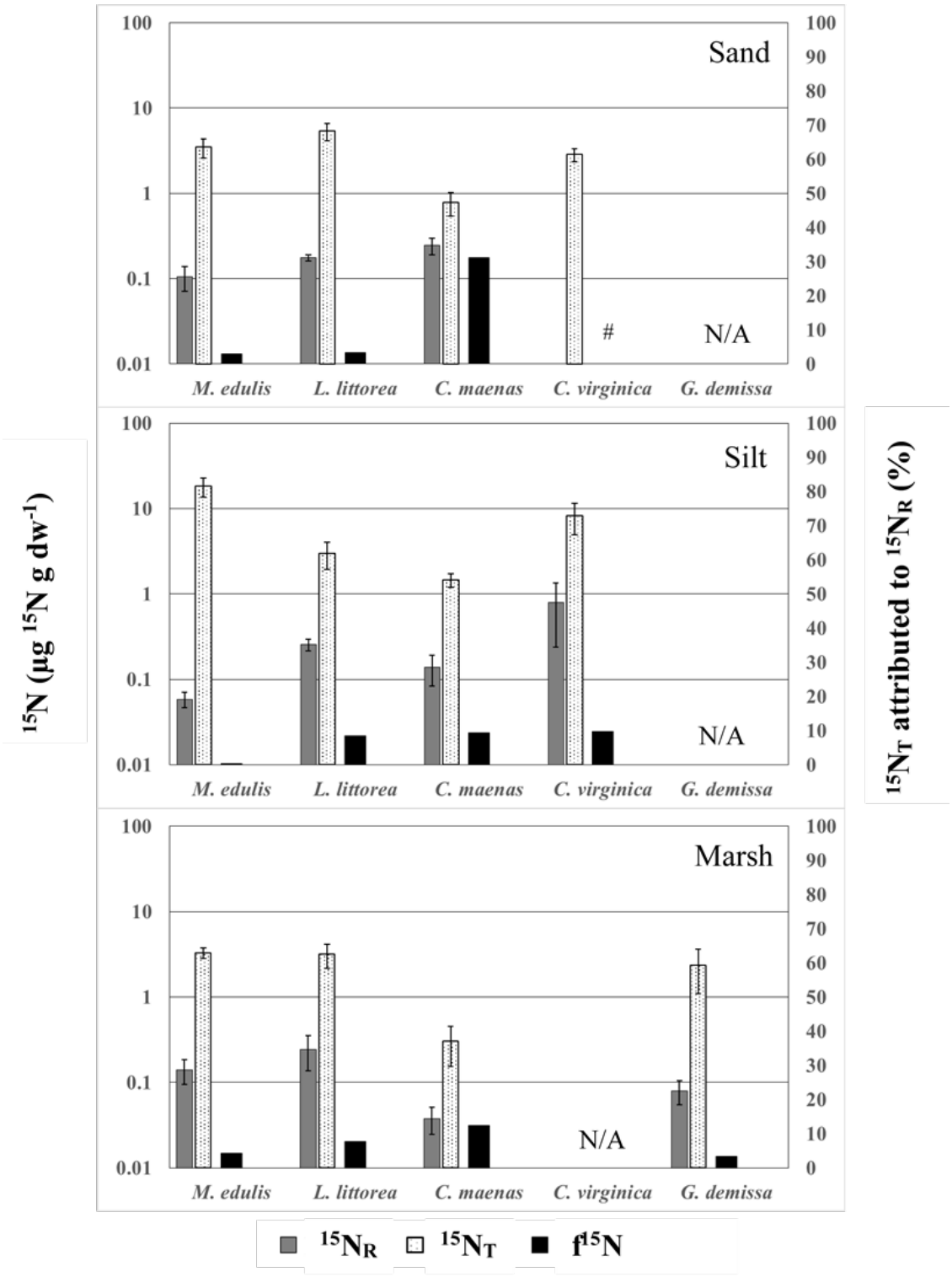

Figure 10.4. Epifaunal ^{15}N concentrations. Temporal mean (se) ^{15}N tracer epifaunal tissue concentrations for each mesocosm (Sand, Silt, and Marsh). $^{15}N_R$ and $^{15}N_T$ tissue are represented by the gray and hatched bars. The solid black bar ($f^{15}N$) represents the percent of $^{15}N_T$ that can be attributed to $^{15}N_R$. *C. virginica* is missing $^{15}N_R$ data (#) due to high background in GC/ECD. N/A denotes organisms that were not used.

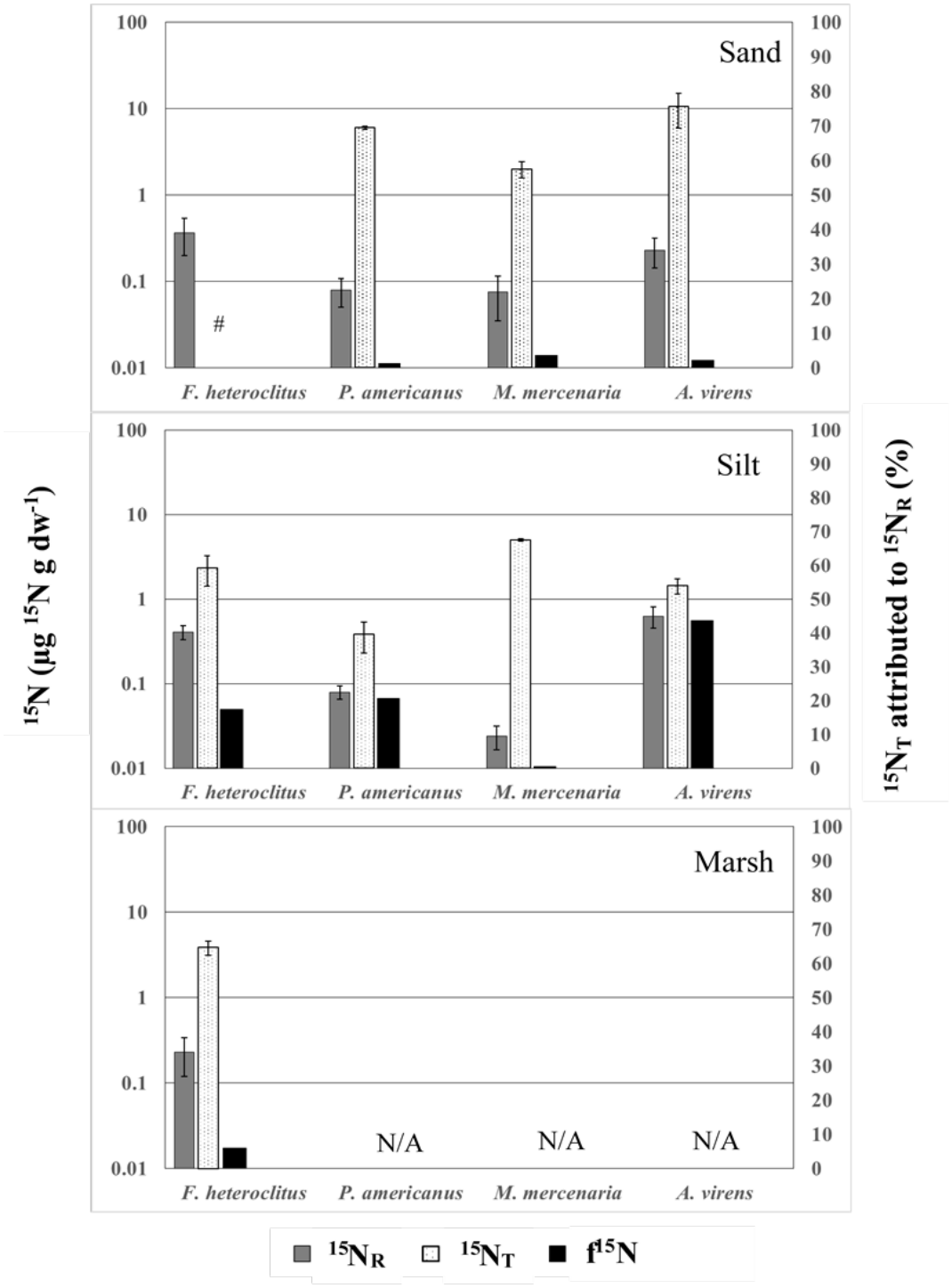

Figure 10.5. Infaunal and Fish ^{15}N concentrations. Temporal mean (se) ^{15}N tracer fish and infaunal tissue concentrations for each mesocosm (Sand, Silt, and Marsh). $^{15}N_R$ and $^{15}N_T$ tissue are represented by the gray and hatched bars. The solid black bar ($f^{15}N$) represents the percent of $^{15}N_T$ that can be attributed to $^{15}N_R$. *F. heteroclitus* $^{15}N_T$ tissue concentrations were not available for the sand mesocosm. N/A denotes organisms that were not used.

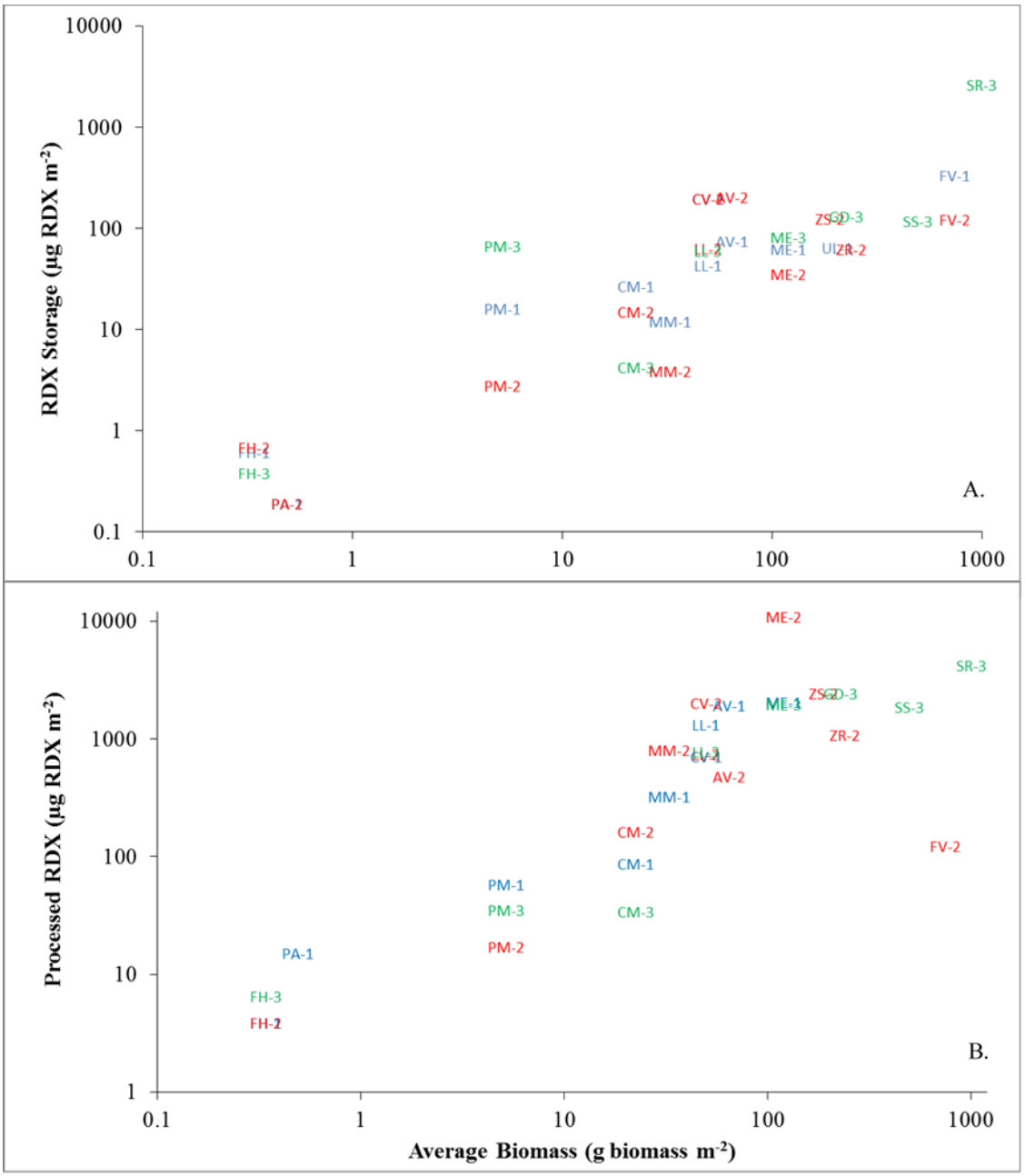

Figure 10.6. Storage of RDX on an Ecosystem Scale: Panel A. represents the intact RDX derived from the $^{15}N_R$ values for each species. The intact RDX storage values and the average biomasses are reported in Table 1S. While panel B. represents the processed and retained RDX derived from $^{15}N_T$ values for each species. The values for panel B are reported in Table 2S. The data points are represented by two digit letter code and a dash followed by a number denoting mesocosm type that is color coded (Sand-1 'blue', Silt-2 'red', and marsh-3 'green'). Values for *F. vesiculosus* (FV-1) and *U. lactuca* (UL-1) for the sand mesocosm were not plotted due to suspected high amounts of luxury uptake of DI^{15}N produced from RDX mineralization (Table 10.2).

Table 10.1. Species List. Scientific and common names for each species by mesocosm.

Scientific Name	Common Name	Experiment
Fucus vesiculosus	bladderwrack	sand, silt
Ulva lactuca	sea lettuce	sand
Zostera marina	marine eelgrass	silt
Spartina alterniflora	smooth cordgrass	marsh
Mytilus edulis	blue mussel	sand, silt, marsh
Geukensia demissa	ribbed mussel	marsh
Mercenaria mercenaria	hard clam	sand, silt
Crassostrea virginica	eastern oyster	sand, silt
Littorina littorea	common periwinkle	sand, silt, marsh
Alitta virens	sandworm	sand, silt
Fundulus heteroclitus	mummichog	sand, silt, marsh
Pseudopleuronectes americanus	winter flounder	sand, silt
Carcinus maenas	green crab	sand, silt, marsh

Table 10.2. Species linear regression comparison: Coefficients of determination (r^2) for linear regressions of $^{15}N_R$ and $^{15}N_T$ tissue concentrations as a function of aqueous RDX. N/A denotes mesocosms where the species was not used and # indicates where species were used but a regression was not obtained do to missing species data for a mesocosm.

Species	Sand		Silt		Marsh	
	$^{15}N_R$	$^{15}N_T$	$^{15}N_R$	$^{15}N_T$	$^{15}N_R$	$^{15}N_T$
F. vesiculosus	0.65	0.029	0.41	0.68	N/A	N/A
U. lactuca	0.52	0.11	N/A	N/A	N/A	N/A
Z. marina rhizome	N/A	N/A	0.48	0.24	N/A	N/A
Z. marina shoot	N/A	N/A	< 0.01	0.58	N/A	N/A
S. alterniflora root	N/A	N/A	N/A	N/A	0.43	0.18
S. alterniflora shoot	N/A	N/A	N/A	N/A	< 0.01	0.22
M. edulis	0.35	0.35	0.24	0.60	0.48	0.067
G. demissa	N/A	N/A	N/A	N/A	0.021	0.20
M. mercenaria	0.56	< 0.01	0.27	0.050	N/A	N/A
C. virginica	#	< 0.01	0.23	0.49	N/A	N/A
L. littorea	0.098	0.59	0.030	0.51	0.18	0.16
A. virens	0.60	0.32	0.16	0.21	N/A	N/A
F. heteroclitus	0.19	#	0.18	0.40	0.016	0.19
P. americanus	0.82	0.14	0.043	0.17	N/A	N/A
C. maenas	0.49	0.026	0.17	0.20	< 0.01	0.31
Average r^2 (±se)	0.47 (± 0.21)	0.19 (±0.19)	0.20 (± 0.14)	0.38 (± 0.20)	0.11 (± 0.17)	0.19 (± 0.07)

Table 10.3. Ecosystem level RDX ($^{15}N_R$): Average species biomass values are taken from the literature. The Intact RDX per area was calculated by multiplying the avg. biomass (gdw m^{-2}) by the RDX in tissue (µg RDX g dw^{-1}) derived from $^{15}N_R$ values for each species. Species codes apply to Figure 10.6A. na denotes when a species was not used in the mesocosm.

Species	Species code	Avg. Biomass (gdw m^{-2})	Intact RDX per area (µg RDX m^{-2})			Reference
			Sand	Silt	Marsh	
F. vesiculosus	FV	750	335	123	na	Creed et al. 1996
U. lactuca	UL	206	64	na	na	Nikolaisen et al. 2011
M. edulis	ME	120	62	35	82	McGorty & Custard 1991
M. mercenaria	MM	33	12	3.9	na	Walker and Tenore 1984
C. virginica	CV	50	196	196	na	Mann et al., 2009
L. littorea	LL	50	43	63	60	Buschbaum 2000
A. virens	AV	65	74	202	na	Nielsen et al., 1995
F. heteroclitus	FH	0.34	0.61	0.68	0.38	Lockfield 2011
P. americanus	PA	0.49	0.19	0.19	na	Fairchild et al., 2008
C. maenas	CM	22.5	27	15	4.2	Lovely et al., 2015
POM	PM	5.2	16	2.8	67	Wainright 1990
Z. marina shoot	ZS	190	na	124	na	Santamaria-Gallegos et al. 2000
Z. marina rhizome	ZR	240	na	62	na	Santamaria-Gallegos et al. 2000
S. alterniflora root	SR	1000	na	na	2604	Schubauer and Hopkinson 1983
S. alterniflora shoot	SS	500	na	na	117	Schubauer and Hopkinson 1983
G. demissa	GD	228	na	na	132	Fell et al., 1982

Table 10.4. Ecosystem level RDX ($^{15}N_T$): Average species biomass values are taken from the literature. The Total RDX per area was calculated by multiplying the avg. biomass (gdw m^{-2}) by the RDX in total tissue (µg RDX g dw^{-1}) derived from $^{15}N_T$ values for each species. Species code are a reference for Figure 10.6B. na denotes when a species was not used in the mesocosm.

Species	Species code	Avg. Biomass (g dw m^{-2})	RDX equivalents processed and retained (µg RDX g m^{-2})			Reference
			Sand	Silt	Marsh	
F. vesiculosus	FV	750	20195	123	na	Creed et al. 1996
U. lactuca	UL	206	22777	na	na	Nikolaisen et al. 2011
M. edulis	ME	120	2060	10825	1938	McGorty & Custard 1991
M. mercenaria	MM	33	321	801	na	Walker and Tenore 1984
C. virginica	CV	50	703	2024	na	Mann et al., 2009
L. littorea	LL	50	1324	737	779	Buschbaum 2000
A. virens	AV	65	1912	478	na	Nielsen et al., 1995
F. heteroclitus	FH	0.34	3.9	3.9	6.5	Lockfield 2011
P. americanus	PA	0.49	15	0.94	na	Fairchild et al., 2008
C. maenas	CM	22.5	87	163	34	Lovely et al., 2015
POM	PM	5.2	58	17	35	Wainright 1990
Z. marina shoot	ZS	190	na	2432	na	Santamaria-Gallegos et al. 2000
Z. marina rhizome	ZR	240	na	1079	na	Santamaria-Gallegos et al. 2000
S. alterniflora root	SR	1000	na	na	4212	Schubauer and Hopkinson 1983
S. alterniflora shoot	SS	500	na	na	1858	Schubauer and Hopkinson 1983
G. demissa	GD	228	na	na	2445	Fell et al., 1982

11.0. CONCLUSIONS AND IMPLICATIONS FOR FUTURE RESEARCH/IMPLEMENTATION

Results from the experiments presented herein provide some general conclusions about RDX and TNT behavior in nearshore marine ecosystems, identify future avenues for research, and reveal opportunities for implementation of this work.

A summary discussion of conclusions was presented at the SERDP Underwater Military Munitions Constituents Workshop on Ecological Risk, 23-24 May 2018, Washington Navy Yard, Washington DC.

11.1 Conclusions

RDX and TNT are both reactive in the shallow marine environment. But the fate of these parent compounds is different with respect to biotic uptake / retention, persistence in sediments, and susceptibility for mineralization.

Biota

Both compounds and their primary derivatives are not readily taken up by biota. ^{15}N tracer in biota can account for only a few percent of the amount of parent compound removed from the water column. Marine organisms have low BCFs for both TNT and RDX. Tissue concentrations of ΣTNT and ΣRDX in flora and fauna are small and account for, on average, less than 10% of the ^{15}N tracer found in biota. On one hand these low tissue concentrations suggest that the ecological risks of TNT and RDX are likely to be small at aqueous concentrations in the range of our studies (≤ 1ppm). However, the accumulation of the isotope tracer in excess of tissue ΣTNT and ΣRDX levels indicate that breakdown within organisms is followed by retention of some of those breakdown products. It is not known if those products that are retained represent an additional toxicological risk or not.

Sediments and Retention

Sediments were a larger sink for TNT than for RDX by a factor of four. ^{15}N tracer in sediments accounted for 5-19% vs 1-5% of TNT and RDX removed from the overlying water respectively. For both compounds, the parent compounds and primary derivatives accounted for only a few % of the isotope tracer inventory found in sediments and associated with SPM. Sediments were sites for active transformations of both RDX and TNT the results of those transformations differ for RDX and TNT. It has long been thought that reduction of the nitro groups in TNT can lead to the production of TAT which is covalently bonded to sediments. This mechanism incompletely explains our tracer observations. The total ^{15}N in sediments approximates steady state over time which suggests a limit to the TAT mechanism. Further, the isotope mass balance in TNT experiments was poor and pointed to amino-dinitrotoluenes and unmeasured organic derivative(s) as the principal fate of TNT in all coastal ecotypes (Fig. 11.1). PCA results suggested the likelihood that this missing derivative(s), occurred in the aqueous phase although its formation was associated with sediments or SPM. Isotopic investigations of the bulk dissolved organic nitrogen fractions provided some confirmation that a minimum of 15 to 55% of the missing tracer in the mass balance was in the form of an organic derivative in the water column. Beyond that, we were not able to specifically identify the missing derivative(s). Complete mineralization of TNT (almost solely to NH_4^+) was a minor route of TNT processing. The primary fate of TNT in shallow coastal marine systems appears to be that of transforming

into organic derivatives that may be relatively persistent in both the sediments and water column. The ecological risk associated with the measured amino-dinitrotoluenes can be assessed, but any risk derived from the "missing" derivative(s) remains undefined until those compound(s) can be identified.

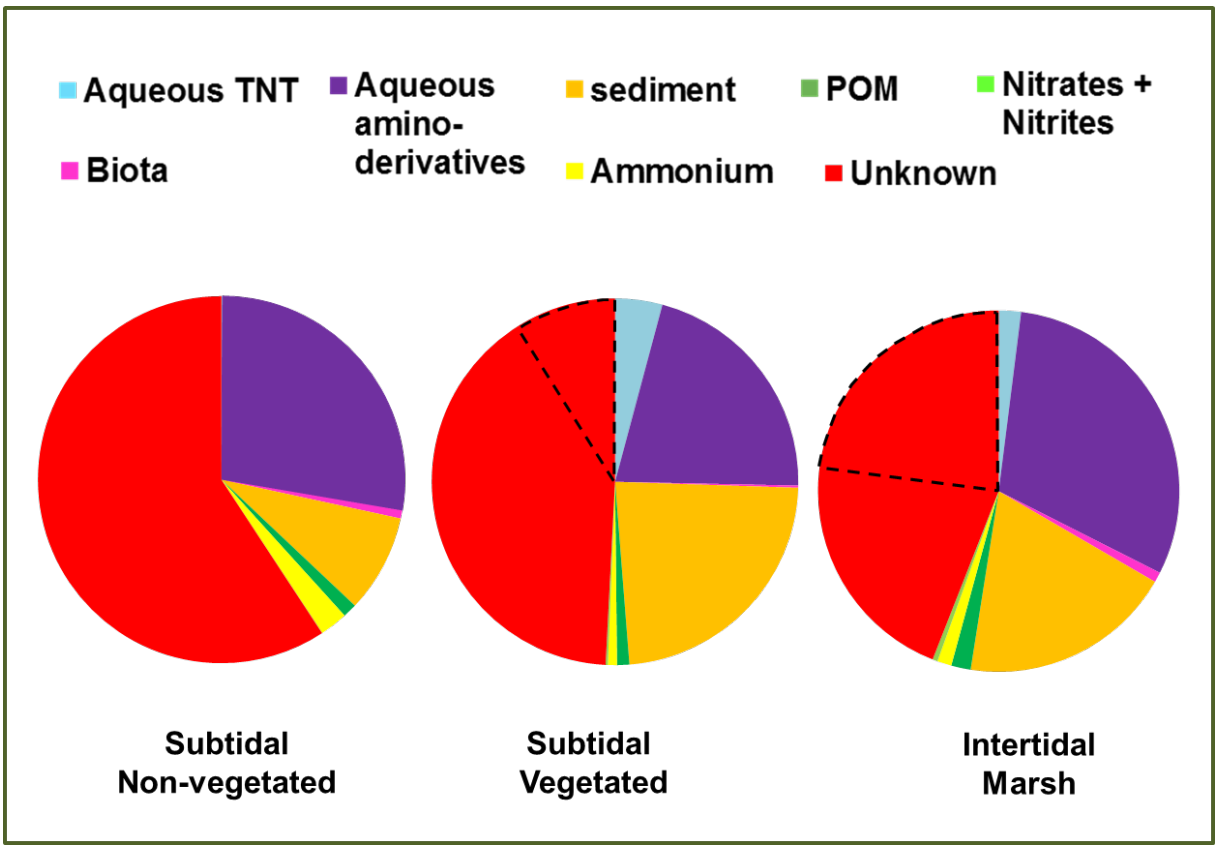

Figure 11.1. Cumulative distribution of isotope tracer in TNT mesocosm experiments. Mass balance is dominated by an unknown and presumed unmeasured organic derivative. The dashed section of the 'unknown' wedge denotes the minimum amount of that fraction that was identified as an organic compound in the aqueous phase. It was assigned using dissolved organic nitrogen (DON) isotope analyses and calculated by difference between the ^{15}N-DON and all other measured aqueous ^{15}N pools. No DON analyses were conducted on the subtidal non-vegetated mesocosm. Mineralization is defined as the sum of the ammonium and nitrate/nitrite fractions. Only trace amounts of labeled N_2 and N_2O were measured.

Mineralization

The fate of RDX was considerably different than that of TNT. RDX mineralization to DIN products accounted for approximately half of the RDX delivered to coastal ecosystems. In the presence of high organic and/or variable redox sediments, mineralization was the dominant fate of RDX. The nitroso-derivatives do not substantially accumulate in sediments or overlying water and instead appear to be transient intermediate species on the path to complete mineralization. Based on isotope mass balance, uncharacterized organic derivatives (those other than TNX,

DNX, and MNX) are the likely the fate of less than 20% of RDX inputs. Nitrous oxide and N_2 gas were the primary terminal mineralization products for RDX, the latter of which is reliant on naturally occurring denitrifying populations to reduce N_2O to N_2 (Fig. 11.2).

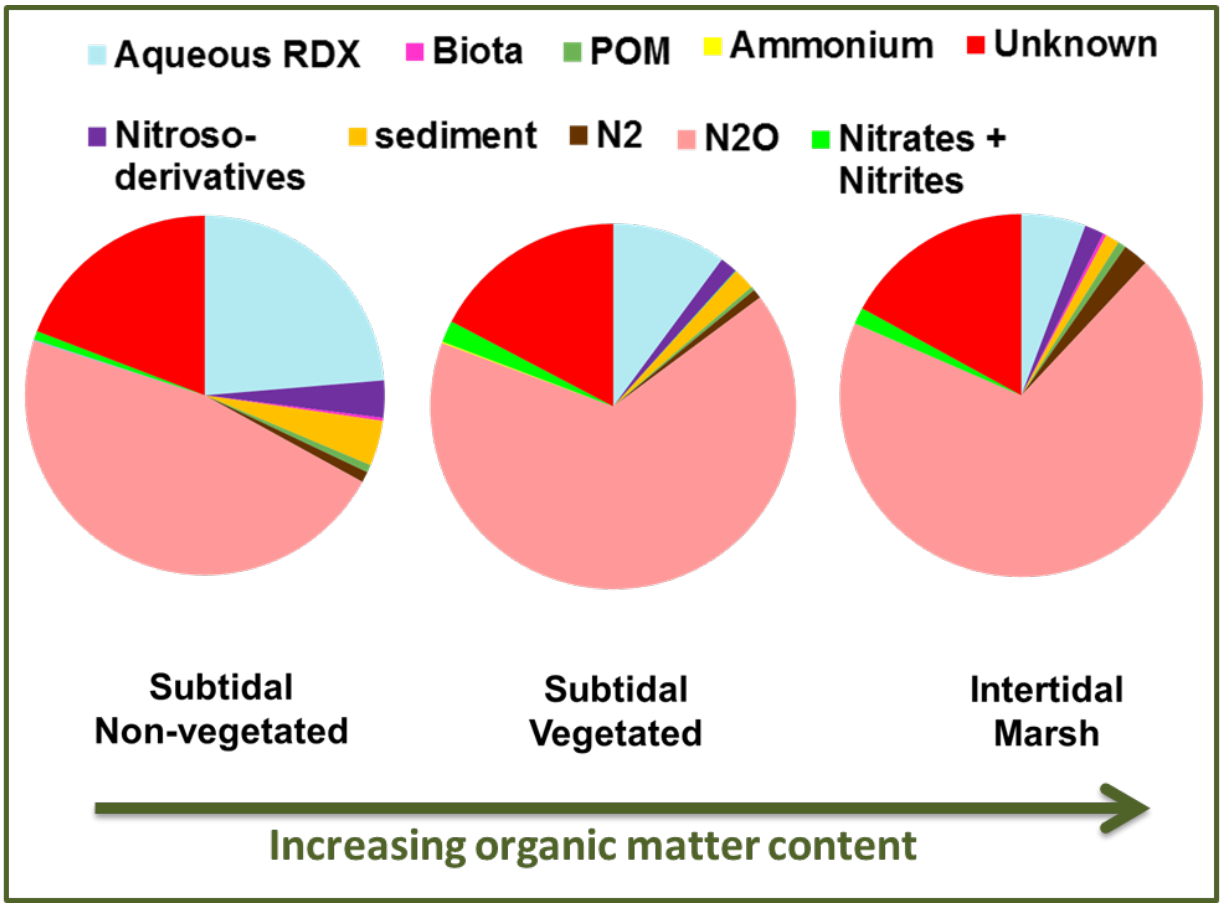

Figure 11.2. Cumulative distribution of isotope tracer in RDX mesocosm experiments. More organic matter equates with less persistence of RDX and derivatives. Mineralization is defined as the sum of the N_2. N_2O, ammonium, and nitrate/nitrite fractions.

11.2 Future Research / /Implementation

Two information gaps emerged from this work as well as a clear direction for transferring approaches developed in this project to DoD end-users.

1) Identify TNT breakdown derivative(s). Based upon the ^{15}N mass balances in labeled TNT experiments, the majority of TNT breakdown in marine settings does not constitute complete mineralization. The derivative or suites of persistent derivatives remain unidentified, and thus the associated potential human health or ecological risk.

2) Resolve the mechanisms of biotransformation and retention within macro flora/fauna. Results indicate that high rates of uptake and internal processing led to 10-fold more ^{15}N tracer in tissues than could be accounted for by measured RDX and nitroso-derivatives. Similar results were found for TNT. It is unclear whether the nature of this ^{15}N retention constitutes incorporation of N (liberated from parent compounds) into tissue biosynthesis, or if unmeasured derivatives accumulate in tissues as adducts or as free metabolites with some associated toxicity. Similar discrepancies between tissue energetics concentrations and bulk tissue isotope tracer levels have also been observed in carbon isotope tracer studies and further resolution of the toxicological significance of this seems warranted.

3) Use isotopic measurements of DIN following the addition of ^{15}N-RDX as a tool to quantify natural attenuation rates of RDX in situ. ^{15}N-RDX underwent significant processing in large open system marine mesoscosms. The majority of that processing was complete mineralization that generated ^{15}N labeled DIN constituents. Establishing directly measured rates of natural attenuation at RDX contaminated sites provides added information when assessing remediation options. This stable isotope approach will be used to quantify natural attenuation in an existing RDX groundwater plume at Naval Base Kitsap in the near future. This work constitutes an important technology transfer from this project to RPMs. The approach holds similar potential for other RDX contaminated soils, sediment, ground and surface waters as well as for other contaminants where nitrogen or carbon stable isotope labeling can be used.

12.0 LITERATURE CITED

33 U.S.C. 1401 et seq. The "Ocean Dumping Act" is the common reference to Title I of the Marine Protection, Research, and Sanctuaries Act of 1972 (MPRSA, P.L. 92-532), as amended.

Ainsworth CC, Harvey SD, Szecsody JE, Simmons MA, Cullinan VI, Resch CT, Mong GH. 1993. Relationship between the Leachability Characteristics of Unique Energetics Compounds and Soil Properties. Project 91PP1800. US Army Biomedical Research and Development Laboratory, Fort Detrick,MD,USA.

Alavi G, Chung M, Lichwa J, D'Alessio M, Ray C. 2011. The fate and transport of RDX, HMX, TNT and DNT in the volcanic soils of Hawaii: A laboratory and modeling study. J. Hazardous Mat. 185: 1600-1604.

Aller RC. 1982. The effects of macrobenthos on chemical properties of marine sediment and overlying water. In Animal-Sediment Relations, eds. P.L. McCall and M.J.S. Tevesz, pp. 52-102. Plenum, New York.

An C, Shi Y, He Y, Huang G, Liang J, Liu Z. 2014. Effect of different carbon substrates on the removal of hexahydro-1,3,5-trinitro-1,3,5-triazine (RDX) and octahydro-1,3,5,7-tetranitro-1,3,5,7-tetrazocine (HMX) by anaerobic mesophilic granular sludge. Water Air Soil Pollut 225. DOI: 10.1007/s11270-014-2174-8

Anderson IC, McGlathery KJ, Tyler AC. 2003. Microbial mediation of 'reactive' nitrogen in a temperate lagoon. Marine Ecology Progress Series 246: 73-84

Anke H, Kuhn A, Weber RWS. 2003. The role of nitrate reductase in the degradation of the explosive RDX (hexahydro-1,3,5-trinitro-1,3,5-triazine) by *Penicillium* sp. AK96151. Mycological Progress 23: 219-225.

Annamaria H, Manno D, Strand SE, Bruce NC, Hawari J. 2010. Biodegradation of RDX and MNX with rhodococcus sp. strain DN22: New insights into the degradation pathway. Environ. Sci. Technol. 44: 9330-6.

Archer D. 1990. The dissolution of calcite in deep sea sediments, an in situ microelectrode study. Ph.D. dissertation, University of Washington, Seattle.

Ariyaratha T, Vlahos P, Smith RW, Fallis S, Groshens T, Tobias C. 2017. Biodegradation and mineralization of isotopically labelled TNT and RDX in anaerobic marine sediments. Environ. Toxicol. Chem. 36: 1170-1180.

Ariyarathna T, Vlahos P, Tobias C, Smith R. 2016. Sorption kinetics of TNT and RDX in anaerobic freshwater and marine sediments: Batch studies. Environ Toxicol Chem. 35: 47-55.

ASTM E1022-94. 2013. Standard Guide for Conducting Bioconcentration Tests with Fishes and Saltwater Bivalve Mollusks, ASTM International, West Conshohocken, PA

ASTDR. 1995. Toxicological Profile for 2,4,6-Trinitrotoluene. US Department of Health and Human Services. Atlanta,GA, USA, http://www.atsdr.cdc.gov/toxprofiles/tp81.pdf.

ASTDR. 2012. Toxicology Profile for RDX. US Department of health and human services. Atlanta, GA, USA, http://www.atsdr.cdc.gov/toxprofiles/tp78.pdf.

Ballentine M, Tobias C, Vlahos P, Smith R, Cooper C. 2015. Bioconcentration of TNT and RDX in coastal marine biota. Arch. Environ. Contam. Toxicol. 68 :718-28.

Ballentine ML, Ariyarathna T, Smith RW, Cooper C, Vlahos P, Fallis S, Groshens TJ, Tobias C. 2016. Uptake and fate of hexahydro-1,3,5-trinitro-1,3,5-triazine (RDX) in coastal marine biota determined using a stable isotopic tracer, 15N - [RDX]. Chemosphere 153:28-38.

Bearden DM. 2007. U.S. disposal of chemical weapons in the ocean: background and issues for congress. Report RL33432.

Belden JB, Lotufo GR, Chambliss CK, Fisher JC, Johnson DR, Boyd RE, Sims JG. 2011. Accumulation of 14 C-trinitrotoluene and related nonextractable (bound) residues in Eisenia fetida. Environmental Pollution 159: 1363-8.

Belden JB, Lotufo GR, Lydy MJ. 2005a. Accumulation of hexahydro-1, 3, 5-trinitro-1, 3, 5-triazine in channel catfish (Ictalurus punctatus) and aquatic oligochaetes (Lumbriculus variegatus). Environmental Toxicology and Chemistry 24: 1962-7.

Belden JB, Ownby DR, Lotufo GR, Lydy MJ. 2005b. Accumulation of trinitrotoluene (TNT) in aquatic organisms: Part 2—Bioconcentration in aquatic invertebrates and potential for trophic transfer to channel catfish (Ictalurus punctatus). Chemosphere 58: 1161-8.

Beller HR. 2002. Anaerobic biotransformation of RDX (hexahydro-1,3,5-trinitro-1,3,5-triazine) by aquifer bacteria using hydrogen as the sole electron donor. Water Res. 36: 2533-2540.

Beller HR Madrid V, Hudson B, McNab WW, Carlsen T. 2004. Biogeochemistry and natural attenuation of nitrate in groundwater at an explosives test facility. Appl. Geochem. 19: 1483-1494.

Bentley R, Dean J, Ells S, Hollister T, LeBlanc G. 1977. Laboratory Evaluation of the Toxicity of Cyclotrimethylene Trinitramine (RDX) to Aquatic Organisms.

Best EP, Zappi ME, Fredrickson HL, Sprecher SL, Larson SL, Ochman M. 1997. Screening of aquatic and wetland plant species for phytoremediation of explosives-contaminated groundwater from the Iowa army ammunition plant. Annals of the New York Academy of Sciences, 829: 179-194.

Best EPH, Sprecher SL, Larson SL, Fredrickson HL, Bader DF. 1999. Environmental behavior of explosives in groundwater from the Milan Army Ammunition Plant in aquatic and wetland plant treatments. Removal, mass balances and fate in groundwater of TNT and RDX. Chemosphere 38:3383-3396.

Bhatt M, Zhao J, Monteil-Rivera F, Hawari J. 2005. Biodegradation of cyclic nitramines by tropical marine sediment bacteria. Journal of Industrial Microbiology and Biotechnology 32: 261-267.

Bhatt M, Zhao J, Halasz A, Hawari J. 2006. Biodegradation of hexahydro-1, 3, 5-trinitro-1, 3, 5-triazine by novel fungi isolated from unexploded ordnance contaminated marine sediment. Journal of Industrial Microbiology and Biotechnology 33: 850-858.

Bhushan B, Halasz A, Spain JC, Hawari J. 2002a. Diaphorase catalyzed biotransformation of RDX via N-denitration mechanism. Biochem. Biophys. Res. Comm. 296: 779-784.

Bhushan B, Halasz A, Spain J, Thiboutot S, Ampleman G, Hawari J. 2002b. Biotransformation of hexahydro-1,3,5-trinitro-1,3,5-triazine (RDX) catalyzed by a NAD(P)H: nitrate oxidoreductase from *Aspergillus niger*. Environ. Sci. Technol. 36: 3104-3108.

Bhushan B, Trott S, Spain JC, Halasz A, Paquet L, Hawari J. 2003. Biotransformation of hexahydro-1,3,5-trinitro-1,3,5-triazine (RDX) by a rabbit liver cytochrome P450: Insight into the mechanism of RDX biodegradation by *Rhodococcus* sp. strain DN22. Appl. Environ. Microbiol. 69: 1347-51.

Boopathy R, Kulpa CF. 1992. Trinitrotoluene (TNT) as a sole nitrogen source for a sulfate-reducing bacterium *Desulfovibrio sp*. (B Strain) isolated from an anaerobic digester. Current Microbiol. 25: 235-241.

Boopathy R, Kulpa CF, Wilson M. 1993. Metabolism of 2,4,6-Trinitrotoluene (TNT) by Desulfovibrio sp. (B strain). Appl. Environ. Microbiol. 39: 270-275.

Boopathy R, Kulpa CF, Manning J. 1998. Anaerobic biodegradation of explosives and related compounds by sulfate-reducing and methanogenic bacteria: A review. Bioresour. Technol. 63: 81-89.

Boopathy R, Widrig DL, Manning J. 1997. In situ bioremediation of explosives-contaminated soil: A soil column study. Bioresour. Technol. 59: 169-176.

Boopathy R. 2014. Biodegradation of 2,4,6-trinitrotoluene (TNT) under sulfate and nitrate reducing conditions. Biologia 69: 1264-1270.

Bose P, Glaze WH, Maddox DS. 1997a. Degradation of RDX by various advanced oxidation processes: I. Reaction Rates. Water Res. 32: 997-1004.

Bose P, Glaze WH, Maddox DS. 1997b. Degradation of RDX by various advanced oxidation processes: II. Organic by-products. Water Res. 32: 1005-1018.

Bradley PM, Chapelle FH, Landmeyer JE, Schumacher JG. 1992. Microbial transformation of nitroaromatics in surface soils and aquifer materials. Appl. Environ. Microb. 60: 2170-2175.

Bradley PM, Dinicola RS. 2005. RDX (Hexahydro-1,3,5-trinitro-1,3,5-triazine) biodegradation in aquifer sediments under manganese-reducing conditions. Biorem. J. 9: 1-8.

Brannon JM PJ. 2002. Environmental Fate and Transport Process Descriptors for Explosives. ERDC/EL TR-02-10. US Army Engineer Research and Development Center, Vicksburg, Miss, USA.

Brannon JM, Adrian GG, Pennington JC, Hayes C, Myers TE. 1992. Slow Release of PCB, TNT and RDX from Soils and Sediments. Technical report EL-92-38. US Army Corps of Engineers, Waterways Experiment Station, Vicksburg, MS, USA.

Brannon JM, Pennington JC. 2002. Environmental Fate and Transport Process Descriptors for Explosives. ERDC/EL TR-02-10. US Army Engineer Research and Development Center, Vicksburg, Miss, USA.

Brannon JM, Price CB, Yost SL, Hayes C, Porter B. 2005. Comparison of environmental fate and transport process descriptors of explosives in saline and freshwater systems. Mar. Pollut. Bull. 50: 247-251.

Brezonik PL. 1997. Denitrification in natural waters. Prog. Water Technol. 8: 373-392.

Brown GI. 1998. The big bang: a history of explosives. Sutton Publishing.

Bruns-Nagel D, Steilnbach K, Gemsa D, von Low E. 2000. Composting (Humification) of nitroaromatic compounds. In Biodegradation of nitroaromatic compounds and explosives; Spain, J. C.; Hughes, J. B.; Knackmuss, H.-J., Eds.; CRC Press: Boca Raton pp. 357-394.

Burken JG, Schnoor JL. 1998. Predictive relationships for uptake of organic contaminants by hybrid poplar trees. Environ. Sci. Technol. 32: 3379-85.

Burton DT, Turley SD, Peters GT. 1994. The acute and chronic toxicity of hexahyro-1,3,5-trinitro-1,3,5-triazine (RDX) to the fathead minnow (*Pimephales promelas*). Chemosphere 29: 567-579.

Camme LM. 1982. Effect of particle size on organic content and microbial abundance within four marine sediments. Mar. Ecol. Prog. Ser. 9: 273-280.

Carpenter DF, McCormick NG, Cornell JH, Kaplan AM. 1978. Microbial transformation of ^{14}C-labeled 2,4,6-trinitrotoluene in an activated-sludge system. Appl. Environ. Microbiol. 35: 949-954.

Casciotti KL, Sigman DM, Hastings MG, Bohlke JK, Hilkert A. 2002. Measurement of the oxygen isotopic composition of nirate in seawater and freshwater using the denitrifier method. Anal. Chem. 74: 4905-4912.

Chai T, Draxler RR. 2014. Root mean square error (RMSE) or mean absolute error (MAE)? - arguments against avoiding RMSE in the literature. Geosci. Model Dev. 7: 1247-1250.

Chappell MA, Porter BE, Price CL, Pettway BA, George RD. 2011. Differential kinetics and temperature dependence of abiotic and biotic processes controlling the environmental fate of TNT in simulated marine systems. Mar. Pollut. Bull. 62: 1736-1743.

Cho C, Bae S, Lee W. 2012. Enhansed degradation of TNT and RDX by bio-reduced iron bearing soil minerals. Advances in Environmental Research 1: 1-14.

Cho Y, Lee B, Oh K. 2008. Simultaneous degradation of nitroaromatic compounds TNT, RDX, atrazine, and simazine by Pseudomonas putida HK-6 in bench-scale bioreactors. Journal of Chemical Technology and Biotechnology 83: 1211-7.

Christensen JP, Murray JW, Devol AH, Codispoti LA. 1987. Denitrification in continental shelf sediments has major impact on the oceanic nitrogen budget. Glob. Biogeochem. Cyc. 1: 97-116.

Chusova O, Nõlvak H, Odlare M, Truu J, Truu M, Oopkaup K, Nehrenheim E. 2015. Biotransformation of pink water TNT on the surface of a low-cost adsorbent pine bark. Biodegradation 26: 375-386.

Clausen J, Robb J, Curry D, Korte N. 2004. A case study of contaminants on military ranges: Camp Edwards, Massachusetts, USA. Environmental Pollution 129: 13-21.

Cline JD. 1969. Spectrophotometric determination of hydrogen sulfide in natural waters. Limnol. Oceanogr. 14: 454-455.

Conder JM, Point TWL, Bowen AT. 2004. Preliminary kinetics and metabolism of 2, 4, 6-trinitrotoluene and its reduced metabolites in an aquatic oligochaete. Aquatic Toxicology 69 :199-213.

Craig HD, Taylor S. 2011. Framework for evaluating the fate, transport, and risks from conventional munitions compounds in underwater environments. Mar. Technol. Soc. J. 45: 35-46.

Crocker FH, Indest KJ, Fredrickson HL. 2006. Biodegradation of the cyclic nitramine explosives RDX, HMX, and CL-20. Appl. Microbiol. Biotechnol. 73:2 74-90.

CRS Report 2007. U.S. Disposal of Chemical Weapons in the Ocean: Background and Issues for Congress. CRS Report for Congress. Resources, Science, and Industry Division.

Cruz-Uribe O, Cheney DP, Rorrer Gl. 2007. Comparison of TNT removal from seawater by three marine macroalgae. Chemosphere 67: 1469-1476.

Darrach MR, Chutjian A, Plett GA. 1998. Trace Explosives signatures from World War II unexploded undersea ordnance. Environmental Science and Technology 32: 1354-1358.

Delaune RD, Reddy KR. 2005. Redox potential. Hillel D (ed), In Encyclopedia of Soils in the Environment, Academic Press, pp. 366-371.

Department of Defense Strategic Environmental Research and Development Program (SERDP). 2010. Statement of Need.

Devol AH. 2008. Denitrification Including Annamox. In Nitrogen and the Marine Environment.263-292. Eds. Capone, D. G.; Bronk D. A.; Mulholland, M. R., Carpenter, E. J. Academic Press.

Di Toro DM. 1985. A particle interaction model of reversible organic chemical sorption. Chemosphere 14: 1503-1538.

Dontsova KM, Yost SL, Šimunek J, Pennington JC, Williford CW. 2006. Dissolution and transport of TNT, RDX, and composition B in saturated soil columns. J. Environ. Qual. 35: 2043-2054.

Dontsova KM, Hayes C, Pennington JC, Porter B. 2008. Sorption of high explosives to water-dispersable clay: influence of organic carbon, aluminosilicate clay, and extractable iron. J. Environ. Qual. 38: 1458-1465.

Douglas TA, Johnson L, Walsh M, Collins C. 2009. A time series investigation of the stability of nitramine and nitroaromatic explosives in surface water samples at ambient temperature. Chemosphere 76: 1-8.

DRDC 2004. Evaluation of underwater contamination by explosives and metals at Point Amour, Labrador and in the Halifax Harbour area. DRDC Valcartier TR 2004-125. Defence Research and Development, Toronto, Canada.

Drzyzga O, Bruns-Nagel D, Gorontzy T, Blotevogel K, Gemsa D, Lo¨w E. 1998. Mass balance studies with 14C-labeled 2,4,6-Trinitrotoluene (TNT) mediated by an anaerobic Desulfovibrio species and an aerobic Serratia species. Current Microbiology 37: 380-386.

Duque E, Haidour A, Godoy F, Ramos JL. 1997. 2,4,6-Trinitrotoluene (TNT) transformation by clostridia isolated from a munition-fed bioreactor: comparison with non-adapted bacteria. J. Ind. Microbiol. Biotechnol. 18: 82-88.

Ek H, Dave G, Nilsson E, Sturve J, Birgersson G. 2006. Fate and effects of 2, 4, 6-trinitrotoluene (TNT) from dumped ammunition in a field study with fish and invertebrates. Arch. Environ. Contam Toxicol 51: 244-52.

Elovitz MS, Weber EJ. 1999. Sediment-mediated reduction of 2,4,6-Trinitrotoluene and fate of the resulting aromatic (poly)amines. Environ. Sci. Technol. Lett. 33: 2617-2625.

Eriksson J, Frankki S, Shchukarev A, Skyllberg U. 2004. Binding of 2,4,6-trinitrotoluene, aniline, and nitrobenzene to dissolved and particulate soil organic matter. Environ. Sci. Technol. 38: 3074-3080.

Esteve-Nunez A, Ramos JL. 1998. Metabolism of 2,4,6-Trinitrotoluene by Pseudomonas sp. JLR11. Environ. Sci. Technol. 32: 3802-3808.

Esteve-Núñez A, Caballero A, Ramos JL. 2001. Biological degradation of 2,4,6-trinitrotoluene. Microbiology and Molecular Biology Reviews 65:335-352.

Felt DR, Bednar A, Arnett C, Kirgan R. 2009. Bio-Geochemical Factors That Affect RDX Degradation. Proceedings of the Annual International Conference on Soils, Sediments, Water and Energy 14: Article 17.

Fiorella PP, Spain JC. 1997. Transformation of 2,4,6-trinitrotoluene by Pseudomonas pseudoalcaligenes JS52. Appl. Environ. Microbiol. 63: 2007-2015.

Finneran KT, Kwon M, Drew SR. 2007. Biodegradation of RDX by stimulating humic substance- and Fe(III) - reduction. Final report:ER-1377. Strategic Environmental Research and Development Program, Arlington, VA.

Freedman DL, Sutherland KW. 1998. Biodegradation of hexahydro-1,3,5-trinitro-1,3,5-triazine (RDX) under nitrate-reducing conditions. Water Science and Technology 38: 33-40.

Fournier D, Halasz A, Spain J, Fiurasek P, Hawari J. 2002. Determination of key metabolites during biodegradation of hexahydro-1,3,5-trinitro-1,3,5-triazine with *Rhodococcus* sp. strain DN22. Appl. Environ. Microbiol. 68: 166-72.

Fournier D, Halasz A, Spain J, Spanggord RJ, Bottaro JC, Hawari, J. 2004. Biodegradation of the hexahydro-1,3,5-trinitro-1,3,5-triazine ring cleavage product 4-nitro-2,4-diazabutanal by *Phanerochaete chrysosporium*. Applied and Environmental Microbiology 70: 1123-1128.

Fuller ME, Heraty L, Condee CW, Vainberg S, Sturchio NC, Böhlke JK, Hatzinger PB. 2016. Relating carbon and nitrogen isotope effects to reaction mechanisms during aerobic or anaerobic degradation of RDX (hexahydro-1,3,5- trinitro-1,3,5-triazine) by pure bacterial cultures. Appl. Environ. Microbiol. 82:3297-3309.

Funk SB, Roberts DJ., Crawford DL, Crawford RL. 1993. Initial-phase optimization for bioremediation of munition compound-contaminated soils. Appl. Environ. Microbiol. 59: 2171-2177.

Gallagher EM, Young LY, McGuiness LM, Kerkhof LJ. 2010. Detecting 2,4,6-Trinitrotoluene utilizing, anaerobic bacteria by 15N and 13C incorporation. Appl. Environ. Microbiol. 76: 1695-1698.

Government Accountability Office (GAO). 2003. DOD needs to develop a comprehensive approach for cleaning up contaminated sites. GAO-04-147.

Gregory KB, Larese-Casanova P, Parkin GF, Scherer MM. 2004. Abiotic transformation of hexahydro-1,3,5-trinito-1,3,5-triazine by Fe II bound to magnetite. Environmental Science and Technology 38: 1408-1414.

Gustafsson O, Gschwend PM.1998.The flux of black carbon to surface sediments on the New England continental shelf. Geochim. Et. Cosmochim.Acta 62: 465–472.

Haderlein SB, Weissmahr KW, Schwarzenbach RP. 1996. Specific adsorption of nitroaromatic explosives and pesticides to clay minerals. Environmental Science and Technology 30: 612-622.

Haidour A, Ramos JL. 1996. Identification of products resulting from the biological reduction of 2,4,6-trinitrotoluene, 2,4-dinitrotoluene and 2,6-dinitrotoluene by Pseudomonas sp. Environ. Sci. Technol. 30: 2365-2370.

Halasz A, Hawari J. 2011. Degradation routes of RDX in various redox systems. ACS Symp. Ser. 1071: 441-462.

Halasz A, Spain J, Paquet L, Beaulieu C, Hawari J. 2002. Insights into the formation and degradation mechanisms of methylene-dinitramine during the incubation of RDX with anaerobic sludge. Environ. Sci. Tech. 36: 633-638.

Halasz A, Manno D, Perreault NN, Sabbadin F, Bruce NC, Hawari J. 2012. Biodegradation of RDX nitroso products MNX and TNX by cytochrome P450 XplA. Environ. Sci. Technol. 46: 7245-51.

Hammett LP. 1937. The effect of structure upon the reactions of organic compounds. Benzene derivatives. J. Am. Chem. Soc. 59: 96-103.

Han L, Sun K, Jin J, Xing B. 2016. Some concepts of soil organic carbon characteristics and mineral interaction from a review of literature. Soil Biol. Biochem. 94: 107-121.

Harrison I, Vane CH. 2010. Attenuation of TNT in seawater microcosms. Water Science and Technology 61: 2531-2538.

Harter DR. 1985. The use and importance of nitroaromatic chemicals in the chemical industry. In Toxicity of nitroaromatic chemical industry. (Institute of toxicology series); Ricket D. E., Eds.; Hemisphere Publishing, New York pp. 1-14.

Hattori A. 1983. Denitrification and dissimilatory nitrate reduction. In: Nitrogen and the marine environment. Eds. Carpenter, E. J.; Capone, D. G. Academic Press, New York, pp. 191-232.

Hatzinger P, Fuller M. 2014. New approaches to evaluate the biological degradation of RDX in groundwater. SERDP Project ER-1607. Final Report.

Hawari J, Halasz A, Groom C, Deschamps S, Paquet L, Beaulieu C, Corriveau A. 2002. Photodegradation of RDX in aqueous solution: A mechanistic probe for biodegradation with *Rhodococcus sp*. Environ. Sci. Technol. 36: 5117-23.

Hawari J, Halasz A, Paquet L, Zhou E, Spencer B, Ampleman G, Thiboutot S. 1998. Characterization of metabolites in the biotransformation of 2,4,6-trinitrotoluene with anaerobic sludge: role of triaminotoluene. Appl. Environ. Microbiol. 64: 2200-2206.

Hawari J, Beaudet S, Halasz A, Thiboutot S, Ampleman G. 2000a. Microbial degradation of explosives: Biotransformation versus mineralization. Appl. Microbiol. Biotechnol. 54: 605-618.

Hawari J, Halasz A, Sheremata T, Beaudet S, Groom C, Paquet L, Rhofir C, Ampleman G, Thiboutot S. 2000b. Characterization of metabolites during biodegradation of hexahydro- 1,3,5-trinitro-1,3,5-triazine (RDX) with municipal anaerobic sludge. Appl. Environ. Microbiol. 66: 2652-2657.

Hedges JI, Keil RG. 1995. Sedimentary organic matter preservation: an assessment and speculative synthesis. Mar. Chem. 49: 81-115.

Hedges JI, Oades JM. 1997. Comparative organic geochemistries of soils and marine sediments. Org. Geochem. 27: 319-361.

Hedges JI, Stern JH. 1984. Carbon and nitrogen determinations of carbonate-containing solids. Limnology and Oceanography 29: 657-663.

Hoffsommer JC, Kubose DA, Glover DJ. 1977. Kinetic isotope effects and intermediate formation for the aqueous alkaline homogenous hydrolysis of 1,3,5-triaza-1,3,5-trinitrocyclohexane (RDX). J. Phys. Chem. 81: 380-385.

Hofstetter TB, Heijman CG, Haderlein SB, Holliger C, Schwarzenbach RP. 1999. Complete reduction of TNT and other (poly)-nitroaromatic compounds under iron-reducing subsurface conditions. Environ. Sci. Technol. 33: 1479-1487.

Holmboe N, Kristensen E. 2002. Ammonium adsorption in sediments of a tropical mangrove forest (Thailand) and a temperate Wadden sea area (Denmark). Wetlands ecology and management 10: 453 - 460.

Holmes R, McClelland J, Sigman D, Fry B, Peterson B. 1998. Measuring $^{15}N\text{-}NH_4^+$ in marine, estuarine and fresh waters: An adaptation of the ammonia diffusion method for samples with low ammonium concentrations. Mar. Chem. 60: 235-243.

Holmes RM, Peterson BJ, Deegan LA, Hughes JE, Fry B. 2000. Nitrogen biogeochemistry in the oligohaline zone of a New England estuary. Ecology 81: 416-32.

Houston JG, Lotufo GR. 2005. Dietary exposure of fathead minnows to the explosives TNT and RDX and to the pesticide DDT using contaminated invertebrates. International Journal of Environmental Research and Public Health 2: 286-92.

Hovatter PS, Talmage SS, Opresko DM, Ross RH. 1997. Ecotoxicity of nitroaromatics to aquatic and terrestrial species at Army superfund sites. ASTM Spec. Tech. Publ. 1317: 117-29.

Howarth RW, Anderson D, Cloern J, Elfring C, Hopkinson C, Lapointe B, Malone T, Marcus N, McGlathery K, Sharpley A, Walker D. 2000. Nutrient pollution of coastal rivers, bays, and seas. Issues in Ecology 7: 1-15.

Hulth S, Aller RC, Canfield DE, Dalsgaard T, Engstrom P, Gilbert F, Sundback K, Thamdrup B. 2005. Nitrogen removal in marine environments: recent findings and future research challenges. Mar. Chem. 94: 125-145.

IARC. 1996. IARC Monographs on the Evaluation of Carcinogenic Risks to Humans. 65, http://monographs.iarc.fr/ENG/Classification/ClassificationsAlphaOrder.pdf.

Jenkins TF, Hewitt AD, Grant CL, Thiboutot S, Ampleman G, Walsh ME, Ranney TA, Ramsey CA, Palazzo AJ, Pennington JC. 2006. Identity and distribution of residues of energetic compounds at army live-fire training ranges. Chemosphere 63: 1280-90.

Jenkins TF, Pennington JC, Ampleman G. 2007. Characterization and Fate of Gun and Rocket Propellant Residues on Testing and Training Ranges: Interim Report 1 . ERDC TR-07-01. Strategic Environmental Research and Development Program, Vicksburg, Miss, USA.

Jones AL, Harwood JL. 1992. Lipid composition of the brown algae Fucus vesiculosus and Ascophyllum nodosum. Phytochemistry 31: 3397-403.

Juhasz AL, Naidu R. 2007. Explosives: Fate, dynamics, and ecological impact in terrestrial and marine environments. Reviews of Environmental Contamination and Toxicology 191: 163-215.

Just CL, Schnoor JL. 2004. Phytophotolysis of hexahydro-1, 3, 5-trinitro-1, 3, 5-triazine (RDX) in leaves of reed canary grass. Environ. Sci. Technol. 38: 290-295.

Kalderis D, Juhasz AL, Boopathy R, Comfort S. 2011. Soils contaminated with explosives: Environmental fate and evaluation of state-of the-art remediation processes (IUPAC technical report). Pure and Applied Chemistry 83: 1407-1484.

Kemper JM, Ammar E, Mitch WA. 2008. Abiotic degradation of hexahydro-1,3,5-trinitro-1,3,5-triazine in the presence of hydrogen sulfide and black carbon. Environ. Sci. Tech. 42: 2118-2123.

Khan MI, Lee J, Park J. 2012. Microbial degradation and toxicity of hexahydro-1,3,5-trinitro-1,3,5-triazine. J. Microbiol. Biotechnol. 22: 1311-1323.

Khan MI, Lee J, Park J. 2013. A toxicological review on potential microbial degradation intermediates of 2,4,6-trinitrotoluene, and its implications in bioremediation. KSCE J. Civ. Eng. 17: 1223-1231.

Kitts CL, Cunningham DP, Unkefer PJ. 1994. Isolation of three hexahydro-1,3,5-trinitro-1,3,5-triazine degrading species of the family Enterobacteriaceae from nitramine explosive-contaminated soil. Appl. Environ. Microbiol. 60: 4608-4611.

Kitts CL, Green CE, Otley RA, Alvarez MA, Unkefer PJ. 2000. Type I nitroreductases in soil enterobacteria reduce TNT (2, 4, 6-trinitrotoluene) and RDX (hexahydro-1, 3, 5-trinitro-1, 3, 5-triazine). Can. J. Microbiol. 46: 278-282.

Kwon MJ, O'Loughlin EJ, Antonopoulos DA, Finneran KT. 2011. Geochemical and microbiological processes contributing to the transformation of hexahydro-1,3,5-trinitro-1,3,5-triazine (RDX) in contaminated aquifer material. Chemosphere 84: 1223-1230.

Lamberton AH, Lindley C, Owston PG, Speakman JC. 1949a. Studies of nitroamines. Part V. Some properties of hydroxymethyl- and aminomethyl-nitroamines. J. Chem. Soc. 1641-1646.

Lamberton AH, Lindley C, Speakman JC. 1949b. Studies of nitroamines. Part VII. The decomposition of methylenedinitroamine in aqueous solutions. J. Chem. Soc. 1650-1656.

Levine B, Furedi E, Gordon D, Barkley J, Lish P. 1990. Toxic interactions of the munitions compounds TNT and RDX in F344 rats. Fundamental and Applied Toxicology 15: 373-80.

Lewis TA, Ederer MM, Crawford RL. 1997. Crawford, D. L. Microbial transformation of 2,4,6-trinitrotoluene. J. Ind. Microbiol. Biotechnol. 18: 89-96.

Long A, Heitman J, Tobias C, Philips R, Song B. 2012. Co-occurring anammox, denitrification and codenitrification in agricultural soils. Appl. Environ. Microbiol. 79: 168-176.

Lotufo GR. 2011. Whole-body and body-part-specific bioconcentration of explosive compounds in sheepshead minnows. Ecotoxicol. Environ. Saf . 74: 301-306.

Lotufo GR, Farrar JD, Inouye LS, Bridges TS, Ringelberg DB. 2001. Toxicity of sediment associated nitroaromatic and cyclonitramine compounds to benthic invertebrates. Environmental Chemistry 20: 1762-1771.

Lotufo GR, Lydy MJ, Rorrer GL, Cruz-Uribe O, Cheney DP. 2009. Bioconcentration, bioaccumulation, and biotransformation of explosives and related compounds in aquatic organisms. In: Sunahara G.I., Lotufo G., Kuperman R.G., Hawari J. (eds) Ecotoxicology of explosives. CRC press, Boca Raton, pp 123-155.

Lotufo GR, Gibson AB, Leslie Yoo J. 2010a. Toxicity and bioconcentration evaluation of RDX and HMX using sheepshead minnows in water exposures. Ecotoxicol Environ Saf 73(7):1653-7.

Lotufo GR, Blackburn W, Marlborough SJ, Fleeger JW. 2010b. Toxicity and bioaccumulation of TNT in marine fish in sediment exposures. Ecotox. Environ. Safety 73,1720-1727.

Lotufo G, Lydy M. 2005. Comparative toxicokinetics of explosive compounds in sheepshead minnows. Arch. Environ. Contam. Toxicol. 49: 206-14.

Lydy MJ, Lasater J, Landrum PF. 2000. Toxicokinetics of DDE and 2-chlorobiphenyl in Chironomus tentans. Arch. Environ. Contam. Toxicol. 38: 163-8.

Lynch JC, Brannon JM, Delfino JJ. 2002. Dissolution rates of three high explosive compounds: TNT, RDX, and HMX. Chemosphere 47: 725-734.

MacDonald JA, Small MJ, Morgan MG. 2009. Quantifying the risks of unexploded ordnance at closed military bases. Environmental Science and Technology 43: 259-265.

Macek T, Mackova M, Káš J. 2000. Exploitation of plants for the removal of organics in environmental remediation. Biotechnol. Adv. 18: 23-34.

Makris KC, Shakya KM, Datta R, Sarkar D, Pachanoor D. 2007. Chemically catalyzed uptake of 2, 4, 6-trinitrotoluene by *Vetiveria zizanioides*. Environmental Pollution 148: 101-106.

Marín-Spiotta E, Gruley KE, Crawford J, Atkinson EE, Miesel JR, Greene S, Cardona-Correa C, Spencer RGM. 2014. Paradigm shifts in soil organic matter research affect interpretations of aquatic carbon cycling: Transcending disciplinary and ecosystem boundaries. Biogeochemistry 117: 279-297.

McCormick NG, Cornell JH, Kaplan AM. 1981. The anaerobic biotransformation of RDX, HMX and acetylated derivatives. Natick Technical report 85-007. U.S. Army Natick Research and Development center, Natick, MA.

McCormick NG, Cornell JH, Kaplan AM. 1985. The anaerobic biotransformation of RDX, HMS, and their acetylated derivatives. AD Report A149464 (TR85-007). Natick, MA: U.S. Army Natick Research and Development Center.

McCormick NG, Feeherry FE, Levinson HS. 1976. Microbial transformation of 2,4,6-Trinitrotoluene and other nitroaromatic compounds. Applied and Environmental Microbiology 31: 949-958.

McDonald J. 2009. Demonstration of the Marine Towed Array on Bahia Salinas del Sur Veiques, Puerto Rico. ESTCP Project MM-0324.

McGlathery KJ, Anderson IC, Tyler AC. 2001. Magnitude and variability of benthic and pelagic metabolism in a temperate coastal lagoon. Marine Ecology Progress Series 216: 1-15.

Menking KM, Musler HM, Fitts JP, Bischoff JL, Anderson RS. 1993. Clay Mineralogical Analyses of the Owens Lake Core . 93-683. Open-File Report, US Geological Survey, Reston,VA.

Meylan WM, Howard PH, Boethling RS, Aronson D, Printup H, Gouchie S. 1999. Improved method for estimating bioconcentration/bioaccumulation factor from octanol/water partition coefficient. Environmental Toxicology and Chemistry 18: 664-72.

Mittal AK. 2003. Military Munitions: DOD Needs to Develop a Comprehensive Approach for Cleaning Up Contaminated Sites . GAO-04-147. Report to house representatives, United States General Accounting Office, Washington,DC.

Miyares PH, Jenkins TF. 1990. Salting-out solvent extraction for determining low levels of nitroaromatics and nitramines in water. Special Report 90-30. US Army Corps of Engineers, Cold Regions Research and Engineering Laboratory, Hanover, NH.

MLA 1996 (6.1) Surveys of the Beaufort's Dyke explosives disposal site. MLA 1996. Fisheries Research Services Report No. 15/96. Marine Laboratory, Aberdeen, MD.

Monteil-Rivera F, Paquet L, Giroux R, Hawari J. 2008. Contribution of hydrolysis in the abiotic attenuation of RDX and HMX in coastal waters. J. Environ. Qual. 37: 858-864.

Monteil-Rivera F, Halasz A, Groom C, Zhao J, Thiboutot S, Ampleman G, Hawari J 2009. Fate and transport of explosives in the environment; a chemist's view. In: Sunahara GI, Lotufo G, Kuperman RG, Hawari J (eds) Ecotoxicology of explosives. CRC Press, Boca Raton, pp 5-33

Montgomery MT, Coffin RB, Boyd TJ, Osburn CL. 2013. Incorporation and mineralization of TNT and other anthropogenic organics by natural microbial assemblages from a small, tropical estuary. Environ. Pollut. 174: 257-264.

Montgomery MT, Coffin RB, Boyd TJ, Smith JP, Walker SE, Osburn CL. 2011. 2,4,6-Trinitrotoluene mineralization and bacterial production rates of natural microbial assemblages from coastal sediments. Environ. Pollut. 159: 3673-3680.

Moore TR. 2003. Dissolved organic carbon in a northern boreal landscape. Global Biogeochem. Cycles 17: 20-1 to 20-8.

Morley M, Yamamoto H, Speitel G, Clausen J. 2006. Dissolution kinetics of high explosives particles in a saturated sandy soil. J. Contam. Hydrol. 85: 141-158.

Morse JW, Mackenzie FT. 1990. Geochemistry of sedimentary carbonates. Elsevier, New York.

Moser DP, Nealson KH. 1996. Growth of facultative anaerobe *Shewanella putrefaciens* by elemental sulfur reduction. Applied and Environmental Microbiology 62: 2100-2105.

Mukhi S, Patiño R. 2008. Effects of hexahydro-1, 3, 5-trinitro-1, 3, 5-triazine (RDX) in zebrafish: General and reproductive toxicity. Chemosphere 72: 726-732.

Mukhi S, Pan X, Cobb GP, Patino R. 2005. Toxicity of hexahydro-1, 3, 5-trinitro-1, 3, 5-triazine to larval zebrafish (Danio rerio). Chemosphere 61: 178-185.

Nipper M, Carr R, Biedenbach J, Hooten R, Miller K, Saepoff S. 2001. Development of marine toxicity data for ordnance compounds. Arch Environ Contam Toxicol 41(3):308-318.

Nipper M, Carr RS, Lotufo GR. 2009. Aquatic toxicology of explosives, In: Sunahara GI, Lotufo G, Kuperman RG, Hawari J (eds). Ecotoxicology of explosives. CRC Press, Boca Raton, pp 77-115.

Nuutinen S, Landrum PF, Schuler LJ, Kukkonen JV, Lydy MJ. 2003. Toxicokinetics of organic contaminants in *Hyalella azteca*. Arch Environ Contam Toxicol 44: 0467-0475.

Ownby DR, Belden JB, Lotufo GR, Lydy MJ. 2005. Accumulation of trinitrotoluene (TNT) in aquatic organisms: Part 1—Bioconcentration and distribution in channel catfish (*Ictalurus punctatus*). Chemosphere 58: 1153-1159.

Pan X, Zhang B, Cobb GP. 2005. Extraction and analysis of trace amounts of cyclonite (RDX) and its nitroso-metabolites in animal liver tissue using gas chromatography with electron capture detection (GC-ECD). Talanta 67: 816-823.

Paquet L, Monteil-Rivera F, Hatzinger PB, Fuller ME, Hawari J. 2011. Analysis of the key intermediates of RDX (hexahydro-1,3,5-trinitro-1,3,5- triazine) in groundwater: occurrence, stability and preservation. J. Environ. Monit. 13: 2304-2311.

Pennington JC, Brannon JM. 2002. Environmental fate of explosives. Thermochimica Acta 384: 163-72.

Pennington JC, Jenkins TF, Ampleman G. 2006. Distribution and Fate of Energetics on DOD Test and Training Ranges :Final Report. ERDC TR-06-13. US Army Corps of Engineers Engineer Research and Development Center, Vicksburg, Miss, USA.

Pennington JC, Lotufo G, Hayes CA, Porter B, George RD. 2011. TNT, RDX, and HMX Association with Organic Fractions of Marine Sediments and Bioavailability Implications. In Chappell MA, Price CL, George RD (ed), In Environmental Chemistry of Explosives and Propellant Compounds in Soils and Marine Systems: Distributed Source Characterization and Remedial Technologies, Vol 1069. American Chemical Society, pp 185-195.

Pennington JC, Myers T, Davis WM, Olin TJ, McDonald TA, Hayes CA, Townsend DM. 1995. Impacts of sorption on in situ bioremediation of explosives-contaminated soils. TR-IRRP-95-1. US Army Engineer Waterways Experiment Station, Washington, DC.

Pennington JC, Bowen R, Brannon JM, Zakikhani M, Harrelson DW, Gunnison D, Mahannah J, Clarke J, Jenkins TF, Gnewuch S. 1999. Draft protocol for evaluating, selecting, and implementing monitored natural attenuation at explosives-contaminated sites. In Technical Report EL-99-10, U.S. Army Engineer Research and Development Center; Vicksburg, MS.

Pennington JC, Patrick Jr. WH. 1990. Adsorption and desorption of 2,4,6-trinitrotoluene by soils. J. Environ. Qual. 19: 559-567.

Pichtel J. 2012. Distribution and fate of military explosives and propellants in soil: A review. Applied and Environmental Soil Science 2012.

Preuss A, Rieger PG. 1995. In biodegradation of nitroaromatic compounds; Spain, J.C., Ed.; Plenum Publishing Co., New York pp. 69-86.

Price CB, Brannon JM, Yost SL. 1998. Transformation of RDX and HMX under controlled Eh/pH conditions. In Technical Report IRRP-98-2, U.S. Army Engineer Waterways Experiment Station; Vicksburg, MS.

Qiao H, Feng H, Liu S, Wang C, Zhang Y, Gao Y, Li W, Yao J, Wang M, Shen D. 2011. The possible reduction pathways of 2,4,6-trinitrotoluene (TNT) by sulfide under simulated anaerobic conditions. Water Sci. Technol. 64: 2474-2482.

Robertson BK, Jjemba PK. 2005. Enhanced bioavailability of sorbed 2,4,6-trinitrotoluene (TNT) by a bacterial consortium. Chemosphere 58: 263-270.

Rodacy PJ, Walker PK, Reber SD, Phelan J, Andre JV. 2000. Explosive detection in the marine environment and on land using ion mobility spectroscopy. A summary of field tests. Sandia National Laboratories, Sandia Report SAND2000-0921.

Roh H, Yu C, Fuller ME, Chu K. 2009. Identification of hexahydro-1, 3, 5-trinitro-1, 3, 5-triazine-degrading microorganisms via ^{15}N-stable isotope probing. Environ. Sci. Technol. 43: 2505-2511.

Ronen Z, Yanovich Y, Goldin R, Adar E. 2008. Metabolism of the explosive hexahydro-1,3,5-trinitro-1,3,5-triazine (RDX) in a contaminated vadose zone. Chemosphere 73: 1492-1498.

Rosen G, Lotufo GR. 2005. Toxicity and fate of two munitions constituents in spiked sediment exposures with the marine amphipod *Eohaustorius estuarius*. Environmental Toxicology and Chemistry 24: 2887-2897.

Rosen G, Lotufo GR. 2007a. Toxicity of explosive compounds to the marine mussel, Mytilus galloprovincialis, in aqueous exposures. Ecotoxicol. Environ. Saf. 68: 228-36.

Rosen G, Lotufo GR. 2007b. Bioaccumulation of explosive compounds in the marine mussel, Mytilus galloprovincialis. Ecotoxicol. Environ. Saf. 68: 237-45.

Rosen G, Lotufo GR. 2010. Fate and effects of composition B in multispecies marine exposures. Environ. Toxicol. Chem. 29: 1330-1337.

Rosenblatt DH, Burrows EP, Mitchell WR, Parmer DL. 1991. Organic explosives and related compounds. In Anonymous The Handbook of Environmental Chemistry, Vol. 3, Spring-Verlag, Berlin, pp Part G.

Sagi-Ben Moshe S, Ronen Z, Dahan O, Weisbrod N, Groisman L, Adar E, Nativ, R. 2009. Sequential biodegradation of TNT, RDX and HMX in a mixture. Environ. Poll. 157: 2231-2238.

Sarrazin M, Dodard SG, Savard K, Lachance B, Robidoux PY, Kuperman RG, Hawari J, Ampleman G, Thiboutot S, Sunahara GI. 2009. Accumulation of hexahydro-1, 3, 5-trinitro-1, 3, 5-triazine by the earthworm *Eisenia andrei* in a sandy loam soil. Environmental Toxicology and Chemistry 28: 2125-2133.

Schmidt CW. 2004. The price of preparing for war. Environ. Health Perspect. 112: A1004-1005.

Schwarzenbach RP, Gschwend PM, Imboden D. 2003. Air-water exchange. In Environmental Organic Chemistry, 2nd ed. John Wiley & Sons, Inc., Hoboken, NJ. 889-890.

Seitzinger S, Harrison JA, Bohlke JK, Bouwman AF, Lowrance R, Peterson B, Tobias C, Van Drecht G. 2006. Denitrification across landscapes and waterscapes: a synthesis. Ecol. Appl. 16: 2064-2090.

Seitzinger SP, Kroeze C, Styles RV. 2000. Global distribution of N_2O emissions from aquatic systems: natural emissions and anthropogenic effects. Chemosphere Glob. Change Sci. 2: 267-279.

Selim HM, Iskandar IK. 1994. Sorption-desorption and transport of TNT and RDX in soils. CRREL report 94-7. U.S. Army Corps of Engineers: Cold Regions Research & Engineering Laboratory, Hanover, NH.

Seth-Smith HM, Edwards J, Rosser SJ, Rathbone DA, Bruce NC. 2008. The explosive-degrading cytochrome P450 system is highly conserved among strains of *Rhodococcus sp*. Appl. Environ. Microbiol. 74: 4550-4552.

Sharma P, Mayes MA, Tang G. 2013. Role of soil organic carbon and colloids in sorption and transport of TNT, RDX and HMX in training range soils. Chemosphere 92: 993-1000.

Shen CF, Guiot SR, Thiboutot S, Ampleman G, Hawari J. 1988. Complete degradation of RDX and HMX in anoxic soil slurry bioreactors: laboratory and pilot-scale experiments. In: Proc. 6th Int. FZK/TNO Conf. Contaminated Soil, Edinburgh. 513-522.

Shen CF, Guiot SR, Thiboutot S, Ampleman G, Hawari J. 1998. Fate of explosives and their metabolites in bioslurry treatment processes. Biodegradation 8: 339-347.

Sheremata TW, Thiboutot S, Ampleman G, Paquet L, Halasz A, Hawari J. 1999. Fate of 2,4,6-Trinitrotoluene and its metabolites in natural and model soil systems. Environ. Sci. Technol. 33: 4002-4008.

Sheremata TW, Halasz A, Paquet L, Thiboutot S, Ampleman G, Hawari J. 2001. The fate of the cyclic nitramine explosive RDX in natural soil. Environmental Science and Technology 35: 1037-1040.

Sheremata TW, Hawari J. 2000. Mineralization of RDX by the white rot fungus *Phanerochaete chrysosporium* to carbon dioxide and nitrous oxide. Environ. Sci. Technol. 34: 3384-3388.

Sigman DM, Casciotti KL, Andreani M, Barford C, Galanter M, Böhlke JK. 2001. A bacterial method for the nitrogen isotopic analysis of nitrate in seawater and freshwater. Anal. Chem. 73: 4145-4153.

Sikka HC, Banerjee S, Pack EJ, Appleton HT. 1980. Environmental fate of RDX and TNT. In Technical Report 81-538, U.S. Army Medical Research and Development Command; Fort Detrick, Frederick, MD.

Simini M, Checkai RT, Kuperman RG, Phillips CT, Kolakowski JE, Kurnas CW, Sunahara GI. 2003. Reproduction and survival of *Eisenia fetida* in a sandy loam soil amended with the nitro-heterocyclic explosives RDX and HMX: The 7th international symposium on earthworm ecology. Cardiff, Wales. Pedobiologia 47: 657-662.

Singh SN. 2013. Biological remediation of explosive residues. Springer, New York.

Singh J, Comfort S, Shea P. 1998. Remediating RDX-contaminated water and soil using zero-valent iron. J. Environ. Qual. 27: 1240-1245.

Sing R, Soni P, Kumar P, Purohit S, Singh A. 2009. Biodegradation of high explosive production effluent containing RDX and HMS by denitrifying bacteria. World J. Microbiol. Biotechnol. 25: 269-275.

Site AD. 2001. Factors Affecting Sorption of Organic Compounds in Natural Sorbent/ Water Systems and Sorption Coefficients for Selected Pollutants. A Review. J. Phys. Chem. 30: 187-439.

Smaal A, Vonck A. 1997. Seasonal variation in C, N and P budgets and tissue composition of the mussel *Mytilus edulis*. Mar. Ecol. Prog. Ser. 153: 167-179.

Smith P, Bogren K. 2001. Determination of nitrate and/or nitrite in brackish or seawater by flow injection analysis colorimeter: QuickChem Method. Methods manual Lachat Instruments.

Smith RW, Tobias C, Vlahos P, Cooper C, Ballentine M, Ariyarathna T, Fallis S, Groshens TJ. 2015a. Mineralization of RDX-derived nitrogen to N_2 via denitrification in coastal marine sediments. Environ. Sci. Technol. 49: 2180-2187.

Smith RW, Vlahos P, Böhlke JK, Ariyarathna T, Ballentine M, Cooper C, Fallis S, Groshens TJ, Tobias C. 2015b. Tracing the Cycling and Fate of the Explosive 2,4,6-Trinitrotoluene in Coastal Marine Systems with a Stable Isotopic Tracer, ^{15}N-[TNT]. Environ. Sci. Technol. 49: 12223-12231.

Smith RW, Vlahos P, Tobias C, Ballentine M, Ariyarathna T, Cooper C. 2013. Removal rates of dissolved munitions compounds in seawater. Chemosphere 92: 898-904.

Smith RW, Vlahos P, Tobias C, Ballentine M, Ariyarathna T, Cooper C. 2014. Corrigendum to "Removal rates of dissolved munitions compounds in seawater." Chemosphere 99: 276-277.

Spain JC. 1995. Biodegradation of nitroaromatic compounds. Annu. Rev. Microbiol. 49: 523-555.

Spain JC, Hughes JB, Knackmuss HJ. 2000. Biodegradation of nitroaromatic compounds and explosives. Lewis Publishers, New York p. 434.

Spalding RF, Fulton JW. 1988. Groundwater munition residues and nitrate near Grand Island, Nebraska, U.S.A. J. Contam. Hydrol. 2: 139-153.

Spanggord R, Mill T, Chou T, Mabey W, Smith J. 1980. Environmental Fate Studies on Certain Munition Wastewater Constituents. Phase III, Laboratory Studies, Final Report. SRI International, Menlo Park, CA, 197, AD-A099256.

Steevens JA, Duke BM, Lotufo GR, Bridges TS. 2002. Toxicity of the explosives 2, 4, 6-trinitrotoluene, hexahydro-1, 3, 5-trinitro-1, 3, 5-triazine, and octahydro-1, 3, 5, 7-tetranitro-1, 3, 5, 7-tetrazocine in sediments to *Chironomus tentans* and *Hyalella azteca*: Low-dose hormesis and high-dose mortality. Environmental Toxicology and Chemistry 21: 1475-1482.

Stelzer RS, Lamberti GA. 2001. Effects of N:P ratio and total nutrient concentration on stream periphyton community structure, biomass, and elemental composition. Limnology and Oceanography 46: 356-367.

Sterner RW, Hessen DO. 1994. Algal nutrient limitation and the nutrition of aquatic herbivores. Annual Review of Ecology and Systematics 1-29.

Stookey LL. 1970. Ferrozine - A new spectrophotometric reagent for iron. Anal. Chem. 42: 779-781.

Sunahara GI, Dodard S, Sarrazin M, Paquet L, Ampleman G, Thiboutot S, Hawari J, Renoux AY. 1999. Ecotoxicological characterization of energetic substances using a soil extraction procedure. Ecotoxicol. Environ. Safety 43: 138-148.

Sunahara GI, Lotufo G, Kuperman RG, Hawari J. 2009. Introduction, In Ecotoxicology of explosives In: Sunahara GI, Lotufo G, Kuperman RG, Hawari J (eds) Ecotoxicology of explosives. CRC Press, Boca Raton, pp 1-3.

Sweeney LM, Okolica MR, Gut CP, Gargas ML. 2012. Cancer mode of action, weight of evidence, and proposed cancer reference value for hexahydro-1, 3, 5-trinitro-1, 3, 5-triazine (RDX). Regulatory Toxicology and Pharmacology 64: 205-224.

Talmage SS, Opresko DM, Maxwel CJ, Welsh CJE, Cretella FM, Reno PH, Daniel FB. 1999. Nitroaromatic munition compounds: environmental effects and screening values. Rev. Environ. Contam. Toxicol. 161: 1-156.

Thompson R, Bayne B. 1974. Some relationships between growth, metabolism and food in the mussel *Mytilus edulis*. Mar. Biol. 27: 317-326.

Thompson KT, Crocker FH, Fredrickson HL. 2005. Mineralization of the cyclic nitramine explosive hexahydro-1,3,5-trinitro-1,3,5-triazine by *Gordonia* and *Williamsia sp*. Appl. Environ. Microbiol. 71: 8265-8272.

Thompson PL, Ramer LA, Schnoor JL. 1999. Hexahydro-1,3,5-triazine translocation in poplar trees. Environmental Toxicology and Chemistry. 18: 279-284.

Tobias CR, Macko SA, Anderson IC, Canuel EA, Harvey JW. 2001. Tracking the fate of a high concentration groundwater nitrate plume through a fringing marsh: A combined groundwater tracer and in situ isotope enrichment study. Limnol. Oceanogr. 46: 1977-1989.

Ullah H, Shah AA, Hasan F, Hameed A. 2010. Biodegradation of trinitrotoluene by immobilized *Bacillus Sp.* YRE1. Pak. J. Bot. 42: 3357-3367.

Urbanski T. 1967. In Chemistry and technology of explosives, Vol III; Laverton, S., Eds.; Pergamon Press: Oxford, 1967; pp 17-77.

US Army Environmental Hygiene Agency (AEHA). 1985. Water Pollution Aspects of Explosive Manufacturing. Technical Guide No. 140.

USARDEC. 2001. Off-Shore Disposal of Chemical Agents and Weapons Conducted by the United States Department of Defense; U.S. Army Research, Development, and Engineering Command: Aberdeen Proving Ground, Maryland. Corporate Information Office. Historical Research and Response Team: Aberdeen Proving Ground, MD.

US EPA. 1994. Nitroaromatics and Nitramines by High Performance Liquid Chromatography (HPLC)-Method 8330. SW846. Office of Solid Waste and Emergency Response. Washington, DC, USA.

US EPA. 1994. SW-846, method 8330, Nitroaromatics and Nitramines by High Performance Liquid Chromatography (HPLC), revision 0, September 1994. Office of Solid Waste and Emergency Response. Washington, DC.

US EPA. 2007. Explosives by Gas Chromatography - Method 8095. Office of Solid Waste and Emergency Response. Washington, DC, USA.

US EPA. 2014a. Technical Fact Sheet – 2,4,6-Trinitrotoluene (TNT). EPA 505-F-14-009. Office of Solid Waste and Emergency Response. Washington, DC, USA. http://www2.epa.gov/sites/production/files/2014-03/documents/ffrrofactsheet_contaminant_tnt_january2014_final.pdf.

US EPA. 2014b. Technical Fact Sheet –Hexahydro-1,3,5-Trinitro- 1,3,5-Triazine (RDX). EPA 505-F-14-008. Office of Solid Waste and Emergency Response. Washington, DC, USA. http://www2.epa.gov/sites/production/files/2014-03/documents/ffrrofactsheet_contaminant_rdx_january2014_final.pdf.

Van Aken B, Yoon JM, Schnoor JL. 2004. Biodegradation of nitro-substituted explosives 2,4,6-trinitrotoluene, hexahydro-1,3,5-trinitro-1,3,5-triazine, and octahydro-1,3,5,7-tetranitro-1,3,5-tetrazocine by a phytosymbiotic methylobacterium sp. associated with poplar tissues (*Populus deltoides x nigra* DN34). Appl. Environ. Microbiol. 70: 508-17.

Vasilyeva GK, Kreslavski VD, Shea PJ, Bollag JM. 2002. Transformation and binding of 2,4,6-trinitrotoluene in soil amended with activated carbon. In: Violante A, Huang P, Bollag J, Gianfreda L. (eds.) Soil mineral-organic matter-microorganism interactions and ecosystem health, 157-168.

Vila M, Lorber-Pascal S, Laurent F. 2007. Fate of RDX and TNT in agronomic plants. Environmental Pollution 148: 148-154.

Walsh ME, Taylor S, Hewitt AD, Walsh MR, Ramsey CA, Collins CM. 2010. Field observation of the persistence of Comp B explosives residues in a salt marsh impact area. Chemosphere 78: 467-473

Wanninkhof R. 1992. Relationship between wind speed and gas exchange over the ocean. J. Geophysical Res. 97: 7373-7382.

Ward BB. 2007. Nitrogen cycling in aquatic environments. In: Hurst C, Crawford R, Garland J, Lipson D, Mills A, Stetzenbach L. Manual of Environmental Microbiology. Eds. Amer. Soc. Microbiol., New York. 511-522

Weber Jr. WJ, Voice TC, Pirbazari M, Hunt GE, Ulanoff DM. 1983. Sorption of hydrophobic compounds by sediments, soils and suspended solids-II. Sorbent evaluation studies. Water Res. 17: 1443-1452.

Weiss RF. 1970. The solubility of nitrogen, oxygen and argon in water and seawater. Deep-Sea Research and Oceanographic Abstracts 17: 721-735.

Weissmahr KW, Sedlak DL. 2000. Effect of metal complexation on the degradation of dithiocarbamate fungicides. Environmental Toxicology and Chemistry 19: 820-826.

Wilbrand J. 1863. Notiz uber Trinitrotoluol. Annalen der Chemie und Parmacie 128: 178-179.

Won WD, DiSalvo LH, Ng J. 1976. Toxicity and mutagenicity of 2,4,6-trinitrotoluene and its microbial metabolites. Appl. Environ. Microb. 31: 576-580.

Xu W, Dana KE, Mitch WA. 2010. Black carbon-mediated destruction of nitroglycerin and RDX by hydrogen sulfide. Environ. Sci. Technol. 44: 6409-6415.

Xue SK, Iskandar IK, Selim HM. 1995. Adsorption-desorption of 2,4,6-trinitrotoluene and hexahydro-1,3,5-trinitro-1,3,5-triazine in soils. Soil Sci. 160: 317-327.

Yamamoto H, Morley MC, Speitel Jr. GE, Clausen J. 2004. Fate and transport of high explosives in a sandy soil: Adsorption and desorption. Soil and Sediment Contamination 13: 459-477.

Yates J, Peckol P. 1993. Effects of nutrient availability and herbivory on polyphenolics in the seaweed *Fucus versiculosus*. Ecology: 1757-1766.

Yong H, Halasz A, Zhao JS, Monteil-Rivera F, Hawari J. 2008. Experimental evidence for in situ natural attenuation of 2,4- and 2,6-dinitrotoluene in marine sediment. Chemosphere 70: 791–799.

Yoo LJ, Lotufo GR, Gibson AB, Steevens JA, Sims JG. 2006. Toxicity and bioaccumulation of 2, 4, 6-trinitrotoluene in fathead minnow (*Pimephales promelas*). Environmental Toxicology and Chemistry 25: 3253-3260.

Yost SL, Pennington JC, Brannon JM, Hayes CA. 2007. Environmental process descriptors for TNT, TNT-related compounds and picric acid in marine sediment slurries. Mar. Poll. Bull. 54: 1262-1266.

Zhang B, Pan X, Cobb GP, Anderson TA. 2005. Use of pressurized liquid extraction (PLE)/gas chromatography-electron capture detection (GC-ECD) for the determination of biodegradation intermediates of hexahydro-1,3,5-trinitro-1,3,5-triazine (RDX) in soils. Journal of Chromatography B: Analytical Technologies in the Biomedical and Life Sciences 824: 277-282.

Zhang B, Pan X, Smith JN, Anderson TA, Cobb GP. 2007. Extraction and determination of trace amounts of energetic compounds in blood by gas chromatography with electron capture detection (GC/ECD). Talanta 72: 612-619.

Zhao XK, Yang GP, Gao XC. 2003. Studies on the sorption behaviors of nitrobenzene on marine sediments. Chemosphere 52: 917-925.

Zhao JS, Greer CW, Thiboutot S, Ampleman G, Hawari J. 2004a. Biodegradation of the nitramine explosives hexahydro-1,3,5-trinitro-1,3,5-triazine and octahydro-1,3,5,7-tetranitro-1,3,5,7-tetrazocine in cold marine sediment under anaerobic and ologotrophic conditions. Can. J. Microbiol. 50: 91-96.

Zhao JS, Spain J, Thiboutot S, Ampleman G, Greer C, Hawari J. 2004b. Phylogeny of cyclic nitramine-degrading psychrophilic bacteria in marine sediment and their potential role in the natural attenuation of explosives. FEMS Microbiol. Ecol. 49: 349-357.

Zheng W, Lichwa J, D'Alessio M, Ray C. 2009. Fate and transport of TNT, RDX, and HMX in streambed sediments: Implications for riverbank filtration. Chemosphere 76: 1167-1177.

Zheng Y, Hou L, Liu M, Liu Z, Li X, Lin X, Yin G, Gao J, Yu C, Wang R, Jiang X. 2016. Tidal pumping facilitates dissimilatory nitrate reduction in intertidal marshes. Sci. Rep. 6. doi: 10.1038/srep21338

Zoh K, Stenstrom MK. 2002. Fenton oxidation of hexahydro-1,3,5-trinitro-1,3,5-triazine (RDX) and octahydro-1,3,5,7-tetranitro-1,3,5,7-tetrazocine (HMX). Water Res. 36: 1331-1341.

13.0 APPENDICES

13.1 Peer Reviewed Publications

Ariyarathna T, Ballentine M ,Vlahos P, Smith RW, , Cooper C., Böhlke J.K, Fallis S., Groshens T, Tobias C. 2019. Tracing the cycling and fate of the munition, Hexahydro-1,3,5-trinitro-1,3,5-triazine in a simulated sandy coastal marine habitat with stable isotopic tracer, ^{15}N-[RDX]. Science and the Total Environment 647: 369-378.

Ariyarathna T, Vlahos P, Smith RW, Fallis S, Groshens T, Tobias C. 2017. Biodegradation and mineralization of isotopically labelled TNT and RDX in anaerobic marine sediments. Environ. Toxicol. Chem. 36: 1170-1180.

Ariyarathna T, Vlahos P, Tobias C, Smith R. 2016. Sorption kinetics of TNT and RDX in anaerobic freshwater and marine sediments: Batch studies. Environ Toxicol Chem. 35: 47-55.

Ballentine M, Tobias C, Vlahos P, Smith R, Cooper C. 2015. Bioconcentration of TNT and RDX in coastal marine biota. Arch. Environ. Contam. Toxicol. 68 :718-28.

Ballentine ML, Ariyarathna T, Smith RW, Cooper C, Vlahos P, Fallis S, Groshens TJ, Tobias C. 2016. Uptake and fate of hexahydro-1,3,5-trinitro-1,3,5-triazine (RDX) in coastal marine biota determined using a stable isotopic tracer, ^{15}N - [RDX]. Chemosphere 153:28-38.

Smith RW, Tobias C, Vlahos P, Cooper C, Ballentine M, Ariyarathna T, Fallis S, Groshens TJ. 2015a. Mineralization of RDX-derived nitrogen to N_2 via denitrification in coastal marine sediments. Environ. Sci. Technol. 49: 2180-2187.

Smith RW, Vlahos P, Böhlke JK, Ariyarathna T, Ballentine M, Cooper C, Fallis S, Groshens TJ, Tobias C. 2015b. Tracing the Cycling and Fate of the Explosive 2,4,6-Trinitrotoluene in Coastal Marine Systems with a Stable Isotopic Tracer, 15N-[TNT]. Environ. Sci. Technol. 49: 12223-12231.

Smith RW, Vlahos P, Tobias C, Ballentine M, Ariyarathna T, Cooper C. 2013. Removal rates of dissolved munitions compounds in seawater. Chemosphere 92: 898-904.

13.2 Presentations

Ariyarathna, T., Ballentine, M., Vlahos, P., Smith, R.W., Cooper, C., Bohlke, J., Fallis, S., Groshens, T., Tobias, C. Tracking the Fate of Explosive-Trinitrotriazine (RDX) in Coastal Marine Ecosystems Using Stable Isotopic Tracer – Poster. Meeting of the American Geophysical Union. December 2017.

Ariyarathna, T., Vlahos, P., Ballentine, M., Smith, R., Cooper, C., Böhlke, J., Fallis, S., Groshens, T., Tobias, C. 2016. Tracking the fate of explosive-Trinitrotriazine (RDX) in coastal marine ecosystems using stable isotopic tracers. The 22nd Annual Meeting of North Atlantic Chapter - Society of Environmental Toxicology and Chemistry. Amherst, Massachusetts.

Smith, R., Vlahos, P., Ariyarathna, T., Ballentine, M., Cooper, C., Böhlke, J., Fallis, S., Groshens, T., Tobias, C. 2016. Tracing the cycling and fate of individual organic molecules using isotopically labeled "tracer" molecules. A case study from military chemical munitions. Organic Geochemistry Gordon Research Seminar and Conference. Holderness, New Hampshire.

Ariyarathna, T., Vlahos, P., Ballentine, M., Smith, R., Cooper, C., Tobias, C. 2015. Tracking the metabolism of explosives in coastal marine ecosystems using stable isotopic tracers: Role of sediment. North America 36th Annual Meeting of the Society of Environmental Toxicology and Chemistry. Salt Lake City, Utah.

Ballentine, M., Ariyarathna, T., Smith, R., Vlahos, P., Böhlke, J., Fallis, S., Tobias, C. 2015. Biotic uptake and retention of munitions derived nitrogen measured in three simulated coastal habitats. North America 36th Annual Meeting of the Society of Environmental Toxicology and Chemistry. Salt Lake City, Utah.

Smith, R., Vlahos, P., Ariyarathna, T., Ballentine, M., Cooper, C., Böhlke, J., Fallis, S., Groshens, T., Tobias, C. 2015. Tracing the cycling and fate of the explosive 2,4,6-trinitrotoluene (TNT) in coastal marine systems with a stable isotopic tracer, ^{15}N-[TNT]. Society of Environmental Toxicology and Chemistry North American Conference. Salt Lake City, Utah.

Ariyarathna, T., Vlahos, P., Tobias, C., Ballentine, M., Smith, R., Cooper, C. 2015. Tracking the flux and metabolism of explosives in coastal marine ecosystems using stable isotopic tracers: Role of sediment. Annual Aquatic Sciences Meeting of Association for the Sciences of Limnology and Oceanography. Granada, Spain.

Ballentine, M., Ariyarathna, T., Smith, R., Vlahos, P., Böhlke, J., Fallis, S., Tobias, C. 2015. Uptake and retention of munitions derived nitrogen in estuarine biota. The 23rd Biennial Conference of the Coastal and Estuarine Research Federation. Portland, Oregon.

Ballentine, M., Ariyarathna, T., Vlahos, P., Smith, R., Tobias, C. 2015. Uptake and Incorporation of Nitrogen from RDX in Various Estuarine Species Using Stable Nitrogen Isotopes. Spring 2015 Meeting of the New England Estuarine Research Society. Bristol, Rhode Island.

Ariyarathna, T., Vlahos, P., Tobias, C., Smith, R., Ballentine, M., Cooper, C. 2014. Tracking the uptake and metabolism of munitions compounds in coastal marine ecosystems using stable isotopic tracers: Role of sediment. The 24th Annual Meeting of Society of Environmental Toxicology and Chemistry. Basel, Switzerland.

Ballentine, M., Smith, R., Ariyarathna, T., Tobias, C., Vlahos, P. 2014. Tracking Munitions in Two Coastal Marine Ecosystems Using Stable Nitrogen Isotopes: Role of Biota. Europe 24th Annual Meeting of the Society of Environmental Toxicology and Chemistry. Basel, Switzerland.

Smith, R., Ariyarathna, T., Ballentine, M., Cooper, C., Tobias, C., Vlahos, P. 2014. Tracing the cycling and fate of the explosive 2,4,6-Trinitrotoluene (TNT) in marine systems with isotopically labeled ^{15}N-TNT. Society of Environmental Toxicology and Chemistry International Conference. Basel, Switzerland.

Ariyarathna, T., Vlahos, P., Tobias, C., Ballentine, M., Smith, R. 2013. Sorption and anaerobic degradation of explosives in coastal sediments using isotopically labeled compounds. American 34th Annual Meeting of the Society of Environmental Toxicology and Chemistry. Nashville, Tennessee.

Ballentine, M., Smith, R., Ariyarathna, T., Tobias, C., Vlahos, P. 2013. Tracking the uptake and assimilation of TNT and RDX in coastal marine biota using stable nitrogen isotopes. North American 34th Annual Meeting of the Society of Environmental Toxicology and Chemistry. Nashville, Tennessee.

Ariyarathna, T., Vlahos, P., Tobias, C., Smith, R. 2012. Characteristics and sorption kinetics of explosives in Sediments. North American 33rd Annual Meeting of the Society of Environmental Toxicology and Chemistry. Long Beach, California.

Ballentine, M., Smith, R., Tobias, C., Vlahos, P. 2012. Fate of TNT in coastal marine organisms using stable nitrogen isotopes. North American 33rd Annual Meeting of the Society of Environmental Toxicology and Chemistry. Long Beach, California.

Smith, R., Vlahos, P., Tobias, C., Ballentine, M., Ariyarathna, T., Cooper, C. 2012. Behavior of Explosive Compounds in the Marine Environment: The Role of Sediments. North American 33rd Annual Meeting of the Society of Environmental Toxicology and Chemistry. Long Beach, California.

Ballentine, M., Smith, R., Tobias, C., Vlahos, P. 2012. Uptake and partitioning of TNT and RDX in coastal marine organisms. Spring 2012 Meeting of the New England Estuarine Research Society. Block Island, Rhode Island.